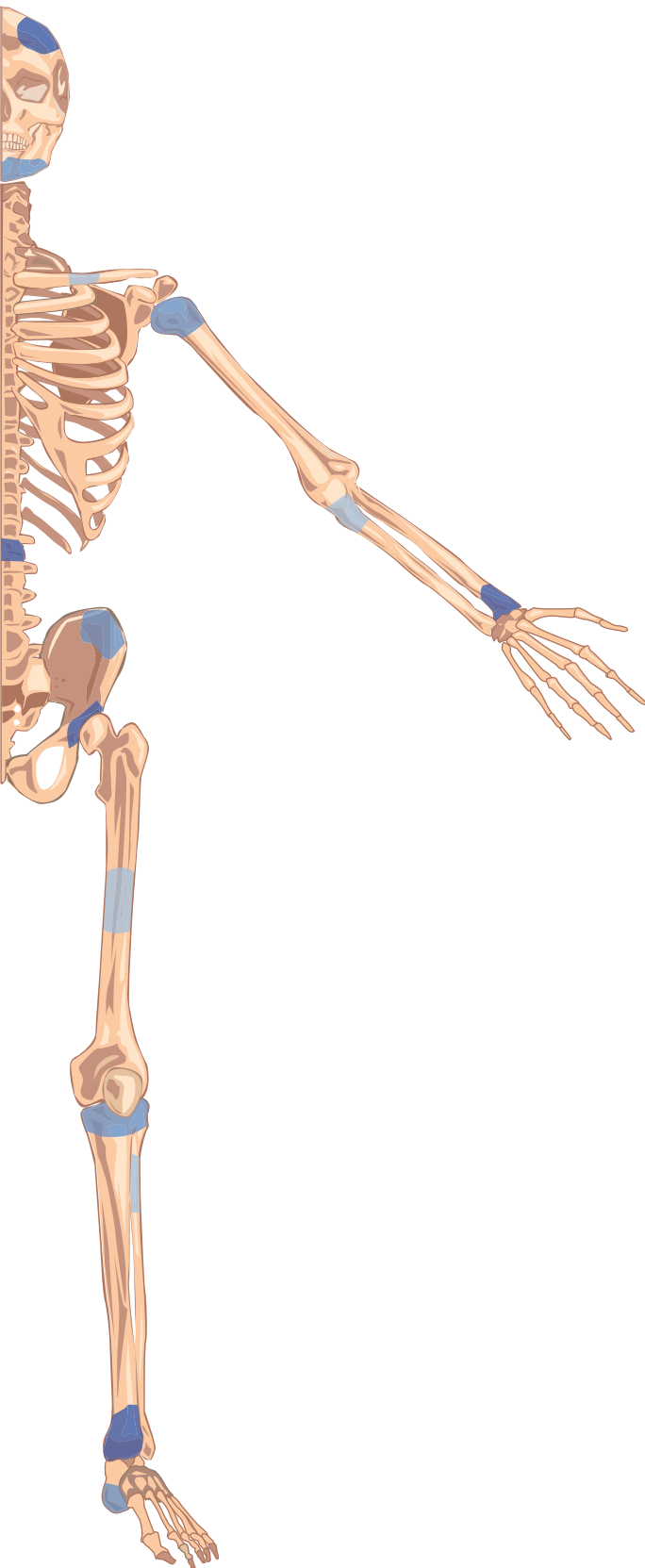


Bone Graft Substitutes

Developed for Trauma
and Orthopaedic Surgery



Johan van der Stok

Bone Graft Substitutes

Developed for Trauma and Orthopaedic Surgery

Johan van der Stok

The printing of this thesis was financially supported by: Erasmus MC, afdeling Orthopaedie Erasmus MC, Nederlandse Orthopaedische Vereniging, Nederlandse Vereniging voor Traumachirurgie, Annafonds, 2Move-Implants BV - Implants for life, 3D Systems - Layerwise NV, Chipsoft BV, Link & Lima Nederland, Livit Orthopedie, Orthopedie Centrum Rotterdam

ISBN: 978-94-6169-641-0

Cover by: Maurice van den Berg, Moop's Art
Layout by: Optima Grafische Communicatie
Printed by: Optima Grafische Communicatie
Publisher: Optima Grafische Communicatie

De digitale versie van dit proefschrift is te vinden op www.e-pubs.nl/?epub=j.vanderstok of door middel van onderstaande QR-code.



© Copyright 2015 J. van der Stok.

All right reserved. No part of this thesis may be reproduced, stored in a retrieval system or transmitted in any form by any means, without prior written permission of the author or, when appropriate, of the scientific journal in which parts of this thesis have been published.

Bone Graft Substitutes Developed for Trauma and Orthopaedic Surgery

Botsubstitutiematerialen ontwikkeld voor gebruik in trauma en orthopaedische chirurgie

Proefschrift

ter verkrijging van de graad van doctor
aan de Erasmus Universiteit Rotterdam
op gezag van de rector magnificus

Prof.dr. H.A.P. Pols

en volgens besluit van het College voor Promoties.

De openbare verdediging zal plaatsvinden op
woensdag 20 mei 2015 om 13:30 uur

door

Johan van der Stok
geboren te Delft



Promotiecommissie

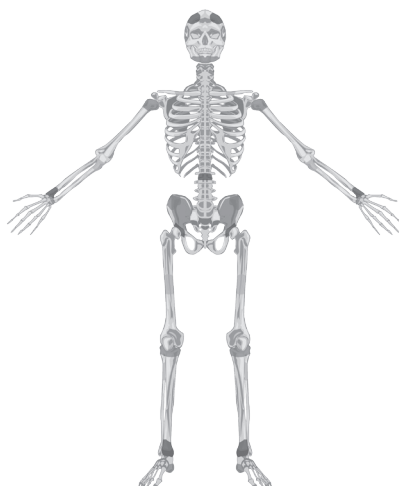
Promotoren: Prof.dr.ir. H. Weinans
Prof.dr. J.A.N. Verhaar
Prof.dr. P. Patka

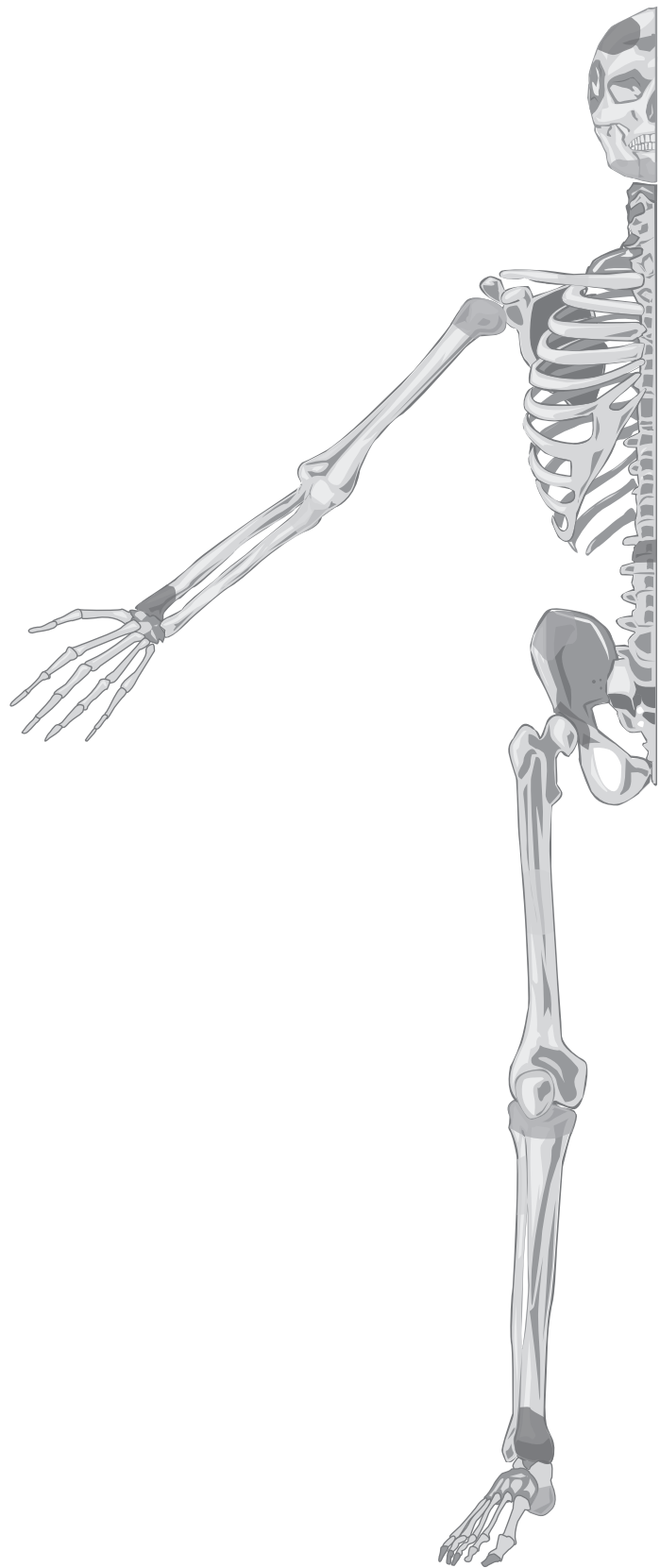
Copromotor: Dr. E.M.M. van Lieshout

Overige leden: Prof.dr. E.B. Wolvius
Prof.dr. M.H.J. Verhofstad
Prof.dr. J. de Boer

Table of contents

1. Introduction	7
2. Bone graft substitutes in the Netherlands	17
3. Calcium phosphate cements	37
4. Porous calcium phosphate ceramics	51
5. Selective laser melting produced porous titanium implants	65
6. Porous titanium implants coated with osteostatin	83
7. Porous titanium implants incorporated with growth factor-loaded gelatin gels	101
8. Porous titanium implants incorporated with BMP-2 loaded fibrin gels	119
9. Chondrogenically differentiated mesenchymal stromal cell pellets	137
10. Conclusion and general discussion	155
11. Summary	167
12. Nederlandse samenvatting	173
13. Appendices	179
References	181
PhD Portfolio	205
List of publications	209
Dankwoord	213
About the author	219





Chapter 1

Introduction

Clinical challenge

Bone grafting was established in the 19th century and has become a common procedure in which bone defects are filled with bone grafts or bone graft substitutes. Bone defects that require bone grafting are encountered in approximately 10% of trauma and orthopaedic surgeries¹. A broad range of different bone grafts or bone graft substitutes have been developed during the past fifty years. All these bone grafts or bone graft substitutes have their strengths and weaknesses, confronting each surgeon with the difficult task to select the most suitable bone graft or bone graft substitute for each trauma and orthopaedic surgical procedure that requires bone grafting.

Bone

The human skeleton contains 206 different bones and these bones show great variation in shape and function. Bone contains three different cell types; osteoblasts, osteocytes, and osteoclasts, which are all involved in the formation, maintenance and remodelling of the extracellular bone matrix. This bone matrix is composed of an inorganic and organic phase. The inorganic phase is mainly responsible for the stiffness of bone and consists of carbonated hydroxyapatite, a calcium phosphate crystal. The organic phase, on the other hand, is mainly responsible for the elasticity of bone and consists of more than 95% of collagen type I. This organic phase of the bones matrix is made by osteoblasts. Therefore osteoblasts lay down an uncalcified matrix of collagen type I fibres and secrete alkaline phosphatase. Alkaline phosphatase is an enzyme that facilitates calcium entrapment and thereby mineralization of the bone matrix. The osteoblasts that become surrounded by mineralized bone matrix differentiate into osteocytes. These osteocytes can communicate with other osteocytes, osteoblasts and/or osteoprogenitor cells on the surface of mineralized bone matrix. Thereby osteocytes act as a mechanosensory system that can regulate bone remodelling, e.g. via synthesized molecules such as sclerostin². Bone remodelling is a continuous process that removes and replaces old or damaged bone matrix. Bone matrix can be degraded by osteoclasts. Osteoclasts are specialized macrophage-like cells located on the bone surface in so called Howship's lacunae or resorption pits. The outer bone surface is covered by periosteum, a membrane that contains progenitor cells that can become osteoblasts. Structurally, bones are made out of cortical (or compact) and trabecular (or cancellous) bone. Cortical bone forms the dense outside layer, and only contains Haversian canals through which small blood vessels and nerve branches run. Trabecular bone forms the interior and is a highly porous structure made of thin trabeculae (100-300µm). This trabecular structure transfers mechanical loads and can adapt to changes in mechanical loading (Wolff's law). Cortical bone is stronger than trabecular bone. Compressive strength of cortical bone varies between

130 and 290MPa, and that of trabecular bone varies between 2 and 38MPa, dependent on its porosity. Also the Young's modulus of cortical bone (ranging from 5-21GPa) is much higher than that of trabecular bone (ranging from 0.01–1.57GPa) ³.

Bone development

Bone development can occur through endochondral ossification and intramembranous ossification ⁴. Endochondral ossification is the process through which long bones (e.g. tibia, femur and radius) are formed, and also occurs in the growth plate (physis) until adolescence. This process begins with mesenchymal stromal cells that become chondrocytes and form a cartilage template. This cartilage template forms into the shape of the future bone and enlarges through chondrocyte proliferation. Chondrocytes in the centre of the cartilage template stop proliferating and then become hypertrophic. Hypertrophic chondrocytes start producing enzymes (e.g. alkaline phosphatase) that initiate mineralization of the extracellular matrix. In addition, they attract blood vessels and osteoclasts through secretion of various cytokines including vascular endothelial growth factor (VEGF) and matrix metalloproteinase (MMP). The mineralized template is, through the attraction of osteoclasts and osteoblasts, remodelled into mature bone.

Intramembranous ossification is the process through which flat bones (e.g. the skull and ribs) form. During this process mesenchymal stromal cells start to form a small, dense cluster of cells, a nodule. Once this nodule has formed, mesenchymal stromal cells differentiate into osteoblasts. Osteoblasts produce osteoid which becomes mineralized and forms the immature bone.

Bone regeneration during fracture repair

Fracture repair progresses through consecutive phases of inflammation, repair and remodelling ⁵. The inflammation phase starts with the formation of a haematoma (a blood clot). Within this haematoma, pro-inflammatory and chemoattractive stimuli are released by degrading platelets and they start to activate neutrophils, monocytes and macrophages and attracting mesenchymal stromal cells. The repair phase follows upon initial stabilization of the fracture. Based on the degree of mechanical stability obtained, this will result in direct or indirect bone formation. Direct bone formation is only seen when there is absolute fracture stability and is capable of restoring fracture gaps that do not exceed 200–500µm. Under these conditions, new Haversian canals crossing the fracture gap are established by remodelling units known as cutting cones ⁶. These remodelling units consist of osteoclasts, that remove bone matrix, and are accompanied by endothelial cells that form new blood

vessels. Subsequently, osteoblasts form new bone that leads to union of the fracture gap. Indirect bone formation is seen when the obtained stabilization allows for a limited degree of micromotion⁷. These micromotions result in the formation of a cartilage template (soft callus) within the medullary canal and inter-cortical areas of the fracture gap⁶. Within these areas, bone is formed through endochondral ossification as the cartilage template mineralizes and is then replaced by bone. Simultaneously, the periosteum and soft tissues that surround the cartilage template will create bone through intramembranous ossification (hard callus), thereby further contributing to bridging the fracture gap. Finally, during the remodelling phase, bone undergoes remodelling to restore its original shape. Overall this process of fracture repair is very efficient, but in 10% of all fractures bone regeneration is insufficient or impaired, resulting in persistent bone defects or the development of delayed unions, malunions or hypertrophic or atrophic non-unions (Figure 1)⁸.

Bone grafting

Bone grafting aims to stimulate insufficient or impaired bone regeneration through enhancing the essential components necessary for bone regeneration. In order to offer all these essential components, an ideal bone graft or bone graft substitute should have the following properties: (1) the biomaterial is fully biocompatible, meaning that it does not elicit any detrimental immunogenic response; (2) it has osteoconductive properties, meaning that the biomaterial provides a scaffold that supports the apposition of bone and the ingrowth of

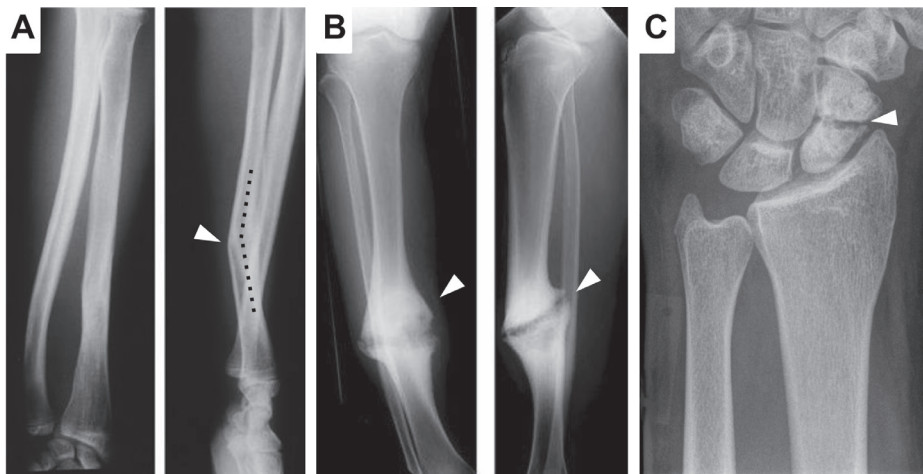


Figure 1: Examples of impaired fracture healing.

Malunion of an antibrachii fracture, black dotted line shows angulation of the radius (A). Hypertrophic non-union of a tibia fracture, indicated by the white arrowhead showing extensive callus formation (B). Atrophic non-union of a scaphoid fracture indicated by the white arrowhead showing a lack of callus formation (C).

vascular tissue^{8,9}; (3) it has osteoinductive properties, meaning that the biomaterial actively recruits osteoprogenitor cells and that it stimulates their differentiation towards active osteoblasts that start to form bone^{8,9}; and/or (4) it has osteogenic properties, meaning that the biomaterial itself contains osteoprogenitor cells or osteoblasts capable of bone regeneration⁸. Finally, the biomaterial should provide sufficient mechanical support to allow for an optimal biomechanical environment in which bone regeneration can occur.

Bone grafts

A bone graft can be taken from the patients' own bone (called an autograft) or from donated bone (called an allograft). Autologous bone is currently considered the gold standard¹⁰ and it can be obtained as cancellous, cortical or vascularised bone grafts.

Cancellous autografts contain a high number of osteogenic cells and high levels of osteoinductive growth factors¹¹. Its trabecular structure offers an osteoconductive scaffold, but it does not offer substantial mechanical support. Cancellous autografts can sometimes be obtained locally, but more often require a secondary surgical site to be harvested. Harvesting bone from the posterior iliac crest offers more bone than harvesting from the anterior iliac crest, but the overall amount of bone that can be harvested is limited. This harvesting procedure is also associated with complications in 30–40% of patients¹², including wound infections, nerve and urethral injury, prolonged or severe postoperative pain, and an increased length of hospital stay¹³. Furthermore harvesting techniques, with a short harvest-to-graft time and adequate interim storage, are essential to maintain the osteogenic and osteoinductive properties of the bone graft¹⁴.

Cortical autografts provide mechanical support, but they contain less osteogenic cells and osteoinductive growth factors than cancellous autografts¹⁵. Due to the dense structure of cortical autografts, bone regeneration is preceded by osteoclasts resorption. This osteoclast activity is estimated to begin two weeks after grafting, and can reduce the mechanical strength by more than 75%¹⁶. This structure also delays revascularisation which can take up to two months. Therefore vascularised cortical autografts are often used (e.g. fibula grafts) because they are better able to maintain mechanical strength after grafting and offer superior osteogenic and osteoinductive properties. However, vascularised cortical autografts require a technically more demanding and time consuming harvesting procedure that includes microsurgery and remains associated with a relatively high failure rate.

Another method to harvest autologous bone is reamer irrigated aspiration (RIA). During this procedure, an inner layer of cortical bone of the femoral canal is reamed and aspirated. The captured aspirate consists of bone and bone marrow and contains a higher concentration of osteoinductive growth factors than cancellous autografts obtained from the iliac

crest¹¹. The RIA method is therefore a viable alternative to cancellous autografts, especially since this harvesting technique is associated with a lower complication rate¹⁷.

Allografts have also been used for many years¹⁸ and are obtained from cadaver bones. Allografts require extensive processing in order to eliminate the risk of disease transmission and to reduce immunogenicity¹⁹. Processing steps include freezing or freeze-drying to devitalize bone. Allografts maintain their osteoconductive matrix, but this processing negatively affects its levels of osteoinductive growth factors and mechanical properties¹⁸. The actual risk of disease transmission is nowadays negligible, but issues of immunogenicity remain a concern²⁰. Allogeneic bone can also be processed as demineralized bone matrix (DBM). Devitalisation and demineralization results in a gel that only contains the matrix proteins (e.g. collagen, glycoproteins and proteoglycans) and growth factors (e.g. bone morphogenetic proteins). This DBM does not provide an osteoconductive matrix nor any mechanical support, although the presence of growth factors should preserve its osteoinductive properties. However the osteoinductive properties of DBM are heavily debated as preserved levels of growth factors are donor dependent and have been found to be extremely low after devitalisation and demineralization processes²¹.

Bone graft substitutes

Bone graft substitutes can be made from various biomaterials and a wide range of products are available for clinical use in trauma and orthopaedic surgery (Table 1).

Calcium phosphate ceramics are probably the most extensively studied group of biomaterials. In 1920, Albee *et al* reported the use of a calcium phosphate ceramic as a bone graft substitute in animal models²⁶. Calcium phosphate ceramics closely resemble the mineral composition of bone. Also calcium sulphate, or plaster of Paris, has been used for more than a century. First reports date back to the late 1800s²⁷, and their interest is based on the fact that calcium sulphate is well-tolerated, relatively cheap and undergoes rapid and complete resorption²⁸. The discovery of bone morphogenetic proteins (BMPs) by Urist in 1965²⁹, led to the development of growth factor enhanced absorbable collagen sponges. In the 1970s, Hench *et al* introduced bioactive glass, which was discovered to have excellent bone-bonding properties^{30, 31}. Also in the 1970s, porous metals were opted to be an interesting bone graft substitute because of their excellent mechanical strength³². In the early 2000s, tantalum was the first porous metal implant introduced in trauma and orthopaedic surgery^{33, 34}. Porous titanium³⁵ and porous magnesium³⁶ implants are still under development for the use of a bone graft substitutes.

Table 1. Biomaterials used as bone graft substitute

Material	Available products ²²⁻²⁵
Calcium-based materials	
Calcium phosphate ceramics	Actifuse, Allogran-N, Allogran-R, Apapore, BoneSave, Camceram, Cellplex TCP, Cerabone, Cerasorb, ChronOS, Conduit TCP, CycLOS, Endobon, ENGIpore, Integra Mozaik, Mastergraft, OpteMx, OsSatura BCP, OsSatura TCP, Ostim, Pro Osteon 500, Repros, SINTIlife, Vitoss
Calcium phosphate cements	Alpha-BSM, Beta-BSM, BoneSource, Calcibon, Callos, CarriGen, ChronOS Inject, Gamma-BSM, GeneX, HydroSet, Nanostim, Norian SRS, Norian Drillable
Calcium sulphate	BonePlast, MIIG X3, OsteoSet, ProDense, Stimulan
Bioglass	Cortoss
Polymer-based materials	
Collagen	Colloss, Healos, Infuse, OP-1, RegenOss, Targobone
Metal-based materials	
Porous titanium	Regenerex
Porous tantalum	Trabecular Metal

Aim and outline of this thesis

The aim of this thesis was to provide a detailed overview of bone graft substitutes that are developed for trauma and orthopaedic surgery, therefore the properties of bone substitute materials and the potential of these biomaterials to enhance bone regeneration were studied in bone defect models.

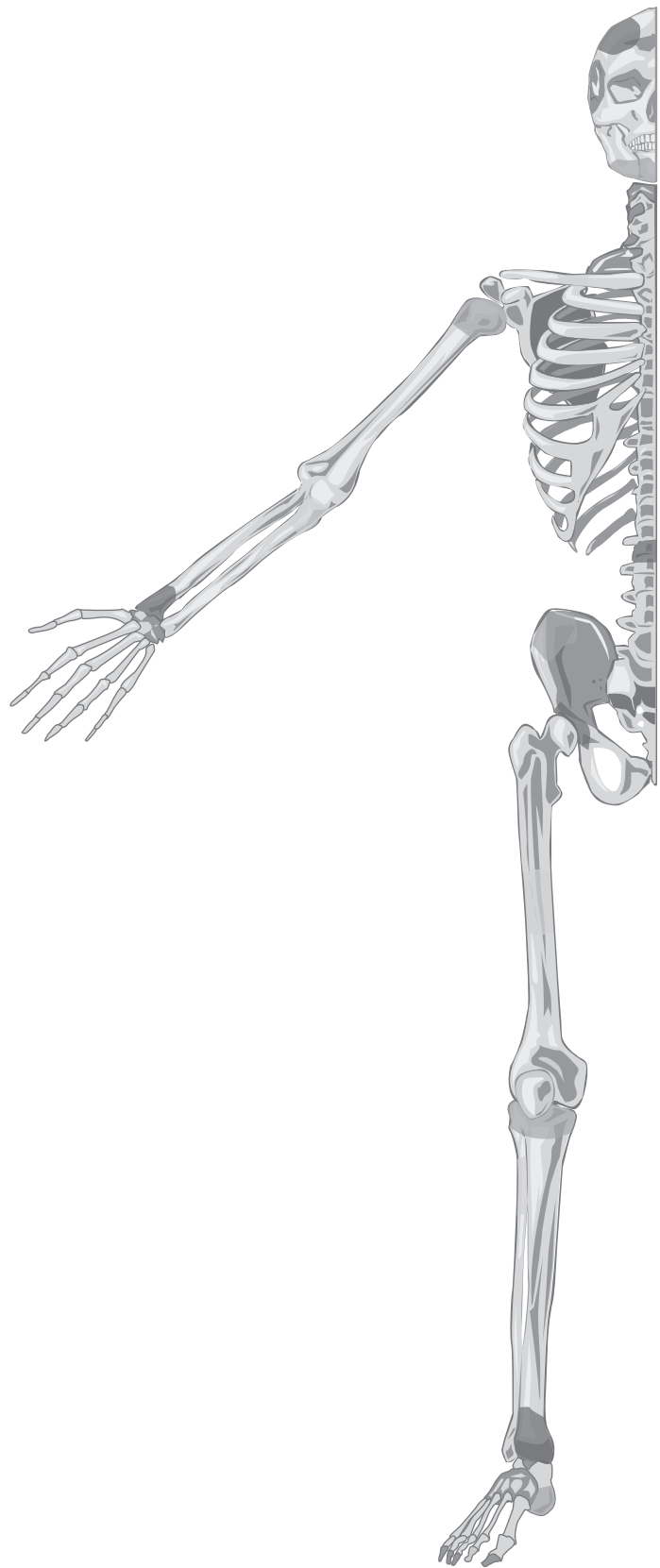
The first part of this thesis focusses on calcium-based bone graft substitutes. **Chapter 2** starts with a comprehensive overview of commercially available bone graft substitutes in trauma and orthopaedic surgery. This overview is based on a systematic literature search that included all 18 calcium-based bone graft substitutes available in the Netherlands (in 2009). This chapter describes the structural, mechanical and biological properties of these bone substitute materials that include calcium phosphate ceramics, calcium phosphate cements, calcium sulphates and bioglass and provides further insight in the current clinical level of evidence to use these bone graft substitutes in trauma and orthopaedic-related indications. In **Chapter 3**, calcium phosphate cements and their use in trauma and orthopaedic-related indications was specifically discussed after a direct comparison of their biological properties in cortical bone defects in goat tibiae. In **Chapter 4**, the potential to enhance

bone regeneration of cortical bone defects of two different calcium phosphate ceramics was evaluated in rats.

The second part of this thesis focusses on the development of porous titanium implants as a new bone graft substitute. In **Chapter 5**, we designed and evaluated two different porous titanium implants and determined their potential to function as a load-bearing osteoconductive scaffold in cortical bone defects in rats. To reinforce porous titanium implants with osteoinductive properties we evaluated several strategies including bioactive surface coatings and incorporation of bioactive gels. In **Chapter 6**, the surface of porous titanium implants was coated with osteostatin, a short peptide that has osteoinductive properties³⁷. In **Chapter 7**, porous titanium implants were incorporated with gelatin nanosphere gels that were designed to release multiple growth factors in a time and dose controlled manner³⁸. In **Chapter 8**, porous titanium implants were incorporated with fibrin gels. These fibrin gels were designed to mimic the fracture haematoma and subsequently loaded with BMP-2.

The final part of this thesis focusses on the use of new stem cell-based approaches to enhance bone regeneration. Stem cells were used to form a cartilage-like tissue that mimics the cartilage template (or soft callus) formed during endochondral ossification. The capacity of this cartilage template to stimulate bone regeneration in atrophic non-unions was determined by implantation of this artificial soft callus in an atrophic non-union model in rats (**Chapter 9**).

This thesis ends with the conclusion and general discussion of the work presented (**Chapter 10**), followed by an English summary **Chapter 11** and a Dutch summary **Chapter 12**.



Chapter 2

Bone graft substitutes in the Netherlands

Johan van der Stok
Esther M.M. van Lieshout
Youssef El-Massoudi
Gerdine H. van Kralingen
Peter Patka

Published as "Bone substitutes in the Netherlands: a systematic literature review" in Acta Biomaterialia;

2011 Feb;7(2):739-50

Abstract

Autologous bone grafting is currently considered as the gold standard to restore bone defects. However, clinical benefit is not guaranteed and there is an associated 8-39% complication rate. This has resulted in the development of alternative (synthetic) bone graft substitutes. The aim of this systematic literature review was to provide a comprehensive overview of literature data of bone graft substitutes registered in the Netherlands for use in trauma and orthopaedic surgery. Brand names of selected products were used as search terms in three available databases: Embase, PubMed and Cochrane. Manuscripts written in English, German or Dutch that reported on structural, biological or biomechanical properties of the pure product or on its use in trauma and orthopaedic surgery were included. The primary search resulted in 475 manuscripts from PubMed, 653 from Embase and 10 from Cochrane. Of these, 218 met the final inclusion criteria. Of each bone substitute material, structural, biological and biomechanical characteristics as well as their clinical indications in trauma and orthopaedic surgery are provided. All included products possess osteoconductive properties but differ in resorption time and biomechanical properties. They have been used for a wide range of clinical applications; however, the overall level of clinical evidence is low. The requirements of an optimal bone graft substitute are related to the size and location of the defect. Calcium phosphates have been used for most trauma and orthopaedic surgery surgical procedures. Calcium sulphates were mainly used to restore bone defects after tumour resection surgery but offer minimal structural support. Bioactive glass remains a potential alternative; however, its use has only been studied to a limited extent.

Introduction

The treatment of fractures remains a continuous challenge for trauma and orthopaedic surgeons. Although most fractures heal uncomplicated, 5-10% of patients encounter problems due to bone defects, impaired fracture healing, or a combination of both⁸. Significant bone defects or post-traumatic complications such as delayed unions, non-unions or malunions may require bone-grafting in order to fill the defect. Bone grafts fill voids, provide support, and therefore may enhance the biological repair of the defect. Bone grafting is a common surgical procedure, carried out in approximately 10% of all skeletal reconstructive surgery cases⁴⁰. Worldwide, an estimated 2.2 million grafting procedures are performed each year^{41, 42}.

Bone healing differs from any other soft tissue since it heals through the generation of new bone rather than by forming fibrotic tissue. Bone repair requires four critical elements: (1) osteogenic cells (e.g. osteoblasts or progenitor cells); (2) osteoinductive signals provided by growth factors; (3) an osteoconductive matrix; and (4) adequate blood and nutrient supply⁴³. Therefore, bone grafts are often described by the terms osteogenicity, osteoinductivity, and osteoconductivity. Osteogenicity is the presence of bone forming cells within the graft^{44, 45}. Osteoinductivity is the ability of a graft to stimulate or promote bone formation⁴⁶. Osteoconductivity is the ability of the graft to function as a scaffold for ingrowth of new bone and sprouting capillaries⁴⁷.

Autologous bone, mostly harvested from the iliac crest, is considered the gold standard since it provides a scaffold for bone ingrowth, contains living bone cells that offer osteogenesis, and contains growth factors that stimulate osteoinduction⁴⁴. However, as the cellular elements do not necessarily survive transplantation, the clinical benefit is not guaranteed¹⁴. In addition, the harvesting of autologous bone lengthens the surgical procedure, and the graft amount may be insufficient, or the form inappropriate. Moreover, autograft harvesting is associated with an 8-39% risk of complications, including: infection, haematoma, nerve and urethral injury, pelvic instability, cosmetic disadvantages, postoperative pain and chronic pain at the donor site^{12, 13, 48, 49}. Furthermore, autografting is normally not recommended for elderly or paediatric patients or for patients with malignant or infectious disease. Alternative strategies like allo-, and xenotransplantation have major biocompatibility disadvantages compared with autografting^{50, 51}, and as such their use is suboptimal.

Due to complications and limitations associated as reported, alternative bone graft substitutes were needed. Based upon the above, the perfect bone substitute material is osteoconductive, osteoinductive, biocompatible, and bioresorbable. Moreover, it should induce minimal or no fibrotic reaction, undergo remodelling and support new bone formation. From a mechanical point of view bone substitute materials should have similar strengths to that of the bone being replaced. Finally, it should be cost-effective and ought to be available in the amount required.

Technological evolution and better understanding of bone-healing biology resulted in the development of numerous alternative bone graft substitutes. Multiple products, containing (combinations of) hydroxyapatite, tricalcium phosphate, dicalcium phosphate, calcium sulphate (plaster of Paris), or bioactive glass are currently available for use in trauma and orthopaedic surgery. However, an evidence-based guideline to assist surgeons in selecting the best product for specific clinical indications is not available yet. The aim of the current study was to provide a comprehensive overview of literature data of bone graft substitutes registered in the Netherlands for use in trauma and orthopaedic surgery. An overview of bone substitute materials, their composition, their biological and biomechanical characteristics as well as their clinical indications in trauma and orthopaedic surgery is provided.

Methods

1. Product selection

Products were selected based upon the following criteria: (1) products composed of (combinations of) calcium phosphate, calcium sulphate or bioactive glass; (2) indicated for use in trauma and orthopaedic surgery; and (3) available in the Netherlands on October 12, 2009. Products were excluded if they could only be used in combination with adjunctive (e.g. bone marrow aspirate, growth factors, or antibiotics) or if they were only indicated for use in craniomaxillofacial surgery.

2. Literature search

Brand names of all products (see Table 1) were used as search terms in three available online databases: Embase, PubMed, and Cochrane. Databases were searched from the earliest date available until July 1, 2010. Titles and abstracts were screened by two researchers (JVDS and YEM). Only papers that reported on structural, biological or biomechanical properties, or on clinical indications in trauma and orthopaedic surgery, and were written in English, German, or Dutch, were considered eligible. The full text of all eligible papers retrieved from PubMed and Cochrane were read by two researchers (JVDS and YEM), papers found in Embase were read by three researchers (JVDS, GHVK, and YEM). All references in the selected manuscripts were reviewed in order to ensure that no papers had been missed with the chosen search strategy. For final inclusion a manuscript had to report on structural, biological or biomechanical properties of the pure product or on their use in trauma and orthopaedic surgery. Data regarding study design, species, structural, biological, biomechanical, and clinical findings were collected in a database, and are summarized below. Manuscripts reporting on clinical indications of bone substitutes for trauma and orthopaedic surgery were given a level of evidence as described by Mahid *et al*⁵².

Table 1. Overview of bone graft substitutes available for clinical use in the Netherlands

Product name	Company	Origin	Chemical composition	Form	Ceramic/ cement*
Calcium phosphate					
Hydroxyapatite					
Cerabone®	Fame Medical Products BV	Bovine	HA	solid	Ceramic
Endobon®	Biomet	Bovine	HA	solid	Ceramic
Ostim®	Heraeus	Synthetic	60% HA / 40% H ₂ O	paste	Cement
Pro Osteon 500®	Biomet	Coral	HA	solid	Ceramic
Tricalcium phosphate					
ChronOS™	Synthes	Synthetic	α-TCP	solid	Ceramic
Vitoss®	Orthovita	Synthetic	β-TCP	solid	Ceramic
Composite					
BoneSave®	Stryker	Synthetic	80% TCP / 20% HA	solid	Ceramic
BoneSource®	Stryker	Synthetic	TTCP / DCP	paste	Cement
Calcibon®	Biomet	Synthetic	62.5% α-TCP / 26.8% DCPA / 8.9% CaCO ₃ / 1.8% HA	paste	Cement
Camceram®	CAM Implants	Synthetic	60% HA / 40% β-TCP	solid	Ceramic
ChronOS™ Inject	Synthes	Synthetic	73% β-TCP / 21% MCPH ₂ O / 5% MHPT	paste	Cement
HydroSet™	Stryker	Synthetic	TTCP / DCP / TSC	paste	Cement
Norian SRS®	Synthes	Synthetic	α-TCP / CaCO ₃ / MCPH ₂ O	paste	Cement
Calcium sulphate					
BonePlast®	Biomet	Synthetic	CaSO ₄	paste	
MIIG® X3	Wright Medical Technology	Synthetic	CaSO ₄	paste	
OsteoSet®	Wright Medical Technology	Synthetic	CaSO ₄	pellets	
Stimulan®	Biocomposites	Synthetic	CaSO ₄	pellets/ paste	
Bioactive glass					
Cortoss®	Orthovita	Synthetic	N.S.	paste	

*ceramic is defined as an inorganic, non-metallic solid prepared by thermal treatment and subsequent cooling⁵³; cement is defined as a product consisting of a liquid solution which hardens *in situ* through a chemical reaction.

CaCO₃: calcium carbonate, CaSO₄: calcium sulphate, DCP: dicalcium phosphate, DCPA: dicalcium phosphate anhydrous, MCPH₂O: monocalcium phosphate monohydrate, MHPT: magnesium hydrogen phosphate trihydrate, H₂O: water, HA: hydroxyapatite, TCP: tricalcium phosphate, TTCP: tetracalcium phosphate, TSC: trisodium citrate, N.S.: not specified.

Results

Eighteen bone graft substitute products were selected. All products were commercially available at July 1, 2010 and the costs per unit range between 100 and 750 Euro. The initial literature search for product name resulted in 475 manuscripts for Pubmed, 653 for Embase and ten for Cochrane. After screening of all titles and abstracts, 195 manuscripts for Pubmed, 230 for Embase and one for Cochrane were considered eligible. Exclusion of 159 duplicates resulted in a total of 267 eligible manuscripts, as shown in Figure 1. After reading the full text of all eligible manuscripts 67 papers had were excluded and 18 were added based upon the reference list. Finally, 218 articles were found to fulfil all inclusion criteria. A detailed overview of the final inclusion per product and subdivision in pre-clinical and clinical studies is given in Table 2.

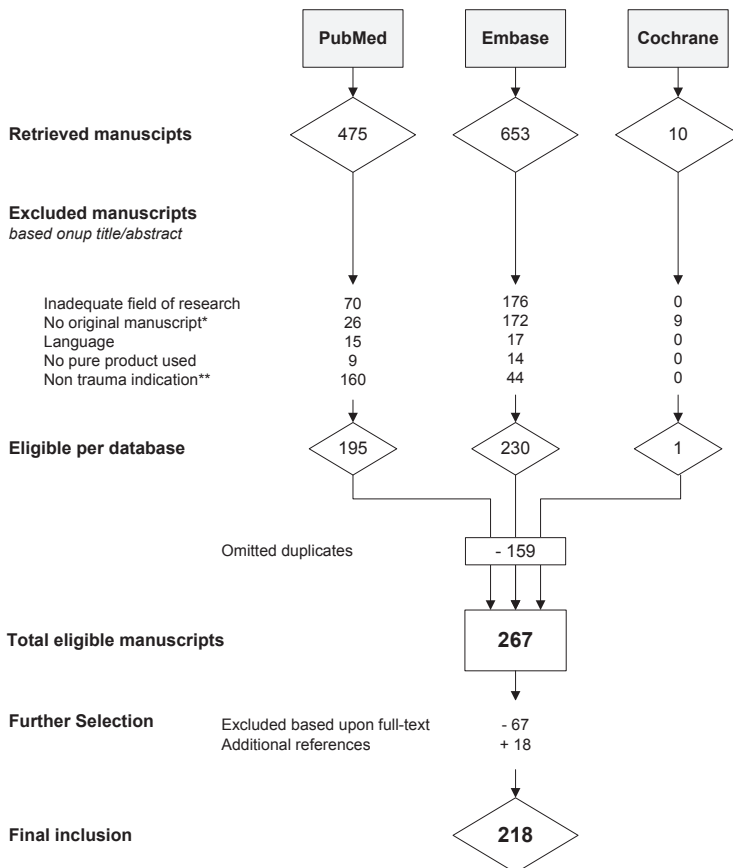


Figure 1: Flow diagram of literature selection process.

Flow diagram of literature selection process. *e.g. reviews, letters, comments, **e.g. dental or craniomaxillofacial surgery.

1. Calcium phosphate

In the eighties, calcium phosphate salts such as tricalcium phosphate (TCP) and hydroxyapatite (HA) were introduced for clinical use. Multiple calcium phosphate are available with different application forms (e.g. pastes, putties, solid matrices, granules). Based upon their chemical composition, calcium phosphates can be separated into hydroxyapatite (HA), tricalcium phosphate (TCP) and composite grafts (Table 1). The latter simply indicating a combination of two or more calcium phosphates.

1.1. Structural properties

Structural properties are related to production methods. Therefore a further subdivision can be made between ceramics and cements. A ceramic is defined as an inorganic, non-metallic solid prepared by thermal treatment and subsequent cooling⁵³, for calcium phosphates ceramics thermal treatment is called sintering. The sintering process removes volatile chemicals and increases crystal size, resulting in a porous and solid material. Cements, first introduced by Brown and Chow⁵⁴, consist of a mixture of calcium phosphates which can be applied as a paste and harden *in situ* due to precipitation reactions.

Hydroxyapatites of ceramic origin are Cerabone[®], Endobon[®] and Pro Osteon 500[®]. Ostim[®] is a hydroxyapatite cement. Hydroxyapatite ceramics have a stoichiometry similar to that of bone mineral^{45,55}. Cerabone[®] and Endobon[®] are of bovine origin and Pro Osteon 500[®] is derived from sea coral (genera *goniopora*). Endobon[®] has a highly crystalline grain size ($1.57 \pm 0.78 \mu\text{m}$) with an apparent density of $0.35\text{-}1.25 \text{g/cm}^3$ ^{56,57}, and has a porosity of 60-80%⁵⁸, including 18% micropores and a pore size of $390\text{-}1,360 \mu\text{m}$ ⁵⁶. Pore sizes of Cerabone[®] and Pro Osteon 500[®] stated in the product information were $100\text{-}1,500 \mu\text{m}$ and $280\text{-}770 \mu\text{m}$, respectively. Ostim[®] is a hydroxyapatite suspension in water, available as a paste.

ChronOS[™] and Vitoss[®] consist of tricalcium phosphate and are both ceramic materials. Tricalcium phosphate has a stoichiometry similar to that of amorphous bone precursors⁵⁵. ChronOS[™] has a particle size of $1.4\text{-}2.8 \text{mm}$ ⁵⁹, and has a porosity of 60-75%⁶⁰⁻⁶² and a pore size of $100\text{-}400 \mu\text{m}$ ^{60,62}.

Included composite grafts of ceramic origin were BoneSave[®] and Camceram[®]. BoneSave[®] consists of 80% TCP and 20% HA. Camceram[®] consist of 60% HA and 40% β -TCP. BoneSource[®], Calcibon[®], ChronOS[™] Inject, HydroSet[™] and Norian SRS[®] are calcium phosphate cements. The setting reaction of calcium phosphate cements leads to the formation of either precipitated hydroxyapatite (PHA) or dicalcium phosphate dihydrate (DCPD). Cements have a solid structure characterized by limited porosity and pore size⁵⁵. BoneSource[®], composed of tetracalcium phosphate and dicalcium phosphate anhydrous, has a porosity of 46%^{63,64} and pore size of $2\text{-}50 \mu\text{m}$ ⁶⁵. Calcibon[®] consists of α -TCP, and has a porosity of 30-40%^{66,67} with a pore size of $<1 \mu\text{m}$ ⁶⁷. Calcibon[®] has a density of 1.84g/cm^3 ⁶⁶ whereas Norian SRS[®] has a density of 1.3g/cm^3 ⁶⁸.

Table 2. Number of publications retrieved from the systematic literature review on bone graft substitutes

Product name	PubMed		Embase		Cochrane		Total eligible	Exclusion	Added references	Final inclusion	Field of study	
	Eligible	Total	Eligible	Total	Eligible	Total						
Calcium phosphate												
Hydroxyapatite												
Cerabone®	3	9	4	0	0	0	7	3	0	3	2	1
Endobon®	22	62	28	0	0	0	48	16	1	29	19	10
Ostim®	23	51	16	2	0	0	29	12	1	16	12	4
Pro Osteon 500®	5	16	8	0	0	0	13	3	0	5	2	3
Tricalcium phosphate												
ChronOS™	51	100	10	0	0	0	14	2	2	9	7	2
Vitoss®	19	59	19	3	0	0	33	16	1	14	6	8
Composite												
BoneSave™	6	15	8	0	0	0	14	5	0	3	1	2
BoneSource®	206	86	17	1	1	1	53	20	2	27	24	3
Calcibon®	7	45	18	0	0	0	25	7	5	15	9	6
Camceram®	1	1	1	0	0	0	2	1	0	0	0	0
ChronOS™ Inject	6	12	6	0	0	0	11	4	0	6	5	1
HydroSet™	2	3	2	0	0	0	4	2	0	2	2	0
Norian SRS®	55	90	45	1	1	1	86	32	3	51	21	30
Calcium sulphate												
Bone Plast®	0	10	1	0	0	0	1	0	0	1	0	1
MIIG X3®	5	6	2	0	0	0	3	0	1	4	1	3
OsteoSet®	30	29	26	3	0	0	47	19	2	20	9	11
Stimulan®	4	20	4	0	0	0	7	3	0	0	0	0
Bioactive glass												
Cortoss®	21	14	40	15	0	0	29	14	2	13	7	6

Database searches were performed until July 1, 2010 (PubMed, Embase and Cochrane). * Pre-clinical studies including biomechanical studies.

1.2. Biological properties

Although highly crystalline TCP and HA derived through thermal treatment do not exist naturally, they have been shown to induce a biologic response similar to that of bone⁵⁵. In general, calcium phosphates are considered to be osteoconductive. However under certain conditions calcium phosphates might also possess osteoinductive properties^{69, 70}. Osteoconductive properties were confirmed for most calcium phosphate products (Table 3), however no data were found for BoneSave[®], Camceram[®] and HydroSet[™]. BoneSource[®] implanted in an extraskeletal site was able to induce bone formation, and is therefore considered to possess osteoinductive properties⁶³. Extraskeletal implantation of Calcibon[®]⁷¹ and Endobon[®]⁷² did not initiate bone formation.

Biodegradability of HA seems related to its appearance. HA ceramics like Endobon[®] and Pro Osteon 500[®] are rather inert⁷³⁻⁷⁸, whereas the HA cement Ostim[®] was shown to be biodegradable by osteoclastic activity⁷⁹⁻⁸⁴. After one year, 70% of the implanted material was resorbed in tibia bone of minipigs⁸⁴, but a recently published study only found minimal resorption of Ostim[®] after an implantation period of twelve weeks in rabbits femora⁸⁵.

Vitoss[®] elicits no cytotoxic reaction in *in vitro* cell cultures⁸⁶. ChronOS[™] and Vitoss[®] are both resorbed over time^{59, 87}. Resorption of these TCP products is mediated by osteoclastic activity and resorption time varies between 6-24 months⁵⁵.

BoneSource[®] and Calcibon[®] support cell growth of osteoblasts in *in vitro* cell cultures, eliciting no cytotoxic reactions⁸⁸⁻⁹⁰. Resorption of composite ceramics is unknown; no data on biodegradation was found for BoneSave[®] and Camceram[®]. All composite cements were shown to be biodegradable. In vertebral bodies, 20% of the applied Calcibon[®] was resolved after one year⁹¹. ChronOS[™] Inject is almost completely resorbed by osteoclastic activity within six months⁹². Norian SRS[®] was biodegraded by osteoclasts⁹³⁻⁹⁶, however one study found no resorption of Norian SRS[®] at twelve weeks after implantation in sheep tibia⁹⁷.

1.3. Biomechanical properties

Calcium phosphates generally provide limited biomechanical support, because they are brittle and have little tensile strength¹⁴¹. Tricalcium phosphates are less brittle compared with hydroxyapatite; however, their degradation results in subsequent loss of mechanical strength over time. An overview of compression strength, Young's modulus, tensile strength and shear strength of each product is given in Table 4. No data was found for BoneSave[®], Camceram[®], ChronOS[™], ChronOS[™] Inject, Ostim[®], Pro Osteon 500[®], and Vitoss[®].

Endobon[®] has an *in vitro* strength of 1-11MPa with a Young's modulus of 20-3,100MPa⁵⁶. *In vivo* tests showed a 2-20MPa compression strength and a Young's modulus of 20-1,200MPa^{58, 98}. Push-out testing of Endobon[®] after 26 weeks implantation in femoral metaphyseal bone of rabbits showed in an interfacial shear stress of 7MPa⁵⁸. Hing *et al* measured compression strength of Endobon[®] before (*in vitro*) and after implantation into rabbit femur condyles

for five weeks. The *in vitro* compression strength was 2-9MPa and the *in vivo* compression strength was 6-11MPa, an increase of 195%⁷³.

Tricalcium phosphates, ChronOSTM and Vitoss[®], were implanted in rabbit tibia and subsequently subjected to torque force. During the study period, torque failure of the grafted tibia increased from 1800Nm after two weeks to 3400Nm after 26 weeks, however torque failures at both time point did not differ significantly between ChronOSTM and Vitoss[®]⁵⁹.

The composite cements BoneSource[®], Calcibon[®], HydroSetTM and Norian SRS[®] have been tested in various biomechanical experiments. Norian SRS[®] has an compression strength of 23-55MPa^{68, 142, 143}, with a tensile strength of 2.1MPa^{142, 143}, and a shear strength of 0.85-1.3MPa¹⁴⁴. In addition, Norian SRS[®] may also be used to augment cortical screws, this results in an increased resistance to torque forces¹⁴⁵. BoneSource[®] has a compression strength of 6.3-34MPa^{146, 147} with a Young's modulus of 3.6-4.7MPa^{117, 148}. Interfacial

Table 3. Overview of porosity, pore size and biological properties

Product name	Porosity (%)	Pore size (µm)	Osteogenic	Osteoinductive	Osteoconductive	Biodegradable
Calcium phosphate						
Hydroxyapatite						
Cerabone [®]	N.D.	(100-1,500)	N.D.	N.D.	Yes ⁸¹	N.D.
Endobon [®]	60-80 ⁵⁸	390-1,360 ⁵⁶	N.D.	No ⁷²	Yes ^{58, 72, 75, 77, 78, 98-102}	No ⁷³⁻⁷⁸
Ostim [®]	N.D.	N.D.	N.D.	N.D.	Yes ^{79-84, 103-105}	Yes ⁷⁹⁻⁸⁴
Pro Osteon 500 [®]	N.D.	(280-770)	N.D.	N.D.	Yes ^{74, 106, 107}	No ¹⁰⁸
Tricalcium phosphate						
ChronOS TM	60-75 ^{59, 61, 62}	100-400 ^{59, 62}	N.D.	N.D.	Yes ^{59, 61, 109-111}	Yes ^{61, 110, 112}
Vitoss [®]	(88-92)	(1-1,000)	N.D.	N.D.	Yes ^{59, 113}	Yes ⁵⁹
Composite						
BoneSave [®]	(50)	(300-500)	N.D.	N.D.	N.D.	N.D.
BoneSource [®]	46 ^{63, 64}	2-50 ⁶⁵	N.D.	Yes ⁶³	Yes ^{64, 114-122}	Yes ^{114, 115, 117, 118, 120}
Calcibon [®]	30-40 ^{66, 67}	<1 ⁶⁷	N.D.	No ⁷¹	Yes ^{67, 71, 91, 123, 124}	Yes ^{91, 125, 126}
Camceram [®]	N.D.	N.D.	N.D.	N.D.	N.D.	N.D.
ChronOS TM Inject	N.D.	N.D.	N.D.	N.D.	Yes ^{92, 96, 127}	Yes ^{92, 96, 127}
HydroSet TM	N.D.	N.D.	N.D.	N.D.	N.D.	N.D.
Norian SRS [®]	(50)	N.D.	N.D.	N.D.	Yes ^{93-97, 128}	Yes ⁹³⁻⁹⁶ /No ⁹⁷
Calcium sulphate						
Bone Plast [®]	N.D.	N.D.	N.D.	N.D.	N.D.	N.D.
MIIG [®] X3	N.D.	N.D.	N.D.	N.D.	Yes ¹²⁹⁻¹³¹	Yes ¹²⁹⁻¹³¹
OsteoSet [®]	N.D.	N.D.	N.D.	N.D.	Yes ¹³²⁻¹³⁵ /No ^{136, 137}	Yes ¹³²⁻¹³⁸
Stimulan [®]	N.D.	N.D.	N.D.	N.D.	N.D.	N.D.
Bioactive glass						
Cortoss [®]	(1)	N.D.	N.D.	N.D.	Yes ¹³⁹	Yes ¹⁴⁰

Data obtained from the suppliers are given between brackets. N.D.: no data available.

bonding strength of BoneSource[®] implanted in dog femora was superior to that of the implanted polymethylmethacrylate (PMMA), which served as a control group¹²¹. Calcibon[®] has a compression strength of 35-55MPa^{66, 149}, with a Young's modulus of 2,500-3,000MPa⁶⁶ and a tensile strength of 4.5MPa¹⁵⁰. Of HydroSet[™], compression strength of 14-24MPa and Young's modulus of 125-240MPa¹⁵¹ and a tensile strengths of 0.11-0.17MPa were recorded¹⁵².

1.4. Clinical indications

Each clinical indication requires specific structural, biological and biomechanical properties of bone substitute materials. An overview of clinical indications in trauma and orthopaedic surgery of each bone graft substitute is given in Table 5.

Hydroxyapatite ceramic Endobon[®] can be used to fill bone defects of several fracture sites; specifically proximal tibia^{77, 100, 155-157}, distal tibia¹⁰⁰, distal radius^{99, 158} and calcaneus¹⁰⁰. It provides adequate mechanical stability in open^{77, 100, 157} and arthroscopic¹⁵⁶ management of tibia plateau fractures. However, in one case refracture of the proximal tibia occurred seven years after implantation¹⁵⁵. Huber *et al* showed treated 24 tibia plateau fractures by using a combination of Ostim[®] and Cerabone[®] resulting in an average Rasmussen tibia score of 26 after one year⁸⁰. Ostim[®] may also be used as sole product for the treatment of fractures of the tibia¹⁰³, calcaneus¹⁰³, or radius^{103, 159, 160}. Bone voids resulting of benign bone tumour resections, located in the humerus, tibia, femur, calcaneus, ileum, fibula, and ulna bone were successfully grafted with Pro Osteon 500[®]¹⁶¹. Besides, Pro Osteon 500[®] was also used for distal radius fractures¹⁶².

Tricalcium phosphates may be used in the upper and lower extremity. Vitoss[®] is an option to treat fractures of the tibia or calcaneus, but was also used in the upper extremity, especially in the humerus¹⁶³. ChronOS[™] was used as bone graft substitute in the posterior stabilization and interlaminar fusion of a vertebral fracture type Magerl B2.3¹⁶¹.

Of the calcium phosphate cements, Norian SRS[®] have been tested most extensively. In the upper extremity, union of fractures of the humerus¹⁶⁴ and distal radius^{128, 165-172} has been achieved. Norian SRS[®] is effective in maintaining realignment of fracture parts after reduction of displaced or comminuted distal radius fractures. This technique resulted in accelerated rehabilitation, and better final outcomes after two years^{166, 168, 169}. In the lower extremities, Norian SRS[®] can be used to fill metaphyseal bone defects in tibia plateau fractures¹⁷³⁻¹⁷⁸. Good to excellent results one year after trauma were shown in 95% of cases¹⁷⁸. Nonetheless, loss of reduction occurred in 8-20% of cases and long term results showed a 20% post-traumatic osteoarthritis rate^{177, 178}. Adding Norian SRS[®] to sliding screw fixation for unstable trochanteric fractures resulted in modest improvement of fracture healing¹⁷⁹. Average movement of sliding screw was significantly reduced by augmentation with Norian SRS[®] after six weeks¹⁸⁰. In calcaneal fractures this bone substitute material allows full weight-bearing four weeks after surgery compared with eight weeks with autologous augmentation¹⁸¹.

Table 4. Overview of biomechanical properties

Product name	Compression Strength (MPa)	Young's modulus (MPa)	Tensile strength (MPa)	Shear strength (MPa)
Calcium phosphate				
Hydroxyapatite				
Cerabone®	(4.2-5.6)	N.D.	N.D.	(1.2-3.4)
Endobon®	1-20 ^{56, 58, 73, 98}	20-3100 ^{56, 58, 98}	N.D.	N.D.
Ostim®	N.D.	N.D.	N.D.	N.D.
Pro Osteon 500®	N.D.	N.D.	N.D.	N.D.
Tricalcium phosphate				
ChronOS™	N.D.	N.D.	N.D.	N.D.
Vitoss®	N.D.	N.D.	N.D.	N.D.
Composite				
BoneSave®	N.D.	N.D.	N.D.	N.D.
BoneSource®	6.3-34 ^{146, 147}	3.6-4.7 ^{117, 148}	(2)	N.D.
Calcibon®	35-55 ^{66, 149}	2500-3000 ⁶⁶	4.5 ⁹⁰	N.D.
Camceram®	N.D.	N.D.	N.D.	N.D.
ChronOS™ Inject	N.D.	N.D.	N.D.	N.D.
HydroSet™	14-24 ¹⁵¹	125-240 ¹⁵¹	0.11-0.17 ¹⁵²	N.D.
Norian SRS®	23-55 ^{68, 142, 143}	N.D.	2.1 ^{142, 143}	0.85-1.3 ¹⁴⁴
Calcium sulphate				
Bone Plast®	N.D.	N.D.	N.D.	N.D.
MIIG® X3	0.6 ¹³⁵	N.D.	N.D.	N.D.
OsteoSet®	0.6-0.9 ^{133, 135}	59 ¹³³	N.D.	N.D.
Stimulan®	N.D.	N.D.	N.D.	N.D.
Bioactive glass				
Cortoss®	91-179 ^{153, 154}	(6400)	(52)	8.4 ¹⁵⁴

Data obtained from the suppliers are given between brackets. N.D.: no data available

Another study shows postoperative full weight-bearing as early as three weeks shows in standard open reduction with internal fixation in calcaneal fractures⁹⁴.

BoneSource® can be used safely when filling of traumatic bone voids is required. Graft sites included the humerus (1), radius (3), femur (1), tibia (9), and calcaneus (7) and reduction was maintained in 83%¹¹⁹. However, BoneSource® alone does not provide adequate fracture stability in distal radius fractures¹⁸². Calcibon® is used for filling of metaphyseal cancellous bone defects and is was used to stabilize traumatic Magerl type A thoracolumbar fractures¹⁸³. Calcibon® augmentation in vertebral bodies improves pain and function and enables the treated vertebral body to regain height^{184, 185}.

Reports on clinical experience with the use of BoneSave[®], Camceram[®], ChronOS[™] Inject and HydroSet[™] without adjunctive in trauma and orthopaedic surgery has not been found.

2. Calcium sulphates

Calcium sulphates (CaSO₄) or Plaster of Paris have been used as bone void filler since the late 1800s²⁰⁰. Calcium sulphate is produced by heating gypsum, resulting in a dry powder. Adding water to this powder results in an exothermic reaction leading to crystallization and hardening of the preparation. Four calcium sulphate products are available in the Netherlands: Bone Plast[®], MIIG[®] X3, OsteoSet[®], and Stimulan[®]. MIIG[®] X3 and OsteoSet[®] are chemically identical; however, MIIG[®] X3 is available in paste, whereas OsteoSet[®] is available in granules or blocks.

2.1. Structural properties

No data on structural properties of calcium sulphate bone substitute materials has been found.

2.2. Biological properties

Calcium sulphates appear to function as a resorbable osteoconductive scaffold that provides the structural framework necessary for angiogenesis and osteogenesis while preventing soft tissue invasion by acting as a void filler; however, they lack not only osteogenic but also osteoinductive properties. Calcium sulphate is considered biocompatible, eliciting little or no macrophagic reaction, and is fully dissolved within 6-12 weeks²⁰¹. MIIG[®] X3 was found to be osteoconductive¹²⁹⁻¹³¹. The use of OsteoSet[®] resulted in a 8-35% new bone ingrowth in animal experiments^{132-135, 201} which was found to be equivalent to autogenous and allogenic bone grafts²⁰¹. However, in two studies no osteoconductive potential of OsteoSet[®] was noted^{136, 137}. No data on osteoconductive properties of Bone Plast[®] and Stimulan[®] were found.

2.3. Biomechanical properties

Compression strength of OsteoSet[®] and MIIG[®] X3 were attained in similar experiments, using *in vivo* samples which were implanted in for 26 weeks in the humerus of dogs. Compression strength of OsteoSet[®] was 0.6-0.9MPa^{133, 135} and of MIIG[®] X3 0.6MPa¹³⁵. Young's modulus of OsteoSet[®] was 59MPa¹³³. No data on biomechanical properties of Bone Plast[®] and Stimulan[®] was found.

2.4. Clinical indications

Calcium sulphate bone substitutes are mainly used to fill bony voids resulting of tumour resection surgery. Kelly *et al* used MIIG[®] X3 to graft bone defects of the distal tibia, patella, calcaneus, ileum, femur, and humerus¹²⁹. But MIIG[®] X3 may also be used to treat both proximal^{130, 135} and distal tibia fractures¹³⁵. Twenty-one tibia plateau fractures were treated

Table 5. Overview of applications in trauma and orthopaedic surgery

Product name	Fractures							Other
	Femur	Tibia plateau	Tibia distal	Calcaneus	Humerus	Radius distal	Vertebra	
Calcium phosphate								
Hydroxyapatite								
Cerabone®	N.D.	V 80	N.D.	N.D.	N.D.	N.D.	N.D.	X
Endobon®	N.D.	V 77, 100, 156, 157	V 100	V 100	N.D.	V 99, 100, 158	N.D.	V 186
Ostim®	N.D.	V 80, 103	X	V 103	N.D.	V 103, 159, 160	N.D.	V 161
Pro Osteon 500®	N.D.	N.D.	N.D.	N.D.	N.D.	V 162	N.D.	V 161
Tricalcium phosphate								
ChronOS™	X	X	N.D.	X	X	X	V 161	X
Vitoss®	N.D.	V 163	V 163	V 163	V 163	N.D.	N.D.	N.D.
Composite								
BoneSave™	N.D.	N.D.	N.D.	N.D.	N.D.	N.D.	N.D.	N.D.
BoneSource®	IV 119	IV 119	N.D.	IV 119	IV 119	IV 119, 182	N.D.	V 187
Calcibon®	N.D.	X	N.D.	X	N.D.	X	91, 123, 183-185	V 188
Camceram®	N.D.	N.D.	N.D.	N.D.	N.D.	N.D.	N.D.	N.D.
ChronOS™ Inject	X	X	N.D.	X	X	X	N.D.	V 189
HydroSet™	N.D.	N.D.	N.D.	N.D.	N.D.	N.D.	N.D.	N.D.
Norian SRS®	179, 180, 190	V 173-178	X	V 94, 181, 191	V 164	128, 165-172	N.D.	V 192
Calcium sulphate								
Bone Plast®	N.D.	N.D.	N.D.	N.D.	N.D.	N.D.	N.D.	V 193
MIIG X3®	N.D.	V 130, 131	V 131	N.D.	N.D.	N.D.	N.D.	V 129
OsteoSet®	N.D.	X	N.D.	X	N.D.	X	N.D.	V 138, 194-197
Stimulan®	N.D.	N.D.	N.D.	N.D.	N.D.	N.D.	N.D.	X
Bioactive glass								
Cortoss®	N.D.	N.D.	N.D.	N.D.	N.D.	V 140	V 198, 199	N.D.

I to VI: The highest clinical level of evidence according to Mahid *et al*⁵²; supporting use for specific indication. x: indicated by manufacturer only. N.D.: no data available.

with MIIG[®] X3 and internal fixation, resulting in complete fracture healing and graft resorption after twelve weeks¹³⁰.

OsteoSet[®] fills defects of the humerus, radius, ulna, femur, tibia, fibula and calcaneus^{138, 194, 196, 197, 202}. However, OsteoSet[®] may not provide sufficient biomechanical support as several stress fractures after grafting have been reported^{195, 196} and a self-limiting local sterile inflammatory reaction occurred in 4-20% of graft sites^{196, 203, 204}. In one case convulsions as complication with elevated calcium was reported after use of OsteoSet[®] in a lumbar fracture²⁰⁵. Also Bone Plast[®] may be indicated as it has been used in pelvic, humerus, calcaneus and femoral bone after aspiration of recurrent aneurysmal bone cysts¹⁹³. No data on Stimulan[®] was found.

3. Bioactive glass

Bioactive glasses are hard, solid (non-porous), materials consisting of four components: sodium oxide, calcium oxide, silicon dioxide (silicate, the main component) and phosphorous⁴⁵. By varying the proportions of sodium oxide, calcium oxide and silicon dioxide, soluble and non-resorbable bone substitute materials can be made²⁰⁶. Cortoss[®] is the only bioactive glass that is available in the Netherlands.

3.1. Structural properties

Bioactive glasses can be manufactured into microspheres, fibers and porous implants. Cortoss[®] is available as a paste, but no data concerning other structural properties of Cortoss[®], such as porosity and pore size, was found.

3.2. Biological properties

Bone substitute grafts within the group of bioactive glass display osteoconductive and also some osteoinductive properties⁴⁵. They are bioactive, as they interact with the body³¹. Bioactivity depends upon the SiO₂ content; the bonding between bone and glass is best if the bioactive glass contains 45-52% SiO₂³¹. The strong graft-bone bonding occurs as a result of the formation of a silicate rich layer after contact with body fluids. On top of this, a layer of hydroxyapatite will form, which directs new bone formation together with protein absorption. The extracellular proteins attract macrophages, mesenchymal stromal cells, and osteoprogenitor cells. Subsequently, the osteoprogenitor cells proliferate into matrix-producing osteoblasts^{30, 31}. Cortoss[®] has osteoconductive properties¹³⁹, but is not resorbed¹⁴⁰. It does not induce cytotoxicity²⁰⁷, and offers biocompatibility and reduced risk of thermal necrosis²⁰⁸.

3.3. Biomechanical properties

Bioactive glass possesses superior mechanical strength compared with calcium phosphates, as a result of a strong graft-bone bonding⁴⁵. Cortoss[®] has a compression strength

of 91-179MPa with a shear strength of 8.4MPa, which is significantly higher than PMMA used as bone cement^{153, 154}. Manufactures information also provides a Young's modulus of 6,400MPa and a tensile strength of 52MPa; however this was not confirmed in other studies.

3.4. Clinical indications

The first reports on clinical applications of bioactive glass emerge in the 1980s²⁰⁹. Since then, bioactive glass has been applied for craniofacial reconstructive surgery, dental surgery and trauma or orthopaedic surgery. Reports on clinical applications of Cortoss[®] are few; no randomized controlled trials have been conducted. Andreassen *et al* evaluated the use of Cortoss[®] for screw augmentation in 37 Weber type B ankle fractures. After two years, no screw loosening occurred¹⁹⁸. The use of Cortoss[®] may relieve pain when used in vertebroplasty^{199, 210}. One case report was published in which successful treatment of an unstable distal radius fracture was described¹⁴⁰.

Discussion

The repair of large bone defects resulting of trauma or disease remains a major problem in trauma and orthopaedic surgery. Treatment options depend upon size and location of the defect, but patient characteristics like bone quality, age, and co-morbidities also affect outcome. The past decade, an increasing number of bone substitute materials became available for use in trauma and orthopaedic surgery. This systemic literature review was conducted in order to provide a comprehensive overview of characteristics and clinical indications of products available in the Netherlands. Eighteen products, varying in composition and structure, have been reviewed. These products are widely available worldwide, therefore the information provided is relevant for many other countries as well.

Structural, biological and biomechanical properties of bone substitute materials are critical in their clinical success. Calcium phosphates may possess osteoinductive properties under certain conditions^{69, 70}. Of the 18 selected products, osteoinductivity was only found with the use of BoneSource[®]. Overall, osteoconductive properties could be confirmed for almost all included calcium phosphates, calcium sulphates and for bioactive glass. Unfortunately, major differences in experimental design (e.g. animal models) and absence of a standardized scoring system to define quality and quantity of new bone formation troubles the direct comparison among included bone substitute materials.

In order to acquire osteoconductive properties, pore size and porosity, and the degradation potential of the bone substitute material are essential. A macroporous structure of pores ranging 150-500µm in size is considered optimal for ingrowth of new bone^{211, 212}. In addition, interconnective pores increases new bone ingrowth^{211, 213, 214}. Microporosity (e.g. pores <5µm) is considered important for bioresorbable properties of the material²¹⁵.

Resorption rates differ substantially between the products, mainly due to their chemical composition. On average, sintered HA is rather inert, and hardly shows any resorption even after ten years. Tricalcium phosphate and calcium phosphate cement composites, on the other hand, are degraded within approximately two years as a result of osteoclastic activity⁵⁵. Calcium sulphates are generally dissolved within 8-12 weeks²¹⁶. Resorption of bioactive glass is variable, and depends upon the relative amounts of sodium oxide, calcium oxide, silicon dioxide, and phosphorous present⁴⁵.

Based upon their structure, hydroxyapatite and tricalcium phosphate ceramics have the advantage of offering a sufficient macroporous structure to facilitate new bone ingrowth. Optimized pore size was confirmed for the products Endobon[®] and ChronOS[™] (Table 3). On the other hand, rather quick resorption of calcium sulphate products provides space for new bone formation and prevents the early formation of fibrotic tissue; however, resorption may be completed before sufficient new bone formation. The same accounts for the biodegradable calcium phosphate cements, however their resorption time is slower compared with calcium sulphate products and depends mainly on their chemical composition.

Besides optimal biological properties, bone substitutes should offer direct structural support to surrounding bone and soft tissues. The biomechanical strength is the resultant of a complex interplay between the bone and bone substitute material. In an ideal situation a bone void is grafted by a bone substitute material that offers biomechanical strength similar as the bone being replaced. However, the biomechanical behavior of bone substitute materials may undergo changes as a resultant of *in vivo* interactions, e.g. osteointegration, bone incorporation, and bioresorption of the substitute materials. The biomechanical properties of bone itself, on the other hand, differ according to their structure (cortical or cancellous) and function (weight-bearing or non weight-bearing). Grafting a defect with a bone substitute material that has a higher initial biomechanical strength than the surrounding bone may result in stress-shielding and subsequent bone resorption at the bone-implant interface, or may lead to delayed fractures along the bone-implant interface. Using a bone substitute material with a lower biomechanical strength than the surrounding bone may lead to delayed fractures due to the lack of biomechanical stability. As mentioned above, the different products have different resorption rates. Provided that the biodegradation process works as designed, each product may ultimately resorb and remodel back into normal bone. If that holds true, the long-term strength of the restored bone may be similar for different products.

Human cortical bone has a compression strength of 130-290MPa and a tensile strength of 90-190MPa, whereas the compression strength of cancellous bone ranges between 2 and 38MPa²¹⁷. None of the included bone substitute materials offers biomechanical strengths similar to cortical bone, although bioactive glass (Cortoss[®]) has a compression strength of 91-197MPa, tensile strength does not reach values comparable to cortical bone^{154, 198}. Calcium phosphates possess compression strengths comparable to cancellous bone, but the main drawback of calcium phosphates remains their limited resistance to tensile and shear

forces, making it vulnerable to crackling and subsequent material failure. Calcium sulphates alone provide minimal structural support and are not suitable in cases where structural support is required (Table 4).

All included bone graft substitutes are available for use in trauma and orthopaedic surgery in the Netherlands and an overview of clinical indications is given in Table 5. No bone graft substitute seems to be suitable for grafting weight-bearing bone defects without additive support. Calcium phosphates may be used to fill metaphyseal bone defects at various locations of the lower extremity. The use of Norian SRS[®] in femur fractures is supported by level II evidence (Table 5). Norian SRS[®], BoneSource[®], Endobon[®] and Ostim[®] have also been used to fill bony defects of the calcaneus, proximal tibia, distal tibia, or proximal femur, but the clinical evidence remains limited to level IV and consists mainly of level V evidence. In the lower extremity, calcium sulphate is rarely used. Most likely because it offers minimal biomechanical strength. Although bioactive glass offers acceptable biomechanical strength, no evidence was found for their use in the lower extremity. Again, in the upper extremity, calcium phosphates are most frequently used. The use of Norian SRS[®] in distal radius fractures is supported by level II evidence. In addition, hydroxyapatite ceramics may also be used in open surgical technique to treat distal radius fractures. Furthermore, bioactive glass Cortoss[®] (Level V) and calcium phosphate Calcibon[®] (Level II) can be used in vertebral fractures as alternative for PMMA. Calcium sulphates are generally used to fill bone defects after tumour resection surgery, however their minimal biomechanical support may result in secondary fractures.

The data of the current systematic literature review show that vital data concerning structural, biological, biomechanical behaviour or the use of bone graft substitute for specific clinical indications is limited or incomplete. Additional high-quality scientific evidence is necessary in order to adequately state the clinical benefit of those products as a bone graft substitute. Evidence regarding their clinical use in trauma and orthopaedic surgery comes mainly from uncontrolled case series (clinical evidence level V). The absence of a control group in this type of research makes it difficult to draw sound conclusions regarding the beneficial effects except the avoidance of autograft or allograft-related complications. Three products have been tested in randomized controlled trials (RCTs); Calcibon[®], BoneSource[®] and Norian SRS[®]. Although not available for use in the Netherlands, and hence not included in this review, a properly designed RCT, and within the literature more well conducted RCTs has also been published on the use of α -BSM²¹⁸. This shows that RCTs on efficacy of bone graft substitutes in trauma and orthopaedic surgery are feasible.

A potential weakness of this study could be the used search strategy which forms the basis of our conclusions. Included products were searched in multiple databases by using product name as search term. By this method we might have missed studies which did not specify the product being used. However, the aim of this systematic review was to provide an overview of available pre-clinical and clinical evidence for the use of bone substitute

materials in clinical practice that may guide surgeons for selecting the best product for a particular clinical indication. Therefore manuscripts not specifying the product being used could not be included. The data shown in this manuscript also show that materials consisting of similar chemical compositions do not necessarily possess the same structural, biological and biomechanical properties. Differences in production methods (sintered materials versus cements), or in micro- and macrostructure also influences the biological and biomechanical behavior of the material *in situ*.

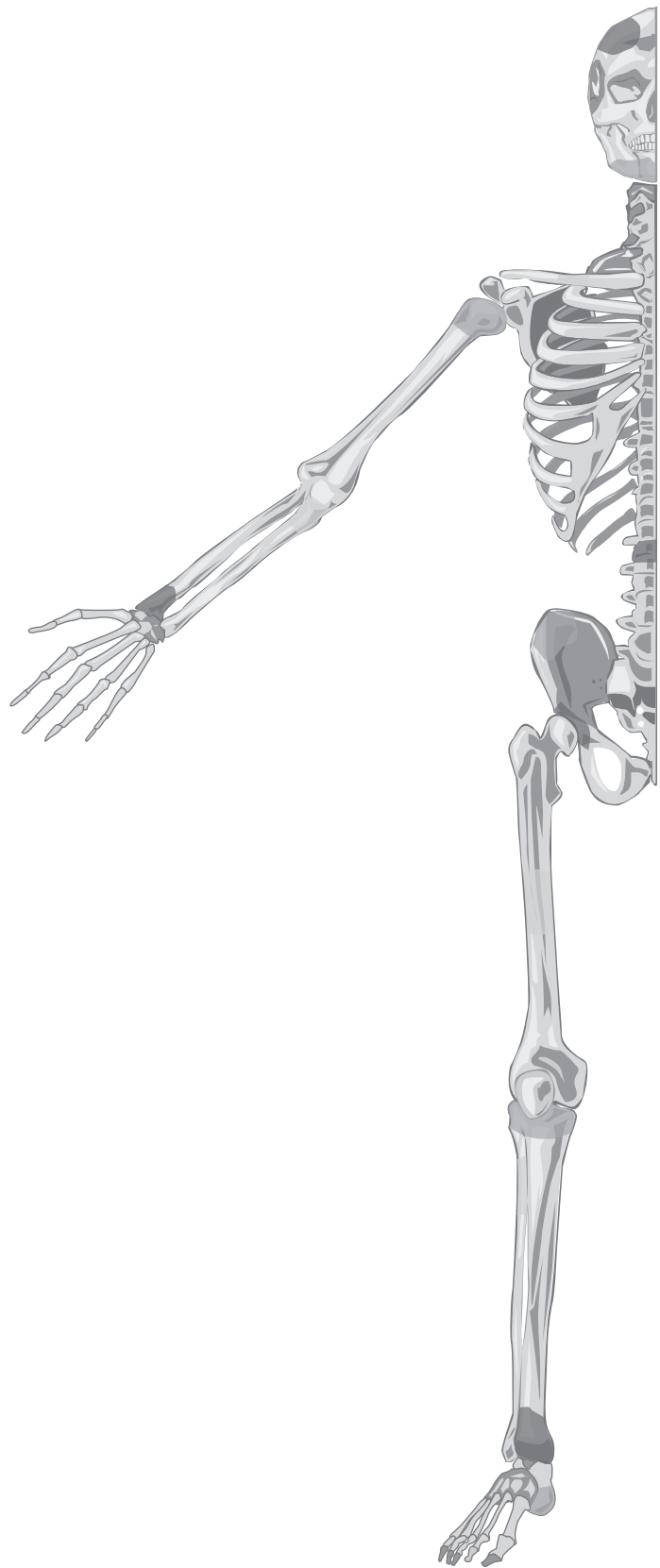
This review focuses on the first and vital step to facilitate new bone formation: the creation of an osteoconductive scaffold, as this will be the first clinical step in the treatment of bone defect. In a majority of cases, an osteoconductive scaffold will provide adequate support and will sufficiently facilitate new bone formation by the invasion of nearby bone forming cells. Only in cases where the surrounding bone has insufficient osteoinductive potential, adjunctive growth stimuli such as bone morphogenetic proteins (BMPs) or bone marrow aspirate may be needed in combination with a void filler. The use of growth factors has been reviewed elsewhere^{219, 220}.

Conclusion

The 18 bone graft substitutes available in the Netherlands represent a variety of forms, structure and chemical composition. Some of them have been investigated thoroughly, for other there is limited data available. Determining which bone graft substitute to use for different clinical indications is based on many factors including the size and location of the bone defect as well as structural, biological and biomechanical properties of the material itself. Calcium phosphates have been used for most trauma and orthopaedic surgery procedures when a grafting is necessary to restore bone defects. Calcium sulphates were mainly used to restore bone defects after tumour resection surgery and do not even offer sufficient biomechanical support to be used. Bioactive glass remains an interesting alternative; however its use in trauma and orthopaedic surgery is only reported in a limited number of studies. To further improve decision making of bone graft substitutes to treat bone defects, more standardized research to explore the full potential of calcium phosphate, calcium sulphate and bioactive glass is recommended.

Acknowledgements

Fonds NutsOhra and Biomet Netherlands B.V. are acknowledged for financial support.



Chapter 3

Calcium phosphate cements

Johan van der Stok

Harrie Weinans

Nicole Kops

Michiel Siebelt

Peter Patka

Esther M.M. van Lieshout

Published as "Properties of commonly used calcium phosphate cements in trauma and orthopaedic surgery"
in Injury; 2013 Oct;44(10):1368-74

Abstract

Since the introduction of calcium phosphate cements (CPCs) in 1985, a number of CPCs became predominantly commercially available for use in trauma and orthopaedic surgery. The aim of this technical note was to provide the relevant knowledge about CPCs that may improve the selection of CPCs for bone defects encountered in trauma and orthopaedic surgery. This includes a classification based on the chemical composition, and details about structural, mechanical and biological properties. Furthermore, the biological performance of each CPC was assessed in an animal study. And finally, a systematic literature search was conducted to provide a comprehensive overview of currently available clinical literature of these CPCs in trauma and orthopaedic surgery.

Introduction

Half of the population sustains at least one fracture during their lifetime²²¹, and the majority of these fractures heal successfully. Successful fracture healing requires the following five elements; (1) osteogenic cells (e.g. osteoblasts), (2) osteoinductive stimuli (e.g. bone morphogenetic proteins); (3) an osteoconductive matrix; (4) adequate blood and nutrient supply, and (5) sufficient mechanical support²²². One or more elements can be compromised due to the existence of a bone defect. Bone defects are treated with bone grafts in order to avoid insufficient fracture healing. Insufficient fracture healing is encountered in 5 to 10% of the fractures, resulting in delayed unions, malunions, or non-unions⁸.

Most commonly used bone graft material is autologous bone. Autologous bone is usually harvested from the iliac crest⁴⁴. However, harvesting autologous bone lengthens the surgical procedure and is associated with complications in 8-39% of patients (e.g. infection, nerve and urethral injury, and postoperative or chronic pain)¹⁷. An alternative option is to use allogeneic bone. However, allogeneic bone grafting is considered suboptimal since it has biocompatibility disadvantages⁵¹. The disadvantages of autologous and allogeneic bone grafts have resulted in the development of alternative (synthetic) bone substitute materials. The most interesting group of bone substitute materials is probably calcium phosphate (CaP), because CaPs mimic the mineral part of natural bone⁵⁵.

CaP-based bone substitutes have been studied for several decades²²³ and they can be categorized into CaP ceramics and CaP cements (CPC)⁵⁵. CaP ceramics are obtained by thermal treatment (sintering), generally resulting in solid grafting materials (e.g. blocks or granules). CPCs, on the other hand, consist of CaP powder that forms a paste upon mixing with a liquid. Mixing is usually done during surgery and the resulting paste becomes solid within several minutes through an isothermic chemical setting reaction. During this setting reaction, the CPCs can be moulded by the surgeon into any desired shape in order to completely fill the defect.

Since the introduction of CPC in 1985 by Brown and Chow, a number of CPCs have become commercially available for trauma and orthopaedic surgery²⁵. Trauma or orthopaedic surgeons are therefore given the opportunity to select a CPC that meets the specific demands of each bone defect that requires bone grafting. The aim of this technical note was to provide a comprehensive overview of knowledge of commonly used CPCs that may improve this selection for bone defects encountered during fracture treatment. The chemical composition and structural, mechanical and biological properties of the four predominantly used CPC products (Table 1) are discussed. In addition, the biological properties were evaluated in a large animal bone defect model. Finally, a systematic literature search was conducted in order to provide insight into the available clinical evidence supporting to use of these CPC products to graft bone defects encountered during fracture treatment.

Table 1. Product specifications

Product	Manufacturer	Available volumes
BoneSource [®]	Stryker	1.5cc, 3cc, 6cc, 15cc, 30cc
Calcibon [®]	Biomet	4cc, 8cc, 16cc
ChronOS [™] Inject	DePuy Synthes	2.5cc, 5cc, 10cc
Norian SRS [®]	DePuy Synthes	3cc, 5cc, 10cc

Calcium phosphate cements

CPCs can be classified based upon the setting product of the CPC into apatite-forming and brushite-forming CPCs. This classification refers to the degree of crystallinity of the CaP formed and has a direct impact on their resorption rate. The resorption of an apatite-forming CPCs is very limited and takes many years, whereas the resorption of brushite-forming CPCs takes place within several months⁵⁵. Commercially available apatite-forming CPCs are BoneSource[®], Calcibon[®], and Norian SRS[®], a brushite-forming CPC is ChronOS[™] Inject (Table 2). CPC products are available in several quantities, ranging from 1.5cc to 30cc (Table 1), and depending on the CPC product the setting reaction will take five (Calcibon[®]) or 15 minutes (Norian SRS[®]) to be completed once the components are mixed (Table 2).

It is necessary to distinguish CPCs from ceramic CaPs. The ceramic CaPs are acquired from heating (sintering) of calcium phosphate powder up to 800-1300°C. This heating results in formation of solid porous blocks or granules that can consist of hydroxyapatite (HA), tricalcium phosphate (TCP) or a combination HA and TCP (composites). Examples of commercially available CaP ceramics are BoneSave[®], Camceram[®], Cerabone[®], ChronOS[™], Endobon[®], Ostim[®], Pro Osteon 500[®], and Vitoss[®]²³.

Table 2. Chemical composition and mixing properties

Product	Chemical composition	Mixing time	Final setting time	Final setting product ⁵⁵
BoneSource [®]	80% TCP / 20% HA	2-4m	5-10m	apatite
Calcibon [®]	62.5% α -TCP / 26.8% DCPA / 8.9% CaCO ₃ / 1.8% HA	1m	5m	apatite
ChronOS [™] Inject	73% β -TCP / 21% MCPH ₂ O / 5% MHPT	1m	11m	brushite
Norian SRS [®]	α -TCP / CaCO ₃ / MCPH ₂ O	1m	15m	apatite

CaCO₃, calcium carbonate; DCPA, dicalcium phosphate anhydrous; HA, hydroxyapatite; MCPH₂O, monocalcium phosphate monohydrate; MHPT, magnesium hydrogen phosphate trihydrate; TCP, tricalcium phosphate.

1. Structural properties

CPCs are generally described as being osteoconductive²²⁴. Osteoconduction is defined as the ability of a graft material to function as a scaffold that allows ingrowth of bone and vascular tissues²¹¹. A scaffold that offers an open porous structure with pore dimensions of 150-500 μm is considered optimal for bone ingrowth²¹¹. CPCs generally form dense structures with limited porosity (Table 3). *In vitro* μCT measurements indicate that the porosity of ChronOSTM Inject is only $5\pm 1\%$, and that the porosity of apatite-CPCs does not exceed 5% (BoneSource[®] $0.4\pm 0.3\%$, Calcibon[®] $0.9\pm 0.5\%$, Norian SRS[®] $0.3\pm 0.2\%$)²²⁵. Furthermore the majority of these pores is smaller than $150\mu\text{m}$. Average pore size of ChronOSTM Inject is $100\mu\text{m}$, and 18% of these pores exceed the size of $150\mu\text{m}$. Average pore sizes of other apatite-CPCs is $\sim 50\mu\text{m}$ and the fraction that exceeds the size of $150\mu\text{m}$ is less than 4%.

2. Mechanical properties

Mechanical properties of a bone substitute material should ideally be comparable to the bone being replaced, however mechanical properties of bone differ according to their structure (cortical or trabecular bone) and function (weight-bearing or non weight-bearing). Compression strength of human cortical bone is in the range of 130 to 190MPa, whereas trabecular bone has a compression strength of 8 to 38MPa. Apatite-CPCs were found to have a compression strength in the range of trabecular bone (Table 3); Calcibon[®] has the highest compression strength ($34\pm 7\text{MPa}$), followed by Norian SRS[®] ($26\pm 7\text{MPa}$) and BoneSource[®] ($14\pm 3\text{MPa}$). The brushite-CPC ChronOSTM Inject has a compression strength that is much lower, it does not exceed values of 1MPa²²⁵.

3. Biological properties

Biological properties of four CPCs were studied in a drill-hole tibia bone defect model in goats¹²⁴. This model allows for a direct comparison of different CPCs. Three months after grafting the drill-hole defects with different CPCs, resorption and bone formation were determined using μCT scanning, histology, and fluorochrome labeling. The study was approved by the institution's Animal Ethics Committee (EUR1540).

Table 3. Structural and mechanical properties

Product	Porosity (%) ²²⁵	Compression strength (MPa) ²²⁵
BoneSource [®]	0.4	14
Calcibon [®]	0.9	34
ChronOS TM Inject	4.5	1
Norian SRS [®]	0.3	26

3.1. Animal experiment

In five skeletally mature female milk goats, each weighing 50-60kg, a drill-hole bone defect model was used in which three holes were created at the diaphysis of the right tibia. Two of the holes were grafted with a CPC and one was left empty, serving as a control. All products were tested in duplicate and randomized over the proximal, distal and middle holes. After three months, the goats were killed and the grafted bone defects were analysed using μ CT, histology, and fluorochrome labeling.

3.2. Surgical procedure

The operation was performed under general anaesthesia induced by an intravenous injection of 0.3ml medetomidine (1mg/ml) followed by 20ml propofol (10mg/ml) and maintained by isoflurane 1.5% through a constant volume ventilator, administered through an endotracheal tube. The goats received prophylactic antibiotics according to the following scheme: 12.5ml amoxicillin (48mg/ml) at the start of the operation and 7.5ml ampicillin (100mg/ml) during the operation; and two and four days after the operation.

Before surgery, the animal was immobilized on its right side and the right limb was shaved, washed, and disinfected with povidone-iodine. A longitudinal incision was made on the medial surface of the tibia, and the bone was exposed by blunt dissection. Three unicortical 2.0mm diameter holes were drilled at low rotational drill speeds and continuous cooling with cold physiologic saline, with an interspace of 2.5cm. The 2.0mm diameter holes were enlarged to 5.0mm diameter and irrigated and packed with sterile cotton gauze, and the calcium phosphate cements were then prepared. Subsequently, the cements were injected into the bone defects and allowed to solidify. Any extruding material was removed. The soft tissues and skin were closed in separate layers with Vicryl sutures. Post-operative analgesia consisted of 0.8ml buprenorphine (300 μ g/ml) and 1.0ml flunixin (50mg/ml) on day one to three after surgery.

3.3. Fluorochrome labeling

The fluorochrome labels were administered intravenously at 14 days (tetracycline hydrochloride, 30mg/kg (Sigma)) and four days (calcein, 10mg/kg intravenously (Sigma)) before they were killed using an overdose pentobarbital.

3.4. μ CT evaluation

The right tibias were taken out and trimmed to a suitable size for μ CT scanning. A 9 μ m resolution protocol (75kV energy, 133 μ A current, 1.0mm Al filter) was used with a SkyScan 1076 μ CT scanner (Bruker micro-CT N.V., Kontich, Belgium). The CT images were reconstructed using NRecon software version 1.5 (Bruker micro-CT N.V., Kontich, Belgium).

3.5. Histological evaluation

After μ CT scanning, each tibia was trimmed to a size suitable for histological processing. Subsequently, all specimens were fixed in paraformaldehyde (4%) overnight, dehydrated in a graded series of ethanol, and embedded in methylmethacrylate (MMA). After polymerisation, undecalcified thin ($6\mu\text{m}$) sections were made with a heavy duty microtome in a transverse direction through the middle of the defect area. Sections were stained using Goldner's trichrome and evaluated with a light microscope (Olympus BX50). Fluorochrome labels were evaluated in unstained sections using an epifluorescence microscope (Axiovert 200MOT/Carl Zeiss) equipped with a double filter block.

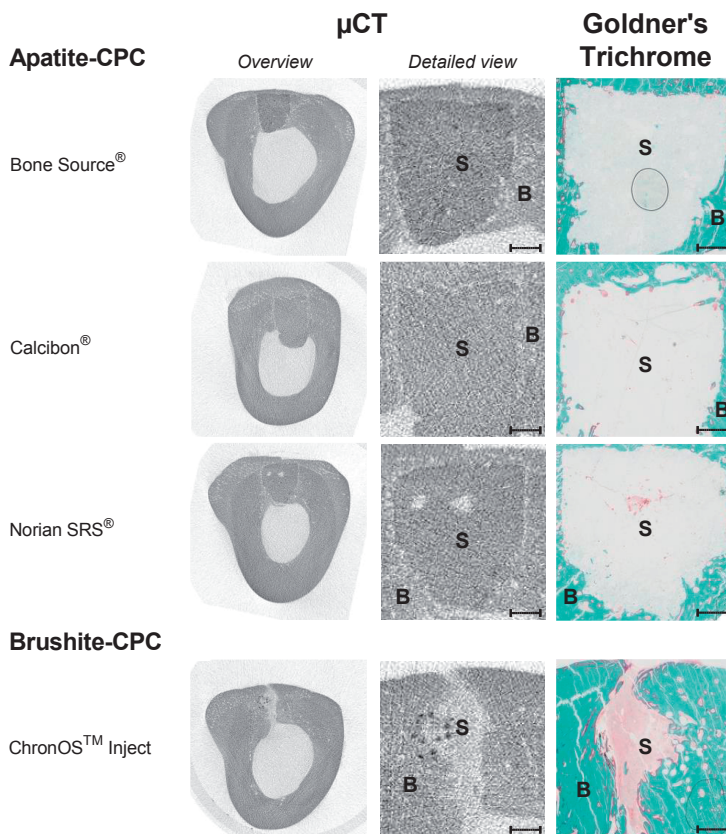


Figure 1: Filling capability of CPCs in a drill-hole defect.

μ CT and corresponding Goldner's trichrome histological images. **S**, bone substitute material; **B**, bone. Bar indicates 1mm.

3.6. Biological properties

The μ CT scans acquired at three months after grafting showed that drill-hole defects remained adequately filled by apatite-based CPCs (BoneSource[®], Calcibon[®], and Norian SRS[®]). This indicates limited resorption of apatite-CPCs whereas using ChronOS[™] Inject resulted in a partially remaining bone defect (Figure 1); the latter is most likely the result of fast resorption of this brushite-CPC. Detailed views of defects with CPCs showed that it is difficult to distinguish CPC from native bone as the radiographic density is very close (BoneSource[®], Norian SRS[®]) or even similar (Calcibon[®], ChronOS[™] Inject) to native bone. These similar radiographic densities obstruct a quantitative analysis from these μ CT images of newly formed bone and remaining CPC volumes.

Histology confirmed that resorption rate of apatite-CPCs is very limited and that, as a result, these CPCs remained largely intact (Figure 2). Calcibon[®] still covered almost the complete defect and hardly any bone ingrowth had appeared within three months. Furthermore little activity of bone formation at the CPC-interface, indicated by the fluorochrome labels, was found in defects grafted with Calcibon[®]. Although BoneSource[®] also covered the majority of the defect, some resorption did take place within the three months follow-up.

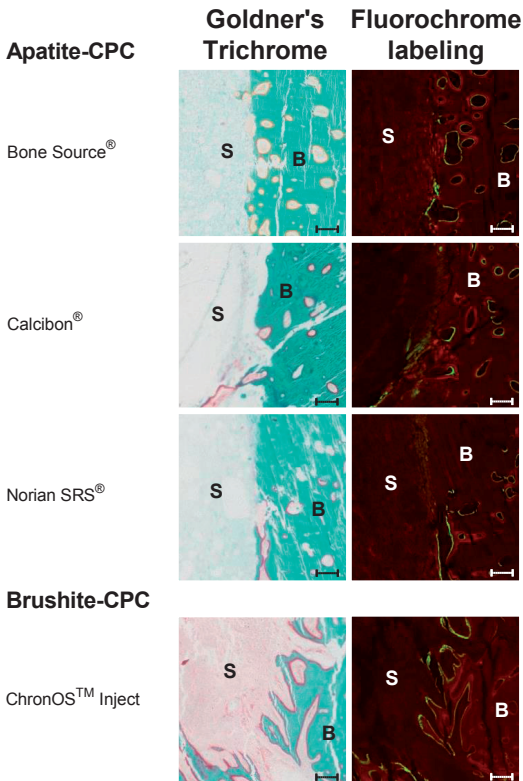


Figure 2: CPC integration and bone forming activity at the CPC-interface.

Goldner's trichrome histological images of the CPC-interface and corresponding fluorochrome images. **S**, substitute material; **B**, bone. Red label is tetracycline and green label is calcein green. Bar indicates 1mm.

The fact that BoneSource[®] resorbed slowly was also shown by Welch *et al*¹¹⁷. In their study, subchondral femoral bone defects in goats were grafted with BoneSource[®], and 38% of the CPC was still present after two years. A similar resorption pattern was also seen for Norian SRS[®]. Apelt *et al* indicated that approximately 5% of Norian SRS[®] was resorbed at six months after grafting a comparable subchondral bone defect in sheep⁹⁶. The minimal appearance of fluorochrome labels at CPC-interface of tibia defects grafted with BoneSource[®] and Norian SRS[®] also indicate little bone forming activity (Figure 2).

Histology of the only brushite-based CPC, ChronOS[™] Inject, indicated indeed that most of CPC was resorbed within three months. This was also shown by Apelt *et al*, who found that only 20% of ChronOS[™] Inject was still present six months after grafting subchondral bone defects in sheep⁹⁶. In the periphery of the defect, ChronOS[™] Inject had resorbed and was replaced by new bone. After three months, only some bits of CPC were found within the center of the defect (Figure 2). Contrary to the limited bone forming activity found for apatite-CPCs, this brushite-CPC seemed to elect a bone formation activity almost throughout the complete CPC-interface (Figure 2).

4. Clinical evidence in fracture treatment

A systematic literature search was conducted using the product names of all products (Table 1) as search terms in PubMed database. PubMed database was searched from the earliest date available until October 26, 2012. The following filters were used: species (human), languages (Dutch, English, or German), search fields (Text word). Retrieved manuscripts were only included when they contained original research on CPC use in trauma and orthopaedic-related indications. Manuscripts were excluded when they only contained data describing *in vitro* (e.g. cellular response or cadaver studies) or animal experiments, or when the CPC was used in other than trauma and orthopaedic-related indications (e.g. dental or craniofacial surgery). All references of included manuscripts were reviewed in order to ensure that no relevant papers had been missed.

The systematic literature search resulted in 78 eligible manuscripts. Thirty-three of these manuscripts were selected for final inclusion, including one additional reference (Table 4). The included manuscripts consisted of ten clinical trials, two case-control studies, 20 case-series and one case-report. The four CPC have been used to graft bone defects encountered in treatment of humerus, radius, femur, tibia, calcaneus, vertebra, and odontoid fractures (Table 5), as well as bone defect encountered during knee or hip revision surgery and treatment of endochondrale bone cysts.

BoneSource[®] was subjected to one multicenter prospective randomized trial¹¹⁹. Metaphyseal bone defects of 38 fractures, including femur, tibia, calcaneus, humerus, and distal radius fractures were grafted with either BoneSource[®] or autologous bone. Adequate reduction was maintained in 83% of the defects treated with BoneSource[®] versus 67% of the defect treated with autologous bone. Furthermore, reduction and injection of BoneSource[®]

was compared with reduction and fixation with K-wires as a treatment for displaced distal radius fractures¹⁸². In their study, all clinical and radiographic parameters were worse after 26 weeks in the BoneSource[®] groups, and they concluded that BoneSource[®] alone does not provide sufficient fixation after reduction of displaced radial fractures.

Calcibon[®] is mostly used for grafting defects resulting of (osteoporotic) vertebral fractures. One prospective trial¹⁸⁴, several prospective^{91, 123, 185} and retrospective¹⁸³ case-series all indicate that grafting with Calcibon[®] gives comparable results to using polymethylmethacrylate (PMMA).

Norian SRS[®] is described in more than 20 manuscripts and has been used as a bone graft for filling bone voids resulting of fractures of the proximal humerus, distal radius, proximal femur, proximal tibia, or calcaneus, as well as in odontoid fractures. Keating *et al* treated 49 lateral tibia plateau fractures with internal fixation and Norian SRS[®]. After one year, 95% had good or excellent Rasmussen knee scores but also 20% showed radiological evidence of post-traumatic osteoarthritis¹⁷⁸. In a randomized controlled trial including 323 patients, percutaneous injection of Norian SRS[®] after closed reduction of displaced distal radius fractures resulted in accelerated rehabilitation and improved clinical outcomes after two years compared with reduction only¹⁶⁹. Norian SRS[®] was used for grafting defects resulting from calcaneal fractures and it allowed full weight-bearing as early as three weeks after open reduction and internal fixation⁹⁴. Furthermore, the use of Norian SRS[®] has used in acetabular cup revision surgery (case-report²²⁶), knee replacement surgery (case-series²²⁷). One study that was designed to treat enchondromas with Norian SRS[®] was stopped because three of the four included patients had severe pain after curettage of enchondroma and subsequent grafting with Norian SRS[®]²²⁸.

ChronOS[™] Inject is indicated for use in femur, tibia, calcaneus, humerus, and radius fractures by the manufacturer, however there were no clinical studies found that describe the use of ChronOS[™] Inject in this indication (Table 5). ChronOS[™] Inject has been used to

Table 4. Number of publications retrieved during the systematic literature search

Products	Inclusion		Exclusion			Additional references	Final
	PubMed Search	<i>In vitro</i> experiments	Animal experiments	Different indication	Other		
Apatite-CPC							
BoneSource [®]	23	9	1	11	1	1	1
Calcibon [®]	5	1	0	0	0	0	4
Norian SRS [®]	48	9	0	6	6	0	27
Brushite-CPC							
ChronOS [™] Inject	2	1	0	0	0	0	1

treat benign bone cysts in children. After treating 24 pediatric patients, ChonOS™ Inject was found to be safe and therefore could provide an alternative treatment for benign bone cysts in children¹⁸⁹.

Table 5. Clinical evidence for CPC use in fracture surgery

Products	Fracture						
	Proximal Humerus	Distal Radius	Proximal Femur	Proximal Tibia	Calcaneal	Vertebral	Odontoid
Apatite-CPC							
BoneSource®	IV ¹¹⁹	IV ^{119, 182}	IV ¹¹⁹	IV ¹¹⁹	IV ¹¹⁹	N.D.	N.D.
Calcibon®	N.D.	x	N.D.	x	x	II ^{91, 183-185}	N.D.
Norian SRS®	V ^{164, 229}	II ^{128, 165-172, 230-232}	II ^{179, 180, 190, 233}	V ¹⁷⁴⁻¹⁷⁷	V ^{94, 181, 234}	N.D.	VI ²³⁵
Brushite-CPC							
ChronOSTM Inject	x	x	x	x	x	N.D.	N.D.

I–VI, the highest clinical level of evidence according to Mahid *et al*⁶² supporting the use for specific indication; x, indicated by manufacturer only; N.D., no data available.

Discussion

Commercially available CPCs have different mechanical, structural and biological properties. Mechanical, structural and biological properties are mainly explained by their chemical composition. Based on chemical composition, CPCs can be classified into apatite-forming and brushite-forming CPCs. This classification may prove helpful in selection of CPCs for bone defects at specific fracture sites. In general, apatite-forming CPCs offer more mechanical strength and have a low resorption rate. Brushite-forming CPCs, on the other hand, offer only limited mechanical strength and have a high resorption rate.

Bone graft substitutes should offer mechanical support to surrounding bone and soft tissues in order to facilitate fracture healing. Apatite-forming CPCs have compression strengths in the range of trabecular bone (Table 3), and may therefore be most suitable to graft defects of metaphyseal bone defect. Brushite-forming CPCs only offer minimal mechanical strength, and they should therefore only be used in situations in which sufficient mechanical stability can already be acquired using fixation hardware. Overall, CPCs do not possess sufficient mechanical strength to be used in cortical or weight-bearing bone defect.

μ CT data indicates that CPCs form a rather dense structure with only a limited amount of pores that may allow bone and vessel ingrowth. The working mechanism in which CPCs can support bone formation is therefore more likely based on gradual resorption of the CPC and subsequent bone formation. Resorption of CPCs is an active process mediated by osteoclasts⁵⁵. The resorption rate is an interplay of chemical composition, structure and volume of the CPC and the availability and activity of osteoclasts. Resorption of CPC should be followed by bone formation until complete regeneration of the bone defects has occurred. The regenerative potential of the surrounding bone should therefore be taken into account, and when rapid bone formation can be expected, fast resorbing brushite-forming CPCs, such as ChronOS™ Inject, may be preferred over apatite-forming CPCs.

CPCs are mostly studied as a bone graft substitute in metaphyseal bone defects (Table 5). Grafted metaphyseal bone defects include fractures of the femur, tibia, calcaneus, humerus, radius, and vertebra. The majority of the studies included in the systematic literature search consist of case-series. Case-series can provide relevant knowledge about the specific indication in which a CPC can be used or the relative safety, however they are not the preferred level of evidence to draw well-founded conclusions on the clinical benefits of using CPCs. Furthermore, the average number of clinical studies performed with each CPC product is surprisingly low, especially for BoneSource®, ChronOS™ Inject and Calcibon® (Table 4). More clinical studies, preferably randomized controlled trials, are therefore desired and can contribute to better understanding of the potential indications and benefits of different CPC products.

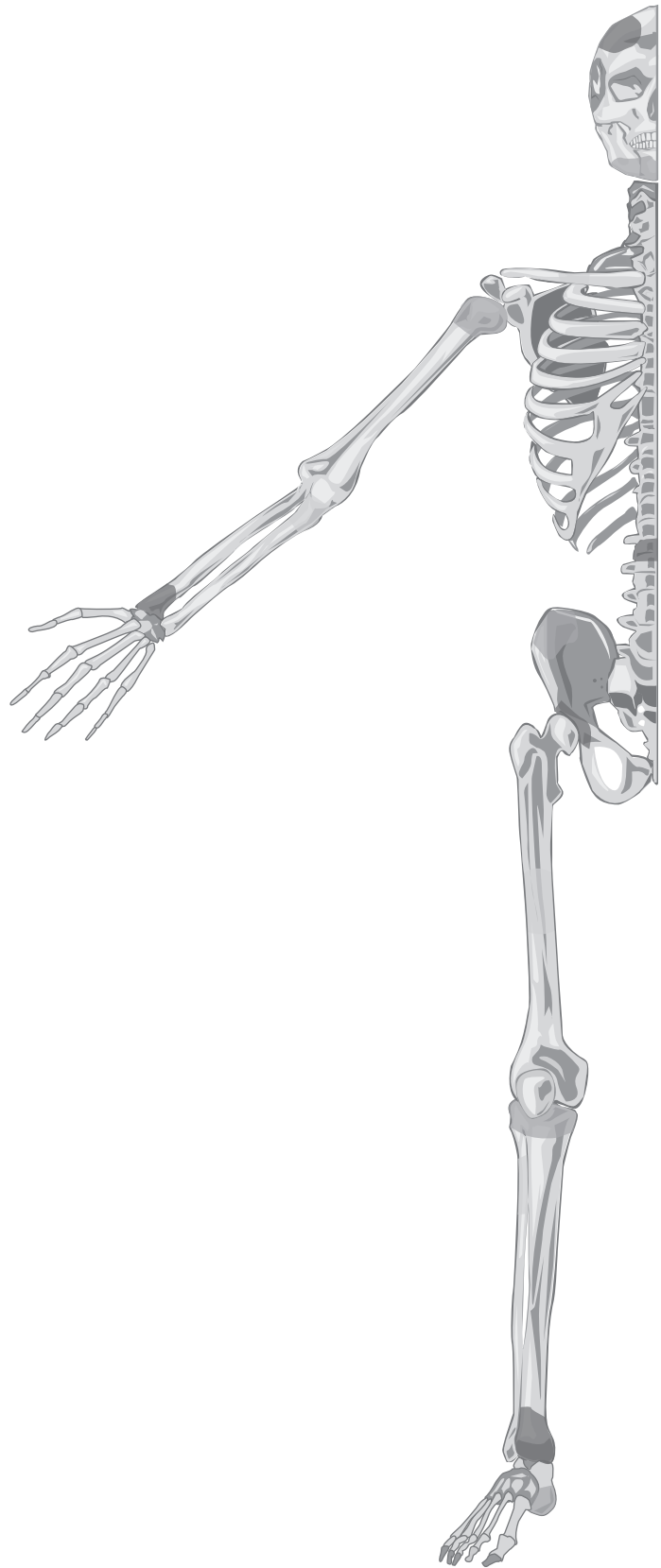
Limitations

There are limitations to this work. Firstly, the selection of CPC products was based upon their availability for use in trauma and orthopaedic surgery in the Netherlands. The included products are widely available and used worldwide, which supports a wide relevance of this paper. On the other side, several other CPC products such as Norian Drillable®, HydroSet®, alpha-BSM® and Callos® were not included. Furthermore, biological properties were studied in a tibia drill-hole defect model. This model has the advantage over other models that it allows for evaluation of multiple CPCs within one animal. This makes direct comparison of the studied CPCs more relevant. On the other hand, this bone defect model might be clinically less relevant, since CPC products are predominantly used to graft metaphyseal bone defects. Therefore, whether metaphyseal bone defects can successfully be grafted with the studied CPC cannot be directly translated from their performance in this model. The biological properties as described here provide important clues that can help to determine which product is most suitable for each type of bone defect encountered during clinical practice. Missing publications which did not explicitly specify the product name cannot be

considered a limitation, since this systematic search was conducted to provide insight into the available clinical evidence of the commercially available CPC products, helping trauma and orthopaedic surgeons to select the most suitable product. Mentioning the product name was therefore essential for this study.

Acknowledgements

We thank Alex Hanssen, Wilma Janssen-Kessels, Maikel Schol and Conrad Van den Broek (Central Animal Laboratory, University Medical Centre Nijmegen, Nijmegen, The Netherlands) for their excellent biotechnical support during the animal experiment. Part of this work was made possible with a grant of the Stichting Annafonds (Project No. 07/37).



Chapter 4

Porous calcium phosphate ceramics

Johan van der Stok

Anindita Chatterjea

Charlène Danoux

Huipin Yuan

Pamala Habibovic

Clemens van Blitterswijk

Harrie Weinans

Jan de Boer

Published as “Inflammatory response and bone healing capacity of two porous calcium phosphate ceramics in critical sized rat long bone defects” in Journal Biomedical Materials Research Part A. 2014

May;102(5):1399-407

Abstract

In the present study, two open porous calcium phosphate ceramics, β -tricalcium phosphate (β -TCP), and hydroxyapatite (HA) were compared in a critical-sized cortical defect in rats. Previous comparisons of these two ceramics showed significantly greater osteoinductive potential of β -TCP upon intramuscular implantation and a better performance in a spinal fusion model in dogs. Results of the current study also showed significantly more bone formation in defects grafted with β -TCP compared to HA; however, both the ceramics were not capable of increasing bone formation to such extent that it bridges the defect. Furthermore, a more pronounced degradation of β -TCP was observed as compared to HA. Progression of inflammation and initiation of new bone formation were assessed for both materials at multiple time points by histological and fluorochrome-based analyses. Until twelve days post-implantation, a strong inflammatory response in absence of new bone formation was observed in both ceramics, without obvious differences between the two materials. Four weeks post-implantation, signs of new bone formation were found in both β -TCP and HA. At six weeks, inflammation had subsided in both ceramics while bone deposition continued. In conclusion, the two ceramics differed in the amount of bone formed after eight weeks of implantation, whereas no differences were found in the duration of the inflammatory phase after implantation or initiation of new bone formation.

Introduction

Autologous bone is currently the gold standard for grafting bone defects. However, the limited availability and post-operative complications associated with the harvesting procedure site have necessitated the search for bone graft substitutes²³⁶. Bone substitute materials such as calcium phosphate (CaP) ceramics, have been used in a widespread of trauma and orthopaedic-related indications^{45, 53, 237}. The interest in CaP ceramics can be attributed to their chemical resemblance with bone mineral and their osteoconductivity⁵³. However, unless additionally endowed with an osteoinductive stimulus, the general performance of CaP ceramics remains inferior to autologous bone.

Osteoinductivity is the ability of a material to induce differentiation of progenitor cells into the osteogenic lineage to form active osteoblasts²³⁸. Differentiation into active osteoblasts is induced through secretion of osteoinductive factors such as bone morphogenetic proteins (BMPs). Addition of osteoinductive factors was therefore thought to be essential to enhance the performance of CaP ceramics. More recently, it was found that some open porous CaP ceramics could induce bone formation in the absence of any osteoinductive factors, making these CaP ceramics potentially suitable as off-the-shelf alternatives to autologous bone^{69, 239-241}.

The osteoinductive performance of open porous CaP ceramics, however, varies strongly and is influenced by chemical composition and structure (e.g. macroporosity, microporosity, surface concavities, surface area and roughness), as recently reviewed²⁴². Four different CaP ceramics were developed and tested *in vivo* by our group²⁴³. Open porous CaP ceramic particles (1-2mm) tested were: β -tricalcium phosphate (β -TCP) ceramic with a specific surface area of 1.2m²/g, phase-pure hydroxyapatite (HA) ceramic with specific surface area of 0.1m²/g and two biphasic ceramics both consisting of HA and β -TCP in a weight ratio 80:20, but sintered at different temperatures to vary microstructural properties and specific surface area (1m²/g versus 0.2m²/g). Twelve weeks after implantation in canine paraspinal muscles (1mL of ceramic particles) and spinal fusion regions (5mL of ceramic particles), the largest difference was found between β -TCP and HA. β -TCP gave five times more bone in both paraspinal muscles (0 versus 20% area of available pore space covered with bone) and spinal fusion regions (5 versus 25% area of available pore space covered with bone).

Implantation at ectopic sites (e.g. intramuscular or subcutaneous) is an established method to screen materials osteoinductive properties since seminal work by Urist in the 1960s²⁹. However, extrapolating this data to clinically relevant bone defects requires evaluation in clinically more relevant models. As bone is not naturally present at the site of bone formation in spinal fusion models, this model cannot be considered fully orthotopic and it remains to be further elucidated whether the osteoinductive performance of β -TCP is relevant in critical-sized orthotopic bone defects. Furthermore, the osteoinductive performance of β -TCP may be the effect of faster degradation and release of microparticles altering

the intrinsic inflammatory phase reaction prior to bone formation²⁴⁴⁻²⁴⁶. Others have shown that bone formation benefits from a mild contained inflammatory reaction, and strong inflammatory reactions can make the environment hostile, and hamper bone formation²⁴⁷.

The aim of the current study was to determine whether the osteoinductive performance of β -TCP is relevant to bone formation in a critical-sized cortical bone defect in rats, compared to the less osteoinductive HA. Furthermore, we aimed to determine the duration of the inflammatory response within this bone defect model after implantation of β -TCP and HA, to assess whether the duration of the inflammatory response could be related to bone formation.

Materials and methods

1. Synthesis and characterization of HA and β -TCP ceramics

In this study two CaP ceramics were investigated: HA and β -TCP. The HA ceramic was prepared from HA powder (Merck) using the dual phase mixing method²⁴⁷ consisting of three steps. First, HA slurry was prepared by mixing 2/3 wt% of calcined HA powder with 1/3 wt% water containing deflocculant (dolphix CE 64, Germany) and binder (carboxymethyl cellulose, Pomosin BC, The Netherlands). Then, two immiscible phases were mixed: water-based HA slurry and polymethylmethacrylate (PMMA) resin with a volume ratio of 1:1. The PMMA resin consisted of PMMA powder, methylmethacrylate (MMA) monomer and naphthalene (<10% v/v %) as an additional fugitive pore maker. Finally, the mixture was polymerized, dried and pyrolyzed and sintered at 1250°C for 8h. The β -TCP ceramic was fabricated by the H₂O₂ method as described previously²⁴⁸ using β -TCP powder purchased from Plasma Biotol (Derbyshire, United Kingdom). The powder was mixed with 2% H₂O₂ solution (1.0g powder/1.20±0.05ml solution) and naphthalene particles (710-1400µm; 100g powder/30g, Fluka Chemie, Zwijndrecht, the Netherlands) at 60°C. The naphthalene was then evaporated at 80°C and the porous bodies were dried, and sintered at 1100°C for 8h. For both CaP ceramics, a lathe was used to produce the cylinders. Subsequently, the cylinders were cut into implants 6mm in length and 3mm in diameter. Implants were cleaned ultrasonically with acetone, 70% ethanol and demineralized water, dried at 80°C, and sterilized by gamma irradiation prior to implantation.

The chemical composition and the crystallinity of the ceramics were analysed using X-ray diffraction (XRD, Miniflex, Rigaku, Japan). The macropore size and porosity of the CaP ceramics were determined by image analysis on thin sections using a KS400 image system (Carl Zeiss, Germany) attached to a light microscope (Nikon, Japan, Objective, X10). Thin sections were made on a Leica diamond saw after embedding CaP ceramics blocks in MMA. The microstructure was evaluated as described previously using a scanning electron

microscope (XL30, Environmental SEM-Field Emission Gun, Philips). Specific surface area of the two ceramics was analysed by mercury intrusion (Micromeritics Instrument).

2. Animal experiment

In total, 34 skeletally mature 18-week-old male Wistar rats were used upon approval by the institution's Animal Ethics Committee (EUR2317). Animals were housed according to national guidelines for the care and use of laboratory animals. A 6mm femoral bone defect was grafted with either HA ($n=14$), β -TCP ($n=14$) or left empty ($n=6$).

The surgical procedures were performed aseptically on a heated plate under general anesthesia (isoflurane 1-3.5% in air). Prior to surgery, the rats received a subcutaneous injection of buprenorphine (0.3mg/ml Temgesic, Schering-Plough B.V., Amstelveen, the Netherlands) at a dose of 0.05mg/kg body weight and enrofloxacin (25mg/ml Baytril, Bayer B.V., Mijdrecht, the Netherlands) at a dose of 5mg/kg body weight. The right thigh was shaved and disinfected with polydine tincture. Then, the femur shaft was exposed by a longitudinal skin incision, and blunt dissection of the underlying fascia between the vastus lateralis muscle and the biceps femoris muscle. Next, a 23mm PEEK plate (RatFix Plate, RISystem, AO Foundation, Davos, Switzerland) was fixated onto the anterolateral side of the femur by three cortical and three distal screws (6.5x0.8 \varnothing mm ShoulderScrews, RISystem, AO Foundation, Davos, Switzerland). Two osteotomies were performed using a saw guide with a wire saw (Drill&Saw guide, RISystem, AO Foundation, Davos, Switzerland) to remove a 6mm large bone segment. The resulting defect was then grafted with one of the implants or left empty (Figure 1). The wound was irrigated with sterile saline and sutured with 5-0 Vicryl sutures. Post-operative care consisted of subcutaneous administration of buprenorphine (0.3mg/ml Temgesic, 0.05mg/kg body weight) as analgesia twice a day for the first three days.

In order to visualize the dynamics of bone growth, rats received sequential subcutaneous injections with fluorochrome labels at four weeks (12.5mg/ml calcein green [CG], 10mg/kg body weight, Sigma Aldrich, Zwijndrecht, the Netherlands) and six weeks (50mg/ml xylenol orange [XO], 100mg/kg body weight, Sigma Aldrich, Zwijndrecht, the Netherlands).

To qualitatively assess the duration of the inflammatory response, two animals from the HA and the β -TCP group were sacrificed after five and twelve days, while one animal from of each group was sacrificed after six weeks. To quantify bone formation, the remaining nine animals in the groups that received either HA or β -TCP were sacrificed after eight weeks. Another six animals in whom the defect was left empty were included to confirm the critical size of the defect.

3. μ CT evaluation

μ CT scans were acquired to provide a qualitative overview of bone integration and resorption of the CaP ceramics and to confirm the critical size of the defect. Right femurs were

collected, fixated in formalin (Merck chemicals, the Netherlands) and kept hydrated during the scanning process by wrapping them in foil. A SkyScan 1076 μ CT scanner (Bruker micro-CT N.V., Kontich, Belgium) was used with an 18 μ m resolution protocol (70kV energy, 100 μ A current, 1.0mm Al/0.25mm Cu filter). CT images were converted into three dimensional reconstructions of cross-sectional images using volumetric reconstruction software NRecon version 1.5 (Bruker micro-CT N.V., Kontich, Belgium).

4. Histology and histomorphometry

After μ CT scanning, fixated samples were kept overnight, dehydrated within an industrial microwave using JFC solution (Leica Microsystems, Rijswijk, The Netherlands) and transferred into MMA solution (L.T.I, Bilthoven, The Netherlands) and polymerized at 37°C within three days. Sections were made at every level of the sample with an approximate thickness of 10 to 15 μ m using a modified interlocked diamond saw (Leica Microtome, Nussloch, Germany). Sections were either stained with 1% methylene blue (Sigma, Zwijndrecht, the Netherlands) and 0.3% basic fuchsin (Sigma, Zwijndrecht, the Netherlands) after etching with an HCl/ethanol mixture for routine histology and histomorphometry or left unstained for epifluorescence microscopy with a light microscope (LM; E600, Nikon, Japan) equipped with a quadruple filter block (XF57, dichroic mirror 400, 485, 558 and 640nm, Omega Filters, Didam, the Netherlands).

Histological sections were qualitatively analysed by light microscopy (Leica), and each section was scored either positive or negative for bone formation. For quantitative histomorphometry, high-resolution digital photographs were made from three randomly selected sections from each sample. Bone and CaP ceramic were manually pseudocoloured green and red, respectively, using Photoshop CS2 (Adobe Systems). A custom-made Matlab script was used to measure the percentage of bone in the available pore area in the total region of implant as well as in the central area of the implant. The central area was defined as the area covered by a rectangle drawn along the points 1mm on either side of the horizontal line running through the center of the implant and 2mm on either side of the vertical line running through the center of the implant. For statistical analysis, a two sided paired Student's *t*-test was used to analyse differences between β -TCP and HA.

Results

1. Characterization of HA and β -TCP ceramics

HA and β -TCP ceramics similar to those used in our previous study were produced²⁴³. Chemical and structural characteristics of the two ceramics are presented in Table 1.

2. μ CT evaluation

μ CT scans showed that none of the six empty defects (control group) show bridging within the eight weeks implantation period, thereby confirming the critical size of the defect (Figure 1A). μ CT scans of defects grafted with HA and β -TCP some limited bone formation originating from the proximal and distal host bone and areas of direct bone-implant

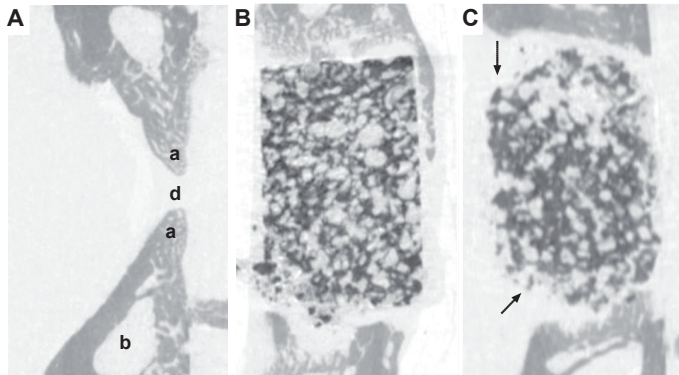


Figure 1: Overview of the rat femoral defect after eight weeks by μ CT.

μ CT evaluation of eight weeks of implantation showed (A) absence of complete bridging of the empty defect confirming its critical size (**a**, the two ends of the bone; **b**, marrow cavity; **d**, the actual defect), (B) maintenance of the shape of the HA implant, and (C) rounding of the edges of the β -TCP implant, suggestive of the more pronounced degradation of β -TCP as compared to HA.

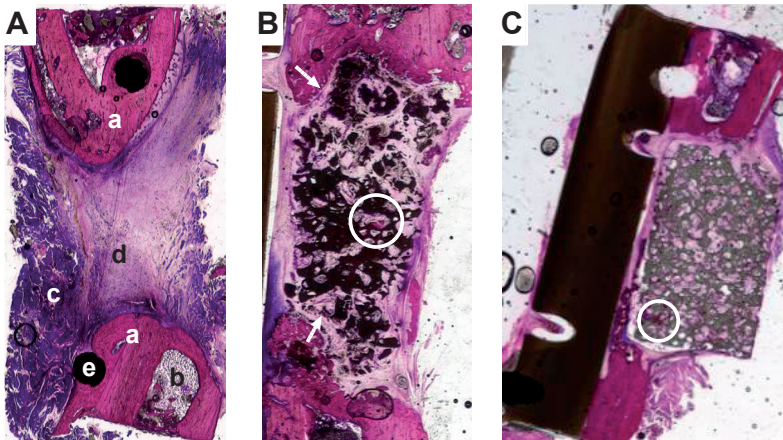


Figure 2: Overview of the rat femoral defect after eight weeks by histology.

Histology findings at eight weeks were very similar to the μ CT scan findings. At eight weeks, incomplete bridging of the empty defect with presence of poorly organized fibrous tissue between the two cut ends of the femur confirmed the critical size of the defect (A), presence of rounded edges in the β -TCP (marked by white arrows), suggested a pronounced degradation at these sites (B) and maintenance of the cylindrical shape of the HA ceramic suggested limited degradation (C). Islands of bone were seen in all the β -TCP and some HA ceramics (encircled areas). The two ends of the bone (**a**); marrow cavity (**b**); muscle surrounding the bone and defect site (**c**); the actual defect (**d**); screws used to hold the PEEK plate in place over the defect (**e**).

contact were limited. Differences in resorption between HA and β -TCP were noted in the defects grafted with the two ceramics. Whereas HA retained its cylindrical shape (Figure 1B), β -TCP clearly showed signs of degradation in the regions closest to the host bone bed (Figure 1C).

Table 1. Physico-chemical characterization of the calcium phosphate ceramics

	HA	β -TCP
Chemistry	HA	90% β -TCP and <10% HA
Sintering Temperatures	1250°C	1100°C
Macroporosity	$\pm 60\%$	$\pm 60\%$
Microporosity*	Low ($\pm 5\%$)	High ($\pm 15\%$)
Surface area	Low (<0.5m ² /g)	High (1.2m ² /g)

*Volume percentage of micropores smaller than 10 μm within the ceramic.

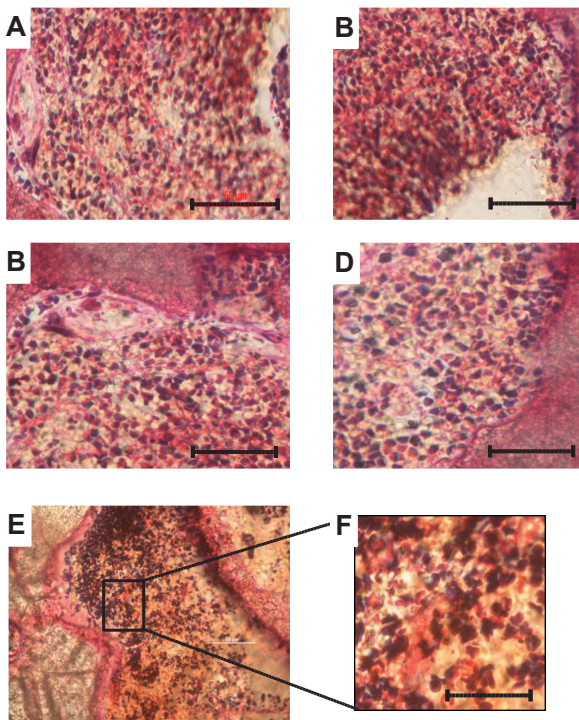


Figure 3: Histological overview of the β -TCP and HA ceramics after five and twelve days.

Rounded cells, probably of inflammatory origin within the pores of the β -TCP and HA ceramics after five days (A and B, respectively) and after twelve days (C and D, respectively). A 40X magnified view of the inflammatory cells in the β -TCP ceramic after twelve days (E) and an enlargement of the black square area (F).

3. Histology and histomorphometry

In line with the μCT scan findings, histology of the empty defects confirmed the critical size of the defect. The defect site was filled with loosely organized fibrous tissue, and no

bridging of the defect occurred (Figure 2A). Rounding of the edges and loss of structure were observed in the β -TCP after eight weeks (Figure 2B), in contrast to HA implants that retained the original shape (Figure 2C). Direct contact between HA or β -TCP and the proximal and distal femoral bone was limited, fibrous tissue had formed at the majority of the interface.

Initiation and progression of inflammation for HA and β -TCP was determined by histology after five and twelve days and six and eight weeks. Clusters of round cells, highly suggestive of inflammatory cells such as monocytes or lymphocytes were found within the pores of both the HA and the β -TCP implants at five and twelve days (Figure 3A to F). No obvious difference was observed between the two ceramics. These cells were not seen in either ceramic after six weeks. Instead, small islands of new bone formation were observed in the pores of both HA (Figure 4A, B) and β -TCP (Figure 4C, D). These results suggested that the cellular infiltration which was probably of inflammatory origin subsided between twelve days and six weeks of implantation, while the bone formation was initiated during this time.

The amount of bone increased between six and eight weeks for both HA and β -TCP. The insets in Figure 4E and F demonstrate the mineralized matrix, bone lining cells and embedded osteocytes which histologically characterize bone. New bone formation was

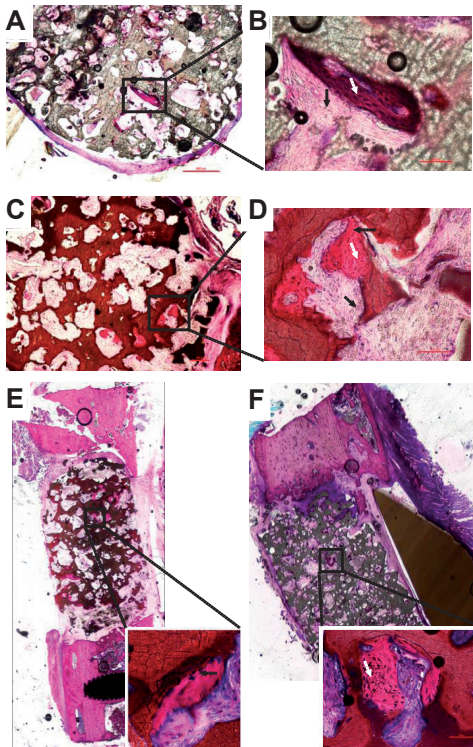


Figure 4: Histological overview of β -TCP and HA ceramics after six and eight weeks.

Absence of the inflammatory cells with concomitant presence of small islands of new bone within the HA (A) and β -TCP (C) ceramics after six weeks. Magnified view of bone formed within the pores of the HA (B) and β -TCP implants (D), (S) ceramic scaffold. Note the presence of osteocytes (white arrows) embedded in the pink matrix and the bone lining cells (dotted black arrows). The rest of the pore was filled by cells with elongated nuclei (fibrous tissue marked by black arrows). After eight weeks, again islands of new bone were observed in both β -TCP (E) and HA (F). The inset images show magnified views of the newly formed bone. Note the presence of osteocytes, bone lining cells and matrix.

observed in all β -TCP implants (9/9) and in seven HA implants (7/9). Total amount of bone formed in defects grafted with β -TCP ceramic was significantly more than that formed in defects grafted with HA ($3.6\pm 2.1\%$ versus $1.4\pm 1.6\%$ respectively of the available pore area was filled with newly formed bone) (Figure 5A). However, no significant difference was found in the amount of bone that formed in the central area of the β -TCP or HA implants, where chances of bone ingrowth from the host bone bed were lowest. While $3.1\pm 2.5\%$ of the available pore area in the central part of the defect was filled with newly formed bone in β -TCP, the corresponding value for HA was $2.5\pm 2.4\%$ (Figure 5B).

Analysis of the fluorochrome markers showed that both CG and XO label were found in areas adjacent to host bone bed, as well as in the central area of the defect (denoted by the rectangle in Figure 5B), suggesting early bone deposition throughout the implanted ceramics. Presence of CG label in the two ceramics indicated that bone formation had started in both HA and β -TCP earlier than four weeks post implantation (Figure 6A, B). Continued deposition and remodeling of bone at eight weeks in the two CaP ceramics was suggested by the presence of the XO label. In the empty defect, fluorochrome markers were only observed at the two ends of the defect, close to the host bone bed, indicating bone deposition and remodeling as a part of the body's intrinsic healing process (Figure 6C).

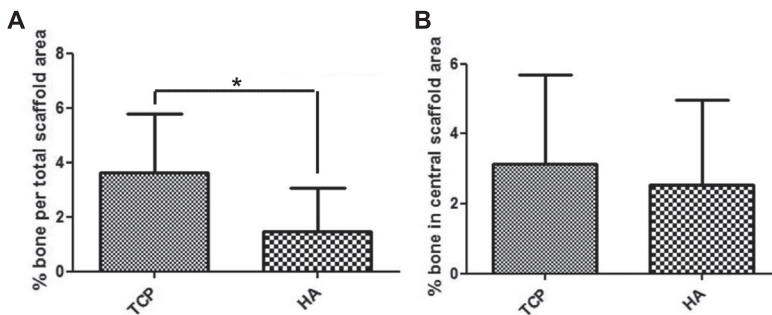


Figure 5: Quantification of bone formed within the pores of HA and β -TCP cylinders.

The amount of bone formed was determined in the available pore area of the total implant (A) and in the center of the implant (B). The error bars represent the standard deviation. Statistical analysis using the Student's paired *t*-test. * $p < 0.05$.

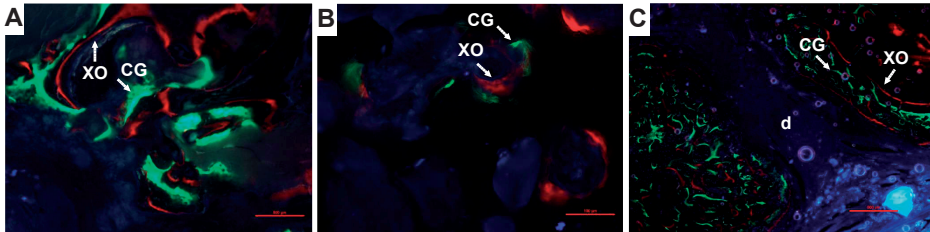


Figure 6: Dynamics of bone deposition within the two ceramics.

Fluorescence microscopy images (original magnification x10) of the fluorochrome markers, calcein green **CG** and xylene orange **XO**, in the center of the β -TCP (A) and HA (B) ceramics. Fluorescence microscopy image (original magnification x4) of the two ends of the femur (C) with the intervening defect (**d**).

Discussion

The present study aimed to determine bone formation in a clinically more relevant critical-sized cortical defect in rats after grafting with open porous β -TCP and HA ceramics, which were previously shown to significantly differ in their osteoinductive potential²⁴³. Our current findings indicated that at the selected implantation site, the amount of bone formed in both ceramics was limited and not sufficient to bridge the defect within the implantation period of eight weeks. Nevertheless, the β -TCP ceramic which had previously demonstrated a superior osteoinductivity as compared to the HA upon heterotopic implantation²⁴³, also resulted in a comparatively greater amount of bone within the critical-sized bone defect used here. Further, based on histological analysis of the inflammatory response elicited post-implantation, we observed that inflammation in both β -TCP and HA subsides between twelve days and six weeks while bone formation was initiated between twelve days and four weeks. Considering that no obvious differences between the two ceramics were observed regarding the timing and the extent of inflammation, neither one of these parameters could be related to the difference in the amount of bone formed.

Comparison between ceramics with known differences osteoinductivity in orthotopic defects are limited. Gosain *et al* demonstrated that HA-TCP cement with higher osteoinductive potential showed superior performance in a critical-sized calvarial sheep model as compared to the non-osteoinductive pure HA cement after one year⁶³. In another study, two BCP ceramics, having similar chemical composition but significantly different microstructure were compared intramuscularly as well as in an iliac wing defect in goats after three months²⁴⁹. The BCP ceramic with a greater surface area as a result of a higher microporosity was more osteoinductive at the heterotopic location and performed significantly better in the iliac wing defect than the non-osteoinductive BCP. Superiority in osteoinductive potential of

the BCP ceramic was also reflected in the larger amount of bone formed after three months in a decorticated transverse process model in goats that represents the first stages of spinal fusion²⁵⁰.

Bone formation observed after implantation of β -TCP and HA ceramics in rats femurs was rather limited compared to bone formation observed after implantation of these ceramics in dogs and goats²⁵⁰, even though bone healing capacity is generally believed to be less in larger animals²⁵¹. Compared to these studies, we used a relatively short implantation period, but this is not believed to be a likely explanation for the low amounts of bone observed as we²⁵² and others^{253, 254} have shown substantial bone healing responses in femoral bone defects within eight weeks. However bone healing capacity is also strongly affected by local biological and biomechanical factors at the site of implantation. Implantation in a cortical bone defect, a weight-bearing orthotopic site, will greatly increase the influence of biomechanical factors on bone healing, whereas biomechanical factors play only a minimal role in ectopic (intramuscular or paraspinal) implantation sites. Both the loading over the defect, as well as the fixation conditions used, may have diminished bone formation by hampering endochondral ossification. However, these conditions mimic clinical relevant bone defects that require bone grafting, because most bone defects result from fractures of long bones. So this weight-bearing orthotopic bone defect might be more suitable for making claims towards the use of these ceramics in specific clinical applications, whereas the ectopic models provide insight in osteoinductive capacity and might help to unravel underlying mechanisms.

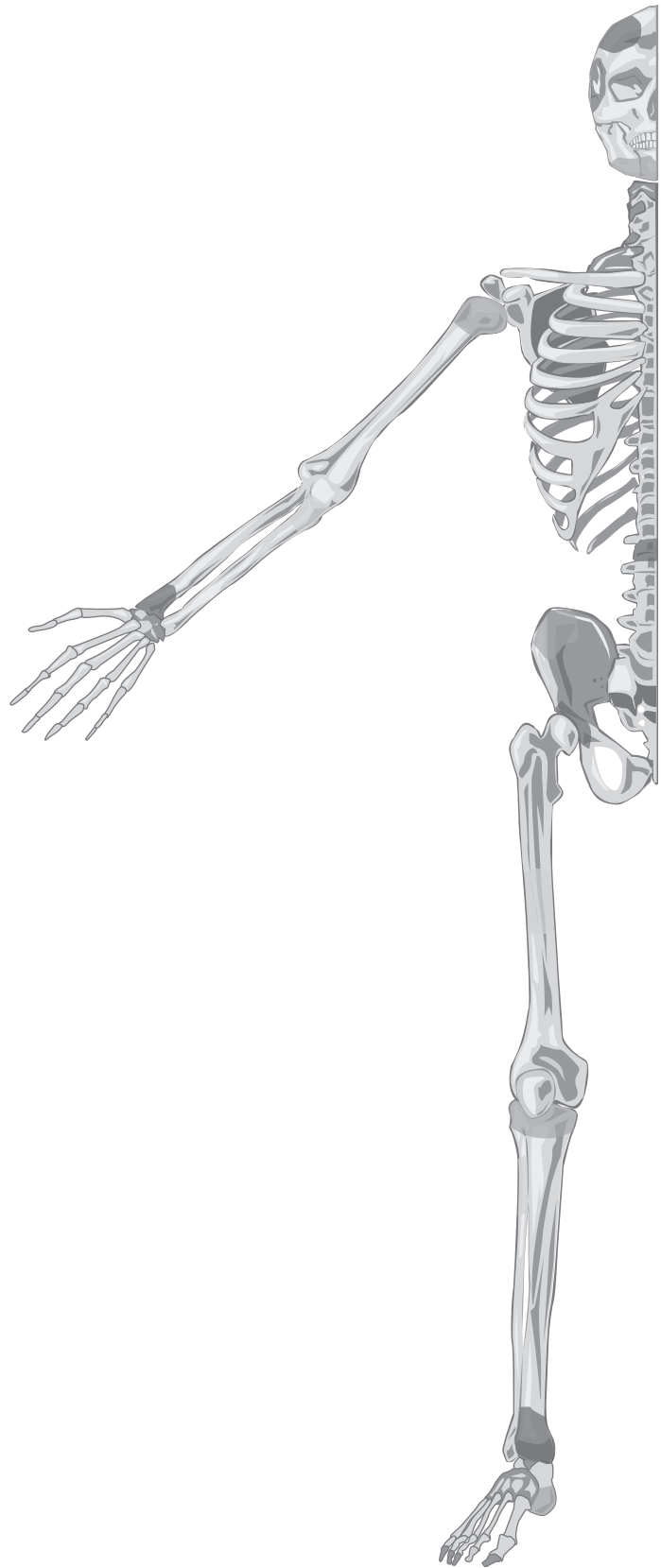
The greater amount of bone formation upon implantation of β -TCP compared to HA, cannot be solemnly attributed to a higher osteoinductive potential of β -TCP. For example, it cannot be excluded that higher microporosity resulting in a twelve times greater surface area positively affected osteoconductive potential of β -TCP. In fact, our finding of a significantly higher percentage of bone in the available pore area in the total region of interest without significant difference within the central portion of the implant, points to the fact that the difference in bone formation between the two CaP ceramics was in the peripheral area. As osteoconduction per definition proceeds from the host bone bed, bone in the periphery of the implant is likely the result of osteoconduction. In the central area of the implant, the material is not in direct contact with the osteogenic cells present in the host bone bed. However, without studies that determine the origin of new bone formation, it is difficult to prove that the bone formed within the central pores of the implant is due to direct differentiation of the inducible osteoprogenitor cells present in the bone marrow or the surrounding muscle, thus osteoinduction.

While our results confirm bone healing capacity is greater with β -TCP as compared to HA, dynamics of inflammation were equal for the two ceramics. β -TCP and HA resulted in an inflammatory reaction during the first two weeks, as is generally seen within bone healing²⁵⁵, which subsides by six weeks. Since we compared two ceramics with different

physico-chemical properties (Table 1), their behavior upon an inflammatory environment may be different (pH-changes, calcium and phosphate ion release). However, this became not apparent in the dynamics of bone formation, since fluorochrome analysis revealed that bone formation had started at around four weeks in both β -TCP and HA.

Acknowledgements

The authors gratefully acknowledge the support of the TeRM Smart Mix Program of The Netherlands Ministry of Economic Affairs and The Netherlands Ministry of Education, Culture and Science.



Chapter 5

Selective laser melting produced porous titanium implants

Johan van der Stok

Olav P. van der Jagt

Saber Amin Yavari

Mirthe F.P. de Haas

Jan H. Waarsing

Holger Jahr

Esther M.M. van Lieshout

Peter Patka

Jan A.N. Verhaar

Amir A. Zadpoor

Harrie Weinans

Published as "Selective laser melting produced porous titanium scaffolds regenerate bone in critical size cortical bone defects" in Journal of Orthopaedic Research. 2013 May;31(5):792-9

Abstract

Porous titanium implants have good mechanical properties that make them an interesting bone substitute material for large bone defects. These implants can be produced with selective laser melting, which has the advantage of tailoring the structure's architecture. Reducing the strut size reduces the stiffness of the structure and may have a positive effect on bone formation. Two implants with struts of 120 μm (titanium-120) or 230 μm (titanium-230) were studied in a load-bearing critical-sized cortical femoral bone defect in rats. The defect was stabilized with an internal plate and treated with titanium-120, titanium-230, or left empty. *In vivo* μCT scans at four, eight, and twelve weeks showed more bone in the defects treated with implants. Finally, 18.4 \pm 7.1 mm^3 (titanium-120, $p=0.015$) and 18.7 \pm 8.0 mm^3 (titanium-230, $p=0.012$) of bone was formed in those defects, significantly more than in the empty defects (5.8 \pm 5.1 mm^3). Bending tests on the excised femurs after twelve weeks showed that the fusion strength reached 62% (titanium-120) and 45% (titanium-230) of the intact contralateral femurs, but there was no significant difference between the two implants. This study showed that in addition to adequate mechanical support, porous titanium implants facilitate bone formation, which results in high mechanical integrity of the treated large bone defects.

Introduction

Bone healing requires: (1) cells that are capable of forming bone (osteogenicity), (2) bioactive factors that can attract such cells and initiate bone formation (osteoinduction), (3) a matrix that guides the bone formation (osteoconduction), (4) adequate vascularisation and (5) initial mechanical support to the surrounding bone, which becomes more important as the size of the defect increases²²².

Bone defects can be treated with autologous bone. Autologous bone is considered the gold standard treatment and is mostly harvested from the iliac crest. However, the harvesting procedure has a complication rate of 10 to 40%, including hemorrhage, nerve, and vascular lesions and post-operative pain¹³. Moreover, the amount and quality of bone that can be harvested is limited, restricting its use in large defects²³⁷. Therefore, large bone defects are currently treated by distraction osteogenesis, vascularised bone (fibula) grafting, or massive cortical allografts²⁵⁶. All treatments have their specific disadvantages, such as multiple surgical procedures, high complication rates, and prolonged periods of immobility and rehabilitation.

The challenge is to develop a bone substitute material that enhances bone healing but also offers adequate mechanical strength. Porous titanium implants are especially interesting, since titanium has superior mechanical properties compared to other synthetic materials such as calcium phosphate ceramics and polymers²³. Although the potential of porous titanium has been recognized for many years, development of open porous structures has been hampered by the limitations of available production techniques²⁵⁷. With production techniques such as plasma spraying²⁵⁸, space-holder techniques²⁵⁹, powder metallurgy²⁶⁰, or sintering of titanium fibers²⁶¹ it remains difficult to produce a porous structure with the desired architecture that meets both osteoconductive and mechanical requirements. For osteoconduction, an open interconnected porous structure with pores in the range of 200-500 μm is required²¹². From a mechanical point of view, the structure should be stiff enough to sustain the physiological loads, but it should not drastically exceed the stiffness of the bone being replaced to avoid stress shielding.

Better control over the structural architecture can be acquired using selective laser melting (SLM)²⁶². SLM allows production of very fine and small porous titanium structures, with struts in the range of 100-200 μm . This enables the possibility of tailoring and optimizing the structural and mechanical properties of the implants while maintaining the required pore dimensions that allow for bone and vessel ingrowth. Thinner titanium struts may result in increased elastic and plastic deformation. Such deformation of the porous structure reduces stress-shielding inside the implants and may provide a biomechanical stimulus for the bone-forming cells, thereby resulting in more bone formation²⁶³.

In this study, we used a critical-sized cortical femur bone defect in a rat to test two hypotheses: (1) porous titanium implants can be a biomechanically strong osteoconductive matrix

for repair of cortical bone defects, (2) thinner strut sizes will result in favorable mechanical properties that will increase bone formation within the titanium implants thereby improving mechanical integrity of the treated bone defect.

Materials and methods

1. Porous titanium implants

Porous titanium implants were produced from Ti6Al4V using SLM (Layerwise, Belgium). Two structural variants were designed using a dodecahedron unit cell as a template structure. One variant consisted of thin titanium struts (titanium-120) and the second variant consisted of thick titanium struts (titanium-230). Both structural variants were produced in two different shapes: (1) cylindrical implants (5mm \varnothing x 10mm) for determining the compression strength and the Young's modulus and (2) femur-shaped implants (6mm mid-diaphyseal segment of the femur bone, Figure 1) for determining the ultimate compression force (UCF) and for *in vivo* implantation. All samples underwent post-production chemical and heat treatment to increase surface roughness. This treatment consisted of (1) immersion in a 5M aqueous NaOH solution at 60°C for 7h, (2) immersion in water at room temperature for 12h, (3) immersion in 5% HCl at 60°C for 5h, (4) immersion in water at room temperature for 24h, (5) heating to 600°C at a rate of 5°C/min in an electric furnace in ambient air pressure, holding the temperature at 600°C for 1h, and subsequent natural cooling in the furnace. The effect of chemical and heat treatment were characterized by scanning electron microscopy (Figure 2).

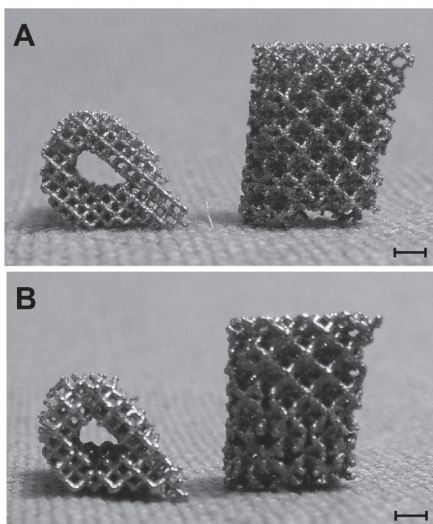


Figure 1: Femur-shaped porous titanium implants.

Titanium-120 structure (A) and titanium-230 structure (B). Bar indicates 1 mm.

2. Structural and mechanical evaluation of porous titanium implants

Porosity, titanium strut thickness, and pore size were determined using a SkyScan 1076 μ CT scanner (Bruker micro-CT N.V., Kontich, Belgium). Compression test were conducted using a Zwick test machine (Zwick GmbH, Ulm, Germany) with a rate of 0.02mm/s. Of each structure, ten cylindrical implants were used in order to determine the compression strength and the homogenized Young's modulus and five femur-shaped implants were used in order to determine the UCF. The 6mm femoral bone segments removed during surgery served as reference for the UCF.

3. Animal experiment

In 27 male Wistar rats, a 6mm cortical bone segment of the right femur was removed and grafted with either titanium-120 ($n=9$) or titanium-230 ($n=9$) or, was left empty in the control group ($n=9$). The local animal ethics committee approved the study. All animals were housed according to the national guidelines for care and use of laboratory animals.

3.1 Surgical procedure

A single dose of antibiotics (enrofloxacin, 5mg/kg body weight) was administered one hour before surgery. The operation was performed aseptically under general anesthesia (1-3.5% isoflurane). The right femur was exposed though a lateral incision of the skin and division of the underlying fascia. A 23mm long PEEK plate (RatFix, AO Foundation, Switzerland) was fixated to the anterolateral plane of the femur. Three proximal and three distal screws fixated the plate. The periosteum was removed over approximately 8mm of the mid-diaphysial region before removal of the 6mm long bone segment. The bone segment was removed

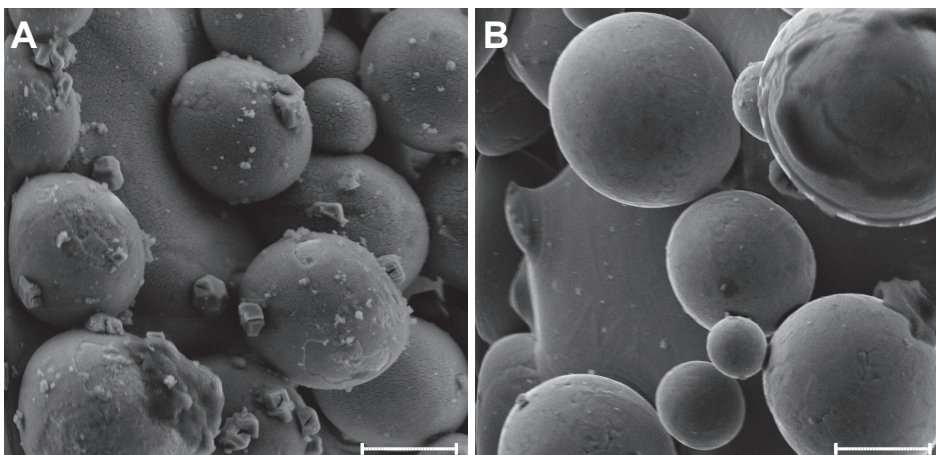


Figure 2: Scanning electron microscopy images of untreated (A) and treated (B) porous titanium surface.

White bar indicates 20 μ m.

with a tailor-made saw guide and a wire saw (RatFix, AO Foundation, Switzerland), and the implant was placed press-fit into the defect site. The fascia and skin were sutured in layers and prophylactic pain medication (buprenorphine, 0.05mg/kg body weight) was administered twice a day for the first three days after surgery. Fluorescent dyes were administered at four (tetracyclin, 25mg/kg body weight), eight (calcein, 25mg/kg body weight), and eleven weeks (xylenol orange, 90mg/kg body weight).

3.2 μ CT evaluation

Immediately after the surgery, while the rats were still under general anesthesia, a SkyScan 1076 μ CT scanner (Bruker micro-CT, Belgium) was used in order to acquire a baseline *in vivo* μ CT scan. A 36 μ m resolution protocol was used at 95kV, 1.0mm Al filter, and 0.6 degree rotation step, resulting in a 15 minute scan. *In vivo* scans were repeated after four, eight, and twelve weeks. For the final *ex vivo* scan, an 18 μ m resolution protocol was used at 95kV, 1.0mm Al/0.25mm Cu filter, and 0.4 degree rotation step (3h scan). The CT images were reconstructed using volumetric reconstruction software NRecon version 1.5 (Bruker micro-CT, Belgium).

The total bone volume (TBV) was defined as the total bone volume within the 6mm bone defect including bone formed around the titanium implants (Figure 3A). The bone volume in pores (BVp) was defined as the bone volume measured within the pore volume (PV) of the titanium implants (Figure 3B), and is also expressed as a percentage of the pore volume (BVp/PV). TBV and BVp were determined using software CTAnalyser version 1.11 (Bruker micro-CT, Belgium).

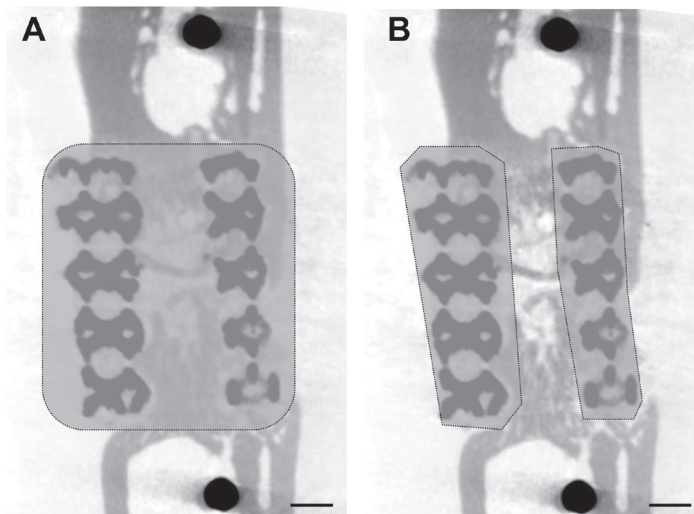


Figure 3: μ CT measurements.

Transversal μ CT image with volume of interest (transparent grey marked area) used for measurements of TBV (A) and BVp (B). Bar indicates 1mm.

This software created a volume of interest (VOI) that specifically captured the volume of the 6mm defect (used for TBV) or the volume of the pores (used for BVp). These VOIs were automatically generated using a custom-made algorithm. After determination of both VOIs, the porous titanium implants was subtracted from the images using a global threshold. An additional eroding step was performed to remove an adjacent $35\mu\text{m}$ layer in order to exclude the metal artifacts at the interface that may interfere with the bone volume measurement. The *in vivo* μCT scan protocol required a further correction for the metal artifacts in order to reduce the interference with the bone measurements performed. Therefore we conducted *in vivo* μCT scans directly after surgery and subtracted the acquired values found from the measurements performed at four, eight and twelve weeks. The *ex vivo* μCT scan protocol generated images in which artifacts were reduced to an absolute minimum. This was confirmed by conducting the described analysis on μCT scans of the empty implants of both structural variants, resulting in TBV and BVp values less than 1mm^3 . Bone volume was then determined after applying a global threshold that was determined on visual inspection and kept the same for all μCT scans analysed.

3.3 Biomechanical evaluation

The final strength of the treated femurs was measured with three-point bending tests conducted on five samples from each group. In these tests, both supports are chosen as close as possible to the bone-implant interfaces (distance $<5\text{mm}$). Small distance between the bone-implant interfaces and the supports ensures that the three-point bending test measures the interface strength of bone and implants as closely as possible. The contralateral femurs served as controls. To ensure that we tested the entire spectrum, we first sorted the treated femurs according to their BVp and then included every other femur. The bending tests were carried out using a Zwick test machine (Zwick GmbH, Germany) as follows: first, the PEEK plate was carefully removed; the femurs were then supported at the proximal and distal side using two plates that were secured with screws. A plate that exceeded the average pore size applied a downward force to the middle of the porous titanium implants, pushing it outside the bone defect. The bending tests were performed at a displacement rate of $2\text{mm}/\text{min}$ until the peak load was reached. The force-displacement curves were recorded and used to determine the maximum force.

3.4 Histological evaluation

Histology was performed on four femurs of each group to study the bone-titanium interface and bone morphology. The specimens were dehydrated in a graded ethanol series, and embedded in methylmethacrylate. Sections of $\sim 20\mu\text{m}$ were obtained using a diamond saw (Leica SP1600) and stained with basic fuchsin 0.3% solution (Sigma) and methylene blue 1% solution (Sigma). Bone stains red with basic fuchsin and fibrous tissue stains blue with

methylene blue. Unstained sections were examined using an epifluorescent microscope (Axiovert 200MOT/Carl Zeiss) with a triple filter block.

4. Statistics

Statistical analyses were performed using SPSS Statistics 17.0 (SPSS Inc, Chicago, Ill). The data are presented as means with standard deviation. One-way Analysis of Variation (ANOVA) and subsequent post-hoc pairwise comparisons with Bonferroni adjustment was used to analyse the differences between the three groups. A repeated measures general linear model was used when examining the longitudinal *in vivo* μ CT data. A Pearsons correlation coefficient was used to determine the correlation between BVp, TBV, and the maximum bending force.

Table 1. Structural and mechanical characteristics of porous titanium implants

	Titanium-120	Titanium-230	Cortical bone (rat)
Porosity (%)	88	68	
Titanium thickness (μm)	120	230	
Pore size (μm)	490 (240-730)	490 (240-730)	
Surface area / volume (μm^2)	0.034	0.018	
Compression strength (MPa)	14.3 \pm 1.7	77.7 \pm 12.8	140 \pm 19 ²⁶⁴
Homogenized Young's modulus (GPa)	0.38 \pm 0.04	1.56 \pm 0.21	8.80 \pm 2.53 ²⁶⁴

Pore size is presented as median and range. Compression strength and homogenized Young's modulus is presented as average \pm SD.

Results

1. Porous titanium implants

The different titanium strut sizes and equal pore dimensions resulted in a porosity of 88% in the titanium-120 implants and 68% in the titanium-230 implants (Table 1). The titanium-120 structure had five-fold lower compression strength and a four-fold lower homogenized Young's modulus than the titanium-230 structure (Table 1). There was a significant difference in the UCF ($p<0.001$). The UCF of the titanium-230 implants (530 \pm 85N) was higher than the corresponding bone segments (441 \pm 31N, $p=0.022$), whereas the UCF of titanium-120 implants (84 \pm 11N) was lower than the corresponding bone segments ($p<0.001$) (Figure 4).

2. μ CT evaluation

Correct positioning of the porous titanium implants was confirmed by μ CT directly after surgery in all animals and no dislocation of the porous titanium implants was detected during the follow-up. The titanium-230 structure remained completely intact in all rats, whereas

breakage of some struts was seen in six of the nine rats given titanium-120. This occurred after either four (two cases) or eight weeks (four cases), but did not result in loss of fixation or complete loss of structural integrity of the implants. The porous titanium implants were well integrated with the adjacent cortical bone and a progression of the bony bridging was observed over time (Figure 5), although in some rats small areas of the adjacent cortical bone underwent changes that may indicate bone resorption (Figure 6). In the empty control group, loss of fixation, due to breakage of the screws, occurred in six out of nine rats. This happened to one rat at four weeks, to four rats at eight weeks, and to one rat at twelve weeks. Those rats were taken out of the experiment at subsequent time points. In the remaining rats, no bridging of the defect had occurred and a consistent pattern of bone resorption of the remaining cortical bone was observed (Figure 7).

Treatment with porous titanium implants resulted in more TBV than in the empty controls at all time points (Figure 8). The increase of TBV was most profound between four and twelve weeks, whereas in the empty controls TBV seemed to have reached a plateau

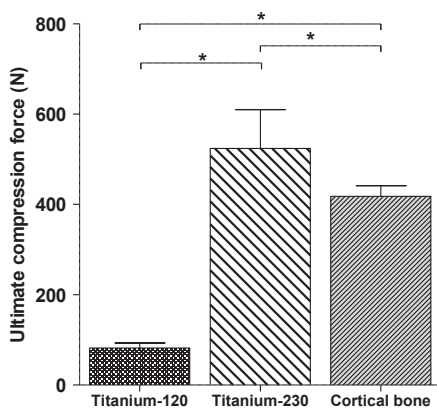


Figure 4: Ultimate compression force of titanium-120, titanium-230, and cortical bone.

Statistical analysis was performed with One-Way analysis of Variance (ANOVA) subsequent post-hoc pairwise with Bonferroni adjustment, * is $p < 0.05$.

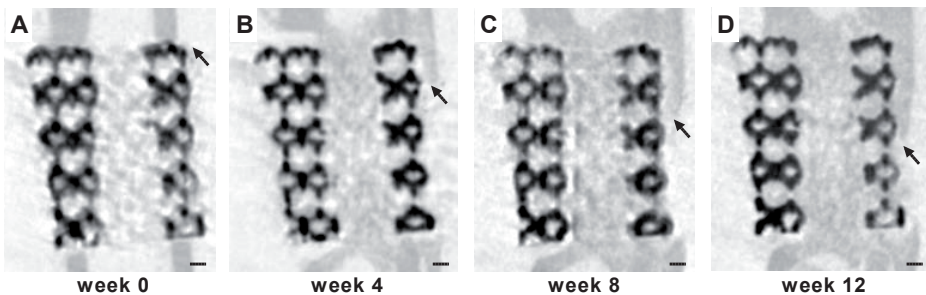


Figure 5: Bony bridging along porous titanium implants.

Progression of bony bridging (arrow) along the porous titanium implants seen on consecutive *in vivo* μ CT scans made of a femur defect treated with titanium-230 at zero (A), four (B), eight (C) and twelve (D) weeks. Black bar indicates 1mm.

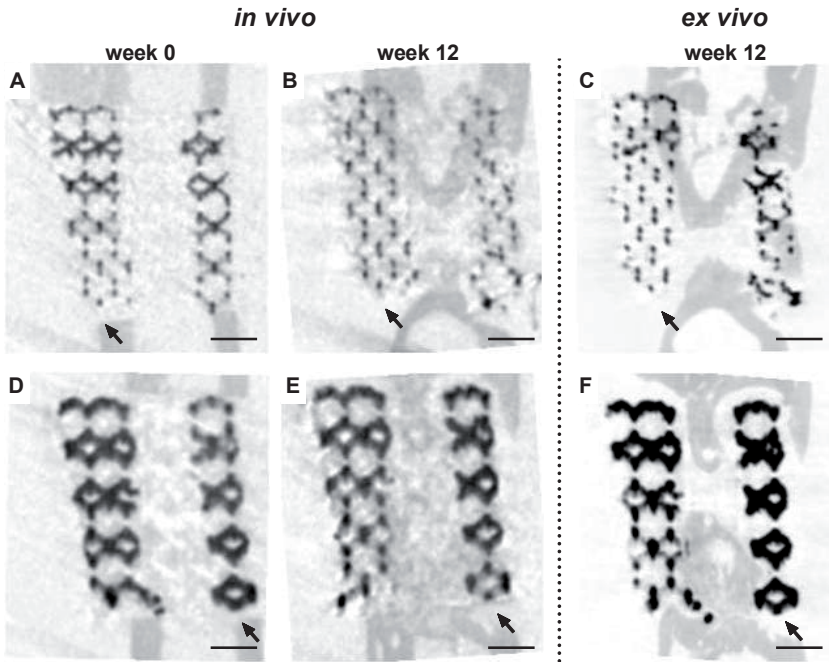


Figure 6: Areas of bone resorption after implantation of porous titanium implants.

μ CT images of titanium-120 (A, B, and C) and titanium-230 (D, E, and F) show small areas of the adjacent cortex that were resorbed during the twelve weeks follow-up (arrows). Black bar indicates 1mm.

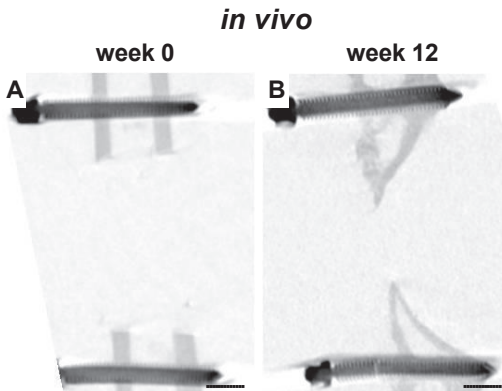


Figure 7: Bone resorption in empty defects.

μ CT images of a defect that was left empty. Extensive resorption of remaining cortex is observed at both proximal and distal bone. Black bar indicates 1mm

phase after eight weeks. At twelve weeks, a significant difference in the TBV ($p=0.008$) was found (Figure 8). The TBV of the titanium-120 group ($18.4\pm 7.1\text{mm}^3$) and the titanium-230 group ($18.7\pm 8.0\text{mm}^3$) was significantly higher than in TBV of the empty control group ($5.8\pm 5.1\text{mm}^3$, $p=0.015$ and $p=0.012$, respectively).

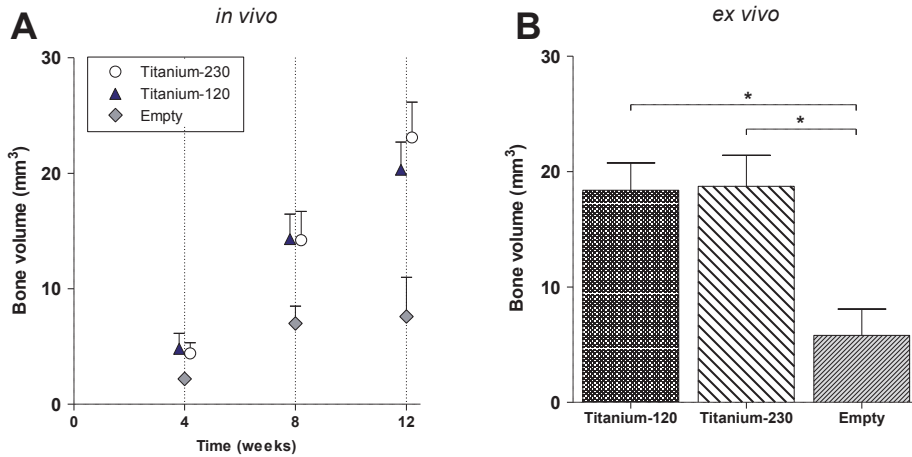


Figure 8: Total bone volume.

Total bone volume (TBV) measured *in vivo* during the study period (A) and *ex vivo* at twelve weeks (B). The *in vivo* measurements were corrected for artifacts using the scan made at time point zero. Statistical analysis was performed with One-Way analysis of Variance (ANOVA) subsequent post-hoc pairwise with Bonferroni adjustment, * is $p < 0.05$.

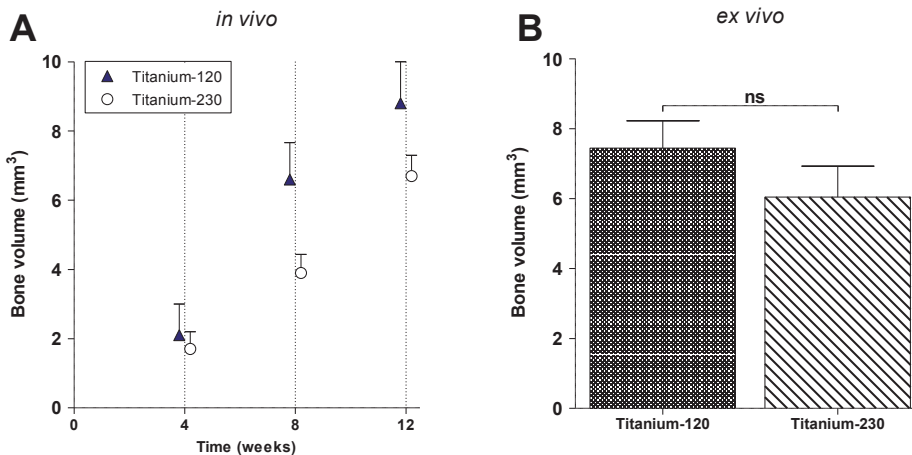


Figure 9: Bone volume in pores.

Bone volume in pores (BVp) measured *in vivo* during the study period (A) and *ex vivo* at twelve weeks (B). The *in vivo* measurements were corrected for artifacts using the scan made at time point zero. Statistical analysis was performed with One-Way analysis of Variance (ANOVA), NS is not statistically significant.

The porous structure of the titanium implants facilitated bone ingrowth given that an increase of BVp was found at all time points (Figure 9A). At twelve weeks, the absolute BVp was $7.4 \pm 2.3 \text{ mm}^3$ in the titanium-120 implants and $6.0 \pm 2.7 \text{ mm}^3$ in the titanium-230 implants ($p = 0.38$) (Figure 9B). This resulted in a BVp/PV of $16 \pm 5\%$ in the titanium-120 and $20 \pm 9\%$ in the titanium-230.

3. Biomechanical evaluation

The intact femurs that served as control broke at a force of 233 ± 27 N. The bending force of the titanium-120-treated femurs was 144 ± 73 N (62% of control) compared with 104 ± 38 N (45% of control) for titanium-230-treated femurs (Figure 10). Except for one case, all samples broke at the titanium-bone interface. BVp measured with μ CT strongly correlated with the maximum bending force for the titanium-120 group ($r^2=0.83$, $p=0.03$). The two treated femurs in which more than 8 mm^3 bone had formed within the pores had a bending force comparable with the intact control femurs (Figure 10B). For the titanium-230 group, the maximum bending force did not seem to relate to BVp ($r^2=0.02$, $p=0.84$).

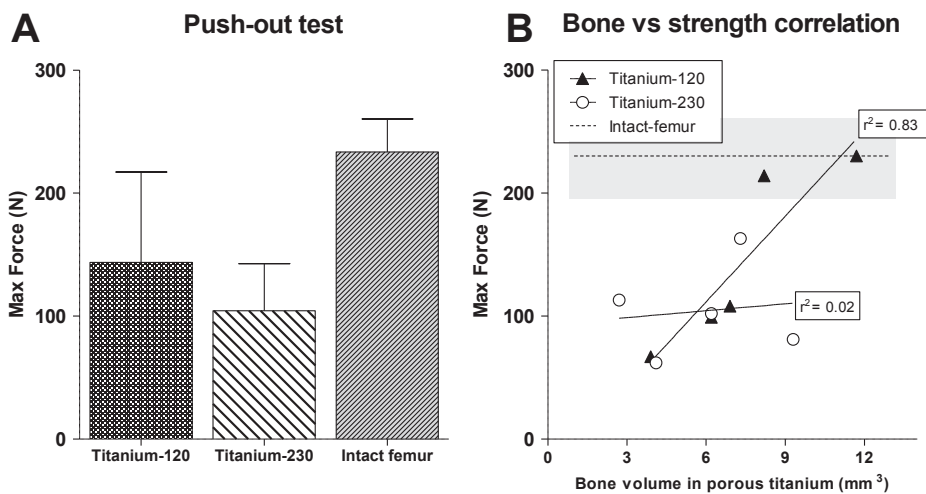


Figure 10: Biomechanical bending test.

Average maximum bending force (A) and bending force correlated to bone in pore volume (B).

4. Histological evaluation

In the histological evaluation, the empty defect sites showed limited bone formation and resorption of the cortical bone at the proximal and distal sites (Figure 11A and F). Within the remaining defect area, abundant fibrous tissue was found.

Histology of the titanium groups revealed formation of a major plug of new bone in the medullary canal at both ends of the bone defect. This bone is most likely formed through the process of direct ossification (Figure 11B and D). The newly formed bone extends from this plug into the porous titanium and the inner space of the implant. Bone was also abundant at the outer area of the implants, showing signs of an attempt to bridge the defect area. The area inside the porous titanium that was not filled with bone was filled with fibrous tissue. The pattern observed correlated well with the bone seen on the corresponding μ CT images (Figure 11G and H).

Bone is directly formed on the surface of the porous titanium implants. At some areas, however, a thin layer of fibrous tissue between the titanium and the bone was observed (Figure 11E). No signs of foreign body reactions or inflammation were detected. In one titanium-120 sample, a possible development of a hypertrophic non-union was seen, since a cluster of chondrocytes was found at a site suspect to breakage of titanium struts (Figure 11C).

The injected fluorochrome labels showed the mineralized bone at four (red), eight (green) and twelve weeks (yellow) (Figure 12). The observed pattern of fluorochrome labels indicate that bone formation was most active around the titanium-bone interface at the proximal and distal ends of the porous titanium implants (Figure 12). Only limited progression of the bridging of the bone defect through the medullary canal was seen between the four and twelve weeks (Figure 12C), since the label injected at four weeks (red) was found close to the most advanced bone fronts (yellow).

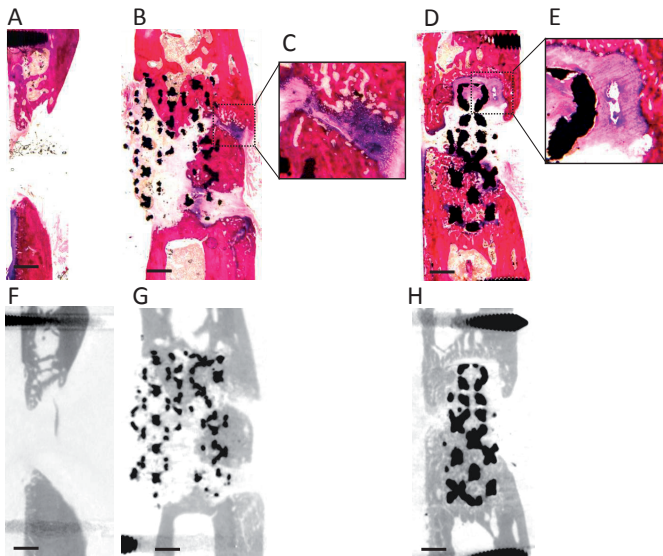


Figure 11: Histology and μ CT.

Histological slides with corresponding μ CT images of an empty defect (A and F), titanium-120 (B and G) and titanium-230 (D and H), including detailed interface view for titanium-120 (C) and titanium-230 (E). Black bar indicates 1mm.

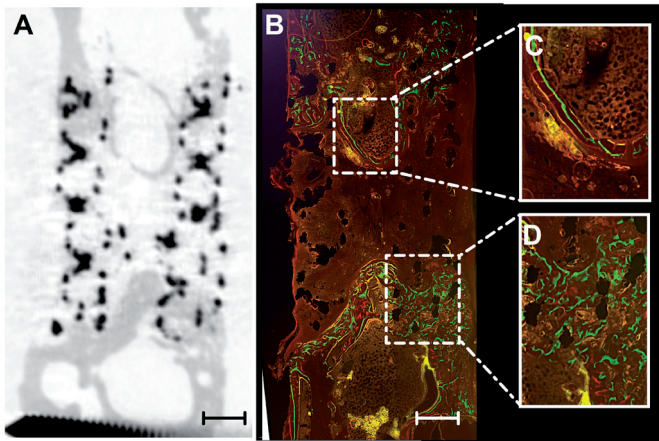


Figure 12: Fluorochrome labelling.

Light microscopy images of the fluorochrome labels of a femur treated with titanium-120 (B) including corresponding μ CT (A) images. Tetracyclin label (four weeks) is red, calcein label (eight weeks) is green and xylenol orange label (twelve weeks) is yellow. Bars indicate 1mm.

Discussion

This longitudinal *in vivo* study supports our first hypothesis that porous titanium implants provide mechanical support in the early phase after implantation, and facilitate bone formation (osteoconduction) over time, resulting in good mechanical strength of the treated femurs after twelve weeks. A lower titanium strut size reduced the homogenized Young's modulus of the implant but did not result in significantly more bone formation or higher mechanical strength of the treated femurs, meaning that these experiments did not support our second hypothesis.

The osteoconductive properties of porous titanium implants were proven by the fact that more bone had formed in the bone defects treated than in the defects that were left empty. This is in line with previous reports that used a metaphyseal bone defect model in rabbits²⁶⁵⁻²⁶⁹. The rat femur bone defect model used here has the advantage that it allows for *in vivo* μ CT scanning to monitor bone formation throughout time. Bone formation was measured using a custom-made algorithm that first removed the metal artifacts and then selected the areas of newly formed bone. Accurate selection of bone was verified using the corresponding histological sections as a reference (Figure 11). The *in vivo* bone measurements showed a gradual increase in bone formation in the rats that received titanium-120 or titanium-230 scaffolds, this bone formation may have still been ongoing, because no plateau phase was reached within the twelve weeks follow-up period (Figure 8A).

The increase in bone regeneration seen in the defects treated with porous titanium implants may be related to the implant structure and its mechanical properties. The structure

of osteoconductive scaffolds is well defined in terms of pore size, interconnectivity, and porosity²¹² and these criteria were met for both structural variants. However, the mechanical properties of the two structural variants were different due to their different strut sizes. Reducing the strut size by ~50% in the titanium-120 structure resulted in a large decrease of the homogenized Young's modulus (Table 1). The measured homogenized Young's modulus for the titanium-120 is close to the lowest range reported in the literature for porous titanium^{259, 265, 270-272} and within the range of human trabecular bone (0.01-2GPa)²⁷³. Such low homogenized Young's modulus allows for more deformation upon loading, and was therefore hypothesized to result in more bone ingrowth in the titanium-120 implants. However, there was not significantly more bone formed after twelve weeks (Figure 9B) and a possible explanation could be that the loads that were applied to the titanium-120 implants after implantation in the femoral bone defect were not able to reach the minimum force required to deform the implants.

Defining the mechanical properties that would have allowed deformation of the porous titanium implants after implantation was complicated by a number of factors. Although the titanium-120 was significantly weaker than the femur segment that it replaced and the titanium-230 was significantly stronger in term of UCF, however bone is able to withstand forces that are at least twice the normal peak loading²⁷⁴. Furthermore, different bones and even different areas of a bone can have different mechanical properties²⁷³. Finally, not all the mechanical loads will be transferred through the porous titanium implants, since a portion of the load will be transferred to the PEEK fixation plate. Preliminary results of a finite element model of this femur bone defect indicates that the division of force is highly dependent on the stiffness of the implants, the contact conditions between the implant and bone, and the mechanical loading²⁷⁵. Moreover, the load distribution changes over time as more bone is generated within the implants. Taking into account all these factors to define the optimal mechanical properties of porous titanium implants remains difficult. One should therefore take the species, the type of bone that needs to be replaced, and the applied fixation methods into account.

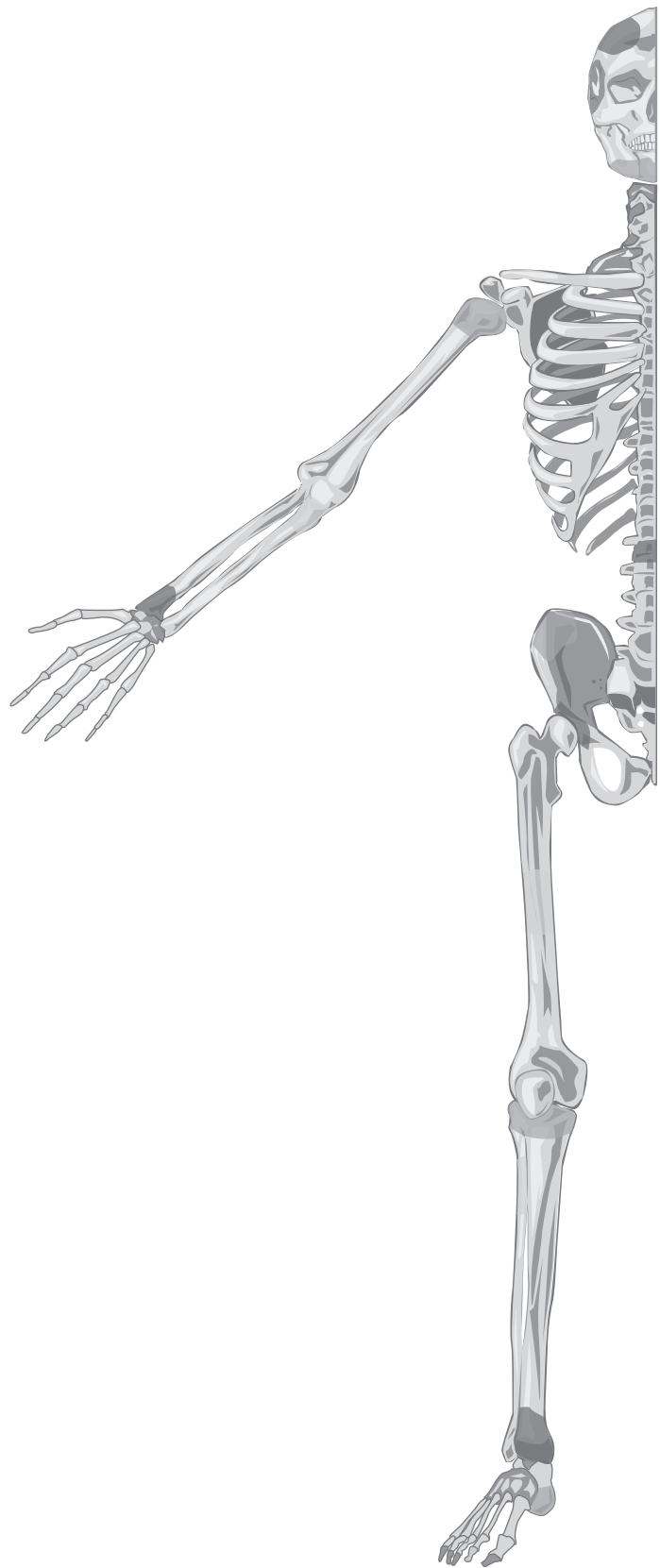
Implantation of the titanium implants provided sufficient support to the bone defect, because it did not result in a loss of fixation, whereas in most rats for which the defect was left empty the PEEK plate fixation failed. The ability to provide sufficient support is likely to have contributed to the bone formation in the defect area but is only made possible by the mechanical properties that allow the porous titanium implants to function as a load-bearing scaffold in this rat femur defect. The final strength of the treated femurs was measured using three-point bending test. In the three-point bending test, the supports were chosen very close to the bone-scaffold interface, so that the bending test more or less measures the interface strength between bones and scaffold and is therefore somewhat similar to torsion test. The bending forces are surprisingly high, taking into account twelve weeks implantation period and that only about 20% of the pore volume was occupied by newly formed bone.

The broken struts seen in the titanium-120 implants, which itself could be explained by the limited compression strength, did not have a negative impact on the maximum bending force. In fact, the maximum bending force was even somewhat higher in the titanium-120 group compared to the titanium-230 group (Figure 10A). Interestingly, there is a strong correlation between the bending force and the bone volume inside the pores for the titanium-120 implants but not for titanium-230. Possible factors other than bone volume that may affect the strength of the treated femurs could be the bone-titanium bonding. Previous studies that used similar heat and surface treatments showed good bone-bonding and even indicated a possible osteoinductive role of the modified surface ²⁷⁶. The larger surface area in the titanium-120 implants (Table 1) may have resulted in a larger area of direct bone-titanium contact. This may explain why bone volume within the pores shows a better correlation with the final mechanical strength for the femurs that received a titanium-120 implants than those that received titanium-230.

The work presented here shows the potential of porous titanium implants, and especially the possibility to function as a load-bearing scaffold may become relevant in clinical cases where conventional fixation methods alone may be insufficient. But before porous titanium can be used in clinical cases, the mechanical properties should be tailored to the human situation. Another aspect of porous titanium that should be further explored is the surface. Surface modifications have been studied by others ²⁷⁷, and it presents a great opportunity to enhance bone-titanium bonding or increase bone formation. A possible example would be the addition of a calcium phosphate coating ²⁷⁸. The surface may also be used to address the main drawback of titanium implants, *i.e.* the risk of infection. Antibiotic coatings have already been developed for solid implants ²⁷⁹, and they may help to reduce the risk of infection. The challenge will be to combine all these different techniques into one porous titanium implants that can withstand thorough experimental testing before proceeding to clinical trials.

Acknowledgements

This research forms part of the Project P2.04 BONE-IP of the research program of the BioMedical Materials institute, co-funded by the Dutch Ministry of Economic Affairs. Osteosynthesis & Trauma Care foundation is acknowledged for financial support.



Chapter 6

Porous titanium implants coated with osteostatin

Johan van der Stok

Daniel Lozano

Yoke Chin Chai

Saber Amin Yavari

Angela P. Bastidas Coral

Jan A.N. Verhaar

Enrique Gómez-Barrena

Jan Schrooten

Holger Jahr

Amir A. Zadpoor

Pedro Esbrit

Harrie Weinans

Published as "Osteostatin-coated porous titanium implants improve early bone regeneration of cortical bone defects in rats" in *Tissue Engineering Part A*. 2015 Mar 10 [Epub ahead of print].

Abstract

A promising bone graft substitute is porous titanium. Porous titanium, produced by selective laser melting (SLM), can be made as a completely open porous and load-bearing scaffold that facilitates bone regeneration through osteoconduction. In this study, the bone regenerative capacity of porous titanium is improved with a coating of osteostatin, an osteoinductive peptide that consists of the 107-111 domain of the parathyroid hormone-related protein (PTHrP) and the effects of this osteostatin-coating on bone regeneration were evaluated *in vitro* and *in vivo*.

SLM-produced porous titanium received an alkali-acid-heat treatment and was coated with osteostatin through soaking in a 100nM solution for 24h or left uncoated. Osteostatin-coated scaffolds contained $\sim 0.1\mu\text{g}$ peptide/g titanium, and *in vitro* 81% was released within 24h. Human periosteum-derived osteoprogenitor cells cultured on osteostatin-coated scaffolds did not induce significant changes in osteogenic (*ALP*, *Col1*, *OCN*, *Runx2*) or angiogenic (*VEGF*) gene expression, however it resulted in an upregulation of *OPG* gene expression after 24h and a lower *RankL:OPG* mRNA ratio. *In vivo*, osteostatin-coated porous titanium implants increased bone regeneration critical-sized cortical bone defects ($p=0.005$). Bone regeneration proceeded until twelve weeks and femurs grafted with osteostatin-coated implants and uncoated implants recovered respectively 66% and 53% of the original femur torque strength ($97\pm 31\text{N}\cdot\text{mm}$ and $77\pm 53\text{N}\cdot\text{mm}$, NS).

In conclusion, the osteostatin-coating improved bone regeneration of porous titanium. This effect was initiated after a short burst-release, and might be related to the observed *in vitro* upregulation of *OPG* gene expression by osteostatin in osteoprogenitor cells. Long-term beneficial effects of osteostatin-coated porous titanium implants on bone regeneration or mechanical strength were not established here and may require optimization of the pace and dose of osteostatin release.

Introduction

Bone grafting is a procedure often performed in trauma, orthopaedic and craniomaxillofacial surgery²⁸⁰ and the current gold standard bone graft is autologous bone⁴⁴. Autologous bone has osteoconductive, osteoinductive, and osteogenic properties and is usually harvested from the iliac crest¹⁰. However, harvesting is associated with complications in 10–40% of the cases¹² and sometimes limited autologous bone is available. These disadvantages motivates the development of bone graft substitutes. An ideal bone graft substitute has osteoconductive, osteoinductive and/or osteogenic properties²⁸¹, while also providing substantial mechanical support. However mechanical support provided by ceramic-based or polymer-based scaffolds is limited and often insufficient to graft cortical bone defects⁵³. Therefore, cortical bone defects may benefit from grafting with mechanically stronger porous metallic-based scaffolds such as porous titanium^{24, 35, 282}, an idea that has already been proposed in the 1970s^{32, 283}.

Today, porous metallic-based implants are used in hip^{284, 285} and knee²⁸⁶ replacement surgery, but also in craniomaxillofacial surgery^{287, 288}. During the past decade, the development of porous titanium has greatly benefitted from the introduction of additive manufacturing techniques. These additive manufacturing techniques, such as selective laser melting (SLM)²⁸⁹, enable the production of fine and precisely controlled porous structures, which can be designed to exactly meet (patient-specific) mechanical properties desired for both trabecular or cortical bone defects²⁹⁰. Manufactured porous titanium implants, containing pores ranging between 460 and 670µm, form a unique mechanically strong osteoconductive scaffold suitable to graft cortical bone defects^{252, 291}. However, porous titanium may be further improved through addition of osteoinductive properties. One successful method to reinforce porous titanium with osteoinductive properties is to incorporate bioactive gels²⁵² but an interesting alternative method might be to make the titanium surface bioactive.

Titanium can be made bioactive through altering the surface chemistry and topography by blasting, etching, or oxidization regimes²⁹², or by deposition of an inorganic (e.g. calcium phosphates) or organic (e.g. peptides) surface coating²⁹³. A recently explored peptide that has potential to equip titanium with osteoinductive properties is osteostatin. Osteostatin is the N-terminal sequence 107-111 of the C-terminal domain of parathyroid hormone (PTH)-related protein (PTHrP). The short length and amino acid composition of this pentapeptide ensures its stability and osteostatin has been shown to stimulate osteoblast activity and inhibit osteoclast activity^{294, 295}. The exact mechanism of action is not well understood, partly because the putative receptor through which osteostatin acts is still unknown, but ceramic-based scaffolds coated with osteostatin have, nevertheless, been shown to enhance bone regeneration *in vivo*^{38, 296}. The aim of this study was to determine the potential benefits on bone regeneration of osteostatin-coated porous titanium.

Materials and Methods

Osteostatin-coated porous titanium was evaluated both *in vitro* and *in vivo*. *In vitro*, osteoprogenitor cells were seeded on porous titanium scaffolds with and without osteostatin coating and their proliferation and differentiation were determined. *In vivo*, porous titanium implants with and without osteostatin were used to graft critical-sized cortical bone defects in rats. Bone regeneration was evaluated with *in vivo* and *ex vivo* micro-computed tomography (μ CT), histological analysis and biomechanical torsion testing.

1. Production of osteostatin-coated and uncoated porous titanium

Disk-shaped (\varnothing 8mm x height 3mm) porous scaffolds were used for *in vitro* experiments while femur-shaped porous scaffolds were used as implants for *in vivo* experiments (Figure 1A). Femur-shaped implants were a copy of the femoral bone segment removed during the *in vivo* experiments and had a height of 6mm, a maximum outer diameter of 5mm and a minimal diameter of 1.3mm leaving an open medullary canal. Porous titanium was produced from Ti6Al4V ELI powder (ASTM B348, grade 23) using SLM (Layerwise N.V., Leuven, Belgium). The porous architecture was based on dodecahedron unit cell design with the following dimensions: 120 μ m strut size, 500 μ m pore size, 88% porosity. Post-production, all porous titanium scaffolds underwent an alkali-acid-heat treatment consisting of (1) immersion in a 5M aqueous NaOH solution at 60°C for 24h; (2) immersion in water at 40°C for 24h; (3) immersion in 0.5mM HCl at 40°C for 24h; (4) heating to 600°C at a rate of 5°C/min in an electric furnace in ambient air pressure, holding the temperature at 600°C for 1h, and subsequent natural cooling²⁹². Osteostatin was coated on the titanium surface by soaking the scaffolds in 1ml of 100nM solution of human PTHrP (107-111) (Bachem, Bubendorf, Switzerland) in phosphate-buffered saline (PBS) at 4°C in constant rotation for

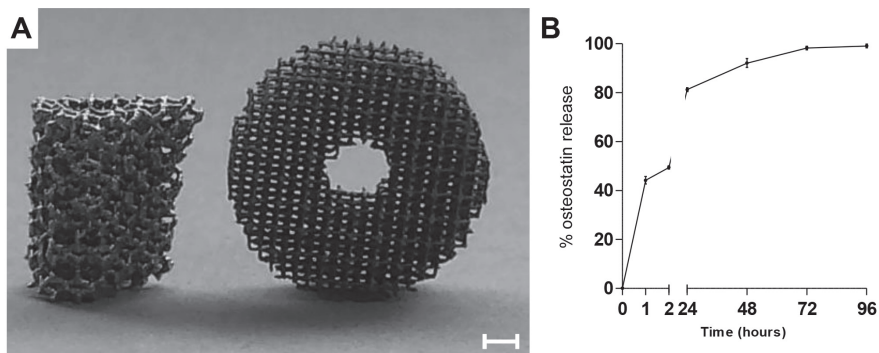


Figure 1: Porous titanium implants coated with osteostatin.

Femur-shaped (left) and disk-shaped (right) porous titanium after alkali-acid-heat treatment (A). Bar indicates 1mm. (B) *In vitro* osteostatin [PTHrP (107-111)] release after loading femur-shaped titanium implants for 24h in 100nM osteostatin in PBS solution (B). Points represent mean \pm SD ($n=3$).

24h. Surface uptake and subsequent release of osteostatin was measured for the rat femur-shaped porous titanium implants through the protein concentration by spectrophotometry absorbance at 280nm, following a standard protocol described elsewhere²⁹⁷.

2. Cell attachment and proliferation

A pool of human periosteal derived cells (hPDCs, six donors, aged 14±2 years, passage 5) were thawed from liquid nitrogen cell bank, expanded in T175 flask, and harvested upon confluence. Cell suspension (*i.e.* 100µl) containing 50,000 cells was drop-seeded onto osteostatin-coated and uncoated disk-shaped scaffolds and incubated statically for 1h to allow cell attachment before being transferred onto a 3D rotator (GrantBio) to perform overnight dynamic rotation seeding²⁹⁸. For cell attachment analysis, cell-seeding efficiency (CSE) was calculated by quantifying total DNA content of the cell-seeded scaffolds ($n=3$) using Quant-iT™ dsDNA HS assay kit (Invitrogen). For cell proliferation assay, cell-seeded scaffolds were transferred into 24-well plates and cultured with DMEM medium (DMEM-GlutaMax™-1, Gibco) containing 10% foetal bovine serum (Gibco), 1% sodium pyruvate, and 1% antibiotics/antimycotics. Then, metabolic activity (PrestoBlue®, Life technologies™) and total DNA content were quantified at defined time points ($n=3$).

3. Cell viability and growth morphology

Cell viability of hPDCs on osteostatin-coated and uncoated scaffolds was determined at 1, 7 and 21 days. Living cells were stained with calcein AM and dead cells with ethidium homodimer (LIVE/DEAD® cell viability kit, Life technologies™). Furthermore, cell morphology was assessed through scanning electron microscopy (SEM). Scaffolds were fixed with 2.5% glutaldehyde, post-fixed with osmium tetroxide, dehydrated in gradually increased alcohol concentrations and chemically dried with hexamethyldisilane. Then, scaffolds were sputtered with gold-palladium coating and cell morphology was observed using SEM coupled with energy dispersive X-ray analysis (FEI XL30 FEG) at 1kV.

4. Osteoblastic, osteoclastic and angiogenic gene expression

Differentiation of hPDCs on osteostatin-coated and uncoated scaffolds was assessed by quantitative, real-time polymerase chain reaction. Briefly, at 1, 7 and 21 days, cells were harvested and the total RNA was extracted using an RNA extraction kit (Qiagen) and subsequently converted into cDNA using cDNA synthesis kit (Fermentas). Expression levels of osteoblastic markers [alkaline phosphatase (*ALP*), collagen type-1 (*Col1*), runt-related transcription factor 2 (*Runx2*), osteocalcin (*OCN*)], osteoclastic markers [receptor activator of nuclear factor kappa-B ligand (*RankL*), osteoprotegerin (*OPG*)], and an angiogenic marker [vascular endothelial growth factor (*VEGF*)] were quantified using Sybr Green primers (Table 1) in a Rotor-Gene sequence detector at 95°C for 3m, 40 cycles of 95°C for 3s, and 60°C for

60s. Expression levels were calculated based on the $2^{-\Delta CT}$ method by normalising values to the housekeeping gene β -Actin.

5. Cortical femoral bone defects in rats

In 20 male Wistar rats, critical-sized cortical femoral bone defects were grafted with osteostatin-coated or uncoated porous titanium implants ($n=10$). The study was approved by Animal Ethics Committee of the Erasmus University (EMC 2811) and Dutch guidelines for care and use of laboratory animals were followed. Prior to surgery, rats were administered antibiotics (enrofloxacin, 5mg/kg body weight) through subcutaneous injection. Surgery was performed aseptically under general anaesthesia (1-3.5% isoflurane). First the right femur was exposed through a lateral skin incision and blunt division of underlying fascia. Then, a 23mm long Poly Ether Ether Ketone (PEEK) plate was fixated to the anterolateral plane using six titanium screws (\varnothing 0.8mm x length 6.5mm). Periosteum was removed over 8mm of the mid-diaphyseal region before a 6mm cortical bone segment was removed with a wire saw and a tailor-made saw guide. Then, an osteostatin-coated or uncoated implant was press-fitted into the defect. Finally, fascia and skin were sutured and pain medication (buprenorphine, 0.05mg/kg body weight) was administered through subcutaneous injection twice a day for three days. Rats were sacrificed after twelve weeks with overdose of pentobarbital (200mg/kg body weight).

6. μ CT evaluation

Bone regeneration was measured using μ CT scans (SkyScan 1076, Bruker micro-CT N.V., Kontich, Belgium). *In vivo* μ CT scans were acquired at four, eight and twelve weeks using a 35 μ m resolution protocol (95kV, 105 μ A current, 1.0mm Al/0.25mm Cu filter, and 0.75 degree rotation step, scan time 14m). Rats were kept under general anaesthesia (1-3.5% isoflurane) during the *in vivo* μ CT scans. *Ex vivo* μ CT scans were acquired after sacrificing the animals using an 18 μ m resolution protocol (95kV, 100 μ A current, 1.0mm Al/0.25mm Cu filter, and 0.5 degree rotation step). μ CT scan images were reconstructed using volumetric reconstruction software NRecon version 1.6.6 (Bruker micro-CT N.V., Kontich, Belgium).

Bone regeneration was expressed as bone volume (BV), which was measured at four specific regions: (1) total BV: the total volume of bone formed within the 6mm defect; (2) outer BV: the bone formed outside the implants; (3) porous BV: the bone formed inside the porous space of the implants; and (4) inner BV: the bone formed in the medullary canal of the implants. BV values were measured using CTAnalyser version 1.13 (Bruker micro-CT N.V., Kontich, Belgium). First the specific region was selected, then the titanium and its border artefacts was excluded from images using a global threshold and by removal of an extra 35 μ m border. Subsequently bone was captured using a second global threshold. Global thresholds were based on visual inspection and were kept constant for all scans. Bone bridging was determined by measuring the shortest remaining gap size between bone

formed at the proximal and distal side of the defect on *ex vivo* scans with DataViewer 1.4 (Bruker micro-CT N.V., Kontich, Belgium).

7. Biomechanical evaluation

The mechanical strength of grafted femurs, and hence the biomechanical functionality of the implants, was measured through torsion tests conducted on eight femurs per group. After sorting all ten grafted femurs according to their total BV after twelve weeks, the two middle femurs were retained for histological analysis, leaving the rest for biomechanical testing. Three contralateral intact femurs were included as controls. After harvesting the femurs, soft tissues and PEEK plates were carefully removed. Specimens were kept in 10% neutral buffered formalin solution for two days, minimizing the effect of formalin conservation on mechanical properties²⁹⁹, and then transferred to PBS. Subsequently, both ends of each femur were embedded in a cold-cured epoxy resin (Technovit 4071, Heraeus Kulzer GmbH, Wehrheim, Germany). On the upper clamping side, the use of a Cardan joint ensured pure rotation without bending. The lower sides were simply fixed. Torsional strength (maximum torque to failure, N.mm) was determined with a rotation rate of 0.5°s^{-1} until failure using a static mechanical testing machine (Zwick GmbH, Ulm, Germany).

8. Histological evaluation

Histology was performed on two femurs. Harvested femurs were fixed in 10% neutral buffered formalin solution for two days, dehydrated in graded ethanol solution from 70 to 100%, and finally embedded in methyl methacrylate. Sections of $\sim 20\mu\text{m}$ were obtained using a diamond saw (Leica SP1600, Rijswijk, the Netherlands) and stained with basic fuchsin 0.3% solution to colour bone tissue purple and methylene blue 1% solution to colour fibrous tissue blue.

9. Statistics

Statistical analyses were performed using SPSS Statistics 20.0 (SPSS Inc, Chicago, Ill). Data is presented as means \pm standard deviation (SD). For *in vitro* experiments, a one-way ANOVA was performed for each time point. For *in vivo* experiments, a linear mixed model was used to determine the interaction between treatment and time and to determine the overall effect of treatment. *Ex vivo* measurements (bone regeneration and biomechanical strength) were tested with an unpaired student's *t*-test. A power calculation (β -value >0.80 , SD $\sim 25\%$) was made to find a true difference in bone regeneration or biomechanical strength of at least 35%. Based on this calculation, $n=10$ was required per experimental group. A *p*-value <0.05 was considered statistically significant.

Results

1. Uptake and release profiles of osteostatin-coated porous titanium

SLM-produced porous titanium scaffolds had an 85% porosity with struts of $163 \pm 43 \mu\text{m}$ and a median pore size of $600 \mu\text{m}$ (range $460\text{--}670 \mu\text{m}$) (Figure 1A). The disk-shaped and femur-shaped scaffolds had a total surface area of respectively $561 \pm 11 \text{mm}^2$ and $314 \pm 47 \text{mm}^2$. The as-produced surface morphology was transferred into nano-scale organized, rod-like TiO_2 crystals by the alkali-acid-heat treatment (Figure 2)³⁰⁰. After soaking for 24h, 30% of the osteostatin in the solution was taken up by the femur-shaped scaffolds, equivalent to 0.02ng peptide/ mm^2 scaffold. This was confirmed by measuring 70% of osteostatin in the remaining solution and resulted in a cumulative dose of $4.7 \pm 0.7 \text{ng}$ osteostatin per femur-shaped scaffold. These femur-shaped scaffolds released $44.2 \pm 1.5\%$ of the osteostatin within 1h, $81.3 \pm 0.8\%$ within 24h, and $98.3 \pm 0.7\%$ within 72h (Figure 1B).

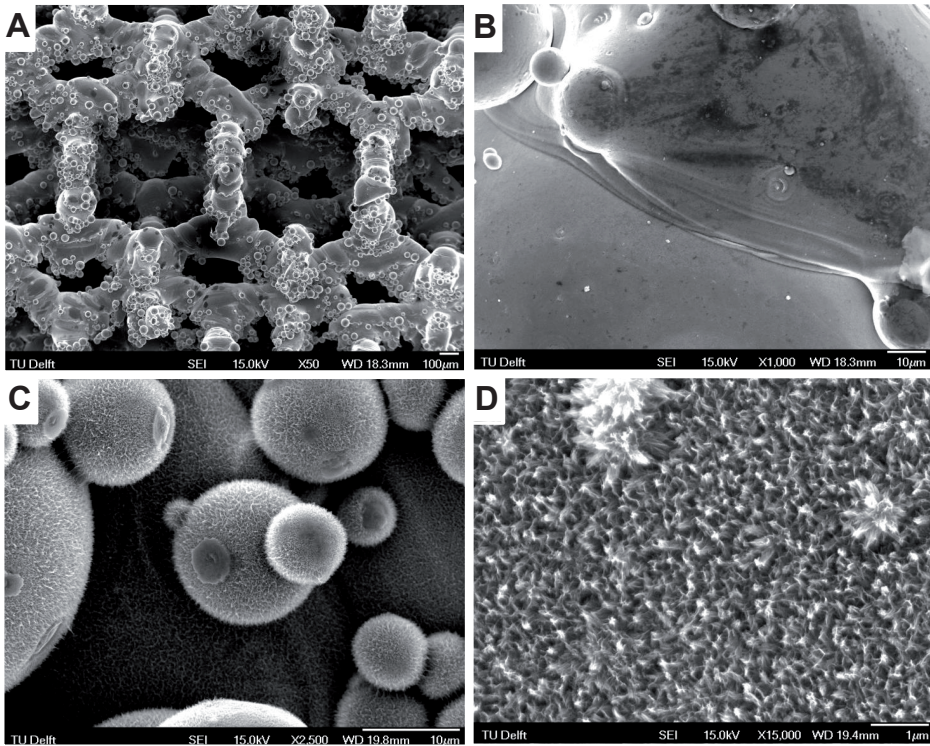


Figure 2: SEM images showing the surface morphology of porous titanium.

Low magnification image of the dodecahedron structure of the porous titanium (A), High magnification image of the as-produced surface morphology (B). High magnification images of the surface morphology after alkali-acid-heat treatment showing the nano-scale organized, rod-like crystal throughout the surface (C-D).

2. Cell attachment and proliferation

Cell-seeding efficiency of hPDCs on osteostatin-coated as well as uncoated scaffolds was ~30% (Figure 3A). Cell proliferation (Figure 3B) and cell metabolic activity (Figure 3C) steadily increased during the 21 days culture period, but on average osteostatin did not lead to significantly more cell activity or proliferation. Only at day 7, total DNA content showed a trend towards more proliferation of hPDCs on osteostatin-coated scaffolds (3008 ± 350 ng versus 2135 ± 609 ng, $p=0.098$).

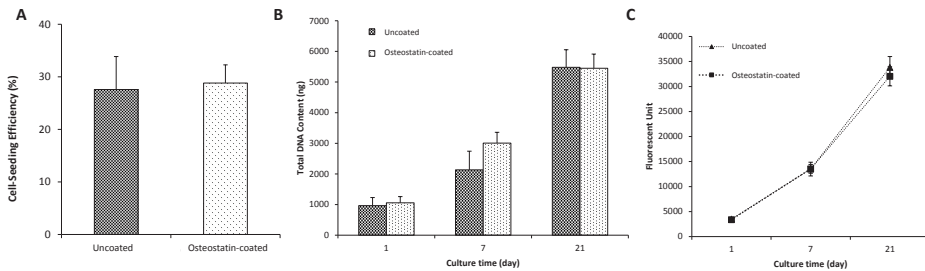


Figure 3: Cell-seeding, proliferation and metabolic activity.

Cell-seeding efficiency (%) after overnight dynamic rotation seeding of 50,000 human periosteum-derived cells (hPDCs) onto osteostatin-coated and uncoated scaffolds (A). Cell proliferation, expressed as total DNA content after culturing hPDCs on implants for 1, 7 and 21 days (B). Metabolic activity of hPDCs cultured on scaffolds, expressed with fluorescent units, after 1, 7 and 21 days (C).

3. Cell viability and growth morphology

Cells attached to osteostatin-coated and uncoated titanium remained viable during the 21 days culture period (Figure 4). Cells were already clearly attached after 1 day, but cell morphology changed from a small rounded shape towards a long and elongated shape at 21 days. No clear differences were observed between cells on osteostatin-coated or uncoated surfaces.

4. Osteoblastic, osteoclastogenic and angiogenic gene expression

Gene expression of *OPG*, an osteoclastogenic marker, was significantly altered with osteostatin-coated scaffolds, whereas osteogenic and angiogenic markers did not show a significant difference (Figure 5). Osteostatin upregulated *OPG* at day 1 ($p<0.05$) and *RankL* was considerably downregulated. As a consequence the *RankL:OPG* ratio was significantly lower for osteostatin-coated scaffolds. At day 21, osteostatin downregulated *OPG* ($p<0.05$) whereas the expression of the other osteogenic (*ALP*, *Col1*, *OCN*, *Runx2*) or angiogenic (*VEGF*) markers measured was not altered through the presence of the osteostatin-coating on the porous titanium implants (Figure 5).

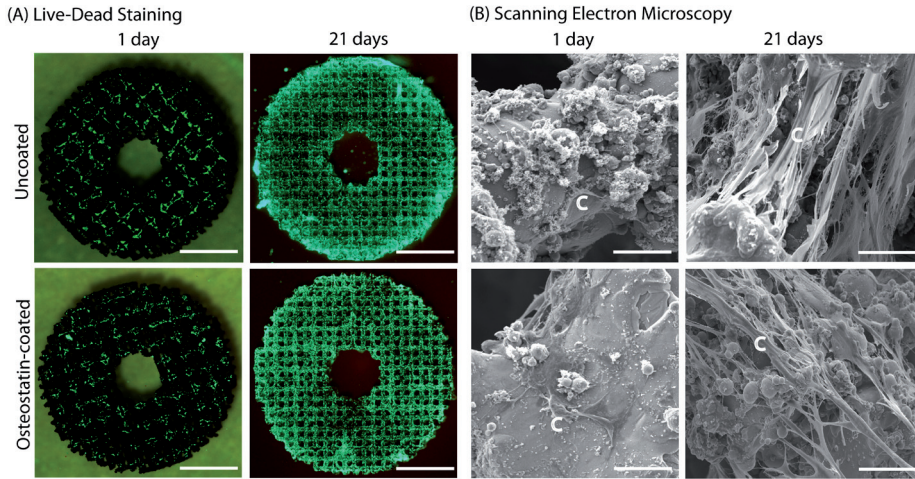


Figure 4: Live-dead staining and SEM images.

Live-dead staining of cell-seeded cylindrical porous titanium scaffolds after 1 and 21 days of culture (A). Viable cells are stained green, dead cells are stained red. White bars indicate 2mm. Scanning electron microscopy of the titanium surface after 1 and 21 days of culture (B), "C" indicates a cell. White bars indicate 50µm.

5. Cortical femoral bone defects in rats

Rats were able to tolerate load-bearing immediately after grafting the defects and all surgical sites healed uneventfully. One rat that received an osteostatin-coated implant was found dead after ten weeks, the cause of death could not be determined and this rat was excluded from further analysis.

6. µCT evaluation

Grafting femur defects with osteostatin-coated porous titanium implants led to more bone regeneration. Although the interaction between time and treatment was not significant ($p=0.09$), running the linear mixed model without the interaction term showed that the main effect of both treatment and time were highly significant ($p=0.005$, $p<0.001$ respectively). After four weeks, total BV of osteostatin-coated implants was $18.5\pm 8.0\text{mm}^3$ compared to $10.4\pm 3.5\text{mm}^3$ of uncoated implants (Figure 6A). Bone regeneration predominantly occurred outside the implant (Figure 6B; outer BV $9.7\pm 5.6\text{mm}^3$ versus $4.4\pm 1.8\text{mm}^3$) and to some extent inside the implant (Figure 6C; porous BV $6.0\pm 2.9\text{mm}^3$ versus $3.7\pm 1.9\text{mm}^3$), but the amount of bone formed within the medullary canal was similar for osteostatin-coated and uncoated implants (Figure 6D; inner BV $2.8\pm 0.9\text{mm}^3$ versus $2.3\pm 1.5\text{mm}^3$).

The total BV of grafted defects continued to increase throughout the follow-up. Osteostatin-coated implants resulted in a total BV of $33.2\pm 18.1\text{mm}^3$ (versus $24.3\pm 13.1\text{mm}^3$ with uncoated implants) after eight weeks and a total BV of $38.5\pm 20.9\text{mm}^3$ (versus $33.7\pm 16.8\text{mm}^3$ with uncoated implants) after twelve weeks. Most bone had formed outside the implants:

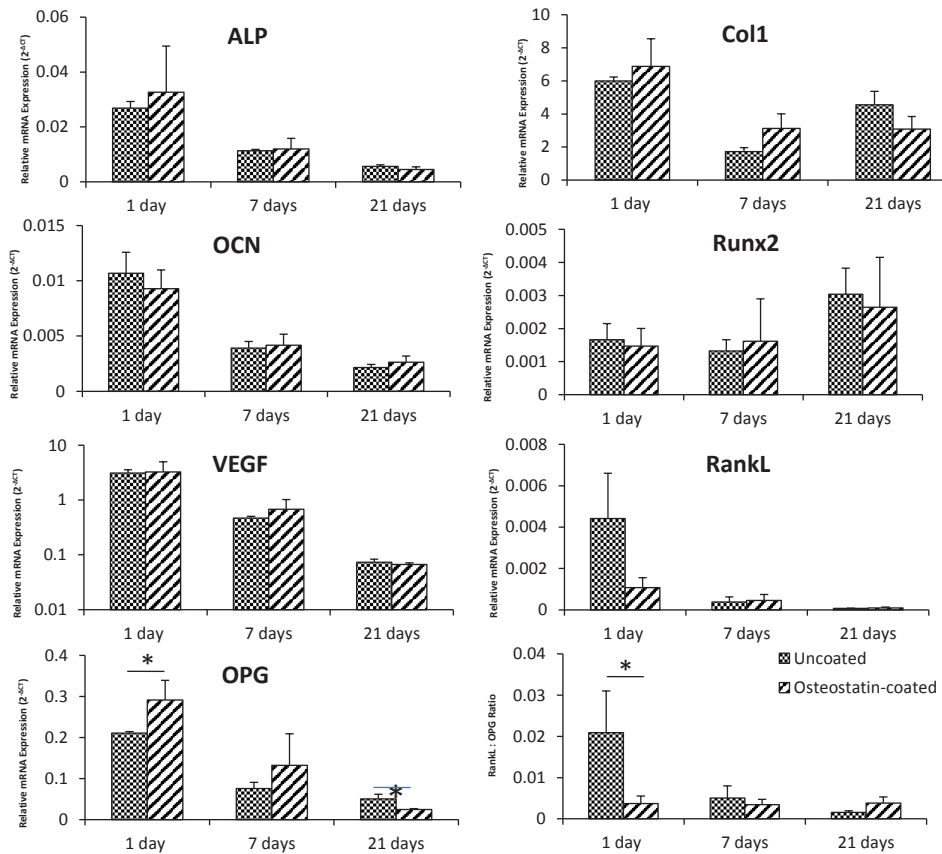


Figure 5: Expression of osteogenic and angiogenic markers.

Effects of osteostatin-coated and uncoated scaffolds on expression of osteogenic markers: (A–D) alkaline phosphatase [*ALP*], collagen type-1 [*Col1*], runt-related transcription factor 2 [*Runx2*], and osteocalcin [*OCN*]. Expression of angiogenic marker and osteoclastogenic markers: (E) vascular endothelial growth factor (*VEGF*), (F–H) receptor activator of nuclear factor kappa-B ligand [*RankL*], osteoprotegerin [*OPG*], and *RankL:OPG* ratio. Expression levels shown are based on the $2^{-\Delta CT}$ method, to normalize values to that of the housekeeping gene. Horizontal bars are used to indicate statistical significant differences ($p < 0.05$).

outer BV was $49 \pm 15\%$ of the total BV for osteostatin-coated implants, and $43 \pm 7\%$ of the total BV for uncoated implants. Porous BV reached $14.2 \pm 6.8 \text{ mm}^3$ with osteostatin and $13.6 \pm 8.3 \text{ mm}^3$ without osteostatin, meaning that respectively $25 \pm 13\%$ and $23 \pm 13\%$ of the porous space was occupied by regenerated bone.

Bone bridging of grafted defects progressed throughout the twelve weeks follow-up and this is clearly shown on *in vivo* μCT scans (Figure 7). Between eight and twelve weeks, bone resorption of adjacent cortical bone was seen when uncoated implants were used (Figure 7). After twelve weeks, the remaining gap of defects grafted with osteostatin-coated implants measured $1.0 \pm 0.8 \text{ mm}$, which was not significantly different from the uncoated implants where a remaining gap of $1.8 \pm 1.5 \text{ mm}$ was measured (Figure 8A and B). Nearly complete

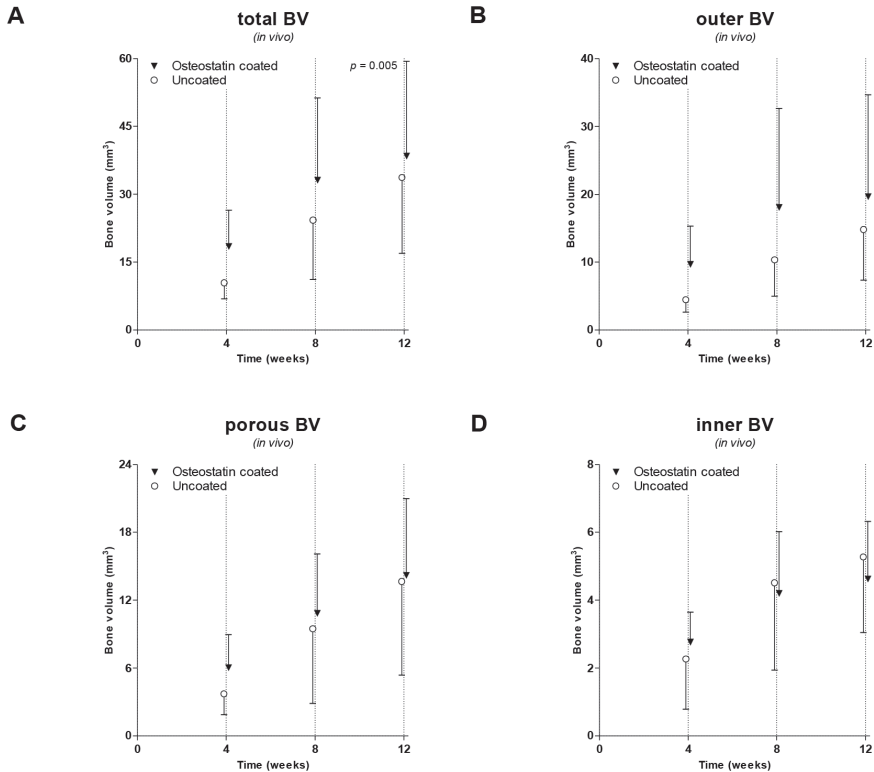


Figure 6: Bone regeneration quantified on *in vivo* μ CT scans made after four, eight and twelve weeks.

Total BV; defined as all bone formed within the 6mm defect (A). Outer BV, defined as bone formed outside the implants (B). Porous BV, defined as bone formed inside the porous space of the implants (C). Inner BV, defined as bone formed in the medullary canal of the implant (D). Values are expressed as mean \pm SD ($n=10$), and a linear mixed model was performed to assess statistical significant differences. A p -value <0.05 was considered as statistically significant.

bridging (defined as gap <0.5 mm) was seen in three defects grafted with osteostatin-coated implants and in two defects grafted with uncoated implants.

7. Biomechanical evaluation

Seven femurs grafted with osteostatin-coated implants, eight femurs grafted with uncoated implants, and three intact femurs were successfully embedded in epoxy resin and subjected to torsion testing. The average maximum failure torque with osteostatin-coated implant was 97 ± 31 N.mm, compared to 77 ± 53 N.mm with uncoated implants (Figure 8C), this was not statistically significant. All femurs failed from the interface of bone-implant except for one, which failed through the implant. Failure torque of femurs with osteostatin-coated implants and uncoated implants reached, respectively, 66% and 53% of that of intact femurs, *i.e.* 146 ± 19 N.mm.

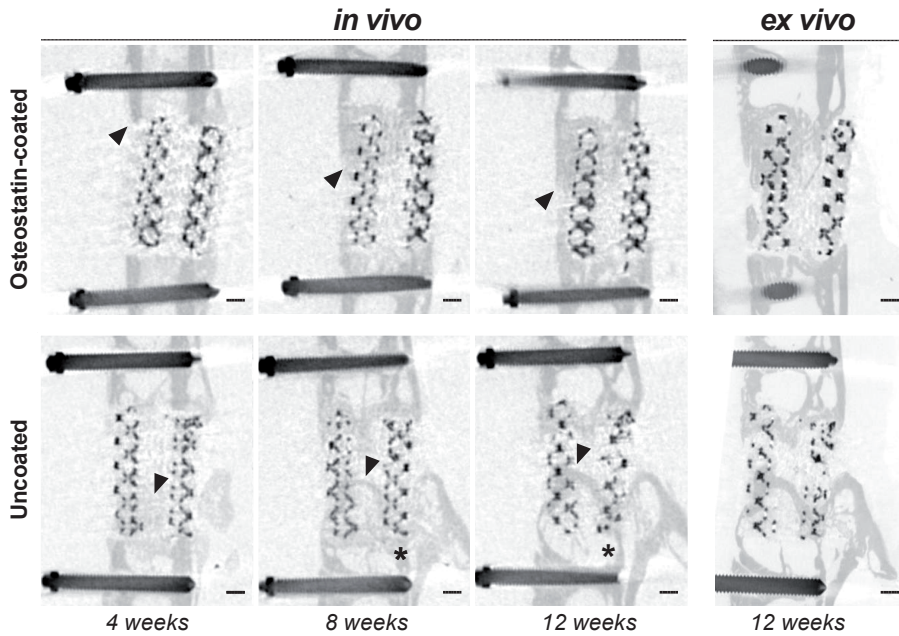


Figure 7: Representative *in vivo* and *ex vivo* μ CT images.

Femur defect grafted with osteostatin-coated (top row) or uncoated (bottom row) porous titanium implants (longitudinal cross-section). Titanium implants and fixation screws appear in black, whereas bone appears in dark grey. Arrows indicate progression of bony bridging during follow-up period. Asterisk depicts area of bone resorption. Black bar indicates 1mm.

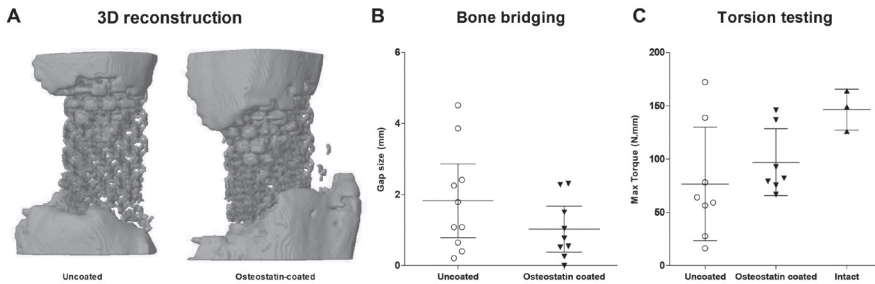


Figure 8: Bone bridging and mechanical strength.

Representative 3D μ CT images of bone bridging upon grafting with osteostatin-coated or uncoated porous titanium implants at twelve weeks (A). Porous titanium implants are shown in transparent grey, whereas bone appears in dark grey. Remaining bone gap (mm) after twelve weeks measured on *ex vivo* μ CT scans (B). Maximum torque to failure (N.mm) during torsion testing of grafted and intact femurs (C). Values are expressed as mean and 95% confidence interval, and an unpaired student's *t*-test was performed to assess for statistical significant differences. A *p*-value <0.05 was considered as statistically significant.

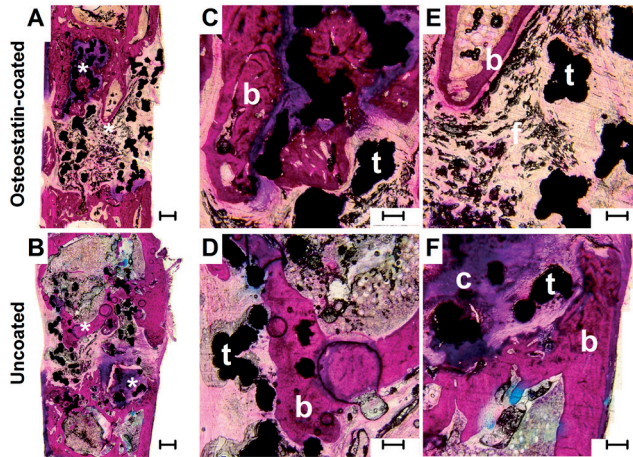


Figure 9: Histological sections of osteostatin-coated and uncoated porous titanium implants.

Representative histological transversal sections of bone defects grafted with osteostatin-coated (upper row) and uncoated (bottom row) porous titanium implants. Sections are stained with basic fuchsin and methylene blue. Basic fuchsin stains bone purple, methylene blue stains fibrous tissue blue. Low magnification overview, black bar indicates 500µm (A, B). Detailed view of areas as noted with an asterisk in A and B (C-F), respectively, 't' indicates titanium, 'b' indicates bone tissue, 'c' indicates cartilage-like tissue and 'f' indicates fibrous-like tissue. Bar represents 200µm.

8. Histological evaluation

Histological evaluation showed no distinct differences in terms of bone morphology or bone-titanium interface between osteostatin-coated and uncoated porous implants at twelve weeks (Figure 9A and B). Regenerated bone consisted mainly of non-woven bone, and direct bone-titanium contact was observed at the proximal and distal sites of the implants (Figure 9C and D). The remaining non-bridged bone gap was mainly filled with fibrous tissue (Figure 9D and E). Occasionally there were also areas of the bone-titanium interface found with a cartilage-like or fibrous-like zone in both groups (Figure 9C and F).

Discussion

An ideal bone graft substitute provides immediate mechanical support and enhance bone regeneration that allows repair of critical-sized bone defects in a short period of time ²⁸⁰. A promising biomaterial suitable to provide sufficient mechanical support to load-bearing bone defects is porous titanium ³⁵. In this study, we showed that the performance of porous titanium can be improved with an osteostatin-coating; since osteostatin-coated implants showed an increase in bone regeneration *in vivo* (Figure 6 and 7).

Osteostatin is a pentapeptide domain (107-111) of PTHrP. PTHrP consists of three major domains and acts as an important modulator of bone formation and bone remodelling ³⁰¹.

The actions of its N-terminal domain (1-36), which shows homology to PTH, are a consequence of the interaction with the PTH/PTHrP receptor 1 (PPR). But the native C-terminal domain (107-139), including osteostatin, seems to act through a PPR-unrelated receptor and increases osteoblast survival and osteoblastic differentiation *in vitro*^{294, 302, 303}. Also, osteostatin was found to enhance bone regeneration *in vivo* in metaphyseal bone defects in rabbits^{37, 38}. These trophic effects, together with its short peptide sequence (Thr–Arg–Ser–Ala–Trp) warranting its stability, make osteostatin an interesting peptide to use as an organic surface coating aimed to enhance bone regeneration of porous titanium.

The SLM-produced porous titanium underwent a post-production alkali-acid-heat treatment³⁰⁴, resulting in a titanium dioxide layer on the surface and altering the surface topography (Figure 2), which has been shown to increase bone regeneration^{276, 292}. Subsequently, this titanium surface was coated with osteostatin by a soaking method used previously for loading osteostatin onto ceramics^{37, 294}. Osteostatin adhesion onto the titanium surface is most likely based on van der Waals' interactions between the indole ring in the C-terminal tryptophan of osteostatin and titanium dioxide and this resulted in a low dose of osteostatin on the surface (0.02ng/mm²). These relatively weak van der Waals' interactions also explain the fast release of osteostatin (Figure 1B). This prompt release was similar to the release of osteostatin from ceramics, and had been capable to enhance trabecular bone volumes of metaphyseal bone defects in rabbits^{37, 38}. This fast release might even be an requisite, since a constant delivery of PTH results in bone resorption whereas only intermittent administration of PTH and PTHrP improved bone mass and bone healing³⁰⁵⁻³⁰⁹. Intermittent administration induces a transient increase in *RankL* that could result in more osteoclastic resorption³¹⁰. The release of osteoblastic growth factors from the resorbed bone matrix can be a source of osteogenic signals that contribute to PTH-induced anabolism. *RankL* may also stimulate the secretion of osteoblastic factors by osteoclasts³¹⁰. Intermittent administration of PTHrP (107-139) also reduced the *RankL:OPG* ratio in human osteoblastic cells *in vitro*³¹¹. These observed differences on bone regeneration between constant and intermittent administration of PTH and PTHrP suggest that altering the pace or dose of osteostatin administration could potentially improve but also diminish its trophic effects on bone regeneration, and improving the osteostatin-coating on titanium surfaces is therefore an interesting topic. Osteostatin-coating on titanium surfaces might be improved using more advanced titanium surface treatments. One treatment that we previously have applied to our porous titanium implants is an anodizing technique that results in the formation of regular and adjustable TiO₂ nanotubes²⁹². Anodizing is especially interesting since others have shown that the size of these TiO₂ nanotubes can be tailored to function as small drug reservoir³¹², and this could be used to improve the osteostatin administration in future research.

Culturing osteoprogenitor cells *in vitro* on porous titanium scaffolds showed a significant effect of osteostatin on the *RankL:OPG* gene expression ratio, leading to a reduction of this ratio at day one (Figure 5). As already mentioned, the *RankL/OPG* system is a major

signalling pathway that regulates differentiation and function of osteoclasts³¹³. *RankL* promotes whereas *OPG* inhibits bone resorption³¹⁴, and this is consistent with the observed accelerated bone regeneration after four weeks *in vivo* (Figure 6). These results are in line with previously published *in vitro* experiments using a mouse osteoblast cell line (MC3T3-E1), showing that *RankL* expression was significantly reduced by addition of osteostatin to cultures at day two and four²⁹⁴. Moreover, in the latter cell line, it was found that osteostatin increased both *OPG* and *VEGF* gene expression through *Src* activation, which presents a mechanism for modulation of osteoblast activity and function³¹⁵. The fact that we did not see a difference in *VEGF* gene expression or expression of osteogenic genes upon osteostatin treatment of hPDCs – in contrast to previous observations in MC3T3-E1 cells^{294,315} – may be explained by differences in: (1) used cell type or (2) time-dependent effects of osteostatin. MC3T3-E1 cells represent immature osteoblasts, whereas hPDCs are multipotent mesenchymal stromalcell-like osteoprogenitors and in previously conducted experiments, the upregulation of osteogenic genes (e.g. *ALP* and *OCN*) was already found to be time-dependent²⁹⁴.

Grafting cortical bone defects with osteostatin-coated porous titanium implants showed significantly more bone regeneration (Figure 6). After four, eight and twelve weeks the difference in total BV was respectively 8mm³, 9mm³ and 5mm³, and this suggest that the advantage of osteostatin-coating decreased over time. However, the interaction of time and treatment only showed a statistical trend ($p=0.09$), more power is necessary to support this observation. Also no significant differences in bone regeneration nor biomechanical strength were found *ex vivo*. Again, we believe this is mainly caused by the limited power of our study design. Due to variability in the surgical procedure and animal response, this bone defect model has a large standard deviation. The group size was not suitable for detecting statistical significant differences that were smaller than 35%. Thus, the observed differences of defects grafted with osteostatin-coated porous titanium implants found after twelve weeks (14% more bone regeneration, 13% increase in biomechanical strength), did not pass the significant threshold imposed by the group size used and require the use of a larger sample size. Additionally have we recently shown that there is a large variation in the degree of implant fixation in our model³¹⁶. This variation, which may allow for excessive micromotion, can explain the observation of a fibrocartilage interface at certain areas of the titanium-bone interface (Figure 9C and F) and needs to be reduced by improving implant fixation.

Porous titanium implants were shown to enhance bone regeneration through osteoconduction^{270, 291, 317-319}. However, to become suitable for grafting load-bearing defects they should be strong enough to sustain mechanical loading but not overly stiff to avoid stress shielding and implant loosening. The mechanical properties of the porous titanium implants used was measured earlier^{290, 319} and are as follows: 14MPa compression strength, 0.4GPa Young's modulus and a fatigue life long enough to allow bone ingrowth and osseointegration. This is sufficient to allow immediate weight-bearing in femur defects and restored up to respectively 53% (uncoated group) and 66% (osteostatin-coated group) of its original

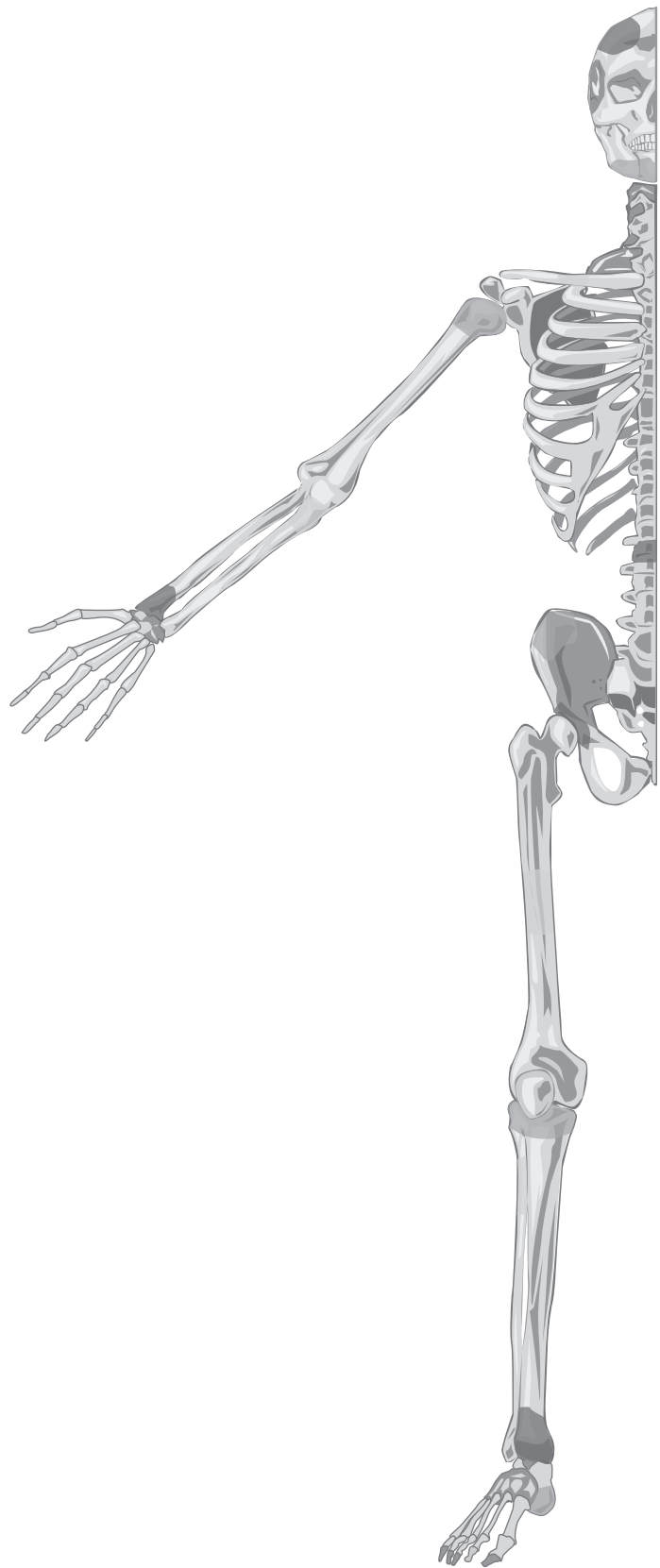
strength (Figure 9). Restoration of mechanical strength is one of the main goals of bone grafting, but the minimal difference in favour of the osteostatin-coated group found here was not significant. A power calculation made based on this data (α -value = 0.05, β -value = 0.80) indicates that an $n=50$ per group would be required to determine if this difference is significant. However, these results were in line with previous experiments^{252, 319}, and underline the potential of porous titanium as a load-bearing osteoconductive scaffold. Combining this load-bearing osteoconductive scaffold with an osteostatin coating capable of enhancing early bone regeneration further improves and accelerates the repair of cortical bone defects grafted with porous titanium implants and might lead to the development of new implants suitable as bone grafts substitutes or implants in trauma, orthopaedic or craniomaxillofacial surgery^{35, 320}.

Conclusions

In this study, osteostatin was used as an organic surface coating to improve bone regeneration upon implantation of porous titanium. *In vivo* experiments showed that porous titanium scaffolds coated with osteostatin enhanced early bone regeneration in critical-sized femoral bone defects in rats. *In vitro* experiments showed that osteostatin results in an early upregulation of *OPG* gene expression, altering the *RankL:OPG* ratio which might be mechanism of action through which *in vivo* early bone regeneration is increased. Optimizing the dose and pace of osteostatin release from the titanium surface remains an interesting topic for future *in vivo* experiments and may show more profound long term effects of osteostatin on bone regeneration of cortical bone defects grafted with porous titanium implants.

Acknowledgements

This research forms part of the Project P2.04 BONE-IP of the research program of the BioMedical Materials Institute, co-funded by the Dutch Ministry of Economic Affairs. D. Lozano has a post-doctoral contract from Spanish Comunidad Autónoma de Madrid (S2009/MAT-1472). Y.C. Chai is a post-doctoral fellow of the Research Foundation-Flanders (FWO: 1.5.172.13N - Interdisc).



Chapter 7

Porous titanium implants incorporated with growth factor-loaded gelatin gels

Johan van der Stok

Huanan Wang

Saber Amin Yavari

Michiel Siebelt

Marjan Sandker

Jan H. Waarsing

Jan A.N. Verhaar

Holger Jahr

Amir A. Zadpoor

Sander C. Leeuwenburgh

Harrie Weinans

Published as “Enhanced Bone Regeneration of Cortical Segmental Bone Defects Using Porous Titanium Scaffolds Incorporated with Colloidal Gelatin Gels for Time- and Dose-Controlled Delivery of Dual Growth Factors” in *Tissue Engineering Part A*. 2013 Dec;19(23-24):2605-14.

Abstract

Porous titanium implants are a promising class of biomaterials for grafting large bone defects, because titanium provides sufficient mechanical support, whereas its porous structure allows bone ingrowth resulting in good osseointegration. To reinforce porous titanium implants with biological cues that enhance and continue bone regeneration, implants can be incorporated with bioactive gels for time and dose controlled delivery of multiple growth factors (GFs). In this study, critical-sized cortical femoral bone defects in rats were grafted with porous titanium implants incorporated with nanostructured colloidal gelatin gels. Gels were loaded with bone morphogenetic protein-2 (BMP-2, 3 μ g), fibroblast growth factor-2 (FGF-2, 0.6 μ g), BMP-2, and FGF-2 (BMP-2/FGF-2, ratio 5:1) or were left unloaded. GF delivery was controlled by fine-tuning the crosslinking density of oppositely charged nanospheres. Grafted femurs were evaluated using *in vivo* and *ex vivo* μ CT, histology, and three-point bending tests. All porous titanium implants containing GF-loaded gels accelerated and enhanced bone regeneration: BMP-2 gels gave an early increase (0-4 weeks), and FGF-2 gels gave a late increase (8-12 weeks). Interestingly, stimulatory effects of 0.6 μ g FGF-2 were similar to a fivefold higher dose of BMP-2 (3 μ g). BMP-2/FGF-2 gels gave more bone outside the porous titanium implants than gels with only BMP-2 or FGF-2, resulted in bridging of most defects and showed superior bone-implant integrity in three-point bending tests. In conclusion, incorporation of nanostructured colloidal gelatin gels capable of time and dose controlled delivery of BMP-2 and FGF-2 in porous titanium implants is a promising strategy to enhance and continue bone regeneration of large bone defects.

Introduction

Regeneration of large bone defects remains a challenging topic in trauma, orthopaedic and maxillofacial surgery²⁸⁰. Despite availability of several biomaterials for bone grafting³²¹, autologous bone remains the clinical gold standard⁴⁴. Nevertheless, well-known drawbacks (e.g. limited amounts and donor site morbidity¹²) provide continuous incentive to develop new biomaterials. A promising new biomaterial for large bone defects is porous titanium. Porous titanium implants directly provide mechanical support after implantation while the porous structure acts as an osteoconductive⁹ implant that facilitates bone regeneration³¹⁹. However, to further enhance and continue bone regeneration in large bone defects, it is necessary to reinforce the bioinert titanium with biological cues stimulating bone regeneration.

Bone regeneration is a cascade of events strongly regulated by spatial and temporal presentation of angiogenic and osteogenic growth factors (GFs)³²². Angiogenic GFs such as fibroblast growth factor-2 (FGF-2) are expressed during early stages of bone regeneration^{322, 323}. In contrast, osteogenic GFs such as bone morphogenetic factor-2 (BMP-2) are expressed in later stages³²⁴. Mimicking this spatiotemporal presentation of GFs by controlled delivery from carrier materials is considered a powerful tool to stimulate bone regeneration³²⁵. Conventional carrier materials (e.g. collagen sponges) have shown poor capacity to control GF delivery, and therefore require a high dose of GF to reach therapeutic effects. However, high doses of GF, especially BMP-2, can cause serious side effects including bone tissue overgrowth, ectopic bone formation, inflammation, and even carcinogenicity³²⁶. This underlines the need for new carrier materials capable of time and dose controlled delivery of multiple GFs³²⁴.

To this end, a new generation of carrier materials recently emerged are shear-thinning and self-healing colloidal gels^{327, 328}. Nanostructured colloidal gels made of oppositely charged gelatin nanospheres can control GF delivery by tailoring the degradation rate of the subpopulation of charged gelatin nanospheres within the gel network. It has been shown that by separately loading FGF-2 and BMP-2 using different species of charged gelatin nanospheres and fine-tuning the cross-linking densities of gelatin particles a sequential release of dual GFs, in terms of early delivery of FGF-2 and sustained delivery of BMP-2, can be obtained³⁹. However, due to the inappropriate dose combination between FGF-2 and BMP-2, the dual GFs delivery resulted into an inhibitory effect on bone regeneration^{329, 330}.

The aim of this study is to enhance bone regeneration of large bone defects using porous titanium implants incorporated with nanostructured colloidal gelatin gels for time and dose controlled delivery of a nanogram dose of FGF-2 and/or a microgram dose of BMP-2. We hypothesize that grafting cortical femoral bone defects in rats with porous titanium implants containing BMP-2/FGF-2 gels results in more bone regeneration than implants containing BMP-2 gels, FGF-2 gels, or unloaded gels. To test this hypothesis, bone regeneration was evaluated using *in vivo* and *ex vivo* μ CT, histology, and three-point bending tests.

Materials and methods

1. Materials

Gelatin A (Gela, from porcine skin, 300 Bloom, isoelectric point (IEP) ~9) and gelatin B (GelB from bovine skin, 225 Bloom, IEP ~5) were purchased from Sigma-Aldrich. Glutaraldehyde (GA, 25 wt% solution in water) was commercially available from Acros Organics. Recombinant human BMP-2 (molecular mass 26kDa (dimer), IEP 7) was purchased from Shanghai Rebone Biomaterials Co., China, and recombinant human FGF-2 (molecular mass 16kDa, IEP 9.6) were supplied by R&D Systems.

2. Preparation and characterization of GF-loaded colloidal gelatin gels

Colloidal gelatin gels were made of oppositely charged gelatin nanospheres³³¹. Briefly, gelatin nanospheres were obtained using a desolvation method and cross-linked using GA. A cross-linking density (defined as molar ratios of GA relative to $[\text{NH}_2]_{\text{gelatin}}$) of one (low) or four (high) was applied to Gela and GelB nanospheres, respectively. That resulted in positively charged Gela and negatively charged GelB nanospheres. Particles size and ζ -potential of gelatin nanospheres were measured using dynamic light scattering (DLS, Zetasizer Nano-Z, Malvern Instruments Ltd.) (Table 1). Lyophilized Gela or GelB nanospheres were mixed with aqueous 1mM NaCl solutions (pH 7) in two separate 1ml BD[®] Luer-lok[™] syringes. A homogeneous gel was obtained by repeated extrusion from both syringes while being connected by a Luer-lok[™] connector. BMP-2/FGF-2 gels were made mixing Gela nanospheres with NaCl solution containing 22 $\mu\text{g/ml}$ FGF-2 and mixing GelB nanospheres with NaCl solution containing 110 $\mu\text{g/ml}$ BMP-2. BMP-2, FGF-2 or unloaded gels were obtained by mixing Gela, GelB or both with 1mM NaCl solution only (Table 2). Gels (solid content of 20 w/v%) were stored at 4°C overnight to allow for complete swelling and GF absorption. Viscoelastic properties were characterized using a rheometer (AR2000ex, TA Instruments). Measurements to assess shear-thinning and self-healing behaviour were performed within the linear viscoelastic region using a flat steel plate geometry (20mm diameter) at 25°C. Briefly, gels were gradually destroyed by applying an oscillatory strain sweep with shear strain increasing from 0.1% to 1000% (1 Hz frequency), meanwhile viscoelastic properties (G' and G'') were monitored. Thereafter, an oscillatory time sweep (5min, 1% strain, 1Hz frequency) was instantaneously applied and gel recovery was recorded.

Table 1. Characteristics of Gela and GelB nanospheres (NS)

Characteristics	Gela NS	GelB NS
Cross-linking density	low (GA/NH ₂ = 1)	high (GA/NH ₂ = 4)
Particle size (swollen state)	430±4nm	247±2nm
Zeta-potential	+9.3±0.3mV	-20.0±0.4mV

Table 2. Preparation of (GF-loaded) colloidal gelatin gels

Gels	GelA	GelB
Unloaded	-	-
FGF-2	22µg/ml FGF-2	-
BMP-2	-	110µg/ml BMP-2
BMP-2/FGF-2	22µg/ml FGF-2	110µg/ml BMP-2

3. Incorporation of GF-loaded gels into porous titanium implants

Selective laser melting (SLM) technique was used to produce porous titanium implants in the shape of the cortical femoral bone segment removed during the animal experiment (Figure 1A) ³¹⁹. The porous structure was based on a dodecahedron template designed with 120µm thick titanium struts and pores ranging from 240 to 730µm. Porosity, compression strength and Young’s modulus are given in Table 3. Post-production, implants underwent an alkali-acid-heat treatment as described previously ²⁷⁶.

Gels were incorporated into the implants using a custom-made gel chamber prior to surgery. First, a implant was placed inside the gel chamber and subsequently the gel chamber was connected to the Luer-lok™ syringes that contained the gels. Then an excess of gel was injected into the chamber resulting in complete filling of the porous titanium implant. Gel-loaded titanium implants were left inside the gel chamber and stored at 4°C until implantation at which superfluous gel around the implants was removed (Figure 1B). Filling efficacy of porous space was visualized using µCT and scanning electron microscopy (SEM). Therefore the gel was prepared with a contrast agent (Hexabrix 320®, Mallinckrodt, Hazelwood, MO, USA) subsequently scanned with a SkyScan 1176 µCT scanner (Bruker micro-CT N.V., Kontich, Belgium). Complete filling of the porous space (55mm³) resulted in a total dose of 3µg BMP-2 and/or 0.6µg FGF-2.

Table 3. Properties of porous titanium implants

Titanium thickness	120µm
Pore size	490µm
Porosity	88%
Pore volume	55mm ³
Compression strength	14MPa
Young’s modulus	0.4GPa

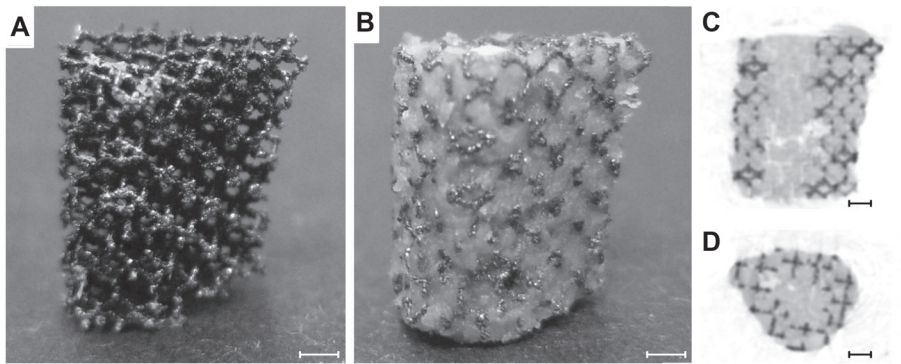


Figure 1: Photographs of porous titanium implants.

Photographs of porous titanium implants in the shape of the 6 mm bone segment that was replaced during the animal experiment before (A) and after (B) incorporation with colloidal gelatin gels. μ CT images of perpendicular (C) and horizontal (D) cross-sections of porous titanium implant (black) incorporated with colloidal gelatin gels containing iodine-based radiographic contrast agent ioxaglate (grey). Scale bar = 1 mm.

4. Animal experiment

In 40 male Wistar rats, a critical-sized cortical femoral bone defect was grafted with porous titanium implants loaded with the four different colloidal gelatin gels (Table 2). The Animal Ethics Committee of the Erasmus University approved the study and Dutch guidelines for care and use of laboratory animals were applied. Before surgery, rats received a single dose of antibiotics (enrofloxacin, 5mg/kg body weight). Surgery was performed aseptically under general anaesthesia (1-3.5% isoflurane). The right femur was exposed through a lateral skin incision and division of underlying fascia. A 23mm long PEEK plate was fixated to the femurs anterolateral plane using three proximal and three distal screws. Periosteum was removed over approximately 8 mm of the mid-diaphyseal region before a 6mm bone segment was removed with a wire saw and a tailor-made saw guide. Subsequently, a gel-loaded porous titanium implant was implanted press-fit into the defect. Finally, fascia and skin were sutured using Vicryl 5-0 and pain medication (buprenorphine, 0.05mg/kg body weight) was administered twice a day for three days.

5. μ CT evaluation

Immediately after surgery, a baseline *in vivo* μ CT scan was acquired (SkyScan 1176 scanner, Bruker micro-CT N.V., Kontich, Belgium) using a 35 μ m resolution protocol (90kV, 0.1mm Cu filter, and 0.5 degree rotation step, 7m scan). *In vivo* scans were repeated after four, eight, and twelve weeks. At twelve weeks, an *ex vivo* scan was made using an 18 μ m resolution protocol (90kV, 0.1mm Cu filter, and 0.2 degree rotation step, 1h scan). CT images were reconstructed using volumetric reconstruction software NRecon version 1.5 (Bruker micro-CT N.V., Kontich, Belgium).

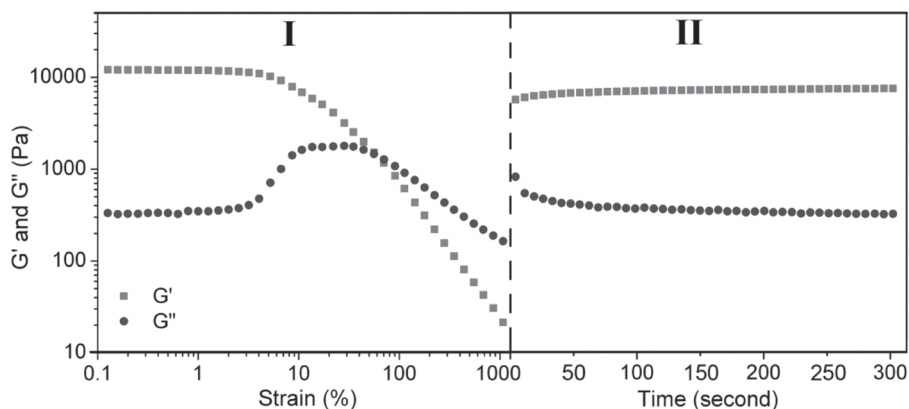


Figure 2: Rheological characterization of colloidal gelatin gels.

Rheological characterization of self-healing behaviour of colloidal gelatin gels (20 w/v% solid content) by monitoring storage moduli G' (square) and loss moduli G'' (circle) as a function of time (region II: oscillatory time sweep with 1% strain and 1Hz frequency) after network destruction by increasing strain from 0.1% to 1000% (region I: oscillatory strain sweep with 1Hz frequency).

Bone formation was expressed as bone volume (BV) and measured at four specific regions: (1) total BV: total volume of bone formed within the 6 mm defect; (2) outer BV: bone formed outside the implant; (3) porous BV: bone formed inside the porous space of the implant; and (4) inner BV: bone formed in the medullary canal of the implant. Specific BVs were measured after selecting the specific region as a volume of interest (VOI) on the scans using a custom-made algorithm within CTAnalyser software version 1.11 (Bruker micro-CT N.V., Kontich, Belgium). After selection of the specific VOIs, titanium was subtracted from the images using a global threshold. Additionally, a $35\mu\text{m}$ layer of the interface was subtracted in order to minimize interference of metal artefacts with BV measurements. BV was then determined after applying a global threshold that was based on visual inspection and was kept constant for all scans. The extent of bone bridging was measured on *ex vivo* scans with DataViewer 1.4 (Bruker micro-CT N.V., Kontich, Belgium).

6. Histology

Histology was performed on five femurs of each group to study bone-titanium interface and bone morphology. After harvesting and removal of surrounding soft tissues, femurs were fixed in 10% neutral buffered formalin solution for two days, dehydrated in graded ethanol solution from 70 to 100%, and finally embedded in methyl methacrylate (MMA). Sections of $\sim 20\mu\text{m}$ were obtained using a diamond saw (Leica SP1600, Rijswijk, The Netherlands) and stained with basic fuchsin 0.3% solution and methylene blue 1% solution. Basic fuchsin stains bone red and methylene blue stains fibrous tissue blue.

7. Mechanical evaluation

Final strength of five grafted femurs from each group was measured using three-point bending tests, intact contralateral femurs served as controls. After harvesting the femurs, soft tissue and the PEEK plate were carefully removed. Specimens were kept in 10% neutral buffered formalin solution for two days followed by phosphate buffered saline, thereby minimizing effects of formalin conservation on mechanical properties²⁹⁹. Bending tests were carried out using a Zwick test machine (Zwick GmbH, Germany) as follows: first, femurs were fixed at both sides using two holding plates that were secured with screws. The fixated femur was supported by two supports (15mm width) and a downward force was applied by a denter (3mm width) to the middle of the anterolateral plane of porous titanium implant. Bending tests were performed at a displacement rate of 2mm/min until peak load was reached. Force-displacement curves were recorded and used to determine the fracture force, maximum replacement and bending stiffness. Bending stiffness was determined by fitting a line to the initial linear portion of the force-displacement curve.

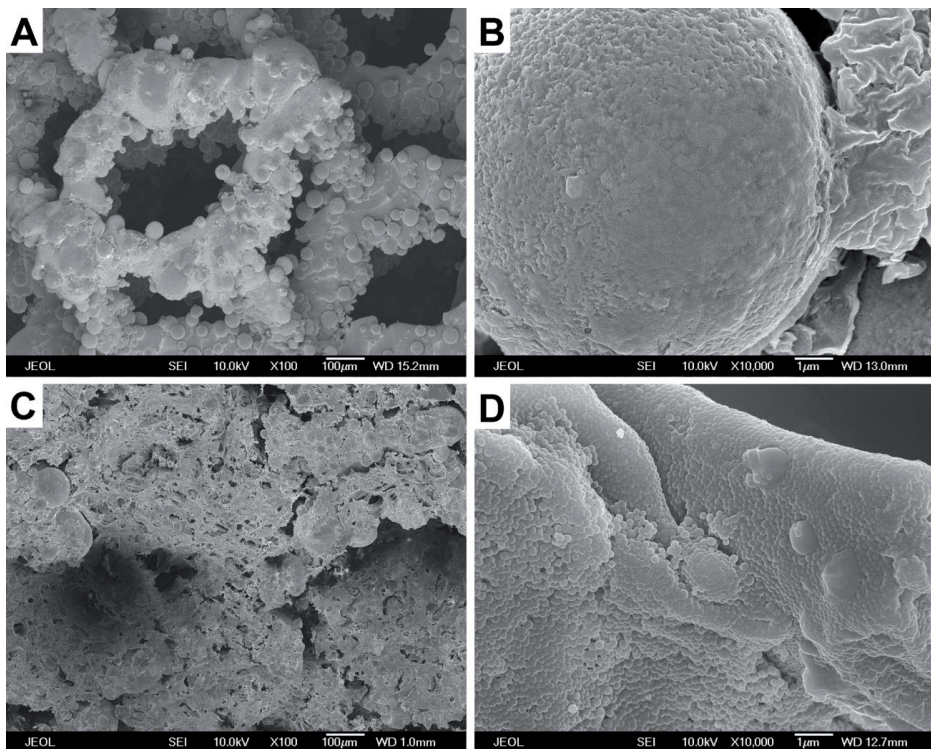


Figure 3: Scanning electron micrographs of porous titanium implants.

Scanning electron micrographs of the porous titanium implants before (A, B) and after (C, D) incorporation of the colloidal gelatin gels. Low (A, C) and high (B, D) magnification.

8. Statistics

Statistical analyses were performed using SPSS Statistics 20.0 (SPSS Inc, Chicago, US). Data is presented as means with standard deviation. One-way Analysis of Variation (ANOVA) and subsequent post-hoc pairwise comparisons with Bonferroni adjustment was used to analyse differences between groups. A p-value <0.05 was considered statistically significant.

Results

1. Gelatin nanosphere-based colloidal gels

Rheological characterization indicates the formation of highly elastic gels, since a storage moduli (G') of 12 kPa was substantially higher than loss moduli (G'') (corresponding to $\tan(\delta)$ values of about 0.03) (Figure 2, region I). Gel networks were gradually destroyed by applying an external increasing shear strain, which led to, the transformation from elastic, solid-like to liquid-like materials ($G' < G''$) at strain exceeding 70%. At the removal of the external destructive shear force, it was observed that the gel strength recovered immediately, with up to 70% of the initial gel elasticity (G') recovered within 5 min (Figure 2, region II).

Colloidal gelatin gels were easily incorporated into porous titanium implants by injection filling process using a custom-made gel chamber resulting in a homogeneous distribution of the gels throughout the porous implants as confirmed by μ CT (Figure 1C and D). SEM shows fused titanium particles forming the porous structure (Figure 3A) and the surface morphology of titanium before (Figure 3B) and after gel incorporation (Figure 3C). After gel incorporation, original surface morphology of titanium was covered by nanoparticulate morphology of colloidal gelatin gels consisting of nanoparticles ranging between 100-200nm in diameter (Figure 3D), whilst the porous architecture of the implants was covered completely by the nanostructure of particulate gel network.

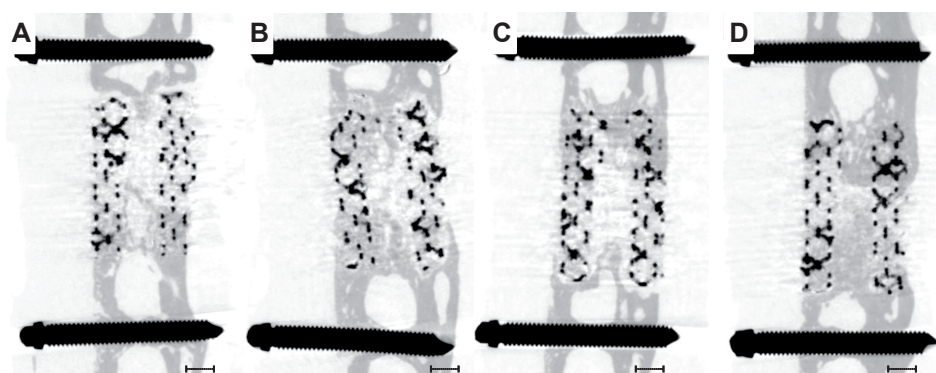


Figure 4: μ CT images of porous titanium implants.

Representative transversal μ CT images of the porous titanium implants containing unloaded (A), FGF-2 (B), BMP-2 (C) or BMP-2/FGF-2 (D) gels after twelve weeks. Porous titanium implants and fixation screws appear in black whereas bone appears in dark grey. Scale bar = 1 mm.

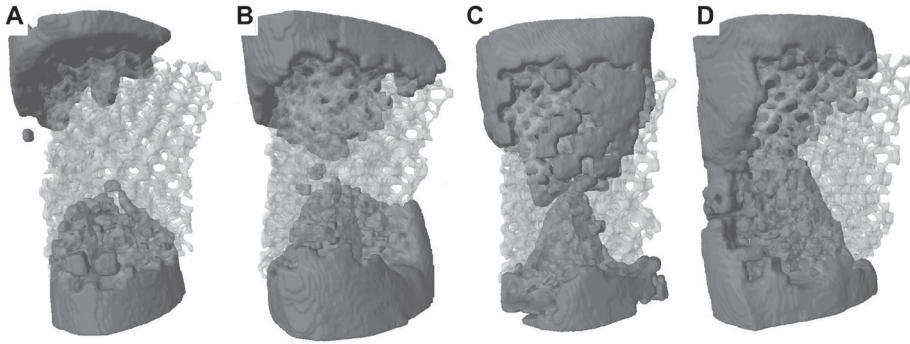


Figure 5: 3D μ CT images of porous titanium implants.

Representative 3D μ CT images of bone bridging the porous titanium implants containing unloaded (A), FGF-2 (B), BMP-2 (C) or BMP-2/FGF-2 (D) gels after twelve weeks. Porous titanium implants are shown in grey whereas bone appears in dark grey.

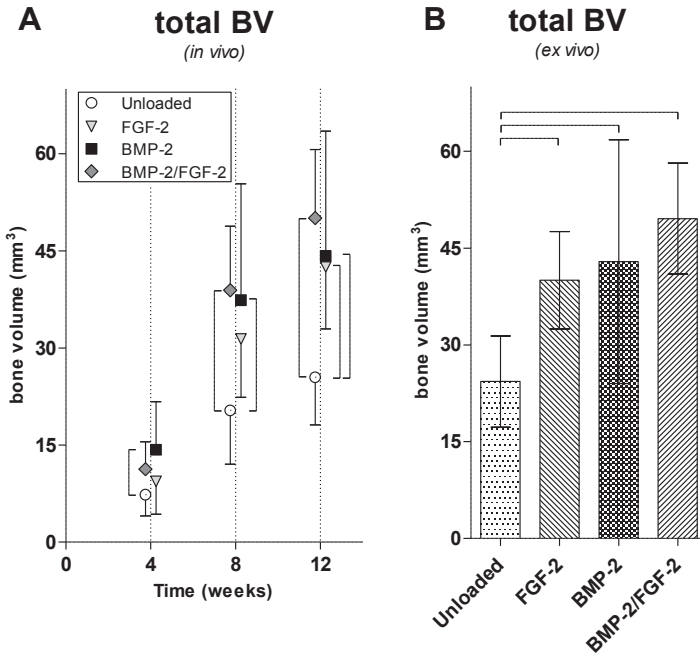


Figure 6: Total bone volume.

In vivo μ CT quantification of total bone volume (BV) at four, eight, and twelve weeks after implantation (A). *Ex vivo* μ CT quantification of total BV after twelve weeks (B). Total BV was defined as total volume of bone formed within the 6mm defect area. Horizontal and vertical bars indicate statistically significant differences ($p < 0.05$) between groups.

2. Animal experiment

Rats were able to tolerate weight-bearing activities immediately after surgery, and implantation sites healed without complications. All animals remained healthy during the entire study period, except one rat that died due to anaesthesia-related complications (BMP-2 group).

3. μ CT evaluation

Correct positioning of porous titanium implant, PEEK-plate, and screws was confirmed directly after surgery in all animals and no dislocation was detected during follow-up. In general, bone regeneration started at bone adjacent to the defect and progressed towards the central area of the defect (Figure 4). Porous titanium implants almost completely bridged the defect (defined as a remaining gap <0.5 mm) in seven rats of the BMP-2/FGF-2 group, seven rats of the BMP-2 group, five rats of the FGF-2 group and one rat of the unloaded group (Figure 5). Average remaining gap distance was 0.33 ± 0.34 mm for the BMP-2/FGF-2 group, 0.51 ± 0.74 mm for the BMP-2 group, 0.83 ± 0.53 mm for the FGF-2 group and 1.20 ± 0.56 mm for the unloaded group.

Porous titanium implants with GF-loaded gels resulted in significantly more bone regeneration than porous titanium implants with unloaded gels after twelve weeks (Figure 6). BMP-2 gels strongly enhanced early bone formation, since total BV was significantly more than with unloaded gels at four weeks (Figure 6A). Total BV continued to increase between four and eight weeks, and reached a plateau phase after eight weeks. FGF-2 gels enhanced bone formation in the later phase, as total BV increased rapidly between four and eight weeks. Finally, FGF-2 gels resulted in 40.0 ± 7.6 mm³ total BV, which was similar to BMP-2 gels (42.9 ± 18.9 mm³). BMP-2/FGF-2 gels continuously enhanced bone formation during the entire follow-up period, resulting in the highest average total BV at twelve weeks (49.6 ± 8.6 mm³) (Figure 6B).

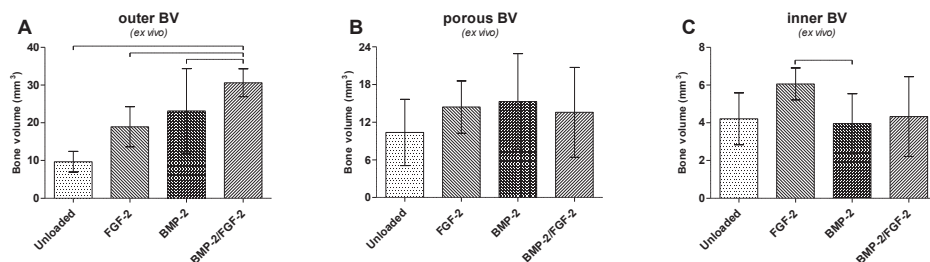


Figure 7: Outer, porous and inner bone volume.

Ex vivo μ CT quantification of outer BV (A), porous BV (B) and inner BV (C) at twelve weeks. Outer BV was defined as bone formed outside the porous titanium implants; porous BV: bone formed inside the porous space of the titanium implants; and inner BV: bone formed in the medullary canal of the implant. Horizontal bars indicate statistical significant differences ($p < 0.05$).

Porous titanium implants with BMP-2/FGF-2 gels resulted in significantly more bone outside the porous titanium implants (outer BV) than those with BMP-2 gels, or FGF-2 gels (Figure 7A). Bone ingrowth into the porous titanium implants (porous BV), however, was not significantly enhanced by GF-loaded gels (Figure 7B). FGF-2 gels resulted in significantly more bone inside the porous titanium implant (inner BV) than BMP-2 gels ($6.1 \pm 0.8 \text{ mm}^3$ versus $4.0 \pm 1.6 \text{ mm}^3$ ($p=0.033$), Figure 7C).

4. Histological evaluation

No distinct differences in terms of bone morphology, bone-titanium bonding or vascularisation between experimental groups were observed (Figure 8A-D). Areas of newly formed bone differed considerably, unloaded gels showed less bone (Figure 8A) than FGF-2 gels (Figure 8B), BMP-2 gels (Figure 8C), and BMP-2/FGF-2 gels (Figure 8D). Bone formation inside the porous space was mainly located at distal and proximal sites and resulted in direct bone-titanium contact (Figure 8G). Direct bone-titanium contact was not found throughout the entire bone-titanium interface. In some areas, a cartilage-like zone was observed (Figure 8E). Fibrous tissue infiltration was occasionally seen inside pores devoid of newly formed bone and within the remaining gap of nearly completely bridged defects (Figure 8F). No remnants of colloidal gelatin gels were detected, and no signs of foreign body reaction or inflammatory response were observed.

5. Mechanical evaluation

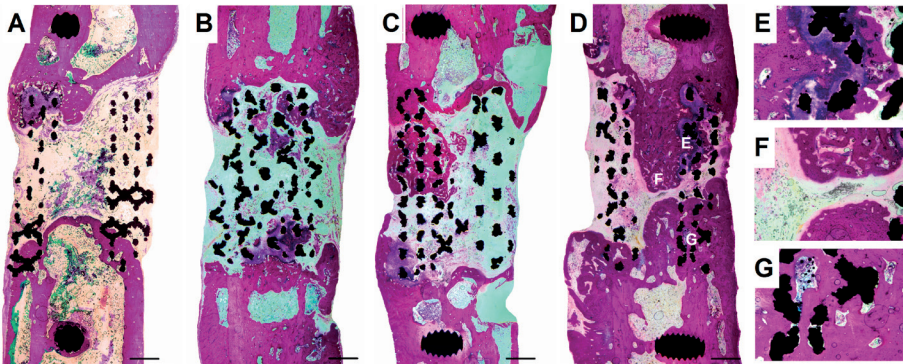


Figure 8: Histological sections of porous titanium implants.

Representative transversal histological sections of the porous titanium implants containing unloaded (A), FGF-2 (B), BMP-2 (C) or BMP-2/FGF-2 (D) gels after twelve weeks as well as high magnification views (E, F and G) of the areas as depicted in figure D. Titanium appears in black whereas bone appears in purple. Scale bar = 1mm.

All grafted femurs broke at approximately 50% of the force required to break the intact contralateral femurs, but fracture force and ultimate displacement did not show statistical

significant differences between the groups (Table 4). The observed fracture location, however, differed substantially. Femurs grafted with implants containing unloaded gels broke at the bone-implant interface (2/5) or through the porous titanium implants (3/5). Similar fracture locations were observed for implants containing FGF-2 gels. In contrast, BMP-2 group consistently broke at the bone-implant interface (4/4) and the BMP-2/FGF-2 group fractured consistently (5/5) through the host bone at ~3 mm distally from the titanium-bone interface.

Discussion

Porous titanium implants have recently received increasing attention as a new biomaterial that can act as an osteoconductive scaffold that provides direct mechanical support in large bone defects at weight-bearing sites²⁸². Advanced additive manufacturing methods, such as SLM, allow precise and reproducible production of porous titanium with full control over the structural design. Thereby the structural design can now be fine-tuned so that porous titanium implants offer optimal mechanical and structural conditions required for bone regeneration³¹⁹. However, porous titanium implants remain bioinert and thereby lacks the ability to provide strong biological cues that can enhance bone regeneration. This lead to the hypothesis that when GF-loaded colloidal gelatin gels are incorporated into porous titanium implants this would result in a biologically active and mechanically strong composite biomaterial that can enhance bone regeneration of large bone defects.

Incorporation of colloidal gelatin gel was easily obtained (Figure 1C and D) owing to shear-thinning and self-healing capacity of the gels, shown by fast recovery from severe network destruction during rheological testing (Figure 2). Moreover, the gels used were previously shown to exhibit a strong capacity for controlled and sustained delivery of multiple GFs by employing different subpopulations of gelatin nanospheres of different cross-linking

Table 4. Fracture locations of the three-point bending tests

Gels	Fracture Force (N)	Ultimate Displacement (mm)	Fracture location			Bending Stiffness (N/mm)	Maximum Moment (N.mm)
			Host bone	Bone-implant interface	Implant		
Unloaded	119±71	2.5±0.9		2/5	3/5	104±19	50±30
FGF-2	122±72	1.9±0.7		3/5	2/5	105±21	51±30
BMP-2	157±69	2.7±0.9		4/4		109±52	66±29
BMP-2/FGF-2	111±38	2.9±1.0	5/5			100±28	47±16
Intact femurs	254±55	0.9±0.3				428±161	107±24

densities. Cross-linking densities of gelatin nanospheres resulted in a rapid delivery of FGF-2 and a sustained delivery of BMP-2, whereas the gelatin gel is resorbed in four weeks³⁹.

Generally, this *in vivo* study confirms the load-bearing and osteoconductive properties of porous titanium implants, as well as the biological efficacy of GFs delivery by nanostructured colloidal gelatin gels. The presence of colloidal gels inside the porous space during the first four weeks did not seem to hamper bone regeneration, because total BVs measured in defects grafted with porous titanium implants that contained unloaded gels were similar to total BVs measured in empty porous titanium implants that were used in our previous study³¹⁹. Although direct bone-titanium contact was observed in all groups, occasionally cartilage-like tissue was formed at parts of the interface (Figure 8E). This cartilage-like tissue may indicate that micromotion had been possible at some areas between the titanium implant and surrounding tissues. Although bone healing generally benefits from a certain degree of micromotion, excessive micromotion is known to inhibit bone calcification at fracture union site³³². This could also explain the fact that, although grafting with titanium implants containing BMP-2/FGF-2 gels or BMP-2 gels resulted in almost complete bridging, none was fully bridged (Figure 8F). Inability to bridge the defect can likely be overcome by using a more rigid plate.

Incorporation of BMP-2/FGF-2 gels resulted in significantly more bone after twelve weeks than incorporation of unloaded gels. However, no significant differences in total BV were observed between different GF-loaded gels. Based on previous studies related to BMP-2 delivery in 6mm cortical bone defects in rat femurs, a BMP-2 dosage of 3µg per defect was considered safe and efficient in stimulating osteogenesis^{253, 333}. The stimulatory effect of BMP-2 gels became apparent during the early stages of bone healing (0-8 weeks), as reflected by significantly more bone at four and eight weeks compared to unloaded gels (Figure 6A). This effect was also observed in a previous *in vivo* study, where BMP-2 gels in rat femoral condyle defects led to significant enhancement of bone formation³⁹. Bone regeneration slowed down after eight weeks, which may be explained by complete depletion of the pool of progenitor cells in and around the bone defect site that are capable of differentiating into osteoblasts upon BMP-2 stimulation.

On the other hand, rapid delivery of 0.6µg FGF-2 per defect resulted in comparable amounts of bone formed after twelve weeks as the sustained delivery of a five times higher doses of BMP-2. This stresses the potent stimulatory effects of low dose FGF-2 (nanograms) on bone regeneration *in vivo*³³⁴. Although FGF-2 is expected to be delivered rapidly from colloidal gelatin gels used³⁹, stimulatory effects were more profound during later stages of bone healing (4-12 weeks) (Figure 6A). It was not possible to elucidate the exact mechanism of action of FGF-2 in this study, but since FGF-2 stimulates proliferation of progenitor cells, it can be speculated that FGF-2 contributed to an expanded pool of osteoprogenitor cells that subsequently can undergo osteogenic differentiation resulting in more bone formation in a later phase^{334, 335}. In addition, angiogenic effects of FGF-2 can potentially lead to enhanced

vascularisation which may become crucial in continuation of bone regeneration after four weeks^{336, 337}. Finally, despite the absence of significant differences in total BV at twelve weeks between BMP-2 gels and FGF-2 gels, significantly more bone was observed within the medullary canal (inner BV) with FGF-2 gels (Figure 7C) suggesting that the proliferative effect of FGF-2 acts stronger on endosteal rather than periosteal cells³³⁸.

BMP-2/FGF-2 gels incorporated into titanium implants resulted in continuous increase in total BV. Total BV after twelve weeks was not statistically different compared to BMP-2 gels or FGF-2 gels, but significantly more bone was formed outside the porous titanium implants. This could be explained by the higher availability and/or more efficient attraction of osteo-progenitor cells from surrounding tissues at the outer side of titanium implants compared to inner region. More interesting is the fact that in a previous study colloidal gelatin gels loaded with 1:1 dose ratio of BMP-2 and FGF-2 (2µg per defect) had inhibitory effects on *in vivo* bone regeneration³⁹. This inhibitory effect was likely caused by overdosing FGF-2 relative to BMP-2. Similar observations on combined delivery of BMP-2 and FGF-2 indicate that higher doses of FGF-2 (micrograms) with lower or equal doses of BMP-2 generally hampered bone formation^{329, 339, 340}. In line with our results, using a 5:1 dose ratio of BMP-2:FGF-2, a lower doses of FGF-2 (nanograms) in combination with higher doses of BMP-2 (micrograms) is found to stimulate osteogenesis^{341, 342}.

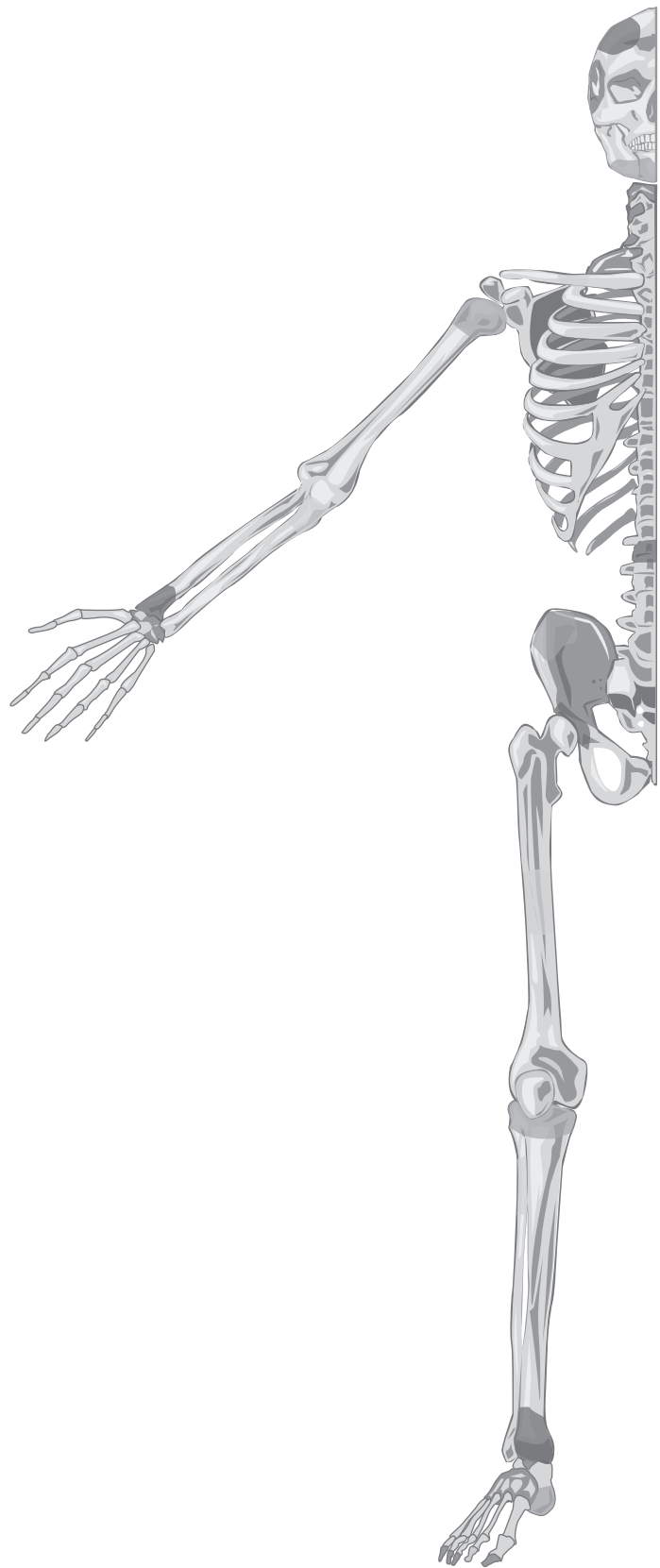
Mechanical strength of grafted femurs was assessed using three-point bending tests, which aimed to evaluate the strength of the interface between porous titanium implants and adjacent host bone. The absence of significant differences in maximum force suggests that only a limited amount of bone ingrowth is effective for complete biomechanical integration of porous titanium implants with adjacent host bone (Table 4). The compression strength of porous titanium implants used here is 14MPa (Table 2). This low strength can explain the fractures that occurred within the titanium implants or at the bone-implant interface when the applied force of the indenter (3mm width) exceeded 100N. The fracture location of femurs grafted with porous titanium implants containing BMP-2/FGF-2 gels is particularly interesting because BMP-2/FGF-2 gels consistently shifted the weakest link from the bone-implant interface towards the host bone at point ~3mm distally of the implant. This observation suggested that the extensive bone formed outside the porous titanium implants incorporated with BMP-2/FGF-2 gels could further strengthen mechanical properties of the implants. Overall, the fact that grafted femurs could already sustain bending forces up to 50% of that required to break an intact femur after twelve weeks, shows the potential of porous titanium implants for grafting large weight-bearing bone defects.

Conclusions

In the current study, porous titanium implants were reinforced with nanostructured colloidal gelatin gels loaded with BMP-2 and/or FGF-2 to graft critical-sized cortical femoral bone defect in rats. Results clearly demonstrated stimulatory effects of time and dose controlled delivery of BMP-2, FGF-2, or both on bone regeneration. Most defects grafted with porous titanium implants containing BMP-2/FGF-2 gels or BMP-2 gels were almost completely bridged after twelve weeks. BMP-2/FGF-2 gels resulted in significantly more bone outside the porous titanium implants. The stimulatory effect of delivery of merely 0.6 μ g FGF-2 per defect was similar to delivery of a five-fold higher dose of BMP-2 (3 μ g per defect). Although three-point bending tests did not show significant differences in fracture force, the pattern of fracture locations indicated that BMP-2/FGF-2 gels enhanced the titanium-bone interface strength thereby shifting the weakest point from the titanium-bone interface to towards the surrounding femoral bone. In summary, incorporation of nanostructured colloidal gelatin gels capable of time and dose controlled delivery of FGF-2 and BMP-2 into porous titanium implants offers a mechanically strong and biologically active composite biomaterial suitable for grafting large bone defects.

Acknowledgements

This research forms part of the Project P2.04 BONE-IP of the research program of the Bio-Medical Materials institute, co-funded by the Dutch Ministry of Economic Affairs. We are also grateful for the support from funding KNAW, China-Netherlands Programme Strategic Alliances (PSA) (No.2008DFB50120).



Chapter 8

Porous titanium implants incorporated with BMP-2 loaded fibrin gels

Johan van der Stok
Marianne K.E. Koolen
Moniek P. de Maat
Saber Amin Yavari
Jacqueline Alblas
Peter Patka
Jan A.N. Verhaar
Esther M.M. van Lieshout
Amir A. Zadpoor
Harrie Weinans
Holger Jahr

Published as "Full regeneration of segmental bone defects using porous titanium implants loaded with BMP-2 containing fibrin gels" in *European Cells and Materials*. 2015 Mar 4;29:141-54

Abstract

Regeneration of load-bearing segmental bone defects is a major challenge in trauma and orthopaedic surgery. The ideal bone graft substitute is a biomaterial that provides immediate mechanical stability, while stimulating bone regeneration to completely bridge defects over a short period of time. Therefore, selective laser melted porous titanium, designed and fine-tuned to tolerate full load-bearing, was filled with a physiologically concentrated fibrin gel loaded with bone morphogenetic protein-2 (BMP-2). This biomaterial was used to graft critical-sized segmental femoral bone defects in rats. As a control, porous titanium implants were either left empty or filled with a fibrin gels without BMP-2. We evaluated bone regeneration, bone quality and mechanical strength of grafted femurs using *in vivo* and *ex vivo* μ CT scanning, histology, and torsion testing. This biomaterial completely regenerated and bridged the critical-sized bone defects within eight weeks. After twelve weeks, femurs were anatomically re-shaped and revealed open medullary cavities. More importantly, new bone was formed throughout the entire porous titanium implants and grafted femurs regained more than their innate mechanical stability: torsional strength exceeded twice their original strength. In conclusion, combining porous titanium implants with a physiologically concentrated fibrin gels loaded with BMP-2 improved bone regeneration in load-bearing segmental defects. This material combination now awaits its evaluation in larger animal models to show its suitability for grafting load-bearing defects in trauma and orthopaedic surgery.

Introduction

A major challenge in trauma and orthopaedic surgery is to successfully repair load-bearing segmental bone defects⁸. This often requires the use of bone grafts or bone graft substitutes to improve bone regeneration by providing an osteoconductive matrix, offering mechanical support, or an osteoinductive and/or osteogenic stimulus²⁸¹. The golden standard bone graft is still autologous bone¹⁰, but the amount of bone that can be harvested is limited and associated with complications in 10-40%¹². These disadvantages motivate the development of biomaterials that can be used as bone graft substitutes²⁸⁰.

A biomaterial that has the potential to become a bone graft substitute is porous titanium^{35, 282, 320}. Nowadays, porous titanium can be manufactured using additive manufacturing techniques such as selective laser melting (SLM)²⁶². This enables the design of porous titanium so that its structure and mechanical strength remains suitable to function as a load-bearing osteoconductive matrix in segmental bone defects³¹⁹. Osseointegration of titanium is optimized through relatively simple chemical and heat treatments that alter the surface chemistry and (nano-) topography³⁰⁰. Thereby the bioinert titanium surface changes into a bioactive surface that allows spontaneous apatite formation and stimulates proliferation and osteogenic differentiation of osteoprogenitor cells²⁹². This surface-treated porous titanium forms a load-bearing osteoconductive matrix, but stimulating bone regeneration and adequate bridging of segmental bone defects may be further improved by addition of effective biological stimuli (*i.e.* osteoinductive cytokines)^{291, 319}.

Bone morphogenetic proteins (BMPs) such as BMP-2 and BMP-7 play a major role in bone regeneration as osteoinductive cytokines²⁹. Their osteoinductive effects have been established in a wide range of species, varying from mice and rats to humans³⁴³. BMP-2 and BMP-7 have received FDA approval for use in trauma and orthopaedic surgery³⁴⁴, but their clinical success is limited³⁴⁵. This might be because a supra-physiological dosage of BMP needs to be loaded onto an absorbable collagen sponge to reach an effect²²⁰. This high dose has been associated with adverse effects including bone tissue overgrowth, ectopic bone formation, inflammation, and even carcinogenicity^{346, 347}. To overcome this, numerous slow-release systems have been developed. Interestingly, these slow-release systems, allowing for controlled release of BMP-2 during several weeks, do not resemble the natural bone regeneration process in which BMP-2 is mainly released during the first few days^{5, 348}.

Bone regeneration starts with the formation of a fibrin clot, often referred to as the fracture haematoma. This fibrin clot forms the natural binding reservoir for osteoinductive cytokines such as BMP-2^{5, 349} and is formed through conversion of fibrinogen by thrombin. Fibrinogen is synthesized in its high molecular weight form, but occurs as a mixture together with partially degraded low molecular weight forms in circulation³⁵⁰. Fibrin gels, made from physiological fibrinogen concentrations (2-4mg/L), are highly permeable to cells³⁵⁰. But at these physiological concentrations, fibrin gels are soft and therefore not suitable for most

clinical applications. As a consequence, commercially available fibrin sealants contain very high fibrinogen concentrations (50-100mg/L)³⁵¹ at the cost of seriously compromising the favorable cellular permeability of these gels. When incorporated into porous titanium, the use of physiologically concentrated fibrin gels becomes feasible as the metal frame ensures mechanical support, then. The surface-treated porous titanium implants may even improve the network organization of fibrin fibers³⁵².

The aim of the current study was to develop a biomaterial capable of improving bone regeneration of segmental bone defects: osteoconductive load-bearing porous titanium filled with physiologically concentrated fibrin gels releasing BMP-2. For this novel combination, the BMP-2 releasing fibrin gel was prepared from purified high molecular weight (HMW) fibrinogen, since HMW fibrinogen increases angiogenesis *in vitro* and *in vivo*.³⁵⁰ To determine whether the angiogenic HMW fibrin gel alone is capable of increasing bone regeneration, porous titanium implants were also filled with HMW fibrin gels without BMP-2 and compared to unfractionated (UNF) fibrin gels. Porous titanium implants incorporated with the three above described fibrin gels were compared to empty porous titanium implants in a critical-sized load-bearing segmental femur defect in rats using *in vivo* (4, 8, and 12 weeks) and *ex vivo* (after 12 weeks) μ CT scans, histology, and biomechanical torsion tests.

Materials and methods

1. Porous titanium implants

Porous titanium implants were produced from Ti6Al4V ELI powder (ASTM B348, grade 23) using selective laser melting (SLM, Layerwise N.V., Leuven, Belgium). The implants were a copy of the replaced femoral bone segment and had a height of 6mm, a maximum outer diameter of 5mm and a minimal inner diameter of 1.3mm (leaving an open medullary canal). The porous architecture was based on a dodecahedron unit cell with a strut width of 120 μ m and an average pore size of 500 μ m to result in 55mm³ porous volume. All implants underwent a post-production alkali-acid-heat treatment consisting of (1) immersion in a 5M aqueous NaOH solution at 60°C for 24h; (2) immersion in water at 40°C for 24h; (3) immersion in 0.5mM HCl at 40°C for 24h; (4) heating to 600°C at a rate of 5°C/min in an electric furnace at ambient air pressure, keeping the temperature at 600°C for 1h, and subsequent natural cooling²⁹². Reproducibility of porous implant architecture (e.g. pore size, titanium strut thickness and porosity) was verified by μ CT (SkyScan 1076; Bruker micro-CT N.V., Kontich, Belgium).

2. Fibrin gel preparation

Fibrin gel preparation was done exactly the same as previously described^{350, 353}. Briefly, plasminogen-rich unfractionated human fibrinogen (Chromogenix, Mölndal, Sweden) was

dissolved in Tris buffer (10mM Tris/HCl, pH 7.4) to a concentration of 5mg/mL. Saturated $(\text{NH}_4)_2\text{SO}_4$ was slowly added to a final concentration of 19% (v/v) and the solution was mixed for 30 minutes at room temperature prior to centrifugation for 10 minutes at 2,000 x g. Repetition of this precipitation step resulted in a HMW fibrinogen pellet (~99% purity), which were dissolved in 5mL of saline and then dialyzed against M199 culture medium, as was the UNF fibrinogen. Purity was determined using standard non-reducing sodium dodecylsulfate polyacrylamide gel electrophoresis and concentrations were calculated using the molar extinction coefficient of fibrinogen (E1% 280 nm for fibrinogen is 15.8). The preparations were stored in single-use aliquots at ~80°C until further use.

In a custom-made mold, the porous titanium implants were filled with 55 μL of either HMW fibrinogen (2mg/mL, HMW-Fb) or UNF fibrinogen (2mg/mL, UNF-Fb) which were clotted with 0.5IU/mL of thrombin (Global Siemens Healthcare, Erlangen, Germany) dissolved in a 4.5mM calcium chloride buffer (Baxter, Utrecht, Netherlands) in a 8.5:1 ratio. HMW fibrin gels with BMP-2 (HWM-BMP-Fb) were made by adding 3 μg BMP-2 (Shanghai Rebone Biomaterials Co., China) in 1mM saline solution to the HWM fibrinogen solution before clotting. Prior to implantation, after clotting the fibrin-filled implants were wrapped in Parafilm[®] and incubated for 15-18h at 6°C to allow completion of crosslinking of the fibrin networks.

3. Scanning electron microscopy (SEM)

To determine filling efficacy and to characterize the structure of the fibrin networks polymerized from HMW and UNF fibrinogen, SEM was used as follows: implants were filled with fibrin gels and fixed in 3% glutaraldehyde for 24h and rinsed with sodium phosphate buffer (0.1M, pH 7.2-7.4; Merck). Samples were then consecutively dehydrated in ascending alcohol concentrations (30%, 50%, 70%, 90% v/v) with three final incubations in 100% ethanol for 10 minutes each. Probes were critical-point-dried in liquid CO_2 and then sputtered with a 30nm gold layer. Samples were analysed in FEI/Philips XL 30 FEG ESEM (Philips) in a high vacuum environment.

4. Load-bearing segmental bone defects

Critical-sized segmental bone defects were made in the femurs of 40 male 16-week-old Wistar rats (446 \pm 32g). Rats were divided into four experimental groups receiving porous titanium implants filled with HMW-BMP-Fb, HMW-Fb, UNF-Fb or were left empty (empty). The Animal Ethics Committee of the Erasmus University approved the study and Dutch guidelines for care and use of laboratory animals were followed. Before surgery, rats received subcutaneous injections of antibiotics (enrofloxacin, 5mg/kg body weight) and pain medication (buprenorphine, 0.05mg/kg body weight). Surgery was performed aseptically under general anaesthesia (1-3.5% isoflurane). The right femur was exposed through a lateral skin incision and separation of underlying fascia. Using three proximal and three distal screws,

a 23x3x2mm polyether ether ketone (PEEK) plate was fixed to the femur anterolateral plane (RISystem, Davos Platz, Switzerland). Periosteum was removed over 8mm of the mid-diaphyseal region before a 6mm cortical bone segment was removed with a wire saw and a tailor-made saw guide. Subsequently, a porous titanium implant was implanted press-fit into the defect. Finally, fascia and skin were sutured. Subcutaneous injection of pain medication (buprenorphine, 0.05mg/kg body weight) was given twice a day for the following three days. Rats were sacrificed after twelve weeks with an overdose of pentobarbital (200mg/kg body weight).

5. μ CT evaluation

Bone regeneration was measured by *in vivo* μ CT scans (SkyScan 1076; Bruker micro-CT N.V., Kontich, Belgium) at four, eight, and twelve weeks and by *ex vivo* μ CT scans on isolated grafted femurs at the end of the experiment. Rats were kept under general anaesthesia (1-3.5% isoflurane) during *in vivo* μ CT scans at 35 μ m resolution (95kV, 105 μ A current, 1.0mm Al/0.25mm Cu filter, and 0.75 degree rotation step, 14 minutes scan). *Ex vivo* μ CT scans were acquired at 18 μ m resolution (95kV, 100 μ A current, 1.0mm Al/0.25mm Cu filter, and 0.5 degree rotation step). μ CT scan images were reconstructed using volumetric reconstruction software NRecon version 1.6.6 (Bruker micro-CT N.V., Kontich, Belgium).

Bone regeneration was expressed as bone volume (BV), which was measured at four specific regions: 1) total BV: the total volume of bone formed within the 6mm defect; 2) porous BV: the bone formed inside the porous space of the titanium implants; 3) outer BV: the bone formed outside the porous titanium implants; and 4) inner BV: the bone formed in the medullary canal of the implants. BV values were measured using CTAnalyser version 1.13 (Bruker micro-CT N.V., Kontich, Belgium). First the specific region was selected, then the titanium and its border artefacts was excluded from images using a global threshold with a value between titanium and bone and removal of an extra 35 μ m border (size of one pixel) surrounding the titanium. Subsequently the bone was extracted by using a second global threshold that differentiated between bone and soft tissue. The global threshold values were chosen on visual inspection and were kept constant for all scans. Bone bridging was assessed on *ex vivo* scans with DataViewer 1.4 (Bruker micro-CT N.V., Kontich, Belgium). Complete bone bridging was defined as bridging of three or more cortices, which was determined by visual inspection. Bone bridging was quantified by measuring the shortest remaining gap size between bone formed at the proximal and distal size of the 6 mm bone defect.

6. Histological evaluation

Histology was performed on two femurs per group that represented the mean of the whole group. To select these two femurs, all ten grafted femurs were sorted according to their total BV after twelve weeks and the two femurs closest to the averaged value were chosen. Harvested femurs were fixed in 10% neutral buffered formalin solution for two days,

dehydrated in ascending alcohol concentrations (70 to 100% v/v), and finally embedded in methyl methacrylate (MMA). Sections of $\sim 20\mu\text{m}$ were obtained using a diamond saw (Leica SP1600, Rijswijk, The Netherlands) and stained with basic fuchsin 0.3% (w/v) solution and methylene blue 1% (w/v) solution to stain bone red and fibrous tissue blue, respectively. Serial sections were then screened for bone formation, bone-implant contact and bone bridging.

7. Biomechanical tests

Mechanical strengths of grafted femurs were measured by a torsion test conducted on the remaining eight femurs of each group. Three contralateral femurs, serving as a reference of intact femurs, were included as controls. After harvesting the femurs, soft tissues and PEEK plate were carefully removed. Specimens were kept in 10% neutral buffered formalin solution for two days, minimizing the effects of formalin conservation on mechanical properties²⁹⁹, and then transferred to PBS. Subsequently, both ends of each femur were embedded in a cold-cured epoxy resin (Technovit 4071, Heraeus Kulzer, Germany). On the upper clamping side, a Cardan joint was used to ensure pure rotation without bending. The lower sides were simply fixed. Tests were performed until failure with a rotation rate of 0.5°s^{-1} using a static mechanical testing machine that could apply a maximum torque of 450N.mm (Zwick GmbH, Ulm, Germany). Torsional strength (maximum torque to failure, N.mm) was determined.

8. Statistics

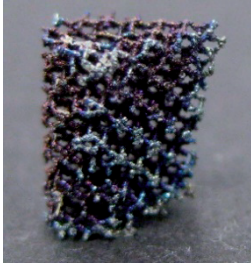
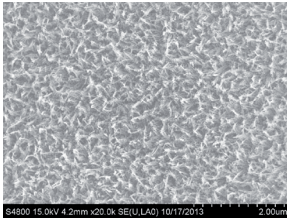
Statistical analyses were performed using SPSS Statistics 20.0 (SPSS, Inc.). Data are presented as means with standard deviations. One-way analysis of variation (ANOVA) and subsequent post hoc pairwise comparisons with Bonferroni adjustment were used to test for differences between the four groups. A power calculation (β -value >0.80 , SD $\sim 25\%$) was made to find a true difference in total BV of at least 35%. Based on this calculation, $n=10$ was required. A p -value <0.05 was considered statistically significant.

Results

1. Porous titanium implants incorporated with fibrin gels

Porous titanium implants were produced using SLM in the anatomical shape of the surgically removed cortical bone segment (Figure 1A). The implants had a porosity of 85% and a pore size ranging from 460-670 μm (Table 1). The alkali-acid-heat treatment resulted in a titanium oxide layer with an irregular nano-scale features (Table 1). Macroscopic inspection and SEM analyses verified that the pores of the titanium implants were completely filled with fibrin gel (Figure 1A-B). The protein fibers of both fibrin gels attached intimately to the

Table 1. Properties of porous titanium implants

Titanium implant	
Titanium thickness	165±43µm
Pore size	577±146µm (range 460–670µm)
Porosity	85%
Pore volume	55mm
Compression strength	14MPa
Young's modulus	0.4GPa
Surface area / volume	0.034µm
Surface composition	Oxygen 35% Titanium 60% Vanadium 2% Aluminium 3%
Surface topography (SEM)	

surface-treated titanium (Figure 1C). In addition, SEM showed clear differences between HMW-Fb and UNF-Fb gels with respect to their nanofiber structures: as compared to the fiber network formed by unfractionated fibrinogen, resulting in a much denser structures with smaller average pore diameters and thinner fibers (Figure 1D), polymerisation of high molecular weight fibrinogen appeared to form a more open network with relatively thicker fibers (Figure 1E).

2. Load-bearing segmental bone defects

All rats were able to tolerate weight-bearing activities immediately after surgery; the implantation sites healed without complications and all animals remained healthy during the follow-up.

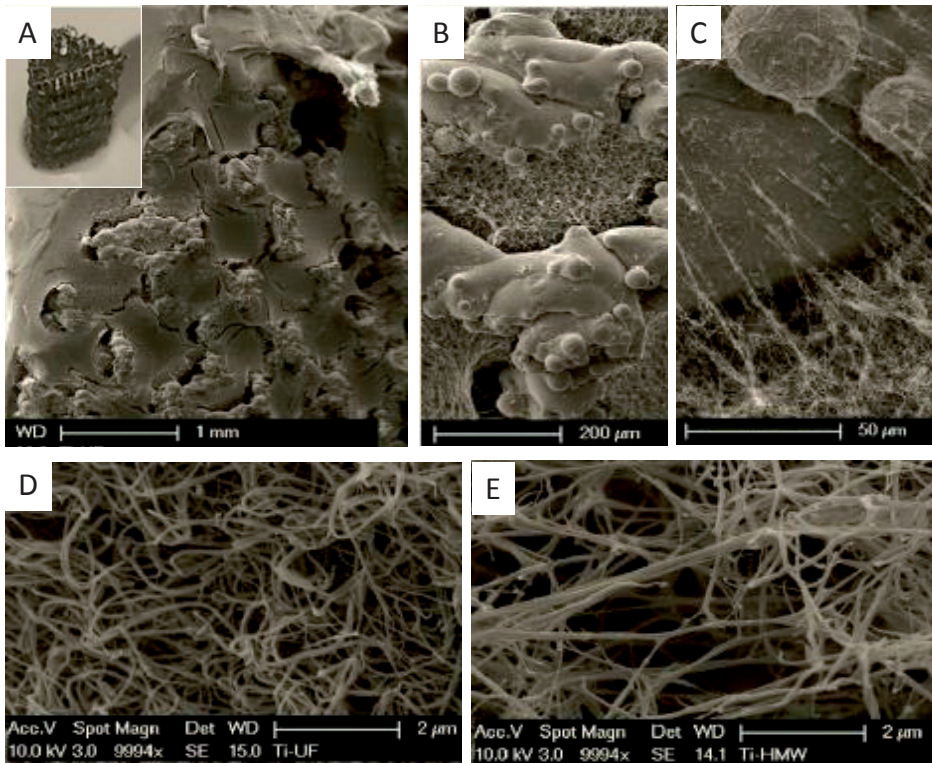


Figure 1: SEM images of fibrin loaded porous titanium implants.

Macroscopic overview, and enlarged details, of a fully fibrin-filled implant (A, B). The fibrin fibers are tightly bound to the implant surface (C). The fiber network resulting from unfractionated fibrinogen is rather dense with thin fibers (D). The fibrin network from HMW fibrinogen reveals an opener, better permeable, structure with slightly thicker fibers (E).

2.1 μCT evaluation

Porous titanium implants with HMW-BMP-Fb gels effectively stimulated bone regeneration (Figure 2). Within four weeks, bone regeneration had occurred throughout the entire length of the porous titanium implants and after eight weeks bridging of the defect was complete. Only minimal bone regeneration was observed in those defects grafted with HMW-Fb containing porous titanium implants and consequently failed to bridge (Figure 2). The load-bearing segmental defects grafted with HMW-BMP-Fb containing porous titanium implants fully restored the original bone architecture after twelve weeks (Figure 2 and 3). Incorporation of HMW-Fb or UNF-Fb did not seem to outperform the empty porous titanium implants (Figure 3).

Quantitative analysis of regenerated bone, based on *in vivo* μCT scans, showed that the total BVs of the HMW-BMP-Fb group increased at each time point and reached an average of $65.1 \pm 14.9 \text{ mm}^3$ after twelve weeks (Figure 4A). This was significantly higher than

all the three control groups. Neither the total BV of the HMW-Fb ($37.7\pm 26.4\text{mm}^3$) group nor that of the UNF-Fb ($32.1\pm 13.4\text{mm}^3$) group was significantly different from the total BV of the empty group ($33.7\pm 16.8\text{mm}^3$) (Figure 4A). Also the porous BV and outer BV of the HMW-BMP-Fb group were significantly higher than that of all three control groups (Figure 4B-C). After twelve weeks, $51\pm 8\%$ of the available pore space of the titanium implants with HMW-BMP-Fb gels was filled with regenerated bone, twice as much as in the HMW-Fb ($24\pm 18\%$) and UNF-Fb ($21\pm 5\%$) group, respectively. The inner BV of the HMW-BMP-Fb group ($3.9\pm 1.6\text{mm}^3$) significantly increased as compared to the control groups after four weeks. Contrary to the HMW-Fb and UNF-Fb groups, the inner BV of the HMW-BMP-Fb decreased over time ($3.1\pm 1.3\text{mm}^3$ at 8 weeks and $2.6\pm 1.3\text{mm}^3$ at 12 weeks) and even became significantly less than in the inner BV of the HMW-Fb group (Figure 4D).

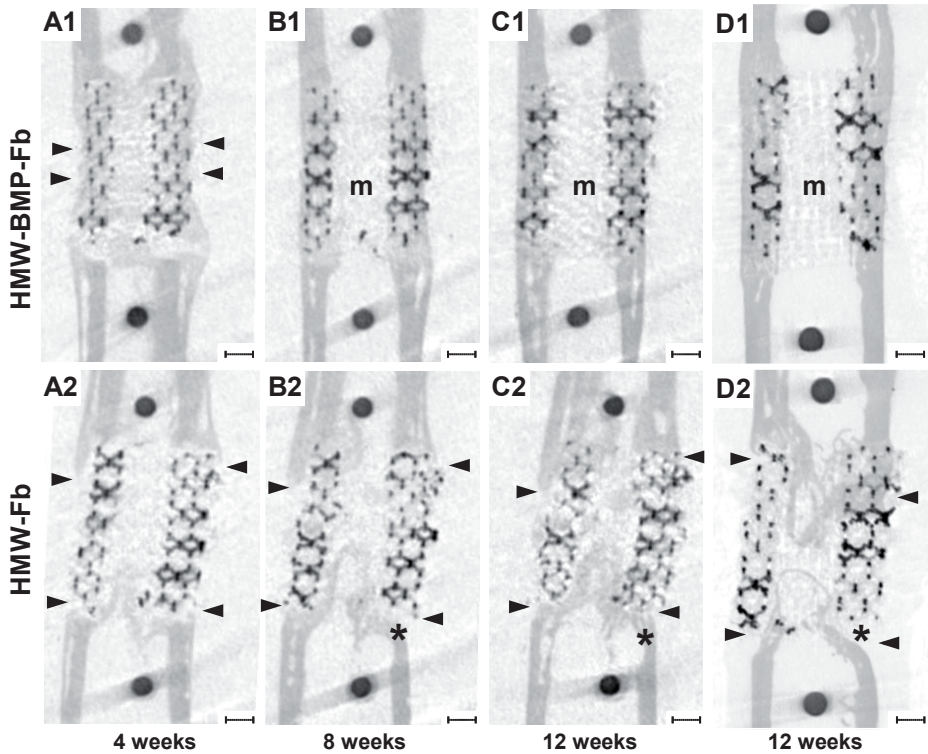


Figure 2: Representative longitudinal μ CT scans illustrating the bone regeneration process.

In vivo scans of defects grafted with porous titanium implants incorporated with high molecular weight fibrin with BMP-2 (HMW-BMP-Fb group) and high molecular weight without BMP-2 (HMW-Fb group) after four (A1-2), eight (B1-2) and twelve weeks (C1-2) as well as *ex vivo* after twelve weeks (D1-2). In the HMW-BMP-Fb group rapid bone regeneration throughout the complete length of the defect is observed already after four weeks (A1, arrows). Between eight and twelve weeks, the cortex and medullary canal (indicated by 'm') are restored in their original shape (B1, C1, and D1). In the HMW-Fb group, bone regeneration is only observed at the proximal and distal side of the porous implants (A2, arrows); this bone is predominantly situated in the medullary canal and insufficiently bridging the defect (D2). Distally from the titanium implants, bone resorption is observed between eight and twelve weeks (asterisk). Bar indicates 1mm.

Bone bridging, determined on *ex vivo* μ CT scans at twelve weeks, was only seen in the cortical defects grafted with porous titanium implants filled with HMW-BMP-Fb gels (Figure 5). Seven defects were completely bridged, and the average remaining gap size in the three defects that were not bridged was 0.8 ± 0.1 mm (Figure 6A). The remaining gap size in the other three experimental groups was 1.8 ± 1.6 mm (HMW-Fb group), 1.9 ± 0.9 mm (UNF-Fb group) and 1.8 ± 1.4 mm (empty group), respectively.

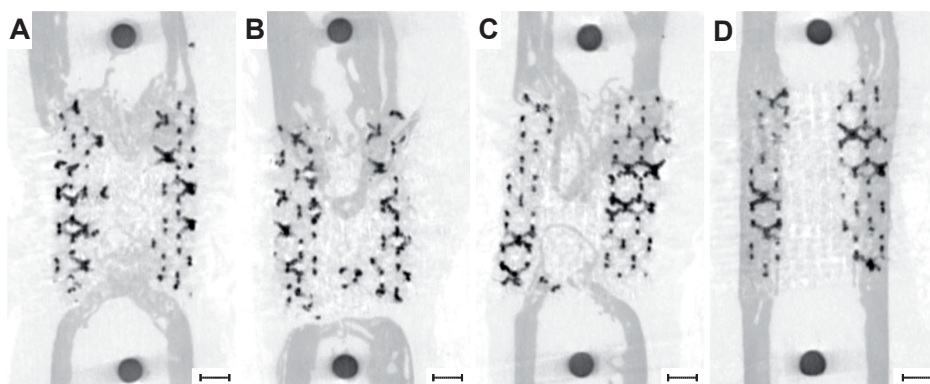


Figure 3: Representative transversal *ex vivo* μ CT images of grafted segmental femur defects. Titanium implants and fixation screws appear in black, whereas bone appears in dark grey. In the empty (A), UNF-Fb (B) and HMW-Fb (C) groups; bone regeneration is predominantly seen at the proximal and distal third of the porous titanium implants. Some new bone has formed inside the porous implants, but most of the newly formed bone is seen in the medullary canal. In the HMW-BMP-Fb group (D), bone regeneration extended throughout the entire porous titanium implants, bridging the defect. Bone formed inside the porous implant, and no bone has been formed inside the medullary canal. Black bar indicates 1 mm.

2.2 Histological evaluation

Bone quality, assessed using light microscopy, showed that in the HMW-BMP-Fb group bone was formed almost exclusively at the site of the original cortex and an intimate contact between the regenerated bone and the titanium implant was found throughout the entire length of the defect (Figure 7D vs. A-C). In the HMW-Fb (Figure 7C), UNF-Fb (Figure 7B) and empty groups (Figure 7A), bone formation occurred predominantly at the distal and proximal sites of the titanium implants that were close to the adjacent cortical bone. This bone formation never extended throughout the entire length of the porous implant. The remaining gaps in the defects were rather filled with amorphous fibrous tissue (Figure 7A, B, and C). Strikingly, in the HMW-BMP-Fb group an open medullary cavity was observed after twelve weeks (Figure 7D), whereas in all control groups bone formation was blocking the medullary cavity (Figure 7A-C).

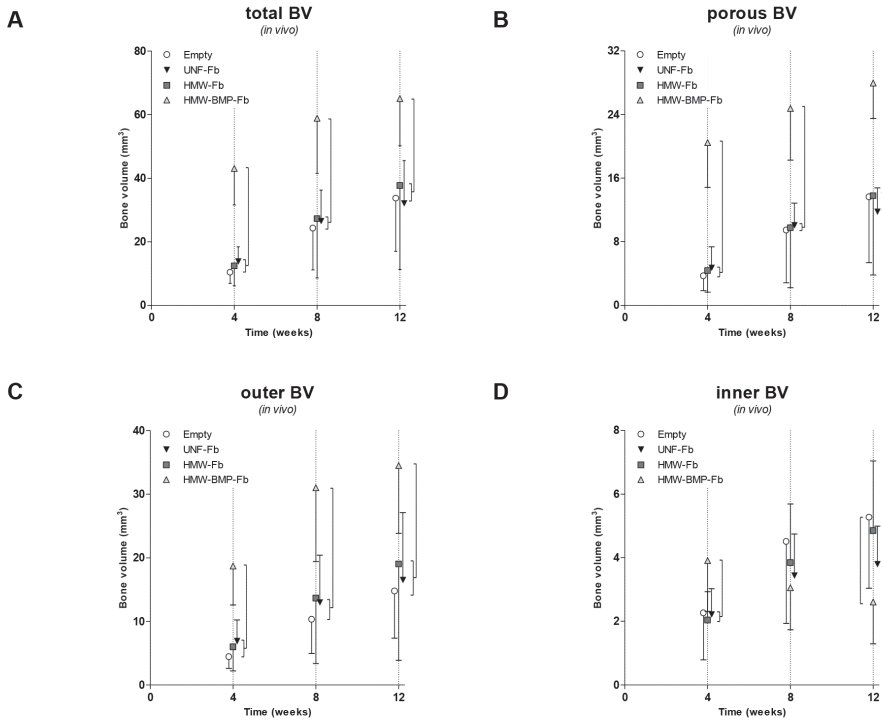


Figure 4: Longitudinal quantification of bone regeneration.

In vivo μ CT scans after four, eight and twelve weeks; total BV (A); defined as all bone formed within the 6 mm defect. Outer BV (B), defined as bone formed outside the titanium implants. Porous BV (C), defined as bone formed inside the porous space of the titanium implants. Inner BV (D), defined as bone formed in the medullary canal of the titanium implants. Values are expressed as mean and SD ($n=10$ per group), and a one-way ANOVA test followed by a post-hoc Bonferroni correction was performed to test for statistically significant difference at each time point. A p -value <0.05 was considered as statistically significant, vertical bars indicate the significant differences found between the groups.

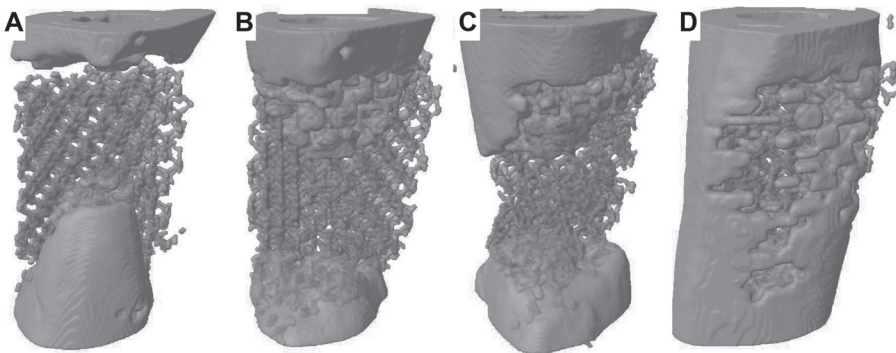


Figure 5: Illustration of bone bridging.

Representative 3D μ CT images showing the average extend of bone bridging of the empty (A), UNF-Fb (B), HMW-Fb (C), as well as the HMW-BMP-Fb (D) group. Porous titanium implants appear in transparent grey, whereas bone appears in dark grey.

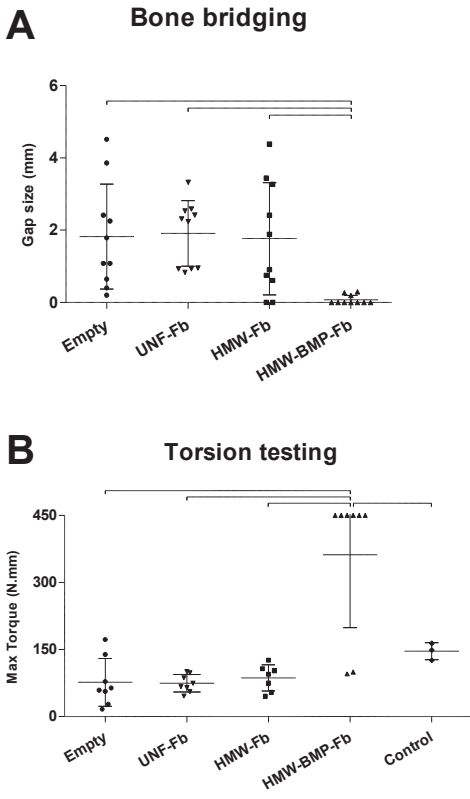


Figure 6: Bone bridging and mechanical strength.

The remaining gap size after twelve weeks was used to indicate bridging success (A). Mechanical femoral strength after implantation of porous titanium implants measured by torsion testing (B). As a positive control, three control femurs were included to provide a reference of a normal strength of femurs during torsion testing. Values are expressed as mean and SD, and a one-way ANOVA test followed by a post-hoc Bonferroni correction was performed to test for statistical significant differences at each time point. A *p*-value <0.05 was considered as statistically significant, horizontal bars indicate significant differences between groups.

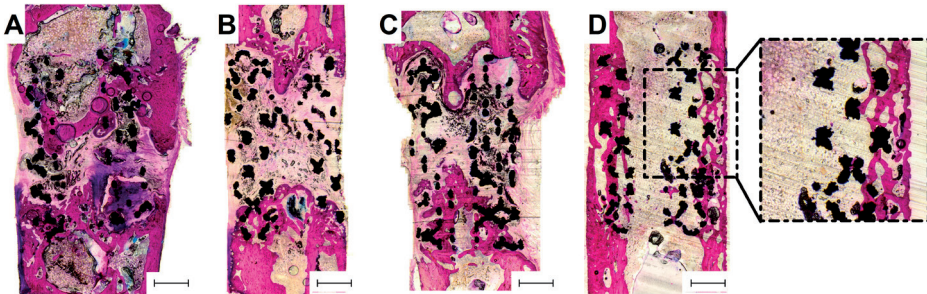


Figure 7: Histological evaluation of bone bridging.

Representative transversal sections of femur defects twelve weeks after implantation of porous titanium implants; empty (A), or incorporated with UNF-Fb (B), HMW-Fb (C) or HMW-BMP-Fb gels (D). Magnification reveals re-colonization of the medulla with small round-shaped cells of a typical bone marrow stroma appearance. Sections are stained with basic fuchsin and methylene blue. Basic fuchsin stains bone purple, methylene blue stains fibrous tissue blue. Black bar indicates 1mm.

2.3 Biomechanical evaluation

Femurs of the HMW-BMP-Fb group reached a significantly higher maximum torque than the three control groups (Figure 6B). The specimens were more than twice as strong as control femurs (248%) and six femurs of this HMW-BMP-Fb group were able to resist the maximum torque (450N.mm) without breaking. Femurs of the HMW-Fb group did not differ in maximum torque from the femurs of the UNF-Fb or empty group. The average maximum torques were 60% (HMW-Fb group, 86 ± 29 N.mm), 51% (UNF-Fb group, 75 ± 20 N.mm), and 53% (empty group, 77 ± 53 N.mm), respectively, of the average maximum torque measured for control femurs (146 ± 19 N.mm) (Figure 6B).

Discussion

An ideal biomaterial that can be used as a bone graft substitute should be able to fully regenerate and bridge load-bearing segmental bone defects within a short period of time²⁸⁰. Our combination of surface-treated porous titanium with BMP-2 containing physiologically concentrated fibrin gels fully regenerated segmental bone defects in rat femurs (Figure 2 and 5) and fully recovered their mechanical strength (Figure 6). Moreover, combining osteoconductive titanium with an osteoinductive BMP-2 releasing fibrin gel resulted in “guided” bone regeneration; *i.e.* new bone was formed throughout the porous titanium implants (Figure 2) to specifically restore the cortex to its native anatomical shape and well as the medullary canal (Figure 3 and 7D).

Biomaterials used for load-bearing segmental defects should offer sufficient support to withstand mechanical loading²⁸¹. A material with such mechanical properties is titanium, and solid titanium implants have been very successfully used in trauma and orthopaedic surgery over the past decades³⁵⁴. However, the notable biomechanical mismatch between solid titanium implants and surrounding bone frequently leads to stress-shielding, subsequent bone resorption and implant loosening³⁵⁵. This limitation can be overcome by using mechanically optimized porous titanium implants^{271, 356}, the development of which greatly benefited from the introduction of additive manufacturing techniques. Techniques such as selective laser melting (SLM)^{262, 357, 358}, electron beam melting (EBM)^{270, 359, 360} or similar additive manufacturing techniques^{265, 317} allow for a personalized, anatomical implant design and control of its structural and mechanical properties alike. Our SLM-based, femur-shaped implants possessed mechanical properties within the physiological range of the host bone, while its fully interconnected porous structure is considered to be within the range required for osteoconduction (Table 1)³¹⁹. Furthermore, the fatigue properties of the porous implants indicate that the biomechanical support is temporary²⁹⁰. The implants were therefore capable of offering sufficient mechanical support *in vivo*, while stimulating bone regeneration through osteoconduction in the segmental bone defects^{252, 319}.

In addition to mechanical support, biomaterials should also offer a surface that facilitates osseointegration, *i.e.* intimate apposition of bone matrix onto the implant surface³⁶¹. The bone-implant interface of most metallic biomaterials including titanium usually consists of an interfacial fibrous-like layer (also called *laminae limitantes*)³⁶¹. The formation of this fibrous-like layer can be avoided by relatively simple treatments that have been shown to improve osseointegration of solid titanium implants²⁷⁷. We optimized the treatment of the porous titanium implants used in this study²⁹², to not only improve apatite formation and cellular attachment, but also cell proliferation and osteogenic differentiation of osteoprogenitor cells²⁹².

Bone graft substitutes should also be able to induce bone regeneration, which can be induced by a variety of bone morphogenetic proteins (BMPs), including BMP-2 and BMP-7³⁶². BMP-2 is mainly released during the first few days of the natural bone regeneration process, and BMP-7 plays a more important role during the later phase⁵. Both BMP-2 and BMP-7 received FDA-approval²²⁰, but their use in humans is currently heavily debated³⁶³. Although the osteoinductive effect of BMP-2 has been demonstrated in a wide variety of species (including rats, rabbits, dogs, sheep and non-human primates)³⁶⁴, it is often argued that one must be cautious in assuming that stromal cells from other species may serve as models for inducible osteogenesis in human marrow stromal cells³⁶⁵. BMP-induced side effects, including cyst-like bone formation and soft tissue swelling, are likely caused by supra-physiological dosages used in humans³⁶³ and these adverse effects were recently reproduced in a similar *in vivo* model as used in this study with BMP-2 concentrations that exceeded 20µg per defect^{253, 333}. In contrast, a dose between 2.5 and 10µg was found to be safe and effective for various other BMP release systems including alginate-based³⁶⁶, poly-L-lactic acid (PLLA)-based³⁶⁷ or silk-based³⁶⁸ scaffolds. Based on these results we used 3 µg BMP-2 per implant. Furthermore, Schmoekel *et al.* demonstrated that with less soluble nonglycosylated BMP-2, the required cytokine dose could even be further reduced³⁶⁹.

Surface-treated porous titanium was loaded with BMP-2 through incorporation in physiologically concentrated fibrin gels. This is different from fibrin gels that have been used in trauma and orthopaedic surgery as "*fibrin glue*", as these sealants are made of highly supra-physiological fibrinogen concentrations³⁵¹. This supra-physiological concentration (50-100 mg/L) ensures quick and effective clotting, and is therefore primarily used as a haemostatic agent. Supra-physiological fibrinogen concentrations were also used to deliver BMP-2 in several bone defect models³⁶⁹⁻³⁷⁹. Schützenberger *et al.* showed that fibrin gels outperformed the currently clinically used absorbable collagen sponges as BMP-release properties of fibrin, in contrast to those of collagen, allow to use 85% less cytokine without compromising the regenerative success³⁸⁰. However, the high fibrinogen concentration of these supra-physiologically concentrated fibrin glues have a limiting effect on cell mobility and ingrowth^{381, 382}. *In vivo*, fibrin constitutes only 0.25% of the volume of a blood clot³⁸³, which was mimicked in the current study by preparing fibrin gels of physiological

concentrations (2-4mg/L). It is tempting to speculate that at these concentrations, fibrin fibers form a more open network that more effectively promoted cell migration and cell ingrowth³⁸⁴. This open network structure and fibrin fiber adherence was perfectly supported by the surface-treated porous titanium (Figure 1C). This temporary fibrin network is not expected to remain intact *in vivo* for more than a few days³⁷⁶, but the results obtained in this study suggest that this is sufficient to adequately induce bone regeneration. Our approach mimics physiological fracture healing, during which BMP-2 is entrapped in the spontaneously formed fracture haematoma to induce differentiation of mesenchymal stromal cells into osteoblasts³⁸⁵. These osteoblast subsequently start to produce more BMP-2 and other important osteogenic cytokines to reach a maximum activity after 4-7 days³⁸⁶.

Physiologically concentrated fibrin gels prepared from HMW fibrinogen were expected to improve bone regeneration, as compared to gels prepared from UNF fibrinogen, because HMW fibrinogen has been shown to promote angiogenesis *in vitro* and *in vivo* in our earlier studies³⁵⁰. UNF fibrin gels contain 30% low molecular weight fibrinogen and, compared to 100% HMW fibrinogen, contamination with more than 10% of LMW fibrinogen gradually decreased the formation of tube-like structure *in vitro* in a dose-depend manner³⁵⁰. However, implants with HMW-Fb gels alone did not enhance bone regeneration and performed similar to implants with UNF-Fb gels or empty porous titanium implants (Figure 2 and 5). BMP-2 release from the fibrin gel is apparently providing the only osteoinductive stimulus,

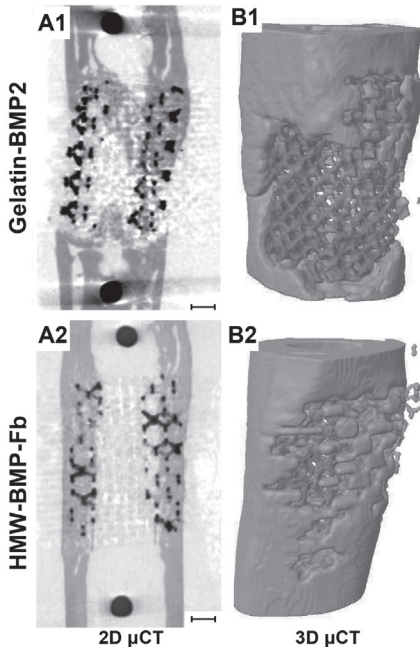


Figure 8: Direct comparison between BMP-2 release from fibrin and gelatin on bone regeneration.

In the same *in vivo* model, using the same type of porous titanium implants and same batch of BMP-2, results from using HMW-BMP-Fb gels (this work) or gelatin nanosphere gels²⁵² were compared. Using gelatin nanosphere gels loaded with 3 μ g BMP-2 predominantly led to bone regeneration outside or inside the porous titanium implants (A1) without bridging the entire defect (B1). In contrast, HMW-BMP-Fb gels (loaded with the same dose of BMP-2) led to complete bridging with restoration of the medullary canal (A2) and the cortex (B2). Bar indicates 1mm.

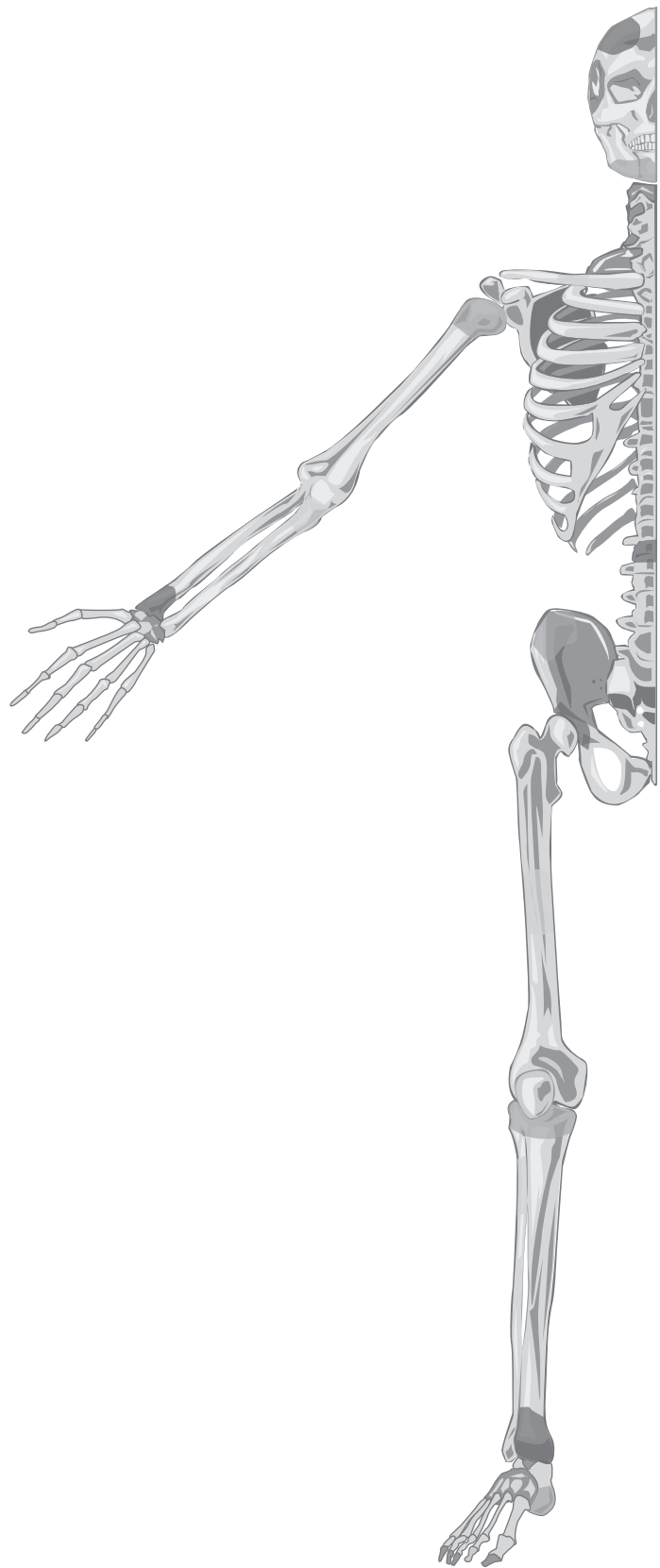
while HMW-Fb may still improve cell migration and angiogenesis. Whether using HMW-Fb to release BMP-2 is indeed better than using UNF-Fb because it improves cell migration or angiogenesis cannot be answered here and is a limitation of our study. But HMW-fibrin gels with BMP-2 clearly outperformed previously used gelatin-based nanosphere gels with BMP-2²⁵², indicating the type of BMP-2 carrier is of crucial importance. Although gelatin gels were capable of a sustained release of BMP-2³⁹, this resulted in bone regeneration that mainly occurred around and inside the porous titanium implants (Figure 8; A1). In addition, bone regeneration in that study did not lead to bridging of the grafted defects within twelve weeks (Figure 8; B1). The mechanical strength also reached only up to only 50% of the original strength in that study³⁹. In contrast, physiological fibrin gels with low doses of BMP-2 boosted bone regeneration in the present study and completely bridged the majority of the grafted defects within four weeks (Figure 8; B2), filling up more than 50% of the porous volume of the titanium implants with regenerated bone. Twelve weeks following the surgery, the grafted femurs were already more than twice as strong as their original strength (*i.e.* control femurs Figure 6).

Conclusion

In this study the developed a new biomaterial combination capable of stimulating complete bone regeneration in load-bearing segmental defects in rat femurs. This optimal combination enabled quick bone regeneration within four weeks and full restoration of the original bone functionality and anatomical shape in this pre-clinical model. Since all used methods have been used separately in trauma and orthopaedic surgery, this combination should be evaluated in a large animal model or a clinical trial and this might result in an efficient bone graft substitute to graft load-bearing segmental bone defects in trauma and orthopaedic surgery.

Acknowledgements

This research forms part of the Project P2.04 BONE-IP of the research program of the Bio-Medical Materials institute, co-funded by the Dutch Ministry of Economic Affairs and was supported by a grant from the Dutch government to the Netherlands Institute for Regenerative Medicine (NIRM, grant No. FES0908). This research project was further supported by the START-Program of the Faculty of Medicine, RWTH Aachen. HW and HJ are receiving EU funding (FP7, HEALTH.2012.2.4.5-2, project number 305815, D-BOARD). Osteosynthesis & Trauma Care foundation is acknowledged for financial support (2011-HWJV).



Chapter 9

Chondrogenically differentiated mesenchymal stromal cell pellets

Johan van der Stok
Marianne K.E. Koolen
Holger Jahr
Nicole Kops
Jan H. Waarsing
Harrie Weinans
Olav P. van der Jagt

Published as "Chondrogenically differentiated mesenchymal stromal cell pellets stimulate endochondral bone regeneration in critical-sized bone defects" in European Cells & Materials. 2014 Feb 19;27:137-48

Abstract

Grafting bone defects or atrophic non-unions with mesenchymal stromal cells (MSCs)-based grafts is not yet successful. MSC-based grafts typically use undifferentiated or osteogenically differentiated MSCs and regenerate bone through intramembranous ossification. Endochondral ossification might be more potent but requires chondrogenic differentiation of MSCs. Here, we determined if chondrogenically differentiated MSC (ch-MSC) pellets could induce bone regeneration in an orthotopic environment through endochondral ossification. Undifferentiated MSC pellets (ud-MSC) and ch-MSC pellets were generated from MSCs of human donors cultured on chondrogenic medium for respectively three (ud-MSC) and 21 (ch-MSC) days. A 6mm femoral bone defect was made and stabilised with an internal plate in 27 athymic rats. Defects were left empty for six weeks to develop an atrophic non-union before they were grafted with ch-MSC pellets or ud-MSC pellets. μ CT scans made four and eight weeks after grafting showed that ch-MSC pellets resulted in significantly more bone than ud-MSC pellets. This regenerated bone could completely bridge the defect, but the amount of bone regeneration was donor-dependent. Histology after seven and fourteen days showed slowly mineralising pellets containing hypertrophic chondrocytes, as well as TRAP-positive and CD34-positive cells around the ch-MSC pellets, indicating osteoclastic resorption and vascularisation typical for endochondral ossification. In conclusion, grafting critical-sized femoral bone defects with chondrogenically differentiated MSC pellets led to rapid and pronounced bone regeneration through endochondral ossification and may therefore be a more successful MSC-based graft to repair large bone defects or atrophic non-unions. But, since bone regeneration was donor-depend, the generation of potent chondrogenically differentiated MSC pellets for each single donor needs to be established first.

Introduction

Bone development and fracture repair occur through intramembranous or endochondral ossification³⁸⁷. In intramembranous ossification, mesenchymal stromal cells (MSCs) differentiate directly into osteoblasts that form bone. In endochondral ossification, MSCs differentiate into chondrocytes, which form a cartilage template⁴. Chondrocytes within this template become hypertrophic and start to secrete cytokines such as vascular endothelial growth factor (VEGF), and enzymes like alkaline phosphatase (ALP) and proteases (e.g. matrix metalloproteinases (MMPs)). Together, these factors stimulate vascularisation and mineralization of the cartilage template, which is subsequently resorbed by attracted osteoclasts and replaced by bone. Which type of ossification predominantly occurs in fracture repair is highly dependent on biomechanical conditions. Absence of motion results in intramembranous ossification, although this is only capable of bridging small gaps (200-500µm), whereas micromotions stimulate endochondral ossification, through which larger fracture gaps are regenerated⁷.

Despite modern treatment, fracture repair remains insufficient or impaired in 10% of all fractures resulting in non-unions or persistent bone defects⁸. Bone defects and atrophic non-unions can be treated with bone grafts, for which the current gold standard material is autologous bone⁴⁴. However, harvesting autologous bone results in a high morbidity rate (10-40%)^{12, 17}, and the amount that can be harvested is limited. These disadvantages fuelled the development of bone graft substitutes. Ideally a bone graft substitute should consist of a biodegradable material that offers direct mechanical support and functions as an osteoconductive scaffold that facilitates bone regeneration. Also the material should provide osteogenic and angiogenic stimuli to enhance bone regeneration and vascularisation²²². Bone graft substitutes currently available for clinical use mainly rely on osteoconductive properties²³. Only in a small case-series, an osteoconductive bone substitute has been combined with MSCs to graft bone defects³⁸⁸. But so far the clinical success of MSC-based grafts remains disappointing³⁸⁹. This may be because those MSC-based grafts contained undifferentiated or osteogenically differentiated MSCs and thus stimulated intramembranous ossification. Differentiation of MSCs towards chondrocytes, and thereby aiming to stimulate endochondral ossification, may be a more successful strategy³⁹⁰.

Chondrogenically differentiated embryonic stem cells³⁹¹, embryonic chondrocytes³⁹² or MSCs³⁹³ can undergo hypertrophy and secrete factors similar to those normally secreted by hypertrophic chondrocytes during endochondral ossification (e.g. VEGF, MMP-13, and ALP). *In vivo*, chondrogenically differentiated MSCs can form bone through endochondral ossification after ectopic implantation in mice^{391, 394-396}. But ectopic implantation does not fully reflect the complex environment of a bone defect or an atrophic non-union. In an orthotopic environment, bone regeneration starts with a low-grade inflammatory phase²⁵⁵, under low-oxygen tensions³⁹⁷, and is continuously exposed to biomechanical stimuli. All

these factors are known to affect MSCs differentiation and survival ³⁹⁸. In this study, we therefore made critical-sized femoral bone defects in rats, and left these defects untreated for six weeks to establish an atrophic non-union. Subsequently the defects were grafted with chondrogenically differentiated MSC pellets to determine whether chondrogenically differentiated MSC pellets remain capable of endochondral ossification in this orthotopic environment. We hypothesized that grafting with chondrogenically differentiated MSC pellets enhances bone regeneration and used grafting with undifferentiated MSC pellets as a control. Bone regeneration was evaluated with the use of μ CT scanning, histology and immunohistochemistry.

Materials and methods

1. Isolation and expansion of human bone marrow cells

Human bone marrow derived MSCs of three donors (donor 1: female, 75 years, donor 2: female, 77 years, donor 3: female, 55 years) were obtained during total hip arthroplasty after informed consent and approval of the local medical ethical committee (METC 2004-142). Bone marrow aspirates were taken from the great trochanter. Heparinized aspirates were seeded at a density of 30 to 100×10^6 nucleated cells per T175 flask. After 24h, non-adherent cells and cell debris were washed out. MSCs were further expanded in low-glucose Dulbecco's modified Eagle medium (DMEM) with 10% fetal calf serum (Lonza) supplemented with 50 μ g/mL of gentamicin, 1.5 μ g/mL of Fungizone (all Invitrogen), 0.1 mM of L-ascorbic acid 2-phosphate and 1ng/mL of fibroblast growth factor 2 (Instruchemie). Cells were cultured at 37°C under humidified conditions and 5% carbon dioxide (CO₂). Medium was changed twice a week. When cultured cells neared confluence, they were trypsinized using 0.05% trypsin and replated at a density of 2,000cells/cm². Cells from the third passage were used for pellet cultures.

2. Culturing of chondrogenically differentiated MSC pellets and undifferentiated MSC pellets

After detachment of cells with 0.05% trypsin, 0.5mL of medium, containing 200,000 cells, was put in a polypropylene tube. Tubes were centrifuged for 8m at 120g. Undifferentiated MSC (ud-MSC) pellets and chondrogenically differentiated MSC (ch-MSC) pellets were maintained for respectively three and 21 days on high-glucose DMEM, supplemented with 50 μ g/mL of gentamicin, 1.5 μ g/mL of Fungizone (Invitrogen), 0.1mM L-ascorbic acid 2-phosphate, 40 μ g/mL L-proline, 1mM of sodium pyruvate (Sigma-Aldrich), 1:100 ITS (BD Biosciences), 10ng/ml of TGF- β 1 (R&D Systems), and 100nM of dexamethasone (Sigma-Aldrich). After maintaining ud-MSC pellets and ch-MSC pellets for respectively three and 21 days, they were directly used for implantation.

3. Animal experiment

Twenty-seven skeletally mature male RNU rats (Charles River) were used as experimental animals (361 ± 36 g body weight). When the animals were 16-weeks-old a critical-sized femoral bone defect was made by removal of 6mm cortical bone, while stabilized with an internal fixation plate. Six weeks later, in a second surgical procedure, bone defects were grafted with ch-MSC pellets ($n=15$) or ud-MSC pellets ($n=12$). The Animal Ethics Committee of the Erasmus University approved the study (ECM 1493) and Dutch guidelines for the care and use of laboratory animals were applied.

4. Surgical procedures

Prior to surgery, prophylactic antibiotics (enrofloxacin, 5mg/kg body weight) and pain medication (buprenorphine, 0.05mg/kg body weight) were administered. Surgical procedures were performed aseptically under general anaesthesia (1-3.5% isoflurane).

During the first surgical procedure, a critical-sized femoral bone defect was made as follows: the right femur was exposed through a lateral skin incision and division of underlying fascia. A 23mm long polyetheretherketone (PEEK) plate was fixated to the anterolateral plane of the femur using three proximal and three distal screws (RatFix, RISystem). Periosteum was removed over approximately 8mm of the mid-diaphyseal region before removal of 6mm cortical bone. Bone was removed with a tailor-made saw guide and a wire. Fascia and skin were sutured in layers using Vicryl 5-0. Antibiotic medication was continued for two days post-surgery, and pain medication was continued for three days.

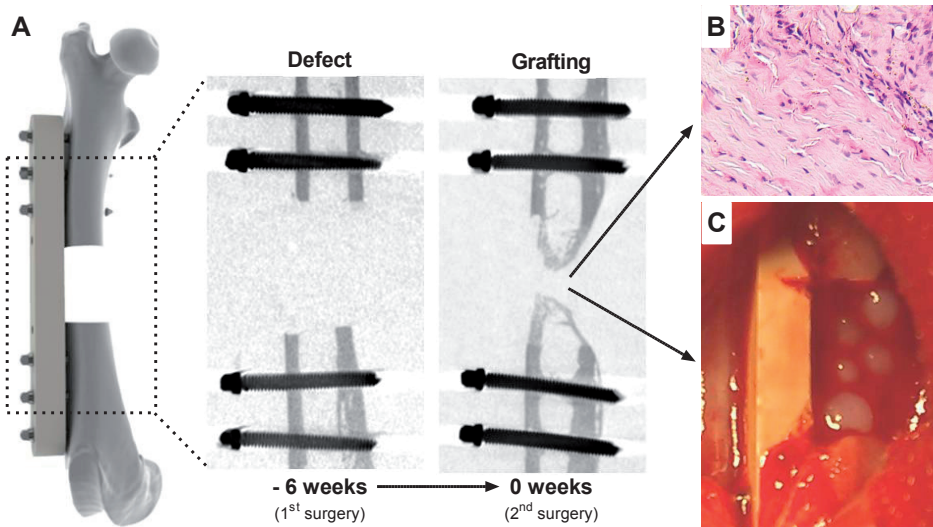


Figure 1: Femur bone defect model.

Critical-sized femur defect with PEEK plate fixation and transversal μ CT images directly after removal of 6mm cortical bone and after six weeks (A). Fibrous tissue that was removed from the defect (B) before six ch-MSC pellets were used to graft the defect (C).

During the second surgical procedure, six weeks later, critical-sized bone defects were grafted with ch-MSC or ud-MSC pellets as follows: the right femur was again exposed through a lateral skin incision and division of underlying fascia. After full exposure of the femur, none of defects had bridged and the defect was filled with fibrous tissue (Figure 1A-B). After debridement and trimming of bone edges at proximal and distal side, defects were grafted with six ch-MSC or ud-MSC pellets (Figure 1C). Pellets were contained inside the defect by closure through intramuscular sutures (Vycril 5-0). Subsequently fascia and skin were sutured. Antibiotic medication was continued for two days post-surgery, pain medication was continued for three days. Rats were killed by an overdose pentobarbital.

5. μ CT evaluation

Bone regeneration was followed longitudinally by *in vivo* μ CT scans, acquired under general anaesthesia (1-3.5% isoflurane). A timeline was acquired by scanning one rat of ch-MSC-group and one rat of ud-MSC-group every week, while the remaining rats ($n=8$ per group) only underwent scans at four and eight weeks to quantify bone regeneration. μ CT scans were made with a SkyScan 1176 scanner (Bruker micro-CT) using a 35 μ m resolution protocol (65kV, 385 μ A current, 1mm Al filter, and 0.5 degree rotation step, resulting in a 7 minute scan). CT images were reconstructed using volumetric reconstruction software NRecon version 1.5 (Bruker micro-CT). Bone volume (BV) was quantified within the 6mm defect after segmentation of calcified tissue from non-calcified tissue using a global threshold. This global threshold was determined based on visual inspection and was kept constant for all scans.

6. Histological and immunohistochemical evaluation

Histology and immunohistochemistry was done on ch-MSC and ud-MSC pellets cultured *in vitro* ($n=3$ per donor) and on grafted femoral bone defects after three, seven and fourteen days ($n=2$ ch-MSC-group, $n=1$ ud-MSC-group at each time point) and after eight weeks ($n=8$ per group). Pellets and grafted femurs were fixed in 10% neutral buffered formalin solution for two days. Grafted femurs were decalcified in 10% EDTA in PBS solution (pH = 7.4) for six weeks. Finally, all specimens were dehydrated in graded ethanol solutions (70 to 100%) and xylene before embedding in paraffin. Six- μ m paraffin sections were cut with a microtome (Leica RM2135). Pellets were stained with haematoxylin-eosin (H&E) and thionin, and immunostained for collagen II, collagen X and VEGF. Grafted femurs were stained with H&E, thionin, and tartrate-resistant acid phosphatase (TRAP), and immunostained for collagen II and CD34.

Collagen II is a marker for chondrogenic differentiation and collagen X is a marker for hypertrophy. Antigen retrieval for collagen II was performed through 30m incubation of sections with 0.1% pronase in PBS, while antigen retrieval for collagen X required 0.1% pepsin in 0.5M acetic acid (pH = 2.0) for two hours. Both collagen II and collagen X stainings

continued with incubation with 1% hyaluronidase in PBS for 30 minutes. Non-specific binding sites were blocked with 10% goat serum in PBS and sections were stained overnight with primary antibodies against collagen II (II/II6B3 antibody, 1:100, Developmental Studies Hybridoma Bank, Iowa City, IA, under contract N01-HD-6-2915 from the National Institute of Child Health and Human Development) or collagen X (1:30, X53, Quartett, Berlin, Germany). To allow the use of monoclonal mouse antibodies on human constructs grafted in a nude rat, we used a method described by Hierck *et al*³⁹⁹. An alkaline-phosphatase-conjugated secondary antibody was used followed by incubation with Neu Fuchsin substrate (Chroma) to demonstrate alkaline-phosphatase activity with a red staining. The positive control for collagen II was bovine cartilage, and for collagen X we used known hypertrophic pellets. An isotype control was taken along as negative control for both stainings.

VEGF is an angiogenic growth factor, and after microwave treatment in 10mM citric acid buffer pH 6.0, sections were blocked with 5% BSA in PBS for 10 min and incubated overnight at 4°C with VEGF antibody (sc-152, Santa Cruz Biotechnology Inc) diluted in 5% bovin serum albumin (BSA) in PBS. Secondary antibodies against human IgG were conjugated with peroxidase (Dako). CD34 is an endothelial cell marker indicating vessel-structures, and antigen retrieval for CD34 was performed through 30m incubation with 0.1% trypsin (Sigma). Non-specific binding sites were blocked with 10% NGS and sections were incubated with primary antibody against rat CD34 (R&D Systems). A biotinylated rabbit antibody followed by alkaline phosphatase conjugated streptavidin and incubation with Neu Fuchsin substrate (Chroma) was used to visualize positive staining. Slides were counterstained with haematoxylin. The positive control for VEGF was human skin and an isotype control was taken along as negative control.

7. Release of angiogenic cytokines

Secretion of angiogenic cytokines was measured in culture medium taken of the ch-MS and ud-MS pellets at the day of implantation using a human cytokine angiogenic multiplex chemiluminescent ELISA (Cat. No. 150251HU, Quansys Biosciences). This angiogenic multiplex measures angiotensin II (Ang-2), fibroblast growth factor-2 (FGF-2), hepatocyte growth factor (HGF), interleukin-8 (IL-8), platelet derived growth factor-BB (PDGF-BB), tissue inhibitor of metalloproteinase 1 and 2 (TIMP-1 and TIMP-2), tumor necrosis factor- α (TNF α), and vascular endothelial growth factor (VEGF). Multiplex chemiluminescent ELISA kits were performed according to the manufacturer's instructions and the plate was imaged using Kodak Digital Science™ Image Station 440CF system (NEN Life Science Products, Inc., Boston, MA, USA). Angiogenic cytokine concentrations were calculated using Q-view software® (Quansys Biosciences).

8. Statistics

The design of this study was aimed to find at least a duplication in the BV formed within the 6mm defect. The standard deviation of BV formed was estimated to be ~50% based on previous work^{252, 319, 400}. A simple power calculation using a students' *t*-test with a β -value of 0.8 indicates that both groups should consist of a minimal of five rats. The final decision to use eight rats per group accounted for loss of animal (e.g. failure of fixation material to stabilize the defect) or loss of donors (e.g. insufficient of unsuccessful chondrogenic differentiation of MSCs). Statistical analyses were performed using SPSS Statistics 20.0 (SPSS Inc, Chicago, Ill). The data are presented as means with standard deviation. Mixed models analysis was used to test for statistical differences between ch-MSC-group and ud-MSC-group, while correcting for donor effect using MSC donor as random factor. A *p*-value less than 0.05 was considered a statistically significant difference.

Results

1. Culturing and characterization of ch-MSC or ud-MSC pellets

Ch-MSC pellets were 2-3mm in diameter and contained hypertrophic chondrocytes surrounded by an extensive extracellular matrix (Figure 2, A1). This extracellular matrix contained high levels of GAGs, collagen II and collagen X, indicated by thionin staining and collagen II and X immunostainings (Figure 2, B1-D1 respectively). VEGF was mainly positive in and around the cells, but not in the extracellular matrix (Figure 2, E1). Ud-MSC

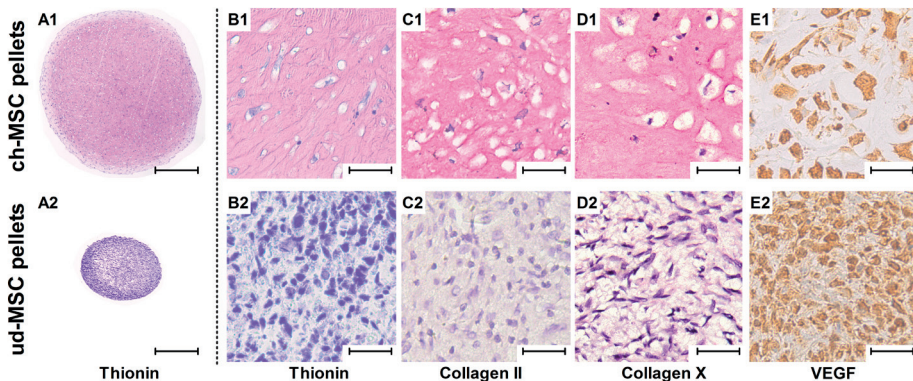


Figure 2: Histology of ch-MSC pellets and ud-MSC pellets before implantation.

Histology of ch-MSC pellets (A1) and ud-MSC pellets (A2): ch-MSC pellets were bigger and generated more extracellular matrix than ud-MSC pellets, bar indicates 500 μ m. Detailed views showed that the extracellular matrix of ch-MSC pellets is rich of GAGs (B1), collagen II (C1) and collagen X (D1), indicating that ch-MSC pellets had undergone hypertrophic chondrogenic differentiation. VEGF was predominantly found in and around the cells (E1). Ud-MSC pellets generated little to none extracellular matrix and had not undergone chondrogenic differentiation (B2, C2, and D2). VEGF was found throughout the pellets (E2). Bar indicates 50 μ m.

pellets were ~1mm in diameter and contained densely packed cells without substantial extracellular matrix (Figure 2, A2). Cells had not undergone chondrogenic differentiation as no GAGs, nor collagen II or collagen X were observed on thionin staining and collagen II and X immunostainings (Figure 2, B2-D2 respectively). VEGF was also produced by ud-MSC pellets and was mainly found in and around the cells (Figure 2, E2). Per donor, approximately 180-200 pellets were cultured from passage three human derived MSCs, which can theoretically result in 0.8–2.7cm³ of ch-MSC pellets.

2. μ CT evaluation

Two weeks after grafting the defects, ch-MSC pellets started to mineralize whereas no mineralization of ud-MSC pellets was observed (Figure 3). Mineralization of ch-MSC pellets started around the pellets and progressed towards the centre. Mineralized pellets also integrated with bone formed at the cortical bone edges. In one defect grafted with ch-MSC pellets of donor 1, bone formation was capable of completely bridging this defect within four weeks (Figure 4). Once this defect was bridged, the original bone architecture was restored through bone remodelling. In other defects grafted with ch-MSC pellets of donor 1 or donor 3, a minimal gap (<0.5mm) remained visible after eight weeks (Figure 5A). Defects grafted with ch-MSC pellets of donor 2 or with ud-MSC pellets showed little bone formation and defects were not bridged.

Bone quantification showed that grafting bone defects with ch-MSC pellets led to significantly more bone regeneration than grafting with ud-MSC pellets ($p=0.041$) (Figure 5B). After four and eight weeks, average BV of all defects grafted with ch-MSC pellets was

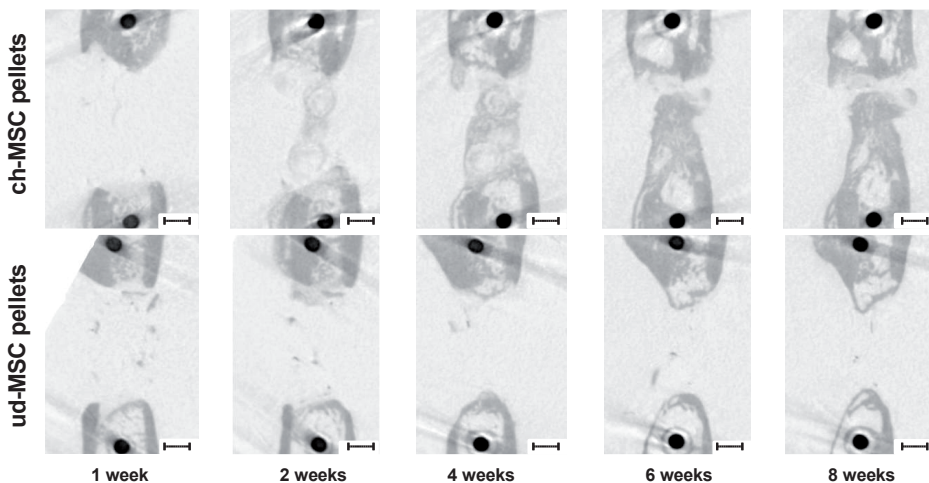


Figure 3: Repeated μ CT scans of defects grafted with ch-MSC pellets or ud-MSC pellets of donor 1.

Ch-MSC pellets mineralize after two weeks, and integrate with adjacent cortical host bone at four weeks. Ud-MSC pellets did not show mineralization throughout the eight week follow-up. Bar indicates 1mm.

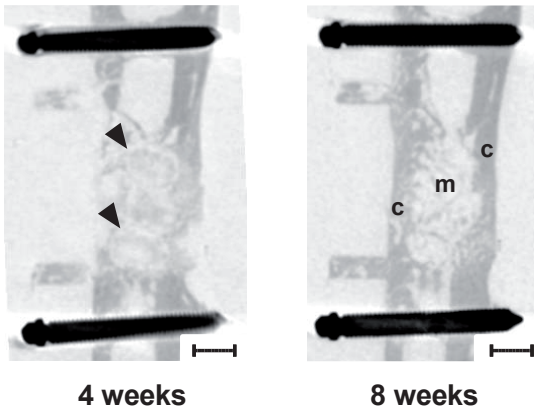


Figure 4: Remodelling of mineralizing ch-MSC pellets

Remodelling of mineralized pellets (4 weeks) restoring the original cortex and medullary canal (8 weeks) of the defect grafted with ch-MSC pellets of donor 1 that showed complete bridging. Black arrow heads depict complete bridging. 'c' indicates the newly formed cortex and 'm' indicates the ongoing restoration of the medullary canal. Bar indicates 1mm.

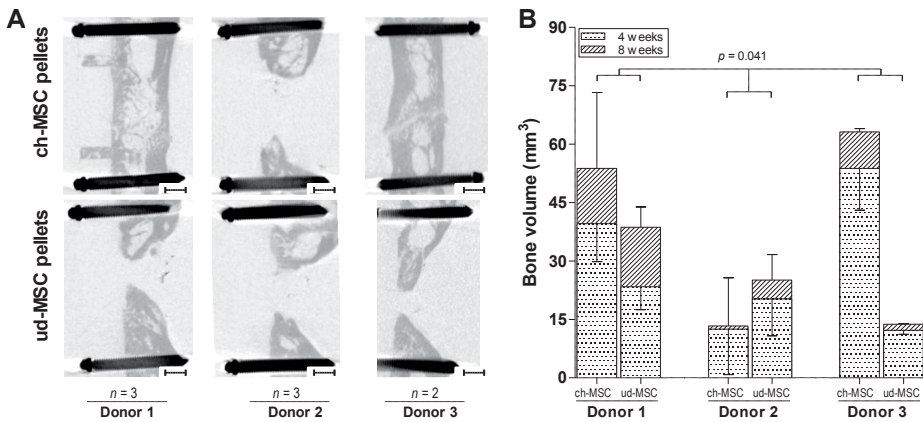


Figure 5: μ CT images of defects grafted with ch-MSC or ud-MSC pellets of all three donors after eight weeks.

Defects grafted with ch-MSC pellets of donor 1 and 3 show more bone formation than grafting with ud-MSC pellets, but defects grafted with ch-MSC pellets of donor 2 showed did not show more bone formation than defects grafted ud-MSC pellets of donor 2 (A). Bar indicates 1mm. Bone volumes measured in 6mm bone defect after four weeks and eight weeks (B).

almost twice as much as defects grafted with ud-MSC pellets (4 weeks $33.1 \pm 18.8 \text{mm}^3$ versus $17.8 \pm 8.6 \text{mm}^3$, 8 weeks $41.8 \pm 24.7 \text{mm}^3$ versus $24.2 \pm 12.2 \text{mm}^3$). This effect was donor dependent, ch-MSC pellets of donor 1 and 3 resulted in BVs of $39.6 \pm 9.7 \text{mm}^3$ (donor 1) and $53.8 \pm 10.7 \text{mm}^3$ (donor 3) after four weeks and $53.8 \pm 19.5 \text{mm}^3$ (donor 1) and $63.2 \pm 0.8 \text{mm}^3$ (donor 3) after eight weeks. But grafting defects with ch-MSC pellets of donor 2 only resulted in $13.3 \pm 12.4 \text{mm}^3$ BV after eight weeks, which was not more than grafting with ud-MSC pellets ($25.1 \pm 6.6 \text{mm}^3$). Compared to donor 2, ud-MSC pellets of donor 1 and 3 resulted in similar BVs and were $36.7 \pm 5.2 \text{mm}^3$ and $13.8 \pm 0.1 \text{mm}^3$ respectively.

3. Histological evaluation

Grafted ch-MSC pellets were clearly visible in the defect after seven and fourteen days (Figure 6, A1-2). They formed a cartilage template that bridged the defect. After seven days, ch-MSC pellets were surrounded by a number of cell layers (Figure 6, B1, C1, and D1). At this time, some vessel-forming activity was detected around the ch-MSC pellets (Figure 6, F1: arrows), without substantial osteoclast activity (Figure 6, E1). After fourteen days, the cartilage template was reduced in size (Figure 6: B1, C1, and D1) and more osteoclast activity was observed along the edges of the remaining ch-MSC pellets (Figure 6, E2: arrows). Areas of osteoclast activity were accompanied by vessel-forming activity and vessel-like structures (Figure 6, F2: arrows). Grafted ud-MSC pellets also remained visible up to fourteen days, but did not form a cartilage template inside the defect (Figure 7, A1-2). After seven and fourteen days, ud-MSC pellets had not undergone chondrogenic differentiation (Figure 7, B1-2, C1-2 and D1-2) and were surrounded by a high number of small round cells. After seven and fourteen days, there was no osteoclast activity (Figure 7, E1-2) but in the surrounding tissue substantial vessel-forming activity was observed (Figure 7, F1-2: arrows).

After eight weeks, grafted ch-MSC pellets were almost completely resorbed and replaced by bone (Figure 8, A1 and B1). Bone close to the remaining gap consisted of woven bone and some small areas of vessel-forming activity were found in the proximity of the fracture gap (Figure 9, A1 and C1: arrows), while the remaining gap consisted of cartilage tissue (Figure 9, B1). In defects grafted with ud-MSC pellets, no cartilage tissue nor remnants of ud-MSC pellets were observed (Figure 8, A2 and B2), and the remaining gap was filled with fibrous tissue (Figure 9, A2 and B2). Within this fibrous tissue, vessel-forming activity was clearly observed (Figure 9, C2: arrows). In both groups, bone observed on histology showed a good correlation with bone seen on corresponding μ CT images (Figure 8, C1-2).

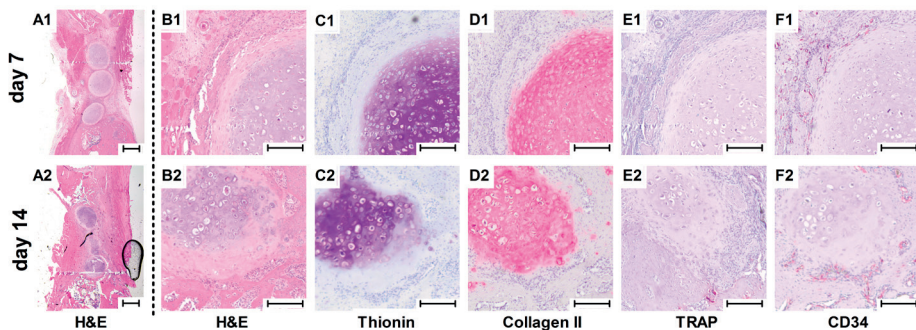


Figure 6: Histology of bone defects grafted with ch-MSC pellets after 7 and 14 days.

Defect grafted with ch-MSC pellets after 7 and 14 days (A1-2), bar indicates 500 μ m. Detailed views show that ch-MSC pellets were surrounded by a number of cell layers (B1-2) and that the extracellular matrix remained rich of GAGs (C1-2) and collagen II (D1-2). Osteoclast activity was observed after 14 days (E1-2: arrows) and some vessel-forming activity was found in the surrounding host tissue (F1-2: arrows), bar indicates 250 μ m.

Ch-MSC pellets of donor 2, which did not stimulate bone regeneration (Figure 5), were smaller in size (~0.5mm) and contained more closely packed cells than ch-MSC pellets of donor 1 (Figure 10, A1-2) or donor 3. Cell nuclei of ch-MSC pellets of donor 2 seemed viable (Figure 10, C2), but the cell nuclei of ch-MSC pellets of donor 1 and donor 3 were smaller or had shrunk and more empty cell lacunae were observed throughout the extracellular matrix (Figure 10, C1). Ch-MSC pellets of donor 1 and 2 had both undergone chondrogenic

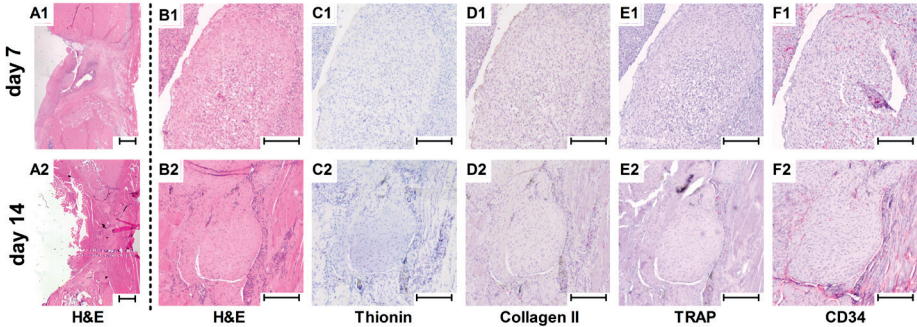


Figure 7: Histology of bone defects grafted with ud-MSC pellets after 7 and 14 days. Defect grafted with ud-MSC pellets after 7 and 14 days (A1-2), bar indicates 500µm. Detailed Detailed views show that ud-MSC pellets were surrounded by small round cells (B1-2). Ud-MSC pellets did not form an extracellular matrix containing GAGs (C1-2) or collagen II (D1-2), indicating that ud-MSC pellets had not undergone chondrogenic differentiation. No osteoclast activity was observed (E1-2), but widespread vessel-forming activity was found in the surrounding host tissue (F1-2: arrows), bar indicates 250µm.

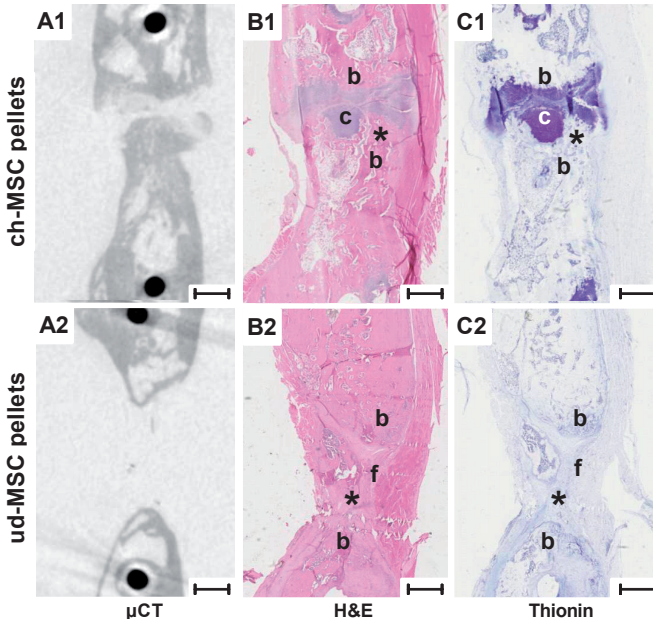


Figure 8: Histology of bone defect grafted with ch-MSC pellets or ud-MSC pellets after eight weeks.

Bone defects grafted with ch-MSC pellets and ud-MSC pellets on corresponding µCT images (A1-2) were stained with respectively H&E (B1-2) or thionin (C1-2). Bone tissue is indicated with 'b', cartilage tissue is indicated with 'c' and fibrous tissue is indicated with 'f'. Asterisk marks area showed in more detail in figure 9. Bar indicates 1mm.

differentiation and consisted of hypertrophic chondrocytes (Figure 10, D1-2 and E1-2), but the extracellular matrix of ch-MSC pellets from donor 2 appeared less structured than the extracellular matrix of ch-MSC pellets from donor 1 (Figure 10, B1-2).

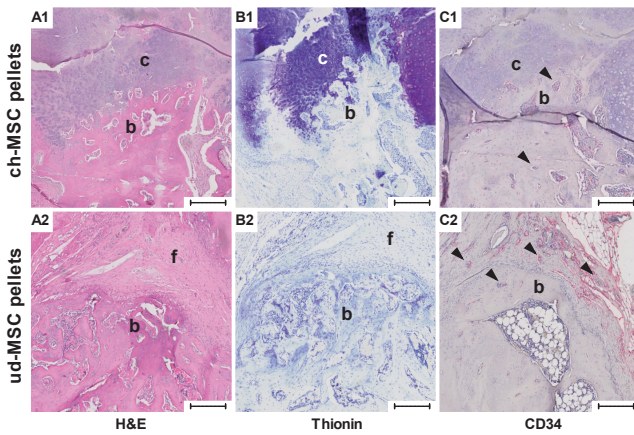


Figure 9: Detailed histology of bone defects grafted with ch-MSC pellets or ud-MSC pellets after eight weeks.

Bone defect grafted with ch-MSC pellets or ud-MSC pellets were stained with respectively H&E (A1-2), thionin (B1-2) and CD34 immunostaining (C1-2). Bone tissue is indicated with 'b', cartilage tissue is indicated with 'c' and fibrous tissue is indicated with 'f'. Arrows indicate vessel forming activity. Bar indicates 250µm.

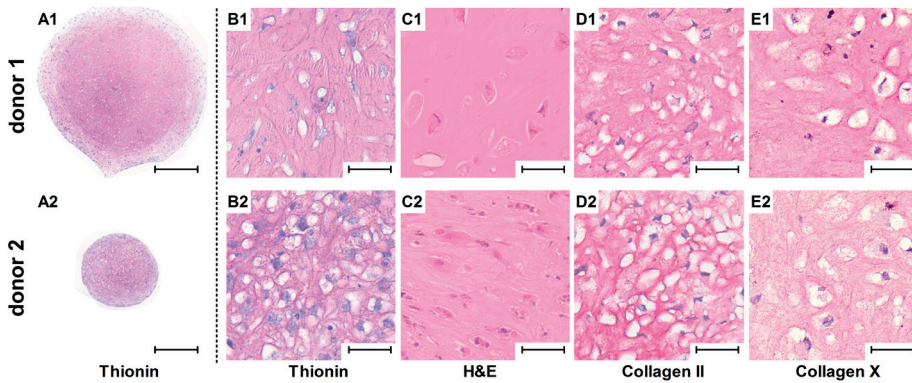


Figure 10: Histology of ch-MSC pellets of donor 1 and 2.

The ch-MSC pellets of donor 1 were bigger than ch-MSC pellets of donor 2 (A1-2). Bar indicates 500µm. Detailed views showed that ch-MSC pellets of donor 1 formed a more structured extracellular matrix (B1-2 and C1-2), although the extracellular matrix of both donors contained collagen II (D1-2) and collagen X (E1-2), indicating that MSC of both donors had undergone hypertrophic chondrogenic differentiation. Bar indicates 50µm.

4. Release of angiogenic cytokines

Release of hTIMP-1 and PDGF-BB is not shown because release of hTIMP-1 exceeded the upper quantification limit (3000pg/ml) and release of PDGF-BB did not exceed the lower quantification limit (1000pg/ml) of the assay. Ch-MSC pellets of all three donors released hVEGF, hTIMP-2, hAng-2, hTNF α , hFGF, and hHGF (Figure 11). Cytokine release of ch-MSC pellets of donor 2 was not different from the cytokine release of the ch-MSC pellets of donor 1 and 3. Compared to ud-MSC pellets, less VEGF was released by ch-MSC pellets and no hIL-8 release was observed.

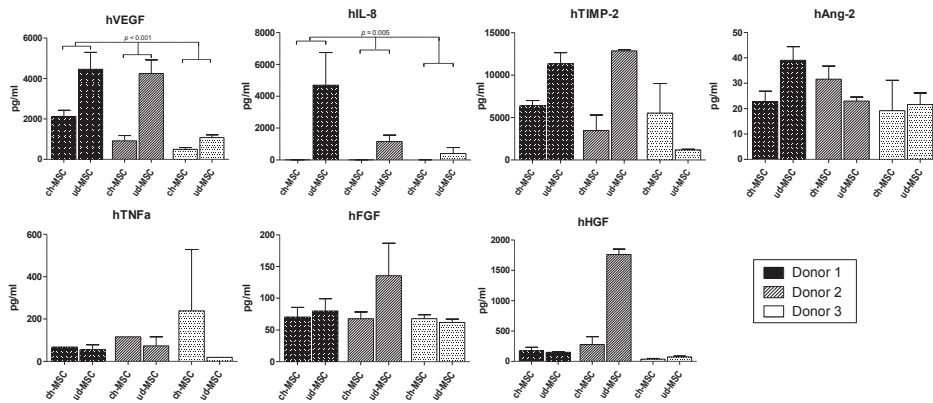


Figure 11: Angiogenic cytokine release.

Angiogenic cytokines released from ch-MSC and ud-MSC pellets in culture medium retrieved before grafting the bone defects.

Discussion

Grafting bone defects and atrophic non-unions with MSC-based grafts is believed to hold great potential⁴⁰¹, but so far clinical results are rather disappointing³⁸⁹. Therefore, instead of stimulating intramembranous ossification with undifferentiated or osteogenically differentiated MSCs, some papers advocate to stimulate endochondral ossification with chondrogenically differentiated MSCs^{393, 395, 396}. In our study, grafting of critical-sized femoral bone defects that were left untreated for 6 weeks with chondrogenically differentiated MSC pellets was found to result in significantly more bone than grafting with undifferentiated MSC pellets (Figure 3 and 5) and we showed that this bone was formed through endochondral ossification (Figure 6). Grafting with chondrogenically differentiated MSC pellets can result in bone regeneration capable of completely bridging the defect (Figure 4). However, the effect of chondrogenically differentiated MSC pellets is donor-dependent (Figure 5).

The complex orthotopic environment that can be encountered during insufficient or impaired fracture repair⁴⁰² were simulated using a critical-sized femoral bone defect model

that was grafted after six weeks. During the first six weeks, untreated defects formed an atrophic non-union and the remaining fracture gap was filled with fibrous tissue (Figure 1C). Grafting these defects with chondrogenically differentiated MSC pellets resulted in large amounts of bone formation through endochondral ossification (Figure 5B). Although extensive bone regeneration was observed in defects grafted with chondrogenically differentiated MSC pellets of donor 1 and 3, only one defect was completely bridged after eight weeks (Figure 4). The inability to bridge the other defect may be explained by a suboptimal method of fixation, because the μ CT images of these defects show the formation of a hypertrophic non-union with a typical horse-shoe or elephant-foot configuration (Figure 5 and 8)⁴⁰³, and the remaining fracture gap contained cartilage tissue (Figure 8 and 9). Although a longer follow-up might have resulted in union, hypertrophic non-unions are usually well treated by providing increased stability over the non-union⁴⁰⁴.

Similar to previous ectopic implantations^{391, 394-396}, we used immunocompromised animals to avoid host-versus-graft reactions against human MSCs. This raised the relevant question whether chondrogenically differentiated MSC pellets remain capable of initiating endochondral ossification in an immunocompetent host. Chondrogenically differentiated MSCs of rat origin have shown to remain capable of initiating endochondral ossification when implanted in immunocompetent rats^{394, 405}. The use of rat MSCs makes it also possible to gain more insight in the influence of a specific immune response of the host to implanted chondrogenically differentiated MSC pellets. Specific immune responses may be the driving factor in the bone regeneration observed, because during endochondral ossification bone regeneration is preceded by osteoclast-mediated degradation of the cartilage template. Osteoclasts are monocyte-derived cells. Furthermore, chondrogenically differentiated MSC pellets that were exposed to IL-1 β , a pro-inflammatory cytokine, showed enhanced accumulation of MMP-13 and increase levels of released stromal cell-derived factor-1, which resulted in more osteoclast recruitment and faster bone regeneration⁴⁰⁶.

Obtaining high yields of MSCs is an important generate sufficient chondrogenically differentiated MSC pellets to be used in clinical applications. MSCs that are capable of undergoing chondrogenic differentiation can be obtained from various tissues including bone marrow, fat, muscle, synovium, periosteum⁴⁰⁷. Bone marrow derived MSCs, used here, have more chondrogenic potential than fat derived MSCs⁴⁰⁸ or muscle derived MSCs⁴⁰⁷. Bone marrow derived MSC can be obtained by a simple percutaneous procedure, and the yield of MSCs obtained can be improved when a concentration device is used that centrifuges a larger volume of bone marrow⁴⁰⁹. Furthermore, the proliferation of obtained MSC can be enhanced by supplementing *in vitro* culture media with FGF-2, or other factors such as platelet-derived growth factor, ascorbic acid and epidermal growth factor⁴¹⁰. More MSCs result in a higher volume of chondrogenically differentiated MSC pellets that can be generated. But with the culturing protocol that we used here, we were able to generate around 200 chondrogenically differentiated MSC pellets per donor. Theoretically this can

result in 2.7 cm³ pellet volume, and is similar to volumes in which commercially available bone substitutes are sold⁴¹¹. Although this volume may not be sufficient or requires the use of additional bone substitutes to graft large bone defects in humans (>2cm), it might already be enough to graft the much smaller fracture gap that is typically seen in an atrophic non-unions (<2mm)⁴⁰³.

VEGF is known to play a key role in endochondral ossification⁴¹² and the release of VEGF could also be to the driving factor through which chondrogenically differentiated MSC pellets can initiate endochondral ossification. VEGF was indeed produced and released by chondrogenically differentiated MSC pellets of all three donors (Figure 11), but endochondral ossification did not occur after grafting with chondrogenically differentiated MSC pellets of donor 2 (Figure 5). The release of VEGF from chondrogenically differentiated MSC pellets was also less than from undifferentiated MSC pellets at the moment of implantation (Figure 11). The cumulative release of VEGF from the chondrogenically differentiated MSC pellets, however, might still be superior after *in vivo* implantation due to prolonged cell survival in low-oxygen environment of the hypertrophic chondrocytes. But the CD34 immunostaining performed on grafted defects after seven and fourteen (Figure 6 and 7) and after 8 weeks (Figure 9) did not suggest that a lot of vessel-forming activity was taking place around chondrogenically differentiated MSC pellets. Vessel formation, however, may have been more controlled and synchronised with the bone formation compared to vessel formation upon grafting with undifferentiated pellets. This possible spatiotemporal role of VEGF in endochondral ossification upon grafting with chondrogenically differentiated MSC pellets warrants further investigation in longitudinal *in vivo* setting.

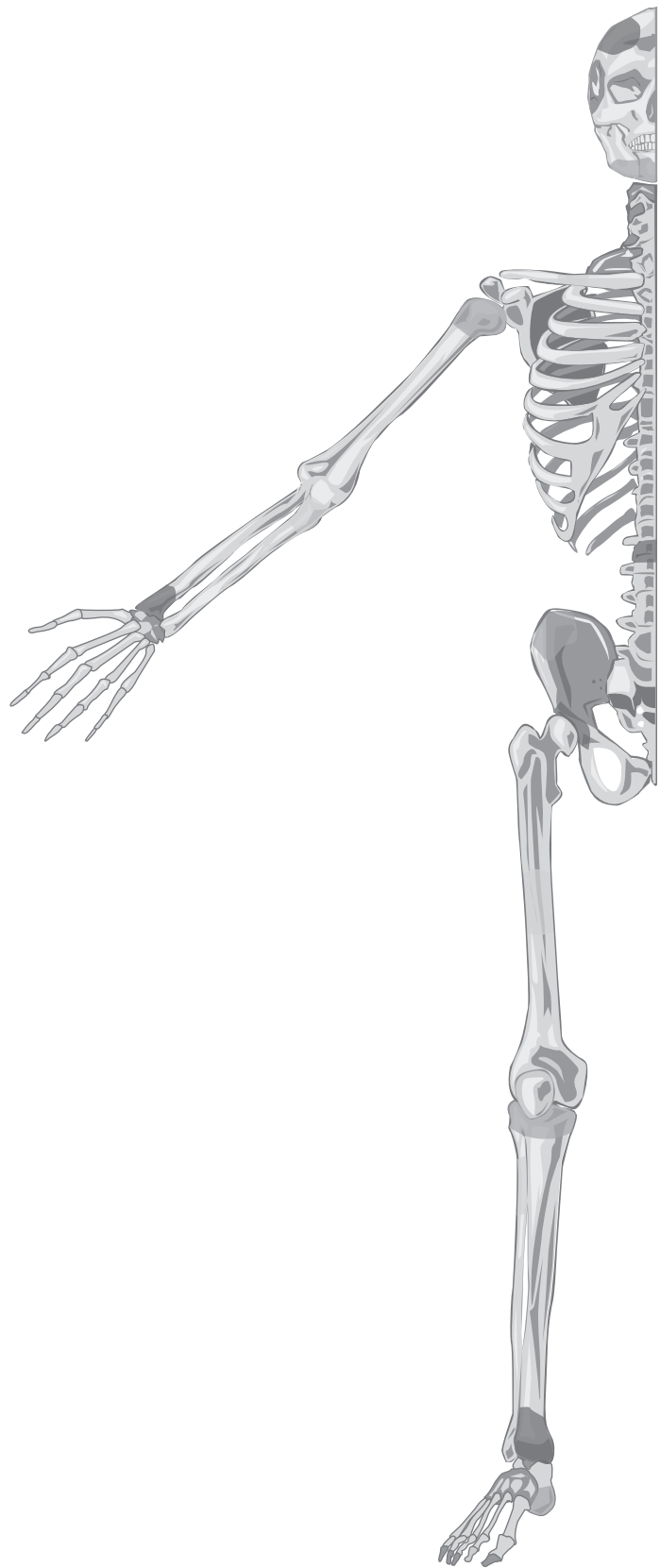
Bone regeneration was after grafting bone defects with chondrogenically differentiated MSC pellets was donor-depend (Figure 5), and this has also been observed after subcutaneous implantation^{393, 394}. The non-potent chondrogenically differentiated MSC pellets of donor 2 did contain hypertrophic chondrocytes that produced VEGF, similar as the potent chondrogenically differentiated MSC pellets of donor 1 and 3 (Figure 8) and there was no clear difference in the release of angiogenic cytokines between the donors (Figure 11). The only difference between the non-potent and the potent chondrogenically differentiated MSC pellets that we could find was their size (Figure 8), non-potent pellets were smaller and contained less extracellular matrix. This may indicate an important role for the extracellular matrix that is generated by chondrogenically differentiated MSC pellets, but on the other hand it has also been suggested that hypertrophic chondrocytes undergoes a transformation into bone^{394, 395, 413}. Determining the exact composition of the extracellular matrix generated by chondrogenically differentiated MSC pellets of a larger number of different donors followed by an *in vivo* implantation to assess their potency to form bone and to determine the survival of these hypertrophic chondrocytes *in vivo* may provide valuable new insights in the mechanism through which chondrogenically differentiated MSCs initiate endochondral ossification and may help to develop protocols to generate potent pellets of each donor.

Conclusion

In conclusion, grafting critical-sized femoral bone defects that were left empty to establish an atrophic non-union with chondrogenically differentiated MSC pellets leads to significantly more bone regeneration than grafting with undifferentiated MSC pellets in athymic rats. With chondrogenically differentiated MSC pellets, bone regenerates rapidly through endochondral ossification, and through bone remodelling leading to restoration of the cortex and the intramedullary space. When this MSC-based approach can be optimized such that sufficient and potent chondrogenically differentiated MSC pellets can be generated for each single patient, grafting with chondrogenically differentiated MSC pellets may become a successful clinical treatment for bone repair in atrophic non-unions and large bone defects.

Acknowledgements

This research forms part of the Project P2.04 BONE-IP of the research program of the BioMedical Materials institute, co-funded by the Dutch Ministry of Economic Affairs and was supported by a grant from the Dutch government to the Netherlands Institute for Regenerative Medicine (NIRM, grant No. FES0908). We thank Dr. R.J. Rottier (Department of Pediatric Surgery, Erasmus MC-Sophia Children's Hospital, Rotterdam, the Netherlands) for the biotechnical support.



Chapter 10

Conclusion and general discussion

The use of bone grafts is over three centuries old. In 1668, a Dutch surgeon named Job van Meek'ren described the repair of a cranial bone defect in a soldier with a piece of skull from a dog ⁴¹⁴. Although this bone graft was quite successful, it was removed two years later because this soldier wanted to return to the church, not due to long term failure of the graft. In succession of Meek'rens first bone graft, Albee introduced autologous bone grafts in the beginning of the 20th century ⁴¹⁵. Autologous bone grafts have been very successful ¹⁰, but their disadvantages including donor site morbidity and limited availability stimulated the development of bone graft substitutes. The majority of these bone graft substitutes are calcium-based, polymer-based or metal-based biomaterials and the aim of this thesis was to determine their potential for trauma and orthopaedic surgery applications.

Definitions and bone defect models

Determining the potential of a biomaterial for trauma and orthopaedic-related indications is difficult because there are no well-defined quantitative tests to compare different biomaterials (**Chapter 2**). In general, the properties of a biomaterial are described with the following criteria: osteoconduction, osteoinduction and osteogenicity ⁹. These terms describe properties of a biomaterial in a qualitative manner, and require evaluation of the biomaterial in at least two different *in vivo* experiments ³⁶⁴. Osteoconduction is determined by grafting a critical-sized bone defect. A critical-sized bone defect was originally defined as “the smallest size bone defect in a particular bone and species of animal that will not heal spontaneously during the lifetime of the animal” ⁴¹⁶. If bone regeneration of a critical-sized bone defect can be improved through grafting with a biomaterial, then this biomaterial is called osteoconductive. However, false claims are often made as many studies lack an empty control group that confirms the critical-size of the defect (**Chapter 2**). Osteoinductive or osteogenic properties are determined through implantation of the biomaterial of interest in an ectopic site (e.g. subcutaneously or intramuscular) ³⁶⁴. If bone is formed in or around the biomaterial following implantation, it will be called osteoinductive or osteogenic. The distinction between osteoinductive and osteogenic properties is subtle and depends on the presence of bone forming cells within the implanted biomaterial. Osteogenic biomaterials already contain bone forming cells, whereas osteoinductive biomaterials contain stimuli (e.g. various growth factors) that attract these bone forming cells from the surrounding tissue ³⁶⁴. So the terms osteoinduction and osteogenicity give insight to the mechanism of action of a biomaterial, but are also not suitable to determine their potential in relevant clinical situations.

To determine the application potential of a biomaterial in a relevant clinical situation where bone regeneration is insufficient (large defects) or impaired (atrophic and hypertrophic non-unions or osteomyelitis) a sufficient animal model that closely mimics these

conditions is required. Although large animal models like goat and sheep more closely resemble human bone⁴¹⁷, we chose to use a critical-sized femur bone defect model in rats. This is also a frequently used model⁴⁰² which is a close representation of the biological and biomechanical conditions that influence bone regeneration during insufficient or impaired bone healing. It also enabled us to easily visualize bone healing in a non-invasive manner with the use of *in vivo* μ CT scanning.

Biomechanical conditions have an important influence on bone regeneration. An unstable environment leads to the formation of a hypertrophic non-union, whereas the complete absence of motion leads to the formation of an atrophic non-union⁴⁰⁴. This makes the degree of biomechanical stabilization in any bone defect model an important variable. In this thesis, adequate stabilization was obtained with rat-specific fixation plates that completely bridged the created segmental bone defects. This fixation plate results in better control over the mechanical environment than previously described fixation by an external frame or by an intramedullary nail⁴⁰². However, the degree of mechanical stabilization showed a substantial variation⁴¹⁸. This variation made our experiments prone to committing a type-II statistical error (false negatives) and thereby small differences between the investigated biomaterials might have been mistakenly disqualified. Reducing the mechanical variation through further development of rat-specific fixation method remains therefore a necessary topic of future research.

Longitudinal follow-up of bone regeneration using *in vivo* μ CT scanning is an excellent non-invasive method to visualize bone regeneration and adaptation⁴¹⁹. Bone quantification through *in vivo* μ CT scanning has been shown to be almost as accurate as histomorphological methods³¹⁴, even in the presence of titanium⁴²⁰. Moreover, *in vivo* μ CT scanning allows for repeated measurements in a single animal. This does not only provide valuable insight into changes in bone volume or bone structure throughout time, but also reduces the number of animals necessary to detect statistical significant differences between experimental groups. Furthermore, bone volumes may be calculated within specific regions of interest. This enabled us to determine how much bone was formed within the pores of a biomaterial (**Chapter 5 to 8**). Currently, *in vivo* μ CT scans are predominantly used to discriminate bone tissue from soft tissue. The next step is to develop a means to discriminate angiogenesis from bone regeneration *in vivo*. Vasculature can already be visualized on *ex vivo* μ CT scans with the use of intravascular solidifying contrast agents⁴²¹. However, new intravascular contrast agents in combination with faster *in vivo* μ CT scans may open up the opportunity to visualize angiogenesis *in vivo*⁴²². *In vivo* visualization of angiogenesis in a bone defect model would be a valuable new tool, because angiogenesis is believed to be a crucial and often limiting factor in the repair of large bone defects⁴²³.

Calcium-based materials

The investigated calcium-based biomaterials in **Chapter 2, 3 and 4** can be categorized into calcium phosphates (subdivided into ceramics and cements), calcium sulphates and bioglass.

Calcium phosphate-based ceramics are obtained by thermal treatment in a process called sintering (**Chapter 2**). This sintering process forms a solid porous material, and most commercially available products are therefore provided in granules or blocks. Whether sintering results in the formation of a hydroxyapatite (HA) or a tricalcium phosphate (TCP) determines the resorption properties of the ceramic. HA ceramics are inert, but TCP ceramics can undergo gradual resorption following osteoclastic activity.

Calcium phosphate ceramics are claimed to be osteoconductive, but only two out of seven commercially available products provided an optimal porous structure for bone ingrowth²¹¹. In addition, the ability to enhance bone regeneration of the investigated osteoconductive HA and TCP ceramics was minimal (**Chapter 4**). Although TCP ceramic performed a little better than HA ceramics, the results of this TCP ceramic was especially disappointing considering that this TCP ceramic was claimed to be as good as autologous bone by others²⁴³. If a calcium phosphate ceramic is selected, it is also important to consider their poor mechanical strength (compression strength <20MPa). Calcium phosphate ceramics are not suitable to be used in defects that are subjected to substantial mechanical loading. Grafting bone defects with ceramics should therefore be combined with additional osteosynthesis materials to provide mechanical stability. Although this raises the question whether these stabilized bone defects require bone grafting to achieve bone bridging^{424, 425}. Clinical indications in which calcium phosphate ceramics have been described are restricted to metaphyseal bone defects tibia, and calcaneal, radial or humeral fractures. But the current level of evidence of these studies mainly consists of case-series (level IV) and case-reports (level V). Proponents of calcium phosphate ceramics often claim there is level I evidence, however this study used TCP ceramics in combination with autologous bone⁴²⁶, and does not evaluate TCP ceramics as a standalone bone graft substitute. Therefore more clinical studies remain necessary to determine the potential of calcium phosphate ceramics in trauma and orthopaedic surgery.

Calcium phosphate-based cements consist of calcium phosphate powders that are mixed with a reagent liquid to form an injectable paste that solidifies through an isothermal reaction. Cements generally form a dense structure with limited porosity that does not exceed more than 5%. Based upon the calcium phosphate powders used, the cement sets into an apatite or a brushite. Apatites and brushites are both calcium minerals, however their different chemical composition affects the resorption rate as well as their mechanical strength. Brushite-based cements resorb quickly, usually within three to six months, but they also possess little to no mechanical strength⁴²⁷. Apatite-based cements resorb very slowly and

complete resorption can take more than ten years, but their mechanical strength is within the range of trabecular bone. Only apatite-based cements and not brushite-based cements are used to graft trauma or orthopaedic-related bone defects. Literature is available on grafting metaphyseal bone defects that occur in humerus, radius, femur, tibia and calcaneus fractures, but also here the level of evidence mainly consists of case-series (level IV) and case-reports (level V). However, there are also a few clinical controlled trials (level II) that use calcium phosphate cements. For distal radius fractures, contradictory outcomes of using apatite-based cements to augment the fracture have been published. The study of Cassidy *et al*¹⁶⁹ claims a better functional outcome after six weeks, but Jeyam *et al*¹⁸² stopped their trial because of more complications, pain and a worse functional outcome in the group receiving the apatite-based cement. In proximal tibia fractures, the use of apatite-based cements is claimed to be better than using autologous bone²¹⁸ or other bone graft substitutes (calcium phosphate ceramics, allografts and demineralized bone matrix)⁴²⁸. Grafting with apatite-based cements reduced the degree of joint surface depression, which might reduce the risk of post-traumatic osteoarthritis after proximal tibia fractures.

Calcium sulphate is produced through heating gypsum, resulting in a dry powder. Adding water to this powder results in an exothermic reaction leading to crystallization and hardening of the calcium sulphate. The formed solid structure dissolves quickly after implantation (within 6 to 12 weeks) and provides no mechanical support. Therefore calcium sulphates are rarely used to fill up bone defects in order to enhance bone regeneration but they might be useful to treat infected fractures sites since they can be impregnated with antibiotics²¹⁶. Bioactive glasses are hard, solid (non-porous) materials, which can be made resorbable through varying the proportions of sodium oxide, calcium oxide and silicon dioxide. Bioactive glass offers more mechanical strength than calcium phosphate cements³, but so far they are only used to fill bone defects resulting from vertebral fractures⁴²⁹.

Metal-based materials

The metal-based biomaterial evaluated in this thesis was titanium. Since titanium offers excellent mechanical properties³⁵, our aim was to develop a bone graft substitute with suitable biological and biomechanical properties for grafting large weight-bearing bone defects.

Porous titanium implants were produced using selective laser melting (SLM), an additive manufacturing technique that was first described in 2006 by Hollander *et al*²⁶². This additive manufacturing technique enabled us to tailor the design of porous titanium implants (Figure 1) and allowed for precise control over the highly porous titanium structures, using only very fine titanium struts (~160µm). Through altering the titanium strut thickness, the mechanical strength of the porous titanium implants can be varied from mechanical properties comparable to trabecular bone to those comparable to cortical bone²⁹⁰. Although it is difficult to

define the optimal mechanical properties of a bone graft substitute material on forehand, porous implants should be strong enough to sustain loading but not overly stiff to avoid stress shielding³. In order to function as an osteoconductive matrix, porous titanium implants were designed with pores sizes that ranging from 460 to 670 μm , which is within the range of pore sizes that are should result in optimal osteoconductive properties²¹¹.

The developed porous titanium implants underwent an additional alkali-acid-heat treatment to optimize their surface chemistry and topography. This alkali-acid-heat treatment was first described by Takemoto *et al*²⁷⁶ and they showed that the acquired surface chemistry that consisted of a titanium oxide layer resulted in osteoinduction. The formation of this titanium oxide layer after alkali-acid-heat treatment was confirmed for the produced porous titanium implants and this modified surface chemistry and topography improved the proliferation of pre-osteoblastic cells and the expression of osteogenic genes *in vitro*²⁹². In addition, others have also shown that this surface treatment positively affects the organization of the fibrin network that forms upon blood-implant contact³⁵². Further supported by two systematically conducted reviews that show the advantage of increasing the surface roughness of titanium^{277, 430}, there is a strong rationale for applying this additional surface treatment to porous titanium implants.

First, the osteoconductive properties of the produced porous titanium implants were evaluated (**Chapter 5**). Grafting segmental defects with two different porous titanium implants resulted in more bone regeneration than leaving the defects empty, which confirms its osteoconductive properties. This finding is supported by several other groups that also designed and produced similar porous titanium implants using either the same manufacturing method (selective laser melting)^{268, 291, 431, 432} or other additive manufacturing techniques^{317, 359, 433-436}. Although, the performance of porous titanium implants as an osteoconductive matrix was not sufficient to result in complete bridging of the segmental bone defects, the implants provided sufficient mechanical support and this resulted up to 50% restoration of the original femur strength after twelve weeks. However, reducing the stiffness of porous

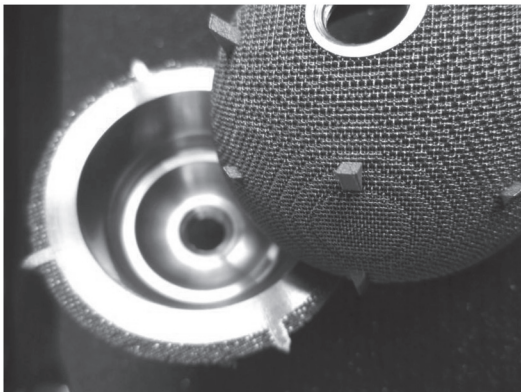


Figure 1: Example of porous titanium implant design.

Selective laser melting is an additive manufacturing technique that allows design of new implants such this acetabular cup.

implants, which was hypothesized to lead to more deformation during implant loading and subsequently more mechanical stimulation to form bone²⁶³, did not result in an improved outcome. In retrospect, not finding this difference is most likely related to the fact that the variability in loads transfer strongly depends on the degree of stability that is achieved after fixation⁴¹⁸.

The potential of porous titanium implants as a bone graft substitute was further explored through reinforcing the implants with osteoinductive stimuli. In **Chapter 6**, an osteoinductive peptide, called osteostatin, was added to the surface of porous titanium implants. Osteostatin is a small pentapeptide domain (107-111) of PTHrP and was used because its short sequence warrants its stability and a very small nanogram dose of this protein proved to be effective in stimulating bone regeneration *in vivo*³⁸. Osteostatin might act through altering the *RankL/OPG* system, which is a major signalling pathway that regulates the differentiation and function of osteoclasts³¹³, and the osteostatin coated porous titanium implants showed an increase of bone formation during the first four weeks after implantation. This might result in faster and better bone-implant integrity directly after implantation, which is known to be important for the long-term survival of non-resorbable implants^{437, 438}. But the osteoinductive stimulus provided through the release of osteostatin in our experiments was not potent enough to result in complete bridging of the grafted segmental defects.

Subsequently an alternative approach to reinforce porous titanium implants with osteoinductive properties was explored. Growth factors were loaded into biogels that were incorporated into the porous space of the titanium implants. First we used a nanostructured colloidal gelatin gel that was found to be capable of a time and dose controlled delivery of multiple growth factors for a prolonged period³⁹ (**Chapter 7**). We showed that the single delivery of either 3µg dose of BMP-2 or a 0.6µg dose of FGF-2 significantly enhanced the bone regenerative capacity. A further increase in bone regeneration around the titanium implants was achieved through combining these two growth factors in a 5:1 ratio. Based on literature using BMP-2 in this defect model, a 3µg BMP-2 dosage can be considered safe and efficient. Further research is mandatory to determine if the use of this nanostructured colloidal gelatin gels can reduce the therapeutic dose necessary in humans because the therapeutic dose of BMP-2 in commercially available carrier materials (e.g. collagen sponges) is extremely high. The supraphysiological dose of BMP-2 is necessary because these carrier materials possess a poor capacity to control the BMP-2 release, but they are also associated with serious side effects that include bone tissue overgrowth, ectopic bone formation, inflammation and even carcinogenicity³⁶³. Although incorporation of growth factor loaded gelatin nanosphere gels into porous titanium implants resulted in a long-term increase in bone regeneration, still this was not sufficient to bridge the grafted segmental defects.

In **Chapter 8**, a fibrin matrix was incorporated within the porous titanium implants because fracture healing naturally starts with the formation of a fibrin matrix, the so-called fracture haematoma. This fibrin network functions as a natural binding reservoir of

numerous cytokines that include, next to BMP-2, also FGF-2, and VEGF. This network is highly permeable to cells and attracts neutrophils and macrophages³⁵⁰ and forms through polymerisation of fibrinogen by thrombin. The results obtained after incorporating a BMP-2 loaded fibrin network inside the porous titanium implants were striking. This resulted in quick and complete regeneration of the cortex. This bone regeneration was guided through the porous titanium implants that precisely preformed the cortical shape and resulted in full functional restoration of the grafted segmental bone defects. The grafted femurs with the regenerated bone around the porous titanium were twice as strong as intact femurs. These stunning results need to be further explained, but it is likely that an optimal balance was achieved between mechanical stabilisation of the defect through the use of the porous titanium implants in combination with an optimal biological environment created through augmenting the natural early phase of fracture healing, the fracture haematoma or fibrin, with an adequate dose of BMP-2. Thereby our goal to develop a bone graft substitute suitable to optimally graft a segmental bone defect in the rat seemed achieved. The next step would be to evaluate the performance of the developed porous titanium implants in a human-size defect, which requires a new set of animal experiments in a larger animal such as goats or sheep.

Cell-based materials

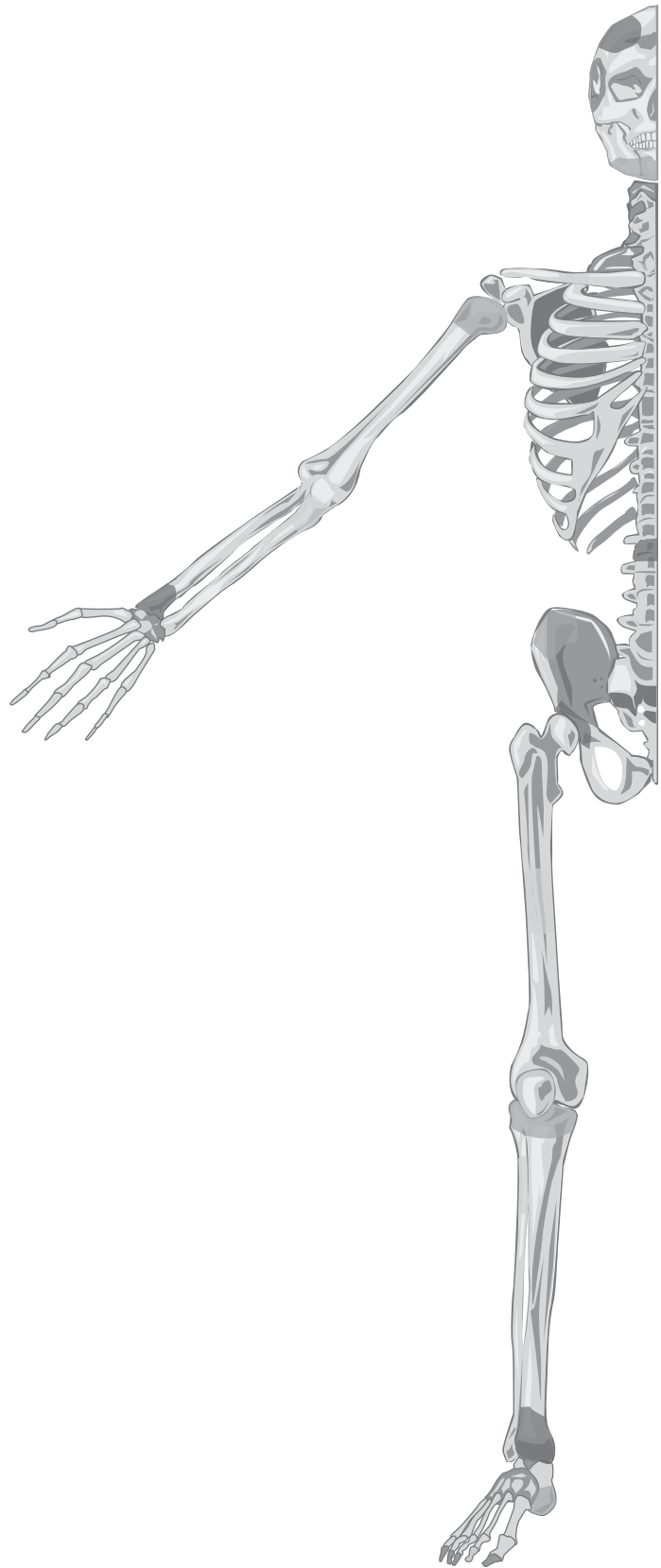
Furthermore, we explored the potential of a cell-based approach to regenerate bone defects. In general, cell-based methods make use of mesenchymal stromal cells because these cells are considered to be the precursors of all musculoskeletal tissues including bone and cartilage⁴³⁹. Usually, mesenchymal stromal cells are differentiated towards osteoblasts and then used to graft bone defects. This approach is already evaluated in a few clinical case-series, but their clinical success is still disappointing³⁸⁹. This might be due to the fact that osteogenic differentiation mimics the process of intramembranous ossification, which is generally believed less efficient than endochondral ossification³²⁴. Endochondral ossification occurs after chondrogenic differentiation and starts with the formation of a cartilage template (or fracture callus). Through chondrogenic differentiation of mesenchymal stromal cells we mimicked the formation of this cartilage template (forming pellets of 1-3mm in diameter) and this effectively improved bone regeneration (**Chapter 9**). These exciting results were recently confirmed by Bahney *et al*⁴¹³ and its potential is more and more recognized⁴⁴⁰. However, several important issues still need to be addressed before a proof-of-principle study of this cell-based method may be conducted in humans. First of all, bone regeneration of chondrogenically differentiated MSC pellets was donor-dependent, which poses a risk that grafting may be unsuccessful. However, this donor-dependency might also help us to unravel the crucial factors through which chondrogenically differentiated MSCs can stimulate

endochondral ossification, since the properties of chondrogenically differentiated MSC pellets of potent and non-potent donors can be extensively studied *in vitro* and *in vivo*. Another important question that needs to be addressed is whether survival of the chondrogenically differentiated MSCs is crucial in order to stimulate endochondral ossification. Bahney *et al*⁴¹³ concluded that survival is crucial because they found that bone formed upon grafting with chondrogenically differentiated MSCs was of donor origin. This finding is contradictory to the general belief that in endochondral ossification the cartilage template is removed by invading osteoclasts and subsequently replaced with bone by surrounding osteoblast⁴. In addition, it has recently been shown by Bourguine *et al* that devitalized chondrogenically differentiated MSC pellets can also stimulate endochondral ossification⁴⁴¹. Devitalized chondrogenically differentiated MSCs can simplify the utility of this cell-based method when allogenic chondrogenically differentiated MSC pellets can generate similar results. Answering this question is the next step, since allogenic chondrogenically differentiated MSC pellets can be made in unlimited amounts in GMP (good manufacturing practice) stem cell laboratories. This would make it possible to produce chondrogenically differentiated pellets as an off-the-shelf product and justifies a proof-of-principle study in humans to show if this method can really become a successful treatment for atrophic non-unions.

Concluding remarks

In conclusion, the repair of bone defects with bone grafts or bone graft substitutes remains a major challenge in trauma and orthopaedic surgery. Although the gold standard bone graft is still autologous bone, the expanding array of available bone graft substitutes offer the attending surgeon the option to choose alternative grafting materials. Selecting the most suitable bone graft substitute for each specific trauma and orthopaedic-related indication requires adequate knowledge of the biomaterial and its potential to regenerate bone defects. In this thesis we learned that evidence to support the use of calcium-based materials for non weight-bearing bone defects is limitedly available, and that these materials are not suitable for weight-bearing bone defects or atrophic non-unions. In a pre-clinical bone defect model, weight-bearing bone defects were successfully grafted with newly developed metal-based materials like porous titanium. Porous titanium is shown to offer a mechanically strong osteoconductive matrix that can be equipped with osteoinductive gels. The best osteoinductive gel so far seemed to be a fibrin gel with a small dose of BMP-2. Furthermore, atrophic non-unions were successfully grafted with chondrogenically differentiated MSC pellets, mimicking the cartilage template of endochondral ossification. Chondrogenically differentiated MSC pellets not only stimulate bone regeneration but also direct adequate revascularisation. The development of these new biomaterials should be continued in large animal models to determine whether they can meet the standard for grafting weight-bearing

bone defects and atrophic non-unions in trauma and orthopaedic-related surgery in the future.



Chapter 11

Summary

Bone grafting, first established in the 19th century, has become a common procedure in trauma and orthopaedic surgeries in which bone defects are filled with bone grafts or bone graft substitutes¹. The current gold standard in bone grafting is the use of autologous bone⁴⁴. Autologous bone has osteoconductive, osteoinductive, and osteogenic properties and is often harvested from the iliac crest¹⁰. However, harvesting of this tissue is associated with complications in 1040% of patients¹² and the availability of autologous bone can be limited. These disadvantages have motivated the development of bone graft substitutes. The aim of this thesis was to critically evaluate the currently available and newly developed bone graft substitutes, and to determine their potential for bone grafting in trauma and orthopaedic surgery.

Bone graft substitutes currently used in trauma and orthopaedic surgery mainly consist of calcium-based materials. An overview of all calcium-based materials available in The Netherlands was provided in **Chapter 2**, and calcium phosphate cements and ceramics were more specifically described in respectively **Chapter 3 and 4**. Calcium phosphate cements and ceramics have different structural, biological, and mechanical properties. Calcium phosphate cements are associated with a solid structure, with little to no pores. Conversely, calcium phosphate ceramics have a porous structure which can facilitate bone ingrowth. In general, calcium-based materials are brittle in nature. Although the compression strength of calcium phosphate cements is comparable to trabecular bone, the compression strength of calcium phosphate ceramics is somewhat less. Therefore both calcium phosphate cements and ceramics are only suitable to graft non weight-bearing bone defects in which adequate mechanical stabilization is guaranteed by the addition of osteosynthesis material. Both subsets have been used to graft metaphyseal bone defects that occur in several fractures, but the clinical level of evidence to use these bone graft substitutes for trauma and orthopaedic-related indications is limited, and requires further evaluation in well-designed clinical trials.

To graft load-bearing bone defects, a new biomaterial based on porous titanium was developed. Porous titanium implants were produced using selective laser melting (SLM). This additive manufacturing technique enabled the design and precise production of porous implants (**Chapter 5**). Through adjusting the porous structure, the implants can be made strong enough to allow weight-bearing while still having a porosity up to 90 %. Grafting weight-bearing segmental cortical femur defects in rats with porous titanium implants enhanced bone regeneration and resulted in a restoration of more than half of the original cortical bone strength.

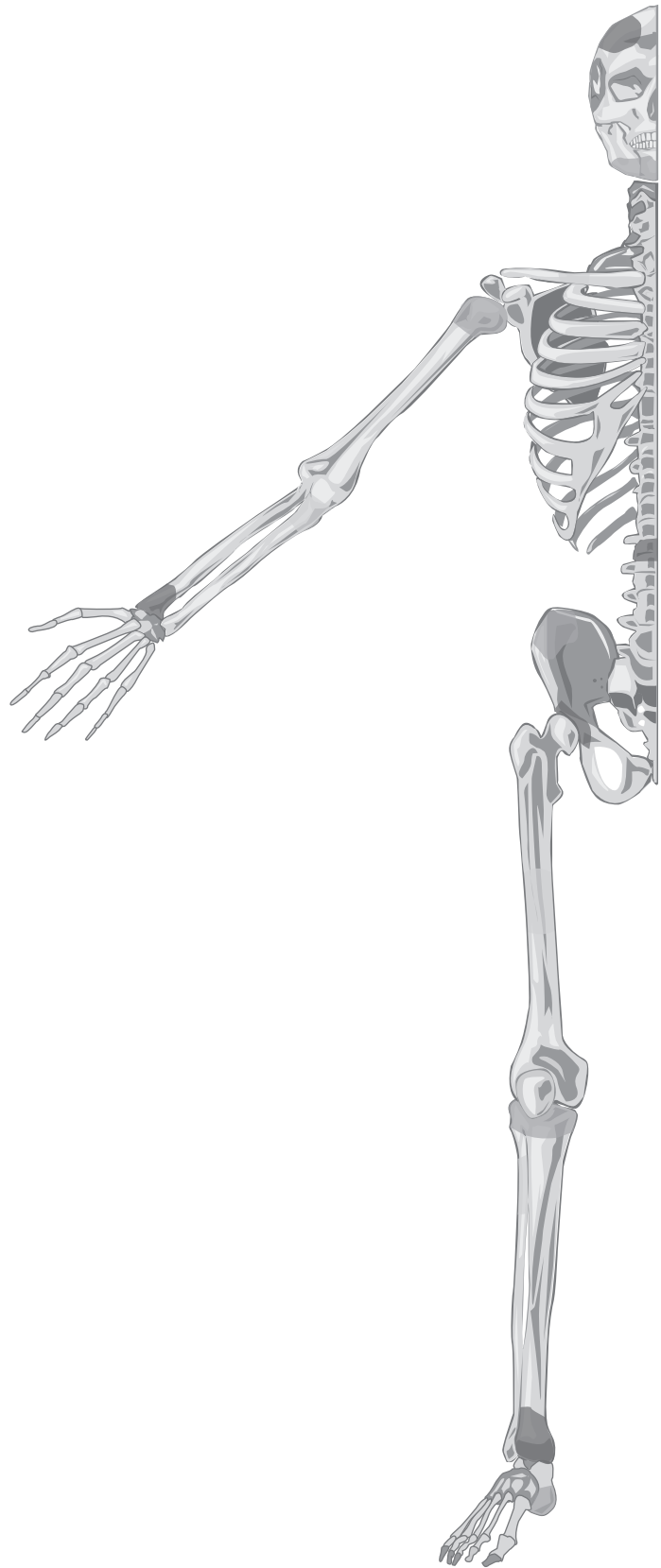
The development of this porous titanium biomaterial was continued by exploration of different strategies to add osteoinductive stimuli. First, porous titanium implants were equipped with an osteostatin-coating (**Chapter 6**). Osteostatin is a small and stable pentapeptide domain (107-111) of PTHrP, which might have osteoinductive properties. Coating the porous titanium implants with osteostatin indeed improved bone regeneration, however this did not improve the mechanical strength of the grafted femur defects in rats.

Alternatively, porous titanium implants were incorporated with growth factor loaded gels. Growth factors with known osteoinductive properties such as bone morphogenetic protein 2 (BMP-2) and fibroblast growth factor 2 (FGF-2) were loaded into two different gels. First, a nanostructured colloidal gelatin gel was used because this gel can control the delivery of multiple growth factors in a time and dose controlled manner (**Chapter 7**). Porous titanium implants loaded with BMP-2 or FGF-2 containing gelatin gels effectively improved bone regeneration. However, bone regeneration occurred mainly around and outside the porous titanium implants. Secondly, a physiologically concentrated fibrin gel was used as this mimics the fracture haematoma, the first phase of bone regeneration (**Chapter 8**). Porous titanium implants loaded with BMP-2 containing fibrin gels also effectively improved bone regeneration. Bone formed exactly within the porous titanium structure and efficient repair of the original cortex was observed. Bone regeneration was much quicker and better aligned within the implant than with previously used gelatin gels, and the majority of the femur defects were fully bridged within eight weeks. Consequently, complete restoration of the original femur strength occurred. Incorporating BMP-2 loaded fibrin gels was therefore the most effective strategy to add a strong osteoinductive stimuli to porous titanium implants.

To graft atrophic non-unions, we determined the potential of a new stem cell-based method. This stem cell-based method used mesenchymal stromal cells that were obtained from human donors. The mesenchymal cells are usually differentiated towards osteoblastic cells, thereby mimicking intramembranous ossification, which is generally believed less effective than endochondral ossification. To mimic endochondral ossification, we differentiated mesenchymal stromal cells towards the chondrogenic pathway (**Chapter 9**). Through chondrogenic differentiation of mesenchymal stromal cells we created small spheres of chondrogenically differentiated MSCs. These spheres were used to graft atrophic non-unions in rats and were shown to effectively stimulate bone regeneration resulting in complete repair of the atrophic non-union. Therefore chondrogenically differentiated MSC spheres may prove an effective clinically successful strategy for atrophic non-unions.

In conclusion, currently available bone graft substitutes for trauma and orthopaedic surgery offer the surgeon a plethora of options, from which it may be difficult to choose the best suitable biomaterial. Non weight-bearing bone defects can be grafted with some of the existing calcium-based bone graft substitutes, whereas weight-bearing bone defects require the development of new (stronger) biomaterials. A biomaterial that shows great potential to graft weight-bearing bone defects in the future is porous titanium that can be applied in combination with active molecules that can be incorporated in the highly porous structure. Potential methodologies include the release of active molecules directly from the surface or release from a substrate (e.g. a gel) that is embedded within the pores. BMP-2 embedded in fibrin gel incorporated in porous titanium provided excellent bone ingrowth and fully repaired weight-bearing cortical femur defects in the rat. Furthermore, a new stem-cell based method, using chondrogenically differentiated MSCs, shows high potential to

enhance bone regeneration in atrophic non-unions in rats. Given their high potential for efficacy as demonstrated in this thesis, both porous titanium implants and chondrogenically differentiated MSCs are worthy of further investigation in large animal studies and clinical trials.



Chapter 12

Nederlandse samenvatting

Bottransplantatie, geïntroduceerd in de 19^e eeuw, is uitgegroeid tot een veel gebruikte procedure in trauma en orthopaedische chirurgie¹. De gouden standaard voor bottransplantatie is het gebruik van lichaamseigen (autoloog) bot⁴⁴. Autoloog bot bezit osteoconductive, osteoinductieve en osteogene eigenschappen en kan onder andere worden verkregen uit de bekkenkam¹⁰. Echter, het verkrijgen van dit autologe bot kan aanleiding zijn tot kleine of zelfs grote complicaties in 10-40% van de patiënten¹². Daarnaast is de hoeveelheid beschikbaar autoloog bot beperkt. Deze nadelen hebben in de afgelopen decennia de ontwikkeling van botsubstitutiematerialen gestimuleerd. Botsubstitutiematerialen die ontwikkeld zijn bestaan voornamelijk uit calcium bevattende keramieken of cementen, of zijn gemaakt van polymeren of metalen. In dit proefschrift werd de bruikbaarheid van deze biomaterialen voor trauma en orthopaedische chirurgie geëvalueerd.

In trauma en orthopaedische chirurgie wordt vooral gebruik gemaakt van calcium gebaseerde biomaterialen. Een overzicht van al deze biomaterialen die beschikbaar zijn als commercieel product in Nederland werd gegeven in **Hoofdstuk 2** en in **Hoofdstuk 3 en 4** werden twee specifieke subgroepen (calciumfosfaat cementen en calciumfosfaat keramieken) meer uitvoerig bestudeerd. Calciumfosfaat cementen en keramieken hebben een verschillende structuur, en daarnaast ook verschillende biologische en mechanische eigenschappen. Over het algemeen zijn de mechanische eigenschappen van calcium bevattende botsubstitutiematerialen beperkt omdat deze biomaterialen broos zijn. Omdat calciumfosfaat cementen bestaan uit een massieve structuur, met weinig tot geen poriën is de compressiesterkte van calciumfosfaat cementen iets is hoger dan de compressiesterkte van calciumfosfaat keramieken. Calciumfosfaat keramieken hebben namelijk een poreuze structuur, met als voordeel dat deze botingroei zou kunnen bevorderen. Omdat de compressiesterkte van zowel calciumfosfaat cementen en calciumfosfaat keramieken over het algemeen lager is dan die van trabeculair bot, kunnen deze calciumrijke biomaterialen alleen gebruikt worden voor niet-gewichtsdragende botdefecten. Calciumfosfaat cementen en keramieken worden gebruikt om metafysaire botdefecten op te vullen die voorkomen bij diverse botbreuken (bv. tibia plateau, distale radius en calcaneus fracturen). Maar het wetenschappelijke bewijs dat het gebruik van deze botsubstitutiematerialen in trauma en orthopaedische chirurgie leidt tot betere uitkomsten is beperkt tot level IV en V studies en vereist nader onderzoek in goed opgezette en gerandomiseerde klinisch onderzoeken.

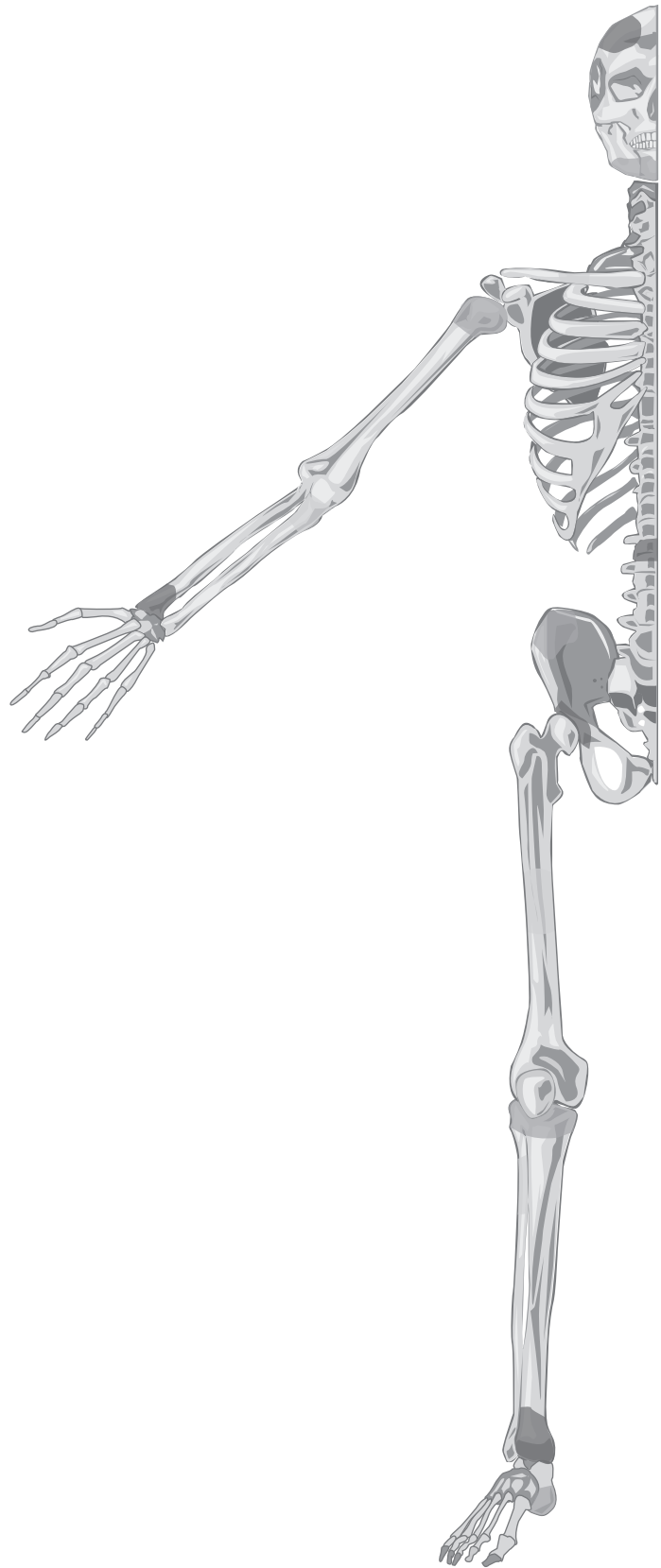
Een nieuw botsubstitutiemateriaal om gewichtsdragende botdefecten te behandelen is poreus titanium. Deze nieuwe poreuze titanium implantaten konden worden gemaakt door middel van selective laser melting (SLM). Selective laser melting is een 3D-print techniek waarmee zeer nauwkeurig een vooraf ontworpen implantaat kan worden geproduceerd (**Hoofdstuk 5**). Door deze techniek, in combinatie met de mechanische eigenschappen van titanium, kon er een volledig poreus titanium implantaat worden ontworpen dat sterk genoeg was voor gewichtsdragende botdefecten. De poreuze titanium implantaten werden vervolgens gebruikt om gewichtsdragende botdefecten in het femur van ratten mee te behandelen. Dit

resulteerde in betere botregeneratie en bijna de helft van de oorspronkelijke botsterkte was na twaalf weken hersteld.

De poreuze titanium implantaten werden op verschillende manieren voorzien van osteo-inductieve stimuli om botregeneratie nog meer te stimuleren. Eerst werd het titanium oppervlak van de poreuze implantaten gecoat met osteostatine (**Hoofdstuk 6**). Osteostatine is een klein en stabiel pentapeptide (domein (107-111) van PTHrP) en dit peptide heeft osteoinductieve eigenschappen. De osteostatine coating verbeterde botregeneratie in de zin dat de botingroei iets sneller verliep, echter dit resulteerde niet in een verbetering van de botsterkte van de behandelde gewichtsdragende botdefecten in ratten. Daarom werden poreuze titanium implantaten vervolgens opgevuld met gelatine-achtige biogels. Deze biogels waren geladen met bone morphogenetic protein 2 (BMP-2) en/of fibroblast growth factor 2 (FGF-2). De speciale nanostructuur van de gelatine-achtige gel zorgde ervoor dat de dosis en de timing van de afgifte van deze twee groeifactoren kon worden gecontroleerd (**Hoofdstuk 7**). Ook deze methode verbeterde de botregeneratie, maar het nieuw gevormde bot bevond zich vooral rondom en niet zozeer binnen in de poreuze structuur van de titanium implantaten. Opnieuw werd er geen volledig herstel van de botsterkte bereikt. Daarom werden poreuze implantaten vervolgens gevuld met een ander soort biogel. Er werd gekozen voor een fibrinegel omdat dit overeen komt met de natuurlijke vorming van een fractuur haematoom, de eerste fase van fractuurgenezing (**Hoofdstuk 8**). Deze fibrinegels werden geladen met BMP-2 en dit resulteerde in een duidelijke verbetering van de botregeneratie in gewichtsdragende botdefecten in ratten. Met behulp van deze BMP-2 bevattende fibrine-gels werd bot geregenereerd binnen de poreuze structuur van de titanium implantaten en werden de botdefecten volledig overbrugd met nieuw gevormd bot. Dit nieuw gevormde bot, in combinatie met de titanium implantaten, resulteerde in een volledig herstel van de oorspronkelijke botsterkte binnen twaalf weken. Deze combinatie van poreuze titanium implantaten met BMP-2 geladen fibrinegels bleek de meest effectieve strategie om gewichtsdragende botdefecten in ratten te herstellen.

Voor de behandeling van atrofische non-unions werd de potentie van een nieuwe, op stamcel-gebaseerde methode, onderzocht (**Hoofdstuk 9**). Voor deze methode werd gebruik gemaakt van menselijke mesenchymale stamcellen. Voorheen werden deze mesenchymale cellen meestal gedifferentieerd tot osteoblasten omdat osteoblasten direct bot kunnen vormen. Deze manier van botregeneratie wordt ook wel intramembraneuze (of directe) ossificatie genoemd. Echter deze vorm van botregeneratie is minder effectief dan endochondrale (of indirecte) ossificatie. Om botregeneratie door middel van endochondrale ossificatie te stimuleren hebben wij mesenchymale stamcellen gedifferentieerd tot hypertrofische chondrocyten. Chondrogene differentiatie van mesenchymale stamcellen resulteerde in de vorming van kleine ronde pellets met een diameter van 1-2mm. Deze pellets komen overeen met de kraakbenige fractuurcallus die ontstaat bij endochondrale verbening en bleken uiterst effectief om atrofische non-unions in ratten mee te herstellen.

Concluderend is er reeds een veelvoud van botssubstitutiematerialen beschikbaar voor trauma en orthopaedische chirurgie. De beschikbare botssubstitutiematerialen zijn alleen geschikt voor niet gewichtsdragende botdefecten, en hiervoor is slechts beperkt wetenschappelijk bewijs beschikbaar. De ontwikkeling van nieuwe botssubstitutiematerialen blijft daarnaast noodzakelijk om in de toekomst ook gewichtsdragende botdefecten of persistente atrofische non-unions te kunnen behandelen. In onze diermodellen werden gewichtsdragende botdefecten succesvol behandeld met poreuze titanium implantaten gevuld met BMP-2 geladen fibrinegels en atrofische non-unions werden succesvol behandeld met de beschreven stamcel-gebaseerde methode. Gezien de goede resultaten van beide beschreven methodes, verdient dit nader onderzocht te worden voor het gebruik in trauma en orthopaedische chirurgie.



Chapter 13

Appendices

References

1. Schnettler R, Markgraf E. *Knockensatzmaterialen und Wachstumsfaktoren*. Stuttgart: Thieme; 1997.
2. Kular J, Tickner J, Chim SM, Xu J. An overview of the regulation of bone remodelling at the cellular level. *Clin Biochem*. 2012;45(12):863-73.
3. An YH. Mechanical properties of bone. Y.H. A, R.A. D, editors. New York: CRC Press; 1999. 41-63 p.
4. Kronenberg HM. Developmental regulation of the growth plate. *Nature*. 2003;423(6937):332-6.
5. Gerstenfeld LC, Cullinane DM, Barnes GL, Graves DT, Einhorn TA. Fracture healing as a post-natal developmental process: molecular, spatial, and temporal aspects of its regulation. *J Cell Biochem*. 2003;88(5):873-84.
6. Einhorn TA. The cell and molecular biology of fracture healing. *Clin Orthop Relat Res*. 1998(355 Suppl):S7-21.
7. Carter DR, Beaupre GS, Giori NJ, Helms JA. Mechanobiology of skeletal regeneration. *Clin Orthop Relat Res*. 1998(355 Suppl):S41-55.
8. Einhorn TA. Enhancement of fracture-healing. *J Bone Joint Surg Am*. 1995;77(6):940-56.
9. Albrektsson T, Johansson C. Osteoinduction, osteoconduction and osseointegration. *Eur Spine J*. 2001;10 Suppl 2:S96-101.
10. Pape HC, Evans A, Kobbe P. Autologous bone graft: properties and techniques. *J Orthop Trauma*. 2010;24 Suppl 1:S36-40.
11. Schmidmaier G, Herrmann S, Green J, Weber T, Scharfenberger A, Haas NP, *et al*. Quantitative assessment of growth factors in reaming aspirate, iliac crest, and platelet preparation. *Bone*. 2006;39(5):1156-63.
12. Banwart JC, Asher MA, Hassanein RS. Iliac crest bone graft harvest donor site morbidity. A statistical evaluation. *Spine (Phila Pa 1976)*. 1995;20(9):1055-60.
13. Younger EM, Chapman MW. Morbidity at bone graft donor sites. *J Orthop Trauma*. 1989;3(3):192-5.
14. Sandhu HS, Grewal HS, Parvataneni H. Bone grafting for spinal fusion. *Orthop Clin North Am*. 1999;30(4):685-98.
15. Burchardt H. Biology of bone transplantation. *Orthop Clin North Am*. 1987;18(2):187-96.
16. Goldberg VM, Stevenson S, Shaffer JW, Davy D, Klein L, Zika J, *et al*. Biological and physical properties of autogenous vascularized fibular grafts in dogs. *J Bone Joint Surg Am*. 1990;72(6):801-10.
17. Dimitriou R, Mataliotakis GI, Angoules AG, Kanakaris NK, Giannoudis PV. Complications following autologous bone graft harvesting from the iliac crest and using the RIA: a systematic review. *Injury*. 2011;42 Suppl 2:S3-15.
18. Delloye C, Cornu O, Druetz V, Barbier O. Bone allografts: What they can offer and what they cannot. *J Bone Joint Surg Br*. 2007;89(5):574-9.
19. Tomford WW. Transmission of disease through transplantation of musculoskeletal allografts. *J Bone Joint Surg Am*. 1995;77(11):1742-54.
20. Ehrler DM, Vaccaro AR. The use of allograft bone in lumbar spine surgery. *Clin Orthop Relat Res*. 2000(371):38-45.
21. Kinney RC, Ziran BH, Hirshorn K, Schlatterer D, Ganey T. Demineralized bone matrix for fracture healing: fact or fiction? *J Orthop Trauma*. 2010;24 Suppl 1:S52-5.
22. Kurien T, Pearson RG, Scammell BE. Bone graft substitutes currently available in orthopaedic practice: the evidence for their use. *Bone Joint J*. 2013;95-B(5):583-97.
23. Van der Stok J, Van Lieshout EMM, El-Massoudi Y, Van Kralingen GH, Patka P. Bone substitutes in the Netherlands - a systematic literature review. *Acta Biomater*. 2011;7(2):739-50.

24. Balla VK, Bodhak S, Bose S, Bandyopadhyay A. Porous tantalum structures for bone implants: fabrication, mechanical and in vitro biological properties. *Acta Biomater.* 2010;6(8):3349-59.
25. Larsson S, Hannink G. Injectable bone-graft substitutes: current products, their characteristics and indications, and new developments. *Injury.* 2011;42 Suppl 2:S30-4.
26. Albee F, Morrison HF. Studies in bone growth: triple calcium phosphate as a stimulus to osteogenesis. *Ann Surg.* 1920;1(1):32-9.
27. Dressmann H. Ueber Knochenplombierung bei Hohlenforming Defekten des Knochens. *Beitr Klin Chir.* 1892;9:804-10.
28. Thomas MV, Puleo DA. Calcium sulfate: Properties and clinical applications. *J Biomed Mater Res B Appl Biomater.* 2009;88(2):597-610.
29. Urist MR. Bone: formation by autoinduction. *Science.* 1965;150(3698):893-9.
30. Hench LL, Paschall HA. Direct chemical bond of bioactive glass-ceramic materials to bone and muscle. *J Biomed Mater Res.* 1973;7(3):25-42.
31. Valimaki VV, Aro HT. Molecular basis for action of bioactive glasses as bone graft substitute. *Scand J Surg.* 2006;95(2):95-102.
32. White EW, Weber JN, Roy DM, Owen EL, Chiroff RT, White RA. Replamineform porous biomaterials for hard tissue implant applications. *J Biomed Mater Res.* 1975;9(4):23-7.
33. Bobynd JD, Stackpool GJ, Hacking SA, Tanzer M, Krygier JJ. Characteristics of bone ingrowth and interface mechanics of a new porous tantalum biomaterial. *J Bone Joint Surg Br.* 1999;81(5):907-14.
34. Tsao AK, Roberson JR, Christie MJ, Dore DD, Heck DA, Robertson DD, *et al.* Biomechanical and clinical evaluations of a porous tantalum implant for the treatment of early-stage osteonecrosis. *J Bone Joint Surg Am.* 2005;87 Suppl 2:22-7.
35. Ryan G, Pandit A, Apatsidis DP. Fabrication methods of porous metals for use in orthopaedic applications. *Biomaterials.* 2006;27(13):2651-70.
36. Witte F, Ulrich H, Palm C, Willbold E. Biodegradable magnesium scaffolds: Part II: peri-implant bone remodeling. *J Biomed Mater Res A.* 2007;81(3):757-65.
37. Lozano D, Trejo CG, Gomez-Barrena E, Manzano M, Doadrio JC, Salinas AJ, *et al.* Osteostatin-loaded onto mesoporous ceramics improves the early phase of bone regeneration in a rabbit osteopenia model. *Acta Biomater.* 2012;8(6):2317-23.
38. Trejo CG, Lozano D, Manzano M, Doadrio JC, Salinas AJ, Dapia S, *et al.* The osteoinductive properties of mesoporous silicate coated with osteostatin in a rabbit femur cavity defect model. *Biomaterials.* 2010;31(33):8564-73.
39. Wang H, Zou Q, Boerman OC, Nijhuis AW, Jansen JA, Li Y, *et al.* Combined delivery of BMP-2 and bFGF from nanostructured colloidal gelatin gels and its effect on bone regeneration in vivo. *J Control Release.* 2013;166(2):172-81.
40. Schnettler R, E. M. *Knochenersatzmaterialien und Wachstumsfaktoren.* Stuttgart: Thieme; 1997.
41. Lewandrowski KU, Gresser JD, Wise DL, Trantol DJ. Bioresorbable bone graft substitutes of different osteoconductivities: a histologic evaluation of osteointegration of poly(propylene glycol-co-fumaric acid)-based cement implants in rats. *Biomaterials.* 2000;21(8):757-64.
42. Muschler GF, Negami S, Hyodo A, Gaisser D, Easley K, Kambic H. Evaluation of collagen ceramic composite graft materials in a spinal fusion model. *Clin Orthop Relat Res.* 1996(328):250-60.

43. Hing KA. Bone repair in the twenty-first century: biology, chemistry or engineering? *Philos Transact A Math Phys Eng Sci.* 2004;362(1825):2821-50.
44. Cypher TJ, Grossman JP. Biological principles of bone graft healing. *J Foot Ankle Surg.* 1996;35(5):413-7.
45. Giannoudis PV, Dinopoulos H, Tsiridis E. Bone substitutes: an update. *Injury.* 2005;36 Suppl 3:S20-7.
46. Urist MR. Bone: formation by autoinduction. *Science.* 1965;150(698):893-9.
47. Burchardt H. The biology of bone graft repair. *Clin Orthop Relat Res.* 1983(174):28-42.
48. Costantino PD, Friedman CD. Synthetic bone graft substitutes. *Otolaryngol Clin North Am.* 1994;27(5):1037-74.
49. Patka P, Haarman HJ, Bakker FC. [Bone transplantation and bone replacement materials]. *Ned Tijdschr Geneesk.* 1998;142(16):893-6.
50. Asselmeier MA, Caspari RB, Bottenfield S. A review of allograft processing and sterilization techniques and their role in transmission of the human immunodeficiency virus. *Am J Sports Med.* 1993;21(2):170-5.
51. Stevenson S, Horowitz M. The response to bone allografts. *J Bone Joint Surg Am.* 1992;74(6):939-50.
52. Mahid SS, Hornung CA, Minor KS, Turina M, Galanduk S. Systematic reviews and meta-analysis for the surgeon scientist. *Br J Surg.* 2006;93(11):1315-24.
53. Dorozhkin SV. Bioceramics of calcium orthophosphates. *Biomaterials.* 2010;31(7):1465-85.
54. Brown WE, Chow LC, inventors; Dental restorative cement pastes. US Patent no. 45184301985.
55. Bohner M. Physical and chemical aspects of calcium phosphates used in spinal surgery. *Eur Spine J.* 2001;10 Suppl 2:S114-21.
56. Hing KA, Best SM, Bonfield W. Characterization of porous hydroxyapatite. *J Mater Sci Mater Med.* 1999;10(3):135-45.
57. Tadic D, Epple M. A thorough physicochemical characterisation of 14 calcium phosphate-based bone substitution materials in comparison to natural bone. *Biomaterials.* 2004;25(6):987-94.
58. Hing KA, Best SM, Tanner KE, Bonfield W, Revell PA. Mediation of bone ingrowth in porous hydroxyapatite bone graft substitutes. *J Biomed Mater Res A.* 2004;68(1):187-200.
59. Walsh WR, Vizesi F, Michael D, Auld J, Langdown A, Oliver R, *et al.* Beta-TCP bone graft substitutes in a bilateral rabbit tibial defect model. *Biomaterials.* 2008;29(3):266-71.
60. Zeman P, Zeman J, Matejka J, Koudela K. [Long-term results of calcaneal fracture treatment by open reduction and internal fixation using a calcaneal locking compression plate from an extended lateral approach]. *Acta Chir Orthop Traumatol Cech.* 2008;75(6):457-64.
61. Knop C, Sitte I, Canto F, Reinhold M, Blauth M. Successful posterior interlaminar fusion at the thoracic spine by sole use of beta-tricalcium phosphate. *Arch Orthop Trauma Surg.* 2006;126(3):204-10.
62. Hiu-Yan Y, Ling Q, Kwong-Man L, Ming Z, Kwok-Sui L, Chun-yiu CJ. Novel approach for quantification of porosity for biomaterial implants using microcomputed tomography (microCT). *J Biomed Mater Res B Appl Biomater.* 2005;75(2):234-42.
63. Gosain AK, Song L, Riordan P, Amarante MT, Nagy PG, Wilson CR, *et al.* A 1-year study of osteoinduction in hydroxyapatite-derived biomaterials in an adult sheep model: part I. *Plast Reconstr Surg.* 2002;109(2):619-30.
64. Gosain AK, Riordan PA, Song L, Amarante MT, Kalantarian B, Nagy PG, *et al.* A 1-year study of hydroxyapatite-derived biomaterials in an adult sheep model: III. Comparison with autogenous bone graft for facial augmentation. *Plast Reconstr Surg.* 2005;116(4):1044-52.

65. Itthichaisri C, Wiedmann-Al-Ahmad M, Huebner U, Al-Ahmad A, Schoen R, Schmelzeisen R, *et al.* Comparative in vitro study of the proliferation and growth of human osteoblast-like cells on various biomaterials. *J Biomed Mater Res A.* 2007;82(4):777-87.
66. Habraken WJ, Wolke JG, Mikos AG, Jansen JA. Injectable PLGA microsphere/calcium phosphate cements: physical properties and degradation characteristics. *J Biomater Sci Polym Ed.* 2006;17(9):1057-74.
67. Link DP, van den Dolder J, Wolke JG, Jansen JA. The cytocompatibility and early osteogenic characteristics of an injectable calcium phosphate cement. *Tissue Eng.* 2007;13(3):493-500.
68. Constantz BR, Ison IC, Fulmer MT, Poser RD, Smith ST, VanWagoner M, *et al.* Skeletal repair by in situ formation of the mineral phase of bone. *Science.* 1995;267(5205):1796-9.
69. Klein C, de Groot K, Chen W, Li Y, Zhang X. Osseous substance formation induced in porous calcium phosphate ceramics in soft tissues. *Biomaterials.* 1994;15(1):31-4.
70. LeGeros RZ. Properties of osteoconductive biomaterials: calcium phosphates. *Clin Orthop Relat Res.* 2002(395):81-98.
71. Ruhe PQ, Hedberg EL, Padron NT, Spauwen PH, Jansen JA, Mikos AG. Biocompatibility and degradation of poly(DL-lactic-co-glycolic acid)/calcium phosphate cement composites. *J Biomed Mater Res A.* 2005;74(4):533-44.
72. Wiltfang J, Merten HA, Wiltfang J. Ectopic bone formation with the help of growth factor bFGF. *J Craniomaxillofac Surg.* 1996;24(5):300-4.
73. Hing KA, Best SM, Tanner KE, Bonfield W, Revell PA. Quantification of bone ingrowth within bone-derived porous hydroxyapatite implants of varying density. *J Mater Sci Mater Med.* 1999;10(10/11):663-70.
74. Jensen SS, Aaboe M, Pinholt EM, Hjørtting-Hansen E, Melsen F, Ruyter IE. Tissue reaction and material characteristics of four bone substitutes. *Int J Oral Maxillofac Implants.* 1996;11(1):55-66.
75. Liebendorfer A, Troster S. [Hydroxyapatite ceramics in clinical application. Histological findings in 23 patients]. *Unfallchirurgie.* 1997;23(2):60-8.
76. Muller-Mai C, Voigt C, Hering A, Rahmzadeh R, Gross U. [Madrepore hydroxyapatite granulates for filling bone defects]. *Unfallchirurg.* 2001;104(3):221-9.
77. Briem D, Linhart W, Lehmann W, Meenen NM, Rueger JM. [Long-term outcomes after using porous hydroxyapatite ceramics (Endobon) for surgical management of fractures of the head of the tibia]. *Unfallchirurg.* 2002;105(2):128-33.
78. Schnettler R, Knoss PD, Heiss C, Stahl JP, Meyer C, Kilian O, *et al.* Enhancement of bone formation in hydroxyapatite implants by rhBMP-2 coating. *J Biomed Mater Res B Appl Biomater.* 2009;90(1):75-81.
79. Schnettler R, Stahl JP, Alt V, Pavlidis T, Dingeldein E, Wenisch S. Calcium phosphate-based bone substitutes. *Eur J Trauma.* 2004.
80. Huber FX, McArthur N, Hillmeier J, Kock HJ, Baier M, Diwo M, *et al.* Void filling of tibia compression fracture zones using a novel resorbable nanocrystalline hydroxyapatite paste in combination with a hydroxyapatite ceramic for the treatment of critical size bone defects (CSD) in rabbits. *J Mater Sci Mater Med.* 2008;19(1):33-8.
81. Huber FX, Berger I, McArthur N, Huber C, Kock HP, Hillmeier J, *et al.* Evaluation of a novel nanocrystalline hydroxyapatite paste and a solid hydroxyapatite ceramic for the treatment of critical size bone defects (CSD) in rabbits. *J Mater Sci Mater Med.* 2008;19(1):33-8.
82. Spies CK, Schnurer S, Gotterbarm T, Breusch S. The efficacy of Biobon and Ostim within metaphyseal defects using the Gottinger Minipig. *Arch Orthop Trauma Surg.* 2009;129(7):979-88.
83. Thorwarth M, Schultze-Mosgau S, Kessler P, Wiltfang J, Schlegel KA. Bone regeneration in osseous defects using a resorbable nanoparticulate hydroxyapatite. *J Oral Maxillofac Surg.* 2005;63(11):1626-33.

84. Spies C, Schnurer S, Gotterbarm T, Breusch S. [Animal study of the bone substitute material Ostim within osseous defects in Gottinger minipigs]. *Z Orthop Unfall*. 2008;146(1):64-9.
85. Brandt J, Henning S, Michler G, Hein W, Bernstein A, Schulz M. Nanocrystalline hydroxyapatite for bone repair: an animal study. *J Mater Sci Mater Med*. 2010;21(1):283-94.
86. Jager M, Fischer J, Schultheis A, Lensing-Hohn S, Krauspe R. Extensive H(+) release by bone substitutes affects biocompatibility in vitro testing. *J Biomed Mater Res A*. 2006;76(2):310-22.
87. van Hemert WL, Willems K, Anderson PG, van Heerwaarden RJ, Wymenga AB. Tricalcium phosphate granules or rigid wedge preforms in open wedge high tibial osteotomy: a radiological study with a new evaluation system. *Knee*. 2004;11(6):451-6.
88. Burstein FD, Williams JK, Hudgins R, Boydston W, Reisner A, Stevenson K, et al. Hydroxyapatite cement in craniofacial reconstruction: experience in 150 patients. *Plast Reconstr Surg*. 2006;118(2):484-9.
89. Rossa C, Jr., Marcantonio E, Jr., Santos LA, Boschi AO, Raddi MS. Cytotoxicity of two novel formulations of calcium phosphate cements: a comparative in vitro study. *Artif Organs*. 2005;29(2):114-21.
90. Oreffo RO, Driessens FC, Planell JA, Triffitt JT. Effects of novel calcium phosphate cements on human bone marrow fibroblastic cells. *Tissue Eng*. 1998;4(3):293-303.
91. Maestretti G, Cremer C, Otten P, Jakob RP. Prospective study of standalone balloon kyphoplasty with calcium phosphate cement augmentation in traumatic fractures. *Eur Spine J*. 2007;16(5):601-10.
92. Kummerle JM, Oberle A, Oechslin C, Böhner M, Frei C, Boeckel I, et al. Assessment of the suitability of a new brushite calcium phosphate cement for cranioplasty - an experimental study in sheep. *J Craniomaxillofac Surg*. 2005;33(1):37-44.
93. Herron S, Thordarson DB, Winet H, Luk A, Bao JY. Ingrowth of bone into absorbable bone cement: an in vivo microscopic evaluation. *Am J Orthop*. 2003;32(12):581-4.
94. Elsner A, Jubel A, Prokop A, Koebeke J, Rehm KE, Andermahr J. Augmentation of intraarticular calcaneal fractures with injectable calcium phosphate cement: densitometry, histology, and functional outcome of 18 patients. *J Foot Ankle Surg*. 2005;44(5):390-5.
95. Acarturk O, Lehmicke M, Aberman H, Toms D, Hollinger JO, Fulmer M. Bone healing response to an injectable calcium phosphate cement with enhanced radiopacity. *J Biomed Mater Res B Appl Biomater*. 2008;86(1):56-62.
96. Apelt D, Theiss F, El-Warrak AO, Zlinszky K, Bettschart-Wolfisberger R, Böhner M, et al. In vivo behavior of three different injectable hydraulic calcium phosphate cements. *Biomaterials*. 2004;25(7-8):1439-51.
97. Gisep A, Wieling R, Böhner M, Matter S, Schneider E, Rahn B. Resorption patterns of calcium-phosphate cements in bone. *J Biomed Mater Res A*. 2003;66(3):532-40.
98. Hing KA, Best SM, Tanner KE, Bonfield W, Revell PA. Biomechanical assessment of bone ingrowth in porous hydroxyapatite. *J Mater Sci Mater Med*. 1997;8(12):731-6.
99. Werber KD, Brauer RB, Weiss W, Becker K. Osseous integration of bovine hydroxyapatite ceramic in metaphyseal bone defects of the distal radius. *J Hand Surg Am*. 2000;25(5):833-41.
100. Helber MU, Ulrich C. [Metaphyseal defect substitute: hydroxylapatite ceramic. Results of a 3 to 4 year follow up]. *Unfallchirurg*. 2000;103(9):749-53.
101. Gierse H, Donath K. Reactions and complications after the implantation of Endobon including morphological examination of explants. *Arch Orthop Trauma Surg*. 1999;119(5-6):349-55.
102. Schnettler R, Dingeldein E, Herr G. [Defect reconstruction using demineralized bone matrix. Experimental studies on piglets]. *Orthopade*. 1998;27(2):80-8.

103. Huber FX, Belyaev O, Hillmeier J, Kock HJ, Huber C, Meeder PJ, *et al.* First histological observations on the incorporation of a novel nanocrystalline hydroxyapatite paste OSTIM in human cancellous bone. *BMC Musculoskelet Disord.* 2006;7:50.
104. Busenlechner D, Tangl S, Mair B, Fugger G, Gruber R, Redl H, *et al.* Simultaneous in vivo comparison of bone substitutes in a guided bone regeneration model. *Biomaterials.* 2008;29(22):3195-200.
105. Huber FX, McArthur N, Heimann L, Dingeldein E, Cavey H, Palazzi X, *et al.* Evaluation of a novel nanocrystalline hydroxyapatite paste Ostim in comparison to Alpha-BSM - more bone ingrowth inside the implanted material with Ostim compared to Alpha BSM. *BMC Musculoskelet Disord.* 2009;10:164.
106. Leupold JA, Barfield WR, An YH, Hartssock LA. A comparison of ProOsteon, DBX, and collagraft in a rabbit model. *J Biomed Mater Res B Appl Biomater.* 2006;79(2):292-7.
107. Feifel H. [Bone regeneration in Pro Osteon 500 alone and in combination with Colloss in the patellar gliding model of the rabbit]. *Mund Kiefer Gesichtschir.* 2000;4 Suppl 2:S527-30.
108. Thalgot J, Fritts K, Giuffre JM, Timlin M. Anterior interbody fusion of the cervical spine with coralline hydroxyapatite. *Spine (Phila Pa 1976).* 1999;24(13):1295-9.
109. Steffen T, Stoll T, Arvinte T, Schenk RK. Porous tricalcium phosphate and transforming growth factor used for anterior spine surgery. *Eur Spine J.* 2001;10 Suppl 2:S132-40.
110. Gaasbeek RD, Toonen HG, van Heerwaarden RJ, Buma P. Mechanism of bone incorporation of beta-TCP bone substitute in open wedge tibial osteotomy in patients. *Biomaterials.* 2005;26(33):6713-9.
111. van der Pol U, Mathieu L, Zeiter S, Bourban PE, Zambelli PY, Pearce SG, *et al.* Augmentation of bone defect healing using a new biocomposite scaffold: an in vivo study in sheep. *Acta Biomater.* 2010;6(9):3755-62.
112. Timmins NE, Scherberich A, Fruh JA, Heberer M, Martin I, Jakob M. Three-dimensional cell culture and tissue engineering in a T-CUP (tissue culture under perfusion). *Tissue Eng.* 2007;13(8):2021-8.
113. Miljkovic ND, Cooper GM, Hott SL, Disalle BF, Gawalt ES, Smith DM, *et al.* Calcium aluminate, RGD-modified calcium aluminate, and beta-tricalcium phosphate implants in a calvarial defect. *J Craniofac Surg.* 2009;20(5):1538-43.
114. Turner TM, Urban RM, Singh K, Hall DJ, Renner SM, Lim TH, *et al.* Vertebroplasty comparing injectable calcium phosphate cement compared with polymethylmethacrylate in a unique canine vertebral body large defect model. *Spine J.* 2008;8(3):482-7.
115. Cavalcanti SC, Pereira CL, Mazzonetto R, de Moraes M, Moreira RW. Histological and histomorphometric analyses of calcium phosphate cement in rabbit calvaria. *J Craniomaxillofac Surg.* 2008;36(6):354-9.
116. Gosain AK, Riordan PA, Song L, Amarante MT, Kalantarian B, Nagy PG, *et al.* A 1-year study of osteoinduction in hydroxyapatite-derived biomaterials in an adult sheep model: part II. Bioengineering implants to optimize bone replacement in reconstruction of cranial defects. *Plast Reconstr Surg.* 2004;114(5):1155-63; discussion 64-5.
117. Welch RD, Berry BH, Crawford K, Zhang H, Zobitz M, Bronson D, *et al.* Subchondral defects in caprine femora augmented with in situ setting hydroxyapatite cement, polymethylmethacrylate, or autogenous bone graft: biomechanical and histomorphological analysis after two-years. *J Orthop Res.* 2002;20(3):464-72.
118. Morio D, Lew D, Krizan K, Keller JC. Short-term bone responses to hydroxyapatite cement. *Implant Dent.* 2002;11(4):376-82.
119. Dickson KF, Friedman J, Buchholz JG, Flandry FD. The use of BoneSource hydroxyapatite cement for traumatic metaphyseal bone void filling. *J Trauma.* 2002;53(6):1103-8.
120. Verheggen R, Merten HA. Correction of skull defects using hydroxyapatite cement (HAC)--evidence derived from animal experiments and clinical experience. *Acta Neurochir (Wien).* 2001;143(9):919-26.

121. Mao K, Yang Y, Li J, Hao L, Tang P, Wang Z, *et al.* Investigation of the histology and interfacial bonding between carbonated hydroxyapatite cement and bone. *Biomed Mater.* 2009;4(4):45003.
122. Rupprecht S, Merten HA, Kessler P, Wiltfang J. Hydroxyapatite cement (BoneSource) for repair of critical sized calvarian defects--an experimental study. *J Craniomaxillofac Surg.* 2003;31(3):149-53.
123. Libicher M, Hillmeier J, Liegibel U, Sommer U, Pyerin W, Vetter M, *et al.* Osseous integration of calcium phosphate in osteoporotic vertebral fractures after kyphoplasty: initial results from a clinical and experimental pilot study. *Osteoporos Int.* 2006;17(8):1208-15.
124. Ooms EM, Wolke JG, van de Heuvel MT, Jeschke B, Jansen JA. Histological evaluation of the bone response to calcium phosphate cement implanted in cortical bone. *Biomaterials.* 2003;24(6):989-1000.
125. Hempel U, Reinstorf A, Poppe M, Fischer U, Gelinsky M, Pompe W, *et al.* Proliferation and differentiation of osteoblasts on Biocement D modified with collagen type I and citric acid. *J Biomed Mater Res B Appl Biomater.* 2004;71(1):130-43.
126. Ooms EM, Wolke JG, van der Waerden JP, Jansen JA. Trabecular bone response to injectable calcium phosphate (Ca-P) cement. *J Biomed Mater Res.* 2002;61(1):9-18.
127. Oberle A, Theiss F, Bohner M, Muller J, Kastner SB, Frei C, *et al.* [Investigation about the clinical use of brushite-and hydroxylapatite-cement in sheep]. *Schweiz Arch Tierheilkd.* 2005;147(11):482-90.
128. Kopylov P, Adalberth K, Jonsson K, Aspenberg P. Norian SRS versus functional treatment in redisplaced distal radial fractures: a randomized study in 20 patients. *J Hand Surg Br.* 2002;27(6):538-41.
129. Kelly CM, Wilkins RM. Treatment of benign bone lesions with an injectable calcium sulfate-based bone graft substitute. *Orthopedics.* 2004;27(1 Suppl):s131-5.
130. Yu B, Han K, Ma H, Zhang C, Su J, Zhao J, *et al.* Treatment of tibial plateau fractures with high strength injectable calcium sulphate. *Int Orthop.* 2009;33(4):1127-33.
131. Watson JT. The use of an injectable bone graft substitute in tibial metaphyseal fractures. *Orthopedics.* 2004;27(1 Suppl):s103-7.
132. Fujishiro T, Bauer TW, Kobayashi N, Kobayashi H, Sunwoo MH, Seim HB, 3rd, *et al.* Histological evaluation of an impacted bone graft substitute composed of a combination of mineralized and demineralized allograft in a sheep vertebral bone defect. *J Biomed Mater Res A.* 2007;82(3):538-44.
133. Urban RM, Turner TM, Hall DJ, Infanger S, Cheema N, Lim TH. Healing of large defects treated with calcium sulfate pellets containing demineralized bone matrix particles. *Orthopedics.* 2003;26(5 Suppl):s581-5.
134. Clokie CM, Moghadam H, Jackson MT, Sandor GK. Closure of critical sized defects with allogenic and alloplastic bone substitutes. *J Craniofac Surg.* 2002;13(1):111-21; discussion 22-3.
135. Urban RM, Turner TM, Hall DJ, Infanger SI, Cheema N, Lim TH, *et al.* Effects of altered crystalline structure and increased initial compressive strength of calcium sulfate bone graft substitute pellets on new bone formation. *Orthopedics.* 2004;27(1 Suppl):s113-8.
136. Kuo SM, Lin LC, Kang PL, Tsai JC, Chang SJ. Evaluation of bone growth using artificial bone substitute (osteoset) and platelet gel mixtures: a preliminarily study in dogs. *Artif Cells Blood Substit Immobil Biotechnol.* 2009;37(2):78-84.
137. Chen WC, Ju CP, Tien YC, Lin JH. In vivo testing of nanoparticle-treated TTCP/DCPA-based ceramic surfaces. *Acta Biomater.* 2009;5(5):1767-74.
138. Zhang DB, Cheng Q, Gu GS. Repair of bone defect caused by bone tumor with OsteoSet: Osteoset absorption and new bone growth characters. *Journal of Clinical Rehabilitative Tissue Engineering Research.* 2007;41:8394-8397.

139. Erbe EM, Clineff TD, Gualtieri G. Comparison of a new bisphenol-a-glycidyl dimethacrylate-based cortical bone void filler with polymethyl methacrylate. *Eur Spine J*. 2001;10 Suppl 2:S147-52.
140. Smit RS, van der Velde D, Hegeman JH. Augmented pin fixation with Cortoss for an unstable AO-A3 type distal radius fracture in a patient with a manifest osteoporosis. *Arch Orthop Trauma Surg*. 2008;128(9):989-93.
141. Martin RB, Chapman MW, Sharkey NA, Zissimos SL, Bay B, Shors EC. Bone ingrowth and mechanical properties of coralline hydroxyapatite 1 yr after implantation. *Biomaterials*. 1993;14(5):341-8.
142. Morgan EF, Yetkinler DN, Constantz BR, Dauskardt RH. Mechanical properties of carbonated apatite bone mineral substitute: strength, fracture and fatigue behaviour. *J Mater Sci Mater Med*. 1997;8(9):559-70.
143. Moore DC, Frankenburg EP, Goulet JA, Goldstein SA. Hip screw augmentation with an in situ-setting calcium phosphate cement: an in vitro biomechanical analysis. *J Orthop Trauma*. 1997;11(8):577-83.
144. Kopylov P, Tagil M, Aspenberg P. Delayed surgery does not reduce the interface strength between the surface of a bone fracture and a self-curing injectable hydroxyapatite (Norian SRS). *Scand J Plast Reconstr Surg Hand Surg*. 2001;35(2):129-33.
145. Eriksson F, Mattsson P, Larsson S. The effect of augmentation with resorbable or conventional bone cement on the holding strength for femoral neck fracture devices. *J Orthop Trauma*. 2002;16(5):302-10.
146. Nitsch A, Patyk A, Schwartz P, Merten HA. [Influence of different mixing fluids on mechanical and micromorphological in vitro qualities of hydroxyapatite cement]. *Mund Kiefer Gesichtschir*. 2005;9(2):89-94.
147. Pierce WA, Welch RD. Acute compressive strength of hydroxyapatite cement. *Trans Orthopd Res Soc*. 1997;22:1014/.
148. Crawford K, Berrey BH, Pierce WA, Welch RD. In vitro strength comparison of hydroxyapatite cement and polymethylmethacrylate in subchondral defects in caprine femora. *J Orthop Res*. 1998;16(6):715-9.
149. Khairoun I, Boltong MG, Driessens FC, Planell JA. Effect of calcium carbonate on clinical compliance of apatitic calcium phosphate bone cement. *J Biomed Mater Res*. 1997;38(4):356-60.
150. Knepper-Nicolai B, Reinstorf A, Hofinger I, Flade K, Wenz R, Pompe W. Influence of osteocalcin and collagen I on the mechanical and biological properties of Biocement D. *Biomol Eng*. 2002;19(2-6):227-31.
151. Clarkin OM, Boyd D, Madigan S, Towler MR. Comparison of an experimental bone cement with a commercial control, Hydroset. *J Mater Sci Mater Med*. 2009;20(7):1563-70.
152. Clarkin O, Boyd D, Towler MR. Comparison of failure mechanisms for cements used in skeletal luting applications. *J Mater Sci Mater Med*. 2009;20(8):1585-94.
153. Boyd D, Towler MR, Wren A, Clarkin OM. Comparison of an experimental bone cement with surgical Simplex P, Spineplex and Cortoss. *J Mater Sci Mater Med*. 2008;19(4):1745-52.
154. Gheduzzi S, Webb JJ, Miles AW. Mechanical characterisation of three percutaneous vertebroplasty biomaterials. *J Mater Sci Mater Med*. 2006;17(5):421-6.
155. Linhart W, Briem D, Amling M, Rueger JM, Windolf J. [Mechanical failure of porous hydroxyapatite ceramics 7.5 years after implantation in the proximal tibia]. *Unfallchirurg*. 2004;107(2):154-7.
156. Attmanspacher W, Dittrich V, Staiger M, Stedtfeld HW. [Arthroscopic management of tibial plateau fractures]. *Zentralbl Chir*. 2002;127(10):828-36.
157. Khodadadyan-Klostermann C, Liebig T, Melcher I, Raschke M, Haas NP. Osseous integration of hydroxyapatite grafts in metaphyseal bone defects of the proximal tibia (CT-study). *Acta Chir Orthop Traumatol Cech*. 2002;69(1):16-21.

158. Sailer R, Lutz M, Zimmermann R, Hackl W, Gabl M, Blauth M. Minimal invasive treatment of displaced metaphyseal fractures of the distal radius - Clinical and radiological results after closed reduction, K-wire fixation and substitution with hydroxyapatite ceramic. *Aktuelle Traumatologie*. 2003;33:26-30.
159. Huber FX, Hillmeier J, Kock HJ, McArthur N, Huber C, Diwo M, *et al.* [Filling of metaphyseal defects with nanocrystalline hydroxyapatite (Ostim) for fractures of the radius]. *Zentralbl Chir*. 2008;133(6):577-81.
160. Huber FX, Hillmeier J, Herzog L, McArthur N, Kock HJ, Meeder PJ. Open reduction and palmar plate-osteosynthesis in combination with a nanocrystalline hydroxyapatite spacer in the treatment of comminuted fractures of the distal radius. *J Hand Surg Br*. 2006;31(3):298-303.
161. Irwin RB, Bernhard M, Biddinger A. Coralline hydroxyapatite as bone substitute in orthopedic oncology. *Am J Orthop*. 2001;30(7):544-50.
162. Wolfe SW, Pike L, Slade JF, 3rd, Katz LD. Augmentation of distal radius fracture fixation with coralline hydroxyapatite bone graft substitute. *J Hand Surg Am*. 1999;24(4):816-27.
163. Hinz P, Wolf E, Schwesinger G, Hartelt E, Ekkernkamp A. A new resorbable bone void filler in trauma: early clinical experience and histologic evaluation. *Orthopedics*. 2002;25(5 Suppl):s597-600.
164. Robinson CM, Page RS. Severely impacted valgus proximal humeral fractures. Results of operative treatment. *J Bone Joint Surg Am*. 2003;85-A(9):1647-55.
165. Kopylov P, Runnqvist K, Jonsson K, Aspenberg P. Norian SRS versus external fixation in redisplaced distal radial fractures. A randomized study in 40 patients. *Acta Orthop Scand*. 1999;70(1):1-5.
166. Sanchez-Sotelo J, Munuera L, Madero R. Treatment of fractures of the distal radius with a remodelable bone cement: a prospective, randomised study using Norian SRS. *J Bone Joint Surg Br*. 2000;82(6):856-63.
167. Kopylov P, Aspenberg P, Yuan X, Ryd L. Radiostereometric analysis of distal radial fracture displacement during treatment: a randomized study comparing Norian SRS and external fixation in 23 patients. *Acta Orthop Scand*. 2001;72(1):57-61.
168. Zimmermann R, Gabl M, Lutz M, Angermann P, Gschwentner M, Pechlaner S. Injectable calcium phosphate bone cement Norian SRS for the treatment of intra-articular compression fractures of the distal radius in osteoporotic women. *Arch Orthop Trauma Surg*. 2003;123(1):22-7.
169. Cassidy C, Jupiter JB, Cohen M, Delli-Santi M, Fennell C, Leinberry C, *et al.* Norian SRS cement compared with conventional fixation in distal radial fractures. A randomized study. *J Bone Joint Surg Am*. 2003;85-A(11):2127-37.
170. Kopylov P, Jonsson K, Thorngren KG, Aspenberg P. Injectable calcium phosphate in the treatment of distal radial fractures. *J Hand Surg Br*. 1996;21(6):768-71.
171. Jupiter JB, Winters S, Sigman S, Lowe C, Pappas C, Ladd AL, *et al.* Repair of five distal radius fractures with an investigational cancellous bone cement: a preliminary report. *J Orthop Trauma*. 1997;11(2):110-6.
172. Tyllianakis M, Giannikas D, Panagopoulos A, Panagiotopoulos E, Lambiris E. Use of injectable calcium phosphate in the treatment of intra-articular distal radius fractures. *Orthopedics*. 2002;25(3):311-5.
173. Horstmann WG, Verheyen CC, Leemans R. An injectable calcium phosphate cement as a bone-graft substitute in the treatment of displaced lateral tibial plateau fractures. *Injury*. 2003;34(2):141-4.
174. Simpson D, Keating JF. Outcome of tibial plateau fractures managed with calcium phosphate cement. *Injury*. 2004;35(9):913-8.
175. Jubel A, Andermahr J, Mairhofer J, Prokop A, Hahn U, Rehm KE. [Use of the injectable bone cement Norian SRS for tibial plateau fractures. Results of a prospective 30-month follow-up study]. *Orthopade*. 2004;33(8):919-27.
176. Engel T, Lill H, Korner J, Verheyden P, Josten C. [Tibial plateau fracture--biodegradable bonecement-augmentation]. *Unfallchirurg*. 2003;106(2):97-101.

177. Lobenhoffer P, Gerich T, Witte F, Tschorne H. Use of an injectable calcium phosphate bone cement in the treatment of tibial plateau fractures: a prospective study of twenty-six cases with twenty-month mean follow-up. *J Orthop Trauma*. 2002;16(3):143-9.
178. Keating JF, Hajducka CL, Harper J. Minimal internal fixation and calcium-phosphate cement in the treatment of fractures of the tibial plateau. A pilot study. *J Bone Joint Surg Br*. 2003;85(1):68-73.
179. Mattsson P, Alberts A, Dahlberg G, Sohlman M, Hyldahl HC, Larsson S. Resorbable cement for the augmentation of internally-fixed unstable trochanteric fractures. A prospective, randomised multicentre study. *J Bone Joint Surg Br*. 2005;87(9):1203-9.
180. Mattsson P, Larsson S. Stability of internally fixed femoral neck fractures augmented with resorb181. Wee AT, Wong YS. Percutaneous reduction and injection of Norian bone cement for the treatment of displaced intra-articular calcaneal fractures. *Foot Ankle Spec*. 2009;2(2):98-106.
182. Jeyam M, Andrew JG, Muir LT, McGovern A. Controlled trial of distal radial fractures treated with a resorbable bone mineral substitute. *J Hand Surg Br*. 2002;27(2):146-9.
183. de Falco R, Scarano E, Di Celmo D, Grasso U, Guarnieri L. Balloon kyphoplasty in traumatic fractures of the thoracolumbar junction. Preliminary experience in 12 cases. *J Neurosurg Sci*. 2005;49(4):147-53.
184. Grafe IA, Baier M, Noldge G, Weiss C, Da Fonseca K, Hillmeier J, et al. Calcium-phosphate and polymethylmethacrylate cement in long-term outcome after kyphoplasty of painful osteoporotic vertebral fractures. *Spine (Phila Pa 1976)*. 2008;33(11):1284-90.
185. Hillmeier J, Meeder PJ, Noldge G, Kock HJ, Da Fonseca K, Kasperk HC. [Balloon kyphoplasty of vertebral compression fractures with a new calcium phosphate cement]. *Orthopade*. 2004;33(1):31-9.
186. Baer W, Schaller P, Carl HD. Spongy hydroxyapatite in hand surgery--a five year follow-up. *J Hand Surg Br*. 2002;27(1):101-3.
187. Joosten U, Joist A, Frebel T, Walter M, Langer M. The use of an in situ curing hydroxyapatite cement as an alternative to bone graft following removal of enchondroma of the hand. *J Hand Surg Br*. 2000;25(3):288-91.
188. Mohanty SS, Bhasme VK, Garg H, Wargantiwar A. The haemophilic pseudotumour - surgical treatment by excision and filling the defect with calcium-phosphate cement granules. *Haemophilia*. 2007;13(2):217-20.
189. Joeris A, Ondrus S, Planka L, Gal P, Slongo T. ChronOS inject in children with benign bone lesions--does it increase the healing rate? *Eur J Pediatr Surg*. 20(1):24-8.
190. Mattsson P, Larsson S. Unstable trochanteric fractures augmented with calcium phosphate cement. A prospective randomized study using radiostereometry to measure fracture stability. *Scand J Surg*. 2004;93(3):223-8.
191. Thordarson DB, Bollinger M. SRS cancellous bone cement augmentation of calcaneal fracture fixation. *Foot Ankle Int*. 2005;26(5):347-52.
192. Csizy M, Buckley RE, Fennell C. Benign calcaneal bone cyst and pathologic fracture--surgical treatment with injectable calcium-phosphate bone cement (Norian): a case report. *Foot Ankle Int*. 2001;22(6):507-10.
193. Clayer M. Injectable form of calcium sulphate as treatment of aneurysmal bone cysts. *ANZ J Surg*. 2008;78(5):366-70.
194. Vigler M, Weigl D, Schwarz M, Ben-Itzhak I, Salai M, Bar-On E. Subtrochanteric femoral fractures due to simple bone cysts in children. *J Pediatr Orthop B*. 2006;15(6):439-42.
195. Gitelis S, Virkus W, Anderson D, Piasecki P, Yao TK. Functional outcomes of bone graft substitutes for benign bone tumors. *Orthopedics*. 2004;27(1 Suppl):s141-4.
196. Kelly CM, Wilkins RM, Gitelis S, Hartjen C, Watson JT, Kim PT. The use of a surgical grade calcium sulfate as a bone graft substitute: results of a multicenter trial. *Clin Orthop Relat Res*. 2001(382):42-50.

197. Mirzayan R, Panossian V, Avedian R, Forrester DM, Menendez LR. The use of calcium sulfate in the treatment of benign bone lesions. A preliminary report. *J Bone Joint Surg Am.* 2001;83-A(3):355-8.
198. Andreassen GS, Hoiness PR, Skraamm I, Granlund O, Engebretsen L. Use of a synthetic bone void filler to augment screws in osteopenic ankle fracture fixation. *Arch Orthop Trauma Surg.* 2004;124(3):161-5.
199. Palussiere J, Berge J, Gangi A, Cotten A, Pasco A, Bertagnoli R, *et al.* Clinical results of an open prospective study of a bis-GMA composite in percutaneous vertebral augmentation. *Eur Spine J.* 2005;14(10):982-91.
200. Dressmann H. Ueber Knochenplombierung bei Hohlenforming Defekten des Knochens. *Beitr Klin Chir.* 1892;9:804-10.
201. Peters CL, Hines JL, Bachus KN, Craig MA, Bloebaum RD. Biological effects of calcium sulfate as a bone graft substitute in ovine metaphyseal defects. *J Biomed Mater Res A.* 2006;76(3):456-62.
202. Gitelis S, Brebach GT. The treatment of chronic osteomyelitis with a biodegradable antibiotic-impregnated implant. *J Orthop Surg (Hong Kong).* 2002;10(1):53-60.
203. Lee GH, Khoury JG, Bell JE, Buckwalter JA. Adverse reactions to OsteoSet bone graft substitute, the incidence in a consecutive series. *Iowa Orthop J.* 2002;22:35-8.
204. Robinson D, Alk D, Sandbank J, Farber R, Halperin N. Inflammatory reactions associated with a calcium sulfate bone substitute. *Ann Transplant.* 1999;4(3-4):91-7.
205. Smith I. Convulsions and Coma Associated with Iatrogenically Elevated CSF Calcium Levels Post Spinal Surgery: A Case Report. *Crit Care Resusc.* 2005;7(3):173-6.
206. Ohtsuki C, Kamitakahara M, Miyazaki T. Bioactive ceramic-based materials with designed reactivity for bone tissue regeneration. *J R Soc Interface.* 2009;6 Suppl 3:S349-60.
207. DiCicco M, Compton R, Jansen-Varnum SA. In vitro evaluation of orthopedic composite cytotoxicity: assessing the potential for postsurgical production of hydroxyl radicals. *J Biomed Mater Res B Appl Biomater.* 2005;72(1):146-55.
208. Evans SL, Hunt CM, Ahuja S. Bone cement or bone substitute augmentation of pedicle screws improves pullout strength in posterior spinal fixation. *J Mater Sci Mater Med.* 2002;13(12):1143-5.
209. Reck R. Tissue reactions to glass ceramics in the middle ear. *Clin Otolaryngol Allied Sci.* 1981;6(1):63-5.
210. Middleton ET, Rajaraman CJ, O'Brien DP, Doherty SM, Taylor AD. The safety and efficacy of vertebroplasty using Cortoss cement in a newly established vertebroplasty service. *Br J Neurosurg.* 2008;22(2):252-6.
211. Blokhuis TJ, Termaat MF, den Boer FC, Patka P, Bakker FC, Haarman HJ. Properties of calcium phosphate ceramics in relation to their in vivo behavior. *J Trauma.* 2000;48(1):179-86.
212. Daculsi G, Passuti N. Effect of the macroporosity for osseous substitution of calcium phosphate ceramics. *Biomaterials.* 1990;11:86-7.
213. Hulbert SF, Young FA, Mathews RS, Klawitter JJ, Talbert CD, Stelling FH. Potential of ceramic materials as permanently implantable skeletal prostheses. *J Biomed Mater Res.* 1970;4(3):433-56.
214. van Eeden SP, Ripamonti U. Bone differentiation in porous hydroxyapatite in baboons is regulated by the geometry of the substratum: implications for reconstructive craniofacial surgery. *Plast Reconstr Surg.* 1994;93(5):959-66.
215. Driskell TD, O'Hara MJ, Sheets HD, Jr., Greene GW, Jr., Natiella JR, Armitage J. Development of ceramic and ceramic composite devices for maxillofacial applications. *J Biomed Mater Res.* 1972;6(1):345-61.
216. Beuerlein MJ, McKee MD. Calcium sulfates: what is the evidence? *J Orthop Trauma.* 2010;24 Suppl 1:S46-51.
217. An YH, Draughn RA. Mechanical testing of bone and bone-implant interface: CRC Press LLC; 1999. 624 p.

218. Russell TA, Leighton RK. Comparison of autogenous bone graft and endothermic calcium phosphate cement for defect augmentation in tibial plateau fractures. A multicenter, prospective, randomized study. *J Bone Joint Surg Am.* 2008;90(10):2057-61.
219. Giannoudis PV, Dinopoulos HT. BMPs: Options, indications, and effectiveness. *J Orthop Trauma.* 2010;24 Suppl 1:S9-16.
220. Termaat MF, Den Boer FC, Bakker FC, Patka P, Haarman HJ. Bone morphogenetic proteins. Development and clinical efficacy in the treatment of fractures and bone defects. *J Bone Joint Surg Am.* 2005;87(6):1367-78.
221. Brinker MR, O'Connor DP. The incidence of fractures and dislocations referred for orthopaedic services in a capitulated population. *J Bone Joint Surg Am.* 2004;86-A(2):290-7.
222. Giannoudis PV, Einhorn TA, Marsh D. Fracture healing: the diamond concept. *Injury.* 2007;38 Suppl 4:S3-6.
223. Patka P. Bone replacement by calcium phosphate ceramics: an experimental study. 1st ed. Amsterdam: Free University Press; 1984.
224. Hannink G, Arts JJ. Bioresorbability, porosity and mechanical strength of bone substitutes: what is optimal for bone regeneration? *Injury.* 2011;42 Suppl 2:S22-5.
225. Van Lieshout EMM, Van Kralingen GH, El-Massoudi Y, Weinans H, Patka P. Microstructure and biomechanical characteristics of bone substitutes for trauma and orthopaedic surgery. *BMC Musculoskelet Disord.* 2011;12(1):34.
226. Muller M, Stangl R. [Norian SRS augmentation in revision of acetabular cup of total hip arthroplasty. A follow up of six patients]. *Unfallchirurg.* 2006;109(4):335-8.
227. Manzotti A, Confalonieri N, Pullen C. Grafting of tibial bone defects in knee replacement using Norian skeletal repair system. *Arch Orthop Trauma Surg.* 2006;126(9):594-8.
228. Welkerling H, Raith J, Kastner N, Marschall C, Windhager R. Painful soft-tissue reaction to injectable Norian SRS calcium phosphate cement after curettage of enchondromas. *J Bone Joint Surg Br.* 2003;85(2):238-9.
229. Robinson CM, Page RS. Severely impacted valgus proximal humeral fractures. *J Bone Joint Surg Am.* 2004;86-A Suppl 1(Pt 2):143-55.
230. Abramo A, Tagil M, Geijer M, Kopylov P. Osteotomy of dorsally displaced malunited fractures of the distal radius: no loss of radiographic correction during healing with a minimally invasive fixation technique and an injectable bone substitute. *Acta Orthop.* 2008;79(2):262-8.
231. Lozano-Calderon S, Moore M, Liebman M, Jupiter JB. Distal radius osteotomy in the elderly patient using angular stable implants and Norian bone cement. *J Hand Surg Am.* 2007;32(7):976-83.
232. Tyllianakis ME, Panagopoulos A, Giannikas D, Megias P, Lambiris E. Graft-supplemented, augmented external fixation in the treatment of intra-articular distal radial fractures. *Orthopedics.* 2006;29(2):139-44.
233. Goodman SB, Bauer TW, Carter D, Casteleyn PP, Goldstein SA, Kyle RF, *et al.* Norian SRS cement augmentation in hip fracture treatment. Laboratory and initial clinical results. *Clin Orthop Relat Res.* 1998(348):42-50.
234. Schildhauer TA, Bauer TW, Josten C, Muhr G. Open reduction and augmentation of internal fixation with an injectable skeletal cement for the treatment of complex calcaneal fractures. *J Orthop Trauma.* 2000;14(5):309-17.
235. Harrop JS, Przybylski GJ. Use of an osteoconductive agent (Norian) in anterior surgical management of odontoid fractures. Technical note. *Neurosurg Focus.* 2000;8(6):e8.
236. Petite H, Viateau V, Bensaid W, Meunier A, de Pollak C, Bourguignon M, *et al.* Tissue-engineered bone regeneration. *Nat Biotechnol.* 2000;18(9):959-63.

237. Damien CJ, Parsons JR. Bone graft and bone graft substitutes: a review of current technology and applications. *J Appl Biomater.* 1991;2(3):187-208.
238. Friedenstein AY. Induction of bone tissue by transitional epithelium. *Clin Orthop Relat Res.* 1968;59:21-37.
239. Yamasaki H, Sakai H. Osteogenic response to porous hydroxyapatite ceramics under the skin of dogs. *Biomaterials.* 1992;13(5):308-12.
240. Yang Z, Yuan H, Tong W, Zou P, Chen W, Zhang X. Osteogenesis in extraskelentially implanted porous calcium phosphate ceramics: variability among different kinds of animals. *Biomaterials.* 1996;17(22):2131-7.
241. Yang ZJ, Yuan H, Zou P, Tong W, Qu S, Zhang XD. Osteogenic responses to extraskelentially implanted synthetic porous calcium phosphate ceramics: an early stage histomorphological study in dogs. *J Mater Sci Mater Med.* 1997;8(11):697-701.
242. Barradas AM, Yuan H, van Blitterswijk CA, Habibovic P. Osteoinductive biomaterials: current knowledge of properties, experimental models and biological mechanisms. *Eur Cell Mater.* 2011;21:407-29; discussion 29.
243. Yuan H, Fernandes H, Habibovic P, de Boer J, Barradas AM, de Ruiter A, *et al.* Osteoinductive ceramics as a synthetic alternative to autologous bone grafting. *Proc Natl Acad Sci U S A.* 2010;107(31):13614-9.
244. Fellah BH, Delorme B, Sohier J, Magne D, Hardouin P, Layrolle P. Macrophage and osteoblast responses to biphasic calcium phosphate microparticles. *J Biomed Mater Res A.* 2010;93(4):1588-95.
245. Lin K, Yuan W, Wang L, Lu J, Chen L, Wang Z, *et al.* Evaluation of host inflammatory responses of beta-tricalcium phosphate bioceramics caused by calcium pyrophosphate impurity using a subcutaneous model. *J Biomed Mater Res B Appl Biomater.* 2011;99(2):350-8.
246. Morel O, Morel N, Jesel L, Freyssinet JM, Toti F. Microparticles: a critical component in the nexus between inflammation, immunity, and thrombosis. *Semin Immunopathol.* 2011;33(5):469-86.
247. Geuze RE, Everts PA, Kruyt MC, Verbout AJ, Alblas J, Dhert WJ. Orthotopic location has limited benefit from allogeneic or autologous multipotent stromal cells seeded on ceramic scaffolds. *Tissue Eng Part A.* 2009;15(11):3231-9.
248. Yuan H, Van Den Doel M, Li S, Van Blitterswijk CA, De Groot K, De Bruijn JD. A comparison of the osteoinductive potential of two calcium phosphate ceramics implanted intramuscularly in goats. *J Mater Sci Mater Med.* 2002;13(12):1271-5.
249. Habibovic P, Yuan H, van den Doel M, Sees TM, van Blitterswijk CA, de Groot K. Relevance of osteoinductive biomaterials in critical-sized orthotopic defect. *J Orthop Res.* 2006;24(5):867-76.
250. Habibovic P, Kruyt MC, Juhl MV, Clyens S, Martinetti R, Dolcini L, *et al.* Comparative in vivo study of six hydroxyapatite-based bone graft substitutes. *J Orthop Res.* 2008;26(10):1363-70.
251. Zoetis T, Tassinari MS, Bagi C, Walthall K, Hurtt ME. Species comparison of postnatal bone growth and development. *Birth Defects Res B Dev Reprod Toxicol.* 2003;68(2):86-110.
252. Van der Stok J, Wang H, Amin Yavari S, Siebelt M, Sandker M, Waarsing JH, *et al.* Enhanced Bone Regeneration of Cortical Segmental Bone Defects Using Porous Titanium Scaffolds Incorporated with Colloidal Gelatin Gels for Time- and Dose-Controlled Delivery of Dual Growth Factors. *Tissue Eng Part A.* 2013;19(23-24):2605-14.
253. Angle SR, Sena K, Sumner DR, Virkus WW, Virdi AS. Healing of rat femoral segmental defect with bone morphogenetic protein-2: a dose response study. *J Musculoskelet Neuronal Interact.* 2012;12(1):28-37.
254. Histing T, Garcia P, Holstein JH, Klein M, Matthys R, Nuetzi R, *et al.* Small animal bone healing models: standards, tips, and pitfalls results of a consensus meeting. *Bone.* 2011;49(4):591-9.
255. Claes L, Recknagel S, Ignatius A. Fracture healing under healthy and inflammatory conditions. *Nat Rev Rheumatol.* 2012;8(3):133-43.

256. Pneumaticos SG, Triantafyllopoulos GK, Basdra EK, Papavassiliou AG. Segmental bone defects: from cellular and molecular pathways to the development of novel biological treatments. *J Cell Mol Med.* 2010;14(11):2561-9.
257. Murr LE, Gaytan SM, Medina F, Lopez H, Martinez E, Machado BI, *et al.* Next-generation biomedical implants using additive manufacturing of complex, cellular and functional mesh arrays. *Philos Transact A Math Phys Eng Sci.* 2010;368(1917):1999-2032.
258. Fujibayashi S, Neo M, Kim HM, Kokubo T, Nakamura T. Osteoinduction of porous bioactive titanium metal. *Biomaterials.* 2004;25(3):443-50.
259. Singh R, Lee PD, Lindley TC, Kohlhauser C, Hellmich C, Bram M, *et al.* Characterization of the deformation behavior of intermediate porosity interconnected Ti foams using micro-computed tomography and direct finite element modeling. *Acta Biomater.* 2010;6(6):2342-51.
260. Dabrowski B, Swieszkowski W, Godlinski D, Kurzydowski KJ. Highly porous titanium scaffolds for orthopaedic applications. *J Biomed Mater Res B Appl Biomater.* 2010;95(1):53-61.
261. Vehof JW, Spauwen PH, Jansen JA. Bone formation in calcium-phosphate-coated titanium mesh. *Biomaterials.* 2000;21(19):2003-9.
262. Hollander DA, von Walter M, Wirtz T, Sellei R, Schmidt-Rohlfing B, Paar O, *et al.* Structural, mechanical and in vitro characterization of individually structured Ti-6Al-4V produced by direct laser forming. *Biomaterials.* 2006;27(7):955-63.
263. Spoerke ED, Murray NG, Li H, Brinson LC, Dunand DC, Stupp SI. Titanium with aligned, elongated pores for orthopedic tissue engineering applications. *J Biomed Mater Res A.* 2008;84(2):402-12.
264. Cory E, Nazarian A, Entezari V, Vartanians V, Muller R, Snyder BD. Compressive axial mechanical properties of rat bone as functions of bone volume fraction, apparent density and micro-ct based mineral density. *J Biomech.* 43(5):953-60.
265. Bandyopadhyay A, Krishna BV, Xue W, Bose S. Application of laser engineered net shaping (LENS) to manufacture porous and functionally graded structures for load bearing implants. *J Mater Sci Mater Med.* 2009;20 Suppl 1:S29-34.
266. Faria PE, Carvalho AL, Felipucci DN, Wen C, Sennerby L, Salata LA. Bone formation following implantation of titanium sponge rods into humeral osteotomies in dogs: a histological and histometrical study. *Clin Implant Dent Relat Res.* 2010;12(1):72-9.
267. Lopez-Heredia MA, Goyenvalle E, Aguado E, Pilet P, Leroux C, Dorget M, *et al.* Bone growth in rapid prototyped porous titanium implants. *J Biomed Mater Res A.* 2008;85(3):664-73.
268. Pattanayak DK, Fukuda A, Matsushita T, Takemoto M, Fujibayashi S, Sasaki K, *et al.* Bioactive Ti metal analogous to human cancellous bone: Fabrication by selective laser melting and chemical treatments. *Acta Biomater.* 2011;7(3):1398-406.
269. Willie BM, Yang X, Kelly NH, Merkow J, Gagne S, Ware R, *et al.* Osseointegration into a novel titanium foam implant in the distal femur of a rabbit. *J Biomed Mater Res B Appl Biomater.* 2011;92(2):479-88.
270. Heinel P, Muller L, Korner C, Singer RF, Muller FA. Cellular Ti-6Al-4V structures with interconnected macro porosity for bone implants fabricated by selective electron beam melting. *Acta Biomater.* 2008;4(5):1536-44.
271. Ryan G, McGarry P, Pandit A, Apatsidis D. Analysis of the mechanical behavior of a titanium scaffold with a repeating unit-cell substructure. *J Biomed Mater Res B Appl Biomater.* 2009;90(2):894-906.
272. Xue W, Krishna BV, Bandyopadhyay A, Bose S. Processing and biocompatibility evaluation of laser processed porous titanium. *Acta Biomater.* 2007;3(6):1007-18.

273. An YN. Mechanical properties of bone. In: An YN, Draughn RA, editors. Mechanical testing of bone and the bone-implant interface. New York: CRC Press; 1999. p. 41-63.
274. Biewener AA. Safety factors in bone strength. *Calcif Tissue Int.* 1993;53 Suppl 1:568-74.
275. Poelert S, Campoli G, Van der Stok J, Amin Yavari S, Weinans H, Zadpoor AA. Relating the microstructure of titanium foam to load distribution and induced bone ingrowth. *ESB2012; Lisbon2012.*
276. Takemoto M, Fujibayashi S, Neo M, Suzuki J, Matsushita T, Kokubo T, *et al.* Osteoinductive porous titanium implants: effect of sodium removal by dilute HCl treatment. *Biomaterials.* 2006;27(13):2682-91.
277. Wennerberg A, Albrektsson T. Effects of titanium surface topography on bone integration: a systematic review. *Clin Oral Implants Res.* 2009;20 Suppl 4:172-84.
278. Narayanan R, Seshadri SK, Kwon TY, Kim KH. Calcium phosphate-based coatings on titanium and its alloys. *J Biomed Mater Res B Appl Biomater.* 2008;85(1):279-99.
279. Zhao L, Wang H, Huo K, Cui L, Zhang W, Ni H, *et al.* Antibacterial nano-structured titania coating incorporated with silver nanoparticles. *Biomaterials.* 2011;32(24):5706-16.
280. Langer R, Vacanti JP. Tissue engineering. *Science.* 1993;260(5110):920-6.
281. Giannoudis PV, Chris Arts JJ, Schmidmaier G, Larsson S. What should be the characteristics of the ideal bone graft substitute? *Injury.* 2011;42 Suppl 2:S1-2.
282. Murr LE, Gaytan SM, Medina F, Lopez H, Martinez E, Machado BI, *et al.* Next-generation biomedical implants using additive manufacturing of complex, cellular and functional mesh arrays. *Philos Trans A Math Phys Eng Sci.* 2010;368(1917):1999-2032.
283. Andersson GB, Gaechter A, Galante JO, Rostoker W. Segmental replacement of long bones in baboons using a fiber titanium implant. *J Bone Joint Surg Am.* 1978;60(1):31-40.
284. Kosashvili Y, Backstein D, Safir O, Lakstein D, Gross AE. Acetabular revision using an anti-protrusion (ilio-ischial) cage and trabecular metal acetabular component for severe acetabular bone loss associated with pelvic discontinuity. *J Bone Joint Surg Br.* 2009;91(7):870-6.
285. Issack PS. Use of porous tantalum for acetabular reconstruction in revision hip arthroplasty. *J Bone Joint Surg Am.* 2013;95(21):1981-7.
286. Meneghini RM, Lewallen DG, Hanssen AD. Use of porous tantalum metaphyseal cones for severe tibial bone loss during revision total knee replacement. Surgical technique. *J Bone Joint Surg Am.* 2009;91 Suppl 2 Pt 1:131-8.
287. Kuttenger JJ, Hardt N. Long-term results following reconstruction. Traini T, Mangano C, Sammons RL, Mangano F, Macchi A, Piattelli A. Direct laser metal sintering as a new approach to fabrication of an isoelastic functionally graded material for manufacture of porous titanium dental implants. *Dent Mater.* 2008;24(11):1525-33.
289. Murr LE, Quinones SA, Gaytan SM, Lopez MI, Rodela A, Martinez EY, *et al.* Microstructure and mechanical behavior of Ti-6Al-4V produced by rapid-layer manufacturing, for biomedical applications. *J Mech Behav Biomed Mater.* 2009;2(1):20-32.
290. Amin Yavari S, Wauthle R, van der Stok J, Riemsag AC, Janssen M, Mulier M, *et al.* Fatigue behavior of porous biomaterials manufactured using selective laser melting. *Mater Sci Eng C Mater Biol Appl.* 2013;33(8):4849-58.
291. de Wild M, Schumacher R, Mayer K, Schkommodau E, Thoma D, Bredell M, *et al.* Bone regeneration by the osteoconductivity of porous titanium implants manufactured by selective laser melting: a histological and micro computed tomography study in the rabbit. *Tissue Eng Part A.* 2013;19(23-24):2645-54.
292. Amin Yavari S, van der Stok J, Chai YC, Wauthle R, Tahmasebi Birgani Z, Habibovic P, *et al.* Bone regeneration performance of surface-treated porous titanium. *Biomaterials.* 2014;35(24):6172-81.

293. Barbas A, Bonnet AS, Lipinski P, Pesci R, Dubois G. Development and mechanical characterization of porous titanium bone substitutes. *J Mech Behav Biomed Mater.* 2012;9:34-44.
294. Lozano D, Manzano M, Doadrio JC, Salinas AJ, Vallet-Regi M, Gomez-Barrena E, *et al.* Osteostatin-loaded bioceramics stimulate osteoblastic growth and differentiation. *Acta Biomater.* 2010;6(3):797-803.
295. Fenton AJ, Kemp BE, Hammonds RG, Jr., Mitchelhill K, Moseley JM, Martin TJ, *et al.* A potent inhibitor of osteoclastic bone resorption within a highly conserved pentapeptide region of parathyroid hormone-related protein; PTHrP[107-111]. *Endocrinology.* 1991;129(6):3424-6.
296. Wang M, VanHouten JN, Nasiri AR, Johnson RL, Broadus AE. PTHrP regulates the modeling of cortical bone surfaces at fibrous insertion sites during growth. *J Bone Miner Res.* 2013;28(3):598-607.
297. Lozano D, Feito MJ, Portal-Nunez S, Lozano RM, Matesanz MC, Serrano MC, *et al.* Osteostatin improves the osteogenic activity of fibroblast growth factor-2 immobilized in Si-doped hydroxyapatite in osteoblastic cells. *Acta Biomater.* 2012;8(7):2770-7.
298. Chai YC, Roberts SJ, Van Bael S, Chen Y, Luyten FP, Schrooten J. Multi-level factorial analysis of Ca²⁺/Pi supplementation as bio-instructive media for in vitro biomimetic engineering of three-dimensional osteogenic hybrids. *Tissue Eng Part C Methods.* 2012;18(2):90-103.
299. Unger S, Blauth M, Schmoelz W. Effects of three different preservation methods on the mechanical properties of human and bovine cortical bone. *Bone.* 2010;47(6):1048-53.
300. Amin Yavari S, Ahmadi SM, Van der Stok J, Wauthle R, Riemsdag AC, Janssen M, *et al.* Effects of bio-functionalizing surface treatments on the mechanical behavior of open porous titanium biomaterials. 2014; 36:109-19.
301. Wysolmerski JJ. Parathyroid hormone-related protein: an update. *J Clin Endocrinol Metab.* 2012;97(9):2947-56.
302. Valin A, Garcia-Ocana A, De Miguel F, Sarasa JL, Esbrit P. Antiproliferative effect of the C-terminal fragments of parathyroid hormone-related protein, PTHrP-(107-111) and (107-139), on osteoblastic osteosarcoma cells. *J Cell Physiol.* 1997;170(2):209-15.
303. Valin A, Guillen C, Esbrit P. C-terminal parathyroid hormone-related protein (PTHrP) (107-139) stimulates intracellular Ca(2+) through a receptor different from the type 1 PTH/PTHrP receptor in osteoblastic osteosarcoma UMR 106 cells. *Endocrinology.* 2001;142(7):2752-9.
304. Takemoto M, Fujibayashi S, Neo M, Suzuki J, Kokubo T, Nakamura T. Mechanical properties and osteoconductivity of porous bioactive titanium. *Biomaterials.* 2005;26(30):6014-23.
305. Stewart AF, Cain RL, Burr DB, Jacob D, Turner CH, Hock JM. Six-month daily administration of parathyroid hormone and parathyroid hormone-related protein peptides to adult ovariectomized rats markedly enhances bone mass and biomechanical properties: a comparison of human parathyroid hormone 1-34, parathyroid hormone-related protein 1-36, and SDZ-parathyroid hormone 893. *J Bone Miner Res.* 2000;15(8):1517-25.
306. Daugaard H, Elmengaard B, Andreassen TT, Lamberg A, Bechtold JE, Soballe K. Systemic intermittent parathyroid hormone treatment improves osseointegration of press-fit inserted implants in cancellous bone. *Acta Orthop.* 2012;83(4):411-9.
307. Andreassen TT, Ejersted C, Oxlund H. Intermittent parathyroid hormone (1-34) treatment increases callus formation and mechanical strength of healing rat fractures. *J Bone Miner Res.* 1999;14(6):960-8.
308. Seebach C, Skripitz R, Andreassen TT, Aspenberg P. Intermittent parathyroid hormone (1-34) enhances mechanical strength and density of new bone after distraction osteogenesis in rats. *J Orthop Res.* 2004;22(3):472-8.
309. Skripitz R, Aspenberg P. Early effect of parathyroid hormone (1-34) on implant fixation. *Clin Orthop Relat Res.* 2001(392):427-32.
310. Jilka RL. Molecular and cellular mechanisms of the anabolic effect of intermittent PTH. *Bone.* 2007;40(6):1434-46.

311. de Gortazar AR, Alonso V, Alvarez-Arroyo MV, Esbrit P. Transient exposure to PTHrP (107-139) exerts anabolic effects through vascular endothelial growth factor receptor 2 in human osteoblastic cells in vitro. *Calcif Tissue Int.* 2006;79(5):360-9.
312. Hu Y, Cai K, Luo Z, Xu D, Xie D, Huang Y, *et al.* TiO₂ nanotubes as drug nanoreservoirs for the regulation of mobility and differentiation of mesenchymal stem cells. *Acta Biomater.* 2012;8(1):439-48.
313. Edwards JR, Mundy GR. Advances in osteoclast biology: old findings and new insights from mouse models. *Nat Rev Rheumatol.* 2011;7(4):235-43.
314. Baril E, Lefebvre LP, Hacking SA. Direct visualization and quantification of bone growth into porous titanium implants using micro computed tomography. *J Mater Sci Mater Med.* 2011;22(5):1321-32.
315. Garcia-Martin A, Acitores A, Maycas M, Villanueva-Penacarrillo ML, Esbrit P. Src kinases mediate VEGFR2 transactivation by the osteostatin domain of PTHrP to modulate osteoblastic function. *J Cell Biochem.* 2013;114(6):1404-13.
316. Amin Yavari S, van der Stok J, Ahmadi SM, Wauthle R, Schrooten J, Weinans H, *et al.* Mechanical analysis of a rodent segmental bone defect model: The effects of internal fixation and implant stiffness on load transfer. *J Biomech.* 2014;47(11):2700-8.
317. Bandyopadhyay A, Espana F, Balla VK, Bose S, Ohgami Y, Davies NM. Influence of porosity on mechanical properties and in vivo response of Ti6Al4V implants. *Acta Biomater.* 2010;6(4):1640-8.
318. Parthasarathy J, Starly B, Raman S, Christensen A. Mechanical evaluation of porous titanium (Ti6Al4V) structures with electron beam melting (EBM). *J Mech Behav Biomed Mater.* 2010;3(3):249-59.
319. Van der Stok J, Van der Jagt OP, Amin Yavari S, De Haas MF, Waarsing JH, Jahr H, *et al.* Selective laser melting-produced porous titanium scaffolds regenerate bone in critical size cortical bone defects. *J Orthop Res.* 2013;31(5):792-9.
320. Alvarez K, Nakajima H. Metallic scaffolds for bone regeneration. *Materials.* 2009;2:790-832.
321. Van der Stok J, Van Lieshout EMM, El-Massoudi Y, Van Kralingen GH, Patka P. Bone substitutes in the Netherlands - a systematic literature review. *Acta Biomater.* 2011;7(2):739-50.
322. Schmid GJ, Kobayashi C, Sandell LJ, Ornitz DM. Fibroblast growth factor expression during skeletal fracture healing in mice. *Dev Dyn.* 2009;238(3):766-74.
323. Carano RAD, Filvaroff EH. Angiogenesis and bone repair. *Drug Discov Today.* 2003;8(21):980-9.
324. Gerstenfeld LC, Einhorn TA. Developmental aspects of fracture healing and the use of pharmacological agents to alter healing. *J Musculoskelet Neuronal Interact.* 2003;3(4):297-303.
325. Chen FM, Zhang M, Wu ZF. Toward delivery of multiple growth factors in tissue engineering. *Biomaterials.* 2010;31(24):6279-308.
326. Carragee EJ, Hurwitz EL, Weiner BK. A critical review of recombinant human bone morphogenetic protein-2 trials in spinal surgery: emerging safety concerns and lessons learned. *Spine J.* 2011;11(6):471-91.
327. Bradley M, Lazim AM, Eastoe J. Stimulus-Responsive Heteroaggregation of Colloidal Dispersions: Reversible Systems and Composite Materials. *Polymers.* 2011;3(3):1036-50.
328. Wang H, Leeuwenburgh SCG, Li Y, Jansen JA. The Use of Micro- and Nanospheres as Functional Components for Bone Tissue Regeneration. *Tissue Eng Part B Rev.* 2012;18(1):24-39.
329. Fujimura K, Bessho K, Okubo Y, Kusumoto K, Segami N, Iizuka T. The effect of fibroblast growth factor-2 on the osteoinductive activity of recombinant human bone morphogenetic protein-2 in rat muscle. *Arch Oral Biol.* 2002;47(8):577-84.

330. Springer ING, Niehoff P, Açil Y, Marget M, Lange A, Warnke PH, *et al.* BMP-2 and bFGF in an irradiated bone model. *J Craniomaxillofacial Surg.* 2008;36(4):210-7.
331. Wang H, Hansen MB, Lowik DW, van Hest JC, Li Y, Jansen JA, *et al.* Oppositely charged gelatin nanospheres as building blocks for injectable and biodegradable gels. *Adv Mater.* 2011;23(12):H119-24.
332. Marsell R, Einhorn TA. The biology of fracture healing. *Injury.* 2011;42(6):551-5.
333. Zara JN, Siu RK, Zhang X, Shen J, Ngo R, Lee M, *et al.* High doses of bone morphogenetic protein 2 induce structurally abnormal bone and inflammation in vivo. *Tissue Eng Part A.* 2011;17(9-10):1389-99.
334. Zellin G, Linde A. Effects of recombinant human fibroblast growth factor-2 on osteogenic cell populations during orthopic osteogenesis in vivo. *Bone.* 2000;26(2):161-8.
335. Guillame-Gentil O, Semenov O, Roca AS, Groth T, Zahn R, Vörös J, *et al.* Engineering the Extracellular Environment: Strategies for Building 2D and 3D Cellular Structures. *Adv Mater.* 2010;22(48):5443-62.
336. Luong LN, Ramaswamy J, Kohn DH. Effects of osteogenic growth factors on bone marrow stromal cell differentiation in a mineral-based delivery system. *Biomaterials.* 2012;33(1):283-94.
337. Tabata Y, Ikada Y. Vascularization effect of basic fibroblast growth factor released from gelatin hydrogels with different biodegradabilities. *Biomaterials.* 1999;20(22):2169-75.
338. Mayahara H, Ito T, Nagai H, Miyajima H, Tsukuda R, Taketomi S, *et al.* In vivo stimulation of endosteal bone formation by basic fibroblast growth factor in rats. *Growth Factors.* 1993;9(1):73-80.
339. Nakamura Y, Tensho K, Nakaya H, Nawata M, Okabe T, Wakitani S. Low dose fibroblast growth factor-2 (FGF-2) enhances bone morphogenetic protein-2 (BMP-2)-induced ectopic bone formation in mice. *Bone.* 2005;36(3):399-407.
340. Takita H, Tsuruga E, Ono I, Kuboki Y. Enhancement by bFGF of osteogenesis induced by rhBMP-2 in rats. *Eur J Oral Sci.* 1997;105(6):588-92.
341. Maegawa N, Kawamura K, Hirose M, Yajima H, Takakura Y, Ohgushi H. Enhancement of osteoblastic differentiation of mesenchymal stromal cells cultured by selective combination of bone morphogenetic protein-2 (BMP-2) and fibroblast growth factor-2 (FGF-2). *J Tissue Eng Regen Med.* 2007;1(4):306-13.
342. Tanaka E, Ishino Y, Sasaki A, Hasegawa T, Watanabe M, Dalla-Bona D, *et al.* Fibroblast Growth Factor-2 Augments Recombinant Human Bone Morphogenetic Protein-2-Induced Osteoinductive Activity. *Ann Biomed Eng.* 2006;34(5):717-25.
343. Murakami N, Saito N, Horiuchi H, Okada T, Nozaki K, Takaoka K. Repair of segmental defects in rabbit humeri with titanium fiber mesh cylinders containing recombinant human bone morphogenetic protein-2 (rhBMP-2) and a synthetic polymer. *J Biomed Mater Res.* 2002;62(2):169-74.
344. Senta H, Park H, Bergeron E, Drevelle O, Fong D, Leblanc E, *et al.* Cell responses to bone morphogenetic proteins and peptides derived from them: biomedical applications and limitations. *Cytokine Growth Factor Rev.* 2009;20(3):213-22.
345. Khan SN, Lane JM. The use of recombinant human bone morphogenetic protein-2 (rhBMP-2) in orthopaedic applications. *Expert Opin Biol Ther.* 2004;4(5):741-8.
346. Woo EJ. Adverse events after recombinant human BMP2 in nonspinal orthopaedic procedures. *Clin Orthop Relat Res.* 2013;471(5):1707-11.
347. Carragee EJ, Hurwitz EL, Weiner BK. A critical review of recombinant human bone morphogenetic protein-2 trials in spinal surgery: emerging safety concerns and lessons learned. *Spine J.* 2014;11(6):471-91.
348. Cho TJ, Gerstenfeld LC, Einhorn TA. Differential temporal expression of members of the transforming growth factor beta superfamily during murine fracture healing. *J Bone Miner Res.* 2002;17(3):513-20.

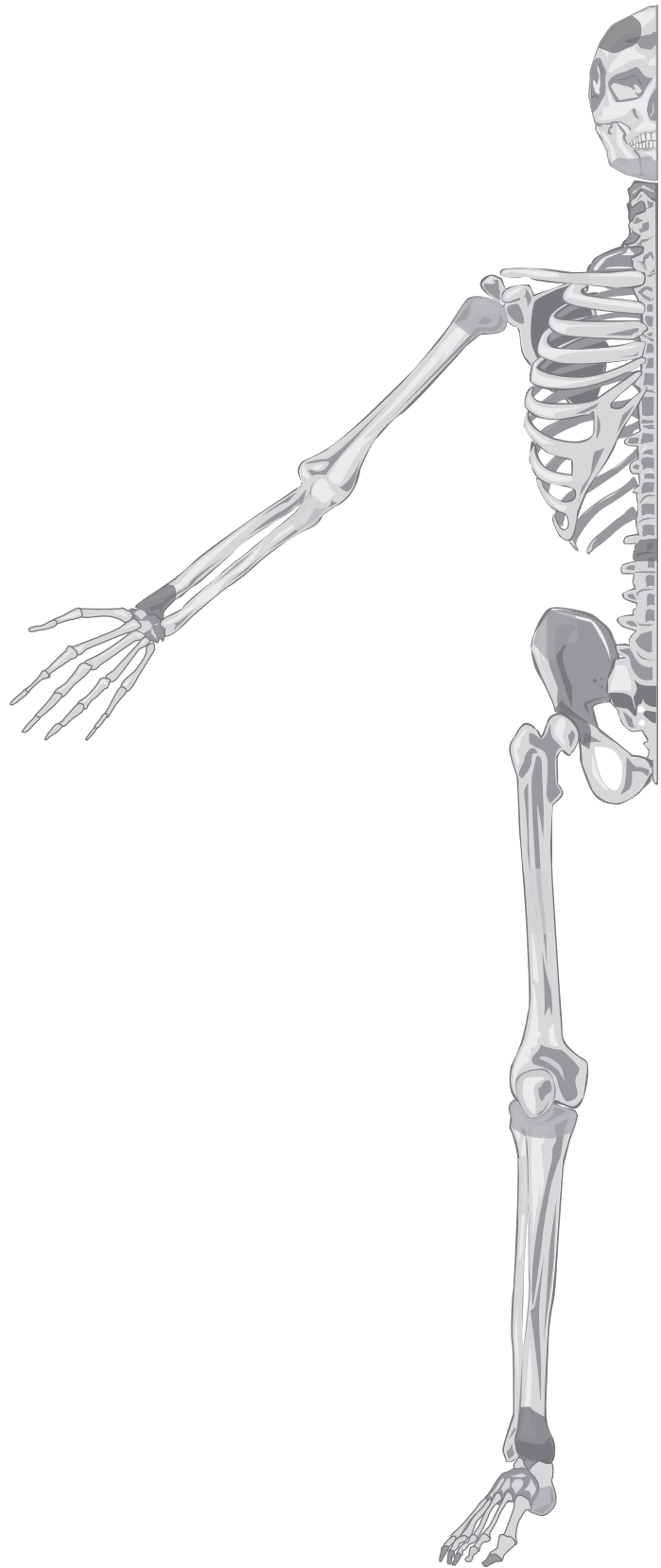
349. Martino MM, Briquez PS, Ranga A, Lutolf MP, Hubbell JA. Heparin-binding domain of fibrin(ogen) binds growth factors and promotes tissue repair when incorporated within a synthetic matrix. *Proc Natl Acad Sci U S A*. 2013;110(12):4563-8.
350. Kaijzel EL, Koolwijk P, van Erck MG, van Hinsbergh VW, de Maat MP. Molecular weight fibrinogen variants determine angiogenesis rate in a fibrin matrix in vitro and in vivo. *J Thromb Haemost*. 2006;4(9):1975-81.
351. Janmey PA, Winer JP, Weisel JW. Fibrin gels and their clinical and bioengineering applications. *J R Soc Interface*. 2009;6(30):1-10.
352. Milleret V, Tugulu S, Schlottig F, Hall H. Alkali treatment of microrough titanium surfaces affects macrophage/monocyte adhesion, platelet activation and architecture of blood clot formation. *Eur Cell Mater*. 2011;21:430-44; discussion 44.
353. Holm B, Nilsen DW, Kierulf P, Godal HC. Purification and characterization of 3 fibrinogens with different molecular weights obtained from normal human plasma. *Thromb Res*. 1985;37(1):165-76.
354. Learmonth ID, Young C, Rorabeck C. The operation of the century: total hip replacement. *Lancet*. 2007;370(9597):1508-19.
355. Niinomi M. Mechanical biocompatibilities of titanium alloys for biomedical applications. *J Mech Behav Biomed Mater*. 2008;1(1):30-42.
356. Murr LE, Amato KN, Li SJ, Tian YX, Cheng XY, Gaytan SM, *et al*. Microstructure and mechanical properties of open-cellular biomaterials prototypes for total knee replacement implants fabricated by electron beam melting. *J Mech Behav Biomed Mater*. 2011;4(7):1396-411.
357. Mullen L, Stamp RC, Brooks WK, Jones E, Sutcliffe CJ. Selective Laser Melting: a regular unit cell approach for the manufacture of porous, titanium, bone in-growth constructs, suitable for orthopedic applications. *J Biomed Mater Res B Appl Biomater*. 2009;89(2):325-34.
358. Stamp R, Fox P, O'Neill W, Jones E, Sutcliffe C. The development of a scanning strategy for the manufacture of porous biomaterials by selective laser melting. *J Mater Sci Mater Med*. 2009;20(9):1839-48.
359. Ponader S, von Wilmsowsky C, Widenmayer M, Lutz R, Heini P, Korner C, *et al*. In vivo performance of selective electron beam-melted Ti-6Al-4V structures. *J Biomed Mater Res A*. 2010;92(1):56-62.
360. Hrabe NW, Heini P, Flinn B, Korner C, Bordia RK. Compression-compression fatigue of selective electron beam melted cellular titanium (Ti-6Al-4V). *J Biomed Mater Res B Appl Biomater*. 2011;99(2):313-20.
361. Puleo DA, Nanci A. Understanding and controlling the bone-implant interface. *Biomaterials*. 1999;20(23-24):2311-21.
362. Groeneveld EH, Burger EH. Bone morphogenetic proteins in human bone regeneration. *Eur J Endocrinol*. 2000;142(1):9-21.
363. Carragee EJ, Hurwitz EL, Weiner BK. A critical review of recombinant human bone morphogenetic protein-2 trials in spinal surgery: emerging safety concerns and lessons learned. *Spine J*. 2011;11(6):471-91.
364. An YH, Friedman RJ. *Animal models in orthopaedic research*. New York: CRC Press; 1999.
365. Diefenderfer DL, Osyczka AM, Garino JP, Leboy PS. Regulation of BMP-induced transcription in cultured human bone marrow stromal cells. *J Bone Joint Surg Am*. 2003;85-A Suppl 3:19-28.
366. Boerckel JD, Kolambkar YM, Dupont KM, Uhrig BA, Phelps EA, Stevens HY, *et al*. Effects of protein dose and delivery system on BMP-mediated bone regeneration. *Biomaterials*. 2011;32(22):5241-51.
367. Wei G, Jin Q, Giannobile WV, Ma PX. The enhancement of osteogenesis by nano-fibrous scaffolds incorporating rhBMP-7 nanospheres. *Biomaterials*. 2007;28(12):2087-96.

368. Bessa PC, Balmayor ER, Hartinger J, Zanoni G, Dopler D, Meinel A, *et al.* Silk fibroin microparticles as carriers for delivery of human recombinant bone morphogenetic protein-2: in vitro and in vivo bioactivity. *Tissue Eng Part C Methods*. 2010;16(5):937-45.
369. Schmoekel H, Schense JC, Weber FE, Gratz KW, Gnagi D, Muller R, *et al.* Bone healing in the rat and dog with nonglycosylated BMP-2 demonstrating low solubility in fibrin matrices. *J Orthop Res*. 2004;22(2):376-81.
370. Chung YI, Ahn KM, Jeon SH, Lee SY, Lee JH, Tae G. Enhanced bone regeneration with BMP-2 loaded functional nanoparticle-hydrogel complex. *J Control Release*. 2007;121(1-2):91-9.
371. Kaipel M, Schutzenberger S, Schultz A, Ferguson J, Slezak P, Morton TJ, *et al.* BMP-2 but not VEGF or PDGF in fibrin matrix supports bone healing in a delayed-union rat model. *J Orthop Res*. 2012;30(10):1563-9.
372. Kim SS, Gwak SJ, Kim BS. Orthotopic bone formation by implantation of apatite-coated poly(lactide-co-glycolide)/hydroxyapatite composite particulates and bone morphogenetic protein-2. *J Biomed Mater Res A*. 2008;87(1):245-53.
373. Koo KH, Lee JM, Ahn JM, Kim BS, La WG, Kim CS, *et al.* Controlled delivery of low-dose bone morphogenetic protein-2 using heparin-conjugated fibrin in the posterolateral lumbar fusion of rabbits. *Artif Organs*. 2013;37(5):487-94.
374. Koo KH, Yeo do H, Ahn JM, Kim BS, Kim CS, Im GI. Lumbar posterolateral fusion using heparin-conjugated fibrin for sustained delivery of bone morphogenetic protein-2 in a rabbit model. *Artif Organs*. 2012;36(7):629-34.
375. La WG, Kwon SH, Lee TJ, Yang HS, Park J, Kim BS. The effect of the delivery carrier on the quality of bone formed via bone morphogenetic protein-2. *Artif Organs*. 2012;36(7):642-7.
376. Schmoekel HG, Weber FE, Seiler G, von Rechenberg B, Schense JC, Schawalder P, *et al.* Treatment of nonunions with nonglycosylated recombinant human bone morphogenetic protein-2 delivered from a fibrin matrix. *Vet Surg*. 2004;33(2):112-8.
377. Schutzenberger S, Schultz A, Hausner T, Hopf R, Zanoni G, Morton T, *et al.* The optimal carrier for BMP-2: a comparison of collagen versus fibrin matrix. *Arch Orthop Trauma Surg*. 2012;132(9):1363-70.
378. Yang HS, La WG, Bhang SH, Jeon JY, Lee JH, Kim BS. Heparin-conjugated fibrin as an injectable system for sustained delivery of bone morphogenetic protein-2. *Tissue Eng Part A*. 2010;16(4):1225-33.
379. Yang HS, La WG, Cho YM, Shin W, Yeo GD, Kim BS. Comparison between heparin-conjugated fibrin and collagen sponge as bone morphogenetic protein-2 carriers for bone regeneration. *Exp Mol Med*. 2012;44(5):350-5.
380. Schutzenberger S, Schultz A, Hausner T, Hopf R, Zanoni G, Morton T, *et al.* The optimal carrier for BMP-2: a comparison of collagen versus fibrin matrix. *Arch Orthop Trauma Surg*. 2013;132(9):1363-70.
381. Nürnberger S, Wolbank S, Peterbauer-Scherb A, Morton TJ, Feichtinger GA, Gugerell A, *et al.* Properties and potential alternative applications in fibrin glue. Von Byern J, I. G, editors. Wien: Springer; 2010.
382. Peterbauer-Scherb A, Danzer M, Gabriel C, van Griensven M, Redl H, Wolbank S. In vitro adipogenesis of adipose-derived stem cells in 3D fibrin matrix of low component concentration. *J Tissue Eng Regen Med*. 2012;6(6):434-42.
383. Weisel JW. The mechanical properties of fibrin for basic scientists and clinicians. *Biophys Chem*. 2004;112(2-3):267-76.
384. Seebach E, Freischmidt H, Holschbach J, Fellenberg J, Richter W. Mesenchymal stroma cells trigger early attraction of M1 macrophages and endothelial cells into fibrin hydrogels, stimulating long bone healing without long-term engraftment. *Acta Biomater*. 2014;10(11):4730-41.
385. Onishi T, Ishidou Y, Nagamine T, Yone K, Imamura T, Kato M, *et al.* Distinct and overlapping patterns of localization of bone morphogenetic protein (BMP) family members and a BMP type II receptor during fracture healing in rats. *Bone*. 1998;22(6):605-12.

386. Kirker-Head CA. Recombinant bone morphogenetic proteins: novel substances for enhancing bone healing. *Vet Surg.* 1995;24(5):408-19.
387. Shapiro F. Bone development and its relation to fracture repair. The role of mesenchymal osteoblasts and surface osteoblasts. *Eur Cell Mater.* 2008;15:53-76.
388. Quarto R, Mastrogiacomo M, Cancedda R, Kutepov SM, Mukhachev V, Lavroukov A, *et al.* Repair of large bone defects with the use of autologous bone marrow stromal cells. *N Engl J Med.* 2001;344(5):385-6.
389. Steinert AF, Rackwitz L, Gilbert F, Noth U, Tuan RS. Concise review: the clinical application of mesenchymal stem cells for musculoskeletal regeneration: current status and perspectives. *Stem Cells Transl Med.* 2012;1(3):237-47.
390. Gawlitta D, Farrell E, Malda J, Creemers LB, Alblas J, Dhert WJ. Modulating endochondral ossification of multipotent stromal cells for bone regeneration. *Tissue Eng Part B Rev.* 2010;16(4):385-95.
391. Jukes JM, Both SK, Leusink A, Sterk LM, van Blitterswijk CA, de Boer J. Endochondral bone tissue engineering using embryonic stem cells. *Proc Natl Acad Sci U S A.* 2008;105(19):6840-5.
392. Oliveira SM, Amaral IF, Barbosa MA, Teixeira CC. Engineering endochondral bone: in vitro studies. *Tissue Eng Part A.* 2009;15(3):625-34.
393. Farrell E, van der Jagt OP, Koevoet W, Kops N, van Manen CJ, Hellingman CA, *et al.* Chondrogenic priming of human bone marrow stromal cells: a better route to bone repair? *Tissue Eng Part C Methods.* 2009;15(2):285-95.
394. Farrell E, Both SK, Odorfer KI, Koevoet W, Kops N, O'Brien FJ, *et al.* In-vivo generation of bone via endochondral ossification by in-vitro chondrogenic priming of adult human and rat mesenchymal stem cells. *BMC Musculoskelet Disord.* 2011;12:31.
395. Scotti C, Tonnarelli B, Papadimitropoulos A, Scherberich A, Schaeren S, Schauerer A, *et al.* Recapitulation of endochondral bone formation using human adult mesenchymal stem cells as a paradigm for developmental engineering. *Proc Natl Acad Sci U S A.* 2010;107(16):7251-6.
396. Oliveira SM, Mijares DQ, Turner G, Amaral IF, Barbosa MA, Teixeira CC. Engineering endochondral bone: in vivo studies. *Tissue Eng Part A.* 2009;15(3):635-43.
397. Brighton CT, Krebs AG. Oxygen tension of healing fractures in the rabbit. *J Bone Joint Surg Am.* 1972;54(2):323-32.
398. Lacroix D, Prendergast PJ. A mechano-regulation model for tissue differentiation during fracture healing: analysis of gap size and loading. *J Biomech.* 2002;35(9):1163-71.
399. Hierck BP, Iperen LV, Gittenberger-De Groot AC, Poelmann RE. Modified indirect immunodetection allows study of murine tissue with mouse monoclonal antibodies. *J Histochem Cytochem.* 1994;42(11):1499-502.
400. Chatterjea A, van der Stok J, Danoux CB, Yuan H, Habibovic P, van Blitterswijk CA, *et al.* Inflammatory response and bone healing capacity of two porous calcium phosphate ceramics in critical size cortical bone defects. *J Biomed Mater Res A.* 2014;102(5):1399-407.
401. Huey DJ, Hu JC, Athanasiou KA. Unlike bone, cartilage regeneration remains elusive. *Science.* 2012;338(6109):917-21.
402. Garcia P, Histing T, Holstein JH, Klein M, Laschke MW, Matthys R, *et al.* Rodent animal models of delayed bone healing and non-union formation: a comprehensive review. *Eur Cell Mater.* 2013;26:1-14.
403. Naimark A, Miller K, Segal D, Kossoff J. Nonunion. *Skeletal Radiol.* 1981;6(1):21-5.
404. Megaw P. Classification of non-union. *Injury.* 2005;36 Suppl 4:S30-7.

405. Farrell E, O'Brien FJ, Doyle P, Fischer J, Yannas I, Harley BA, *et al.* A collagen-glycosaminoglycan scaffold supports adult rat mesenchymal stem cell differentiation along osteogenic and chondrogenic routes. *Tissue Eng.* 2006;12(3):459-68.
406. Scotti C, Piccinini E, Takizawa H, Todorov A, Bourguine P, Papadimitropoulos A, *et al.* Engineering of a functional bone organ through endochondral ossification. *Proc Natl Acad Sci U S A.* 2013;110(10):3997-4002.
407. Sakaguchi Y, Sekiya I, Yagishita K, Muneta T. Comparison of human stem cells derived from various mesenchymal tissues: superiority of synovium as a cell source. *Arthritis Rheum.* 2005;52(8):2521-9.
408. Winter A, Breit S, Parsch D, Benz K, Steck E, Hauner H, *et al.* Cartilage-like gene expression in differentiated human stem cell spheroids: a comparison of bone marrow-derived and adipose tissue-derived stromal cells. *Arthritis Rheum.* 2003;48(2):418-29.
409. Hernigou P, Poignard A, Beaujean F, Rouard H. Percutaneous autologous bone-marrow grafting for nonunions. Influence of the number and concentration of progenitor cells. *J Bone Joint Surg Am.* 2005;87(7):1430-7.
410. Gharibi B, Hughes FJ. Effects of medium supplements on proliferation, differentiation potential, and in vitro expansion of mesenchymal stem cells. *Stem Cells Transl Med.* 2012;1(11):771-82.
411. Van der Stok J, Weinans H, Kops N, Siebelt M, Patka P, Van Lieshout EMM. Properties of commonly used calcium phosphate cements in trauma and orthopaedic surgery. *Injury.* 2013;44(10):1368-74.
412. Patil AS, Sable RB, Kothari RM. Occurrence, biochemical profile of vascular endothelial growth factor (VEGF) isoforms and their functions in endochondral ossification. *J Cell Physiol.* 2012;227(4):1298-308.
413. Bahney CS, Hu DP, Taylor AJ, Ferro F, Britz HM, Hallgrímsson B, *et al.* Stem Cell Derived Endochondral Cartilage Stimulates Bone Healing by Tissue Transformation. *J Bone Miner Res.* 2014;29(5):1269-82..
414. De Long WG, Jr., Einhorn TA, Koval K, McKee M, Smith W, Sanders R, *et al.* Bone grafts and bone graft substitutes in orthopaedic trauma surgery. A critical analysis. *J Bone Joint Surg Am.* 2007;89(3):649-58.
415. Albee FH. Transplantation of a portion of the tibia into the spine for Pott's disease: a preliminary report 1911. *Clin Orthop Relat Res.* 2007;460:14-6.
416. Schmitz JP, Hollinger JO. The critical size defect as an experimental model for craniomandibulofacial non-unions. *Clin Orthop Relat Res.* 1986(205):299-308.
417. Pearce AI, Richards RG, Milz S, Schneider E, Pearce SG. Animal models for implant biomaterial research in bone: a review. *Eur Cell Mater.* 2007;13:1-10.
418. Amin Yavari S, Van der Stok J, Ahmadi SM, Wauthle R, Schrooten J, Weinans H, *et al.* Mechanical analysis of a rodent segmental bone defect model: the effect of internal fixation and implant stiffness on load transfer. *J Biomech.* 2014;47(11):2700-8.
419. Waarsing JH, Day JS, Weinans H. Longitudinal micro-CT scans to evaluate bone architecture. *J Musculoskeletal Neuronal Interact.* 2005;5(4):310-2.
420. Kerckhofs G, Schrooten J, Van Cleynenbreugel T, Lomov SV, Wevers M. Validation of x-ray microfocus computed tomography as an imaging tool for porous structures. *Rev Sci Instrum.* 2008;79(1):013711.
421. Zhang ZY, Teoh SH, Chong MS, Lee ES, Tan LG, Mattar CN, *et al.* Neo-vascularization and bone formation mediated by fetal mesenchymal stem cell tissue-engineered bone grafts in critical-size femoral defects. *Biomaterials.* 2010;31(4):608-20.
422. Nebuloni L, Kuhn GA, Vogel J, Muller R. A novel in vivo vascular imaging approach for hierarchical quantification of vasculature using contrast enhanced micro-computed tomography. *PLoS One.* 2014;9(1):e86562.
423. Gawlitza D, van Rijen MH, Schrijver EJ, Alblas J, Dhert WJ. Hypoxia impedes hypertrophic chondrogenesis of human multipotent stromal cells. *Tissue Eng Part A.* 2012;18(19-20):1957-66.

424. El-Assal MA, Khalifa YE, Abdel-Hamid MM, Said HG, Bakr HM. Opening-wedge high tibial osteotomy without bone graft. *Knee Surg Sports Traumatol Arthrosc.* 2010;18(7):961-6.
425. Zorzi AR, da Silva HG, Muszkat C, Marques LC, Cliquet A, Jr., de Miranda JB. Opening-wedge high tibial osteotomy with and without bone graft. *Artif Organs.* 2011;35(3):301-7.
426. Lerner T, Bullmann V, Schulte TL, Schneider M, Liljenqvist U. A level-1 pilot study to evaluate of ultraporous beta-tricalcium phosphate as a graft extender in the posterior correction of adolescent idiopathic scoliosis. *Eur Spine J.* 2009;18(2):170-9.
427. Van Lieshout EMM, Van Kralingen GH, El-Massoudi Y, Weinans H, Patka P. Microstructure and biomechanical characteristics of bone substitutes for trauma and orthopaedic surgery. *BMC Musculoskelet Disord.* 2011;12:34.
428. Goff T, Kanakaris NK, Giannoudis PV. Use of bone graft substitutes in the management of tibial plateau fractures. *Injury.* 2013;44 Suppl 1:S86-94.
429. Bae H, Hatten HP, Jr., Linovitz R, Tahernia AD, Schaufele MK, McCollom V, *et al.* A prospective randomized FDA-IDE trial comparing Cortoss with PMMA for vertebroplasty: a comparative effectiveness research study with 24-month follow-up. *Spine (Phila Pa 1976).* 2012;37(7):544-50.
430. Junker R, Dimakis A, Thoneick M, Jansen JA. Effects of implant surface coatings and composition on bone integration: a systematic review. *Clin Oral Implants Res.* 2009;20 Suppl 4:185-206.
431. Fukuda A, Takemoto M, Saito T, Fujibayashi S, Neo M, Pattanayak DK, *et al.* Osteoinduction of porous Ti implants with a channel structure fabricated by selective laser melting. *Acta Biomater.* 2011;7(5):2327-36.
432. Chai YC, Kerckhofs G, Roberts SJ, Van Bael S, Schepers E, Vleugels J, *et al.* Ectopic bone formation by 3D porous calcium phosphate-Ti6Al4V hybrids produced by perfusion electrodeposition. *Biomaterials.* 2012;33(16):4044-58.
433. Biemond JE, Eufrazio TS, Hannink G, Verdonschot N, Buma P. Assessment of bone ingrowth potential of biomimetic hydroxyapatite and brushite coated porous E-beam structures. *J Mater Sci Mater Med.* 2011;22(4):917-25.
434. Palmquist A, Snis A, Emanuelsson L, Browne M, Thomsen P. Long-term biocompatibility and osseointegration of electron beam melted, free-form-fabricated solid and porous titanium alloy: experimental studies in sheep. *J Biomater Appl.* 2013;27(8):1003-16.
435. Li X, Feng YF, Wang CT, Li GC, Lei W, Zhang ZY, *et al.* Evaluation of biological properties of electron beam melted Ti6Al4V implant with biomimetic coating in vitro and in vivo. *PLoS One.* 2012;7(12):e52049.
436. Li XK, Yuan CF, Wang JL, Zhang YQ, Zhang ZY, Guo Z. The treatment effect of porous titanium alloy rod on the early stage talar osteonecrosis of sheep. *PLoS One.* 2013;8(3):e58459.
437. Pijls BG, Nieuwenhuijse MJ, Fiocco M, Plevier JW, Middeldorp S, Nelissen RG, *et al.* Early proximal migration of cups is associated with late revision in THA: a systematic review and meta-analysis of 26 RSA studies and 49 survival studies. *Acta Orthop.* 2012;83(6):583-91.
438. Pijls BG, Valstar ER, Nouta KA, Plevier JW, Fiocco M, Middeldorp S, *et al.* Early migration of tibial components is associated with late revision: a systematic review and meta-analysis of 21,000 knee arthroplasties. *Acta Orthop.* 2012;83(6):614-24.
439. Dimarino AM, Caplan AI, Bonfield TL. Mesenchymal Stem Cells in Tissue Repair. *Front Immunol.* 2013;4:201.
440. Nishitani K, Schwarz EM. Regenerative medicine: Cartilage transplants hold promise for challenging bone defects. *Nat Rev Rheumatol.* 2014;10(3):129-30.
441. Bourgine PE, Scotti C, Pigeot S, Tchang LA, Todorov A, Martin I. Osteoinductivity of engineered cartilaginous templates devitalized by inducible apoptosis. *Proc Natl Acad Sci U S A.* 2014;111(49):17426-31.



PhD Portfolio

PhD Portfolio

Name PhD student: Johan van der Stok
 Erasmus MC Department:
 Orthopaedics and Surgery
 Research School: Molecular Medicine

PhD period: Oct 2009 – Dec 2013
 Promotors:
 Prof.dr.ir. H. Weinans,
 Prof.dr. P. Patka
 Prof.dr. J.A.N. Verhaar
 Copromotor:
 Dr. E.M.M. van Lieshout

1. PhD training

	Year	Workload (ECTS)
General courses		
- Laboratory animal science	2009	3,0
- Biomedical English writing and presentation	2010	4,0
Specific courses (e.g. Research school, Medical Training)		
- Regenerative medicine module 1	2010	1,5
- Regenerative medicine module 5	2011	2,0
- AMIE Imaging course	2011	1,4
- COST NAMIBO training school	2012	1,4
Seminars and workshops		
- Seminar Zuid-West Nederland overleg trauma (ZWOT)	2010-2014	0,4
- Workshop Basic introduction on SPSS	2011	0,6
- Workshop InDesign CS6	2013	0,2
Presentations		
- Various presentations at research meetings at the department of orthopaedics	2010 – 2013	4,0
(Inter)national conferences: poster presentation		
- Porous titanium as treatment for large segmental bone defects, Orthopaedic Research Society annual meeting: San Francisco, United States	2012	1,0
- Guided bone regeneration in critical defects using porous titanium scaffolds loaded with gelatin nanosphere-based gels for controlled release of BMP-2 and FGF-2, BMM/TeRM annual meeting: Ermelo, The Netherlands	2012	1,0
(Inter)national conferences – podium presentation		
- Titanium foam in segmental defects of rat femora, BMM/TeRM annual meeting, Ermelo, The Netherlands	2011	>5,0
- Titanium foam in segmental defects of rat femora, BoneTec 4th annual meeting, Hannover, Germany	2011	
- Titanium foam in segmental defects of rat femora, European Orthopaedic Research Society 19th annual meeting, Vienna, Switzerland.	2011	

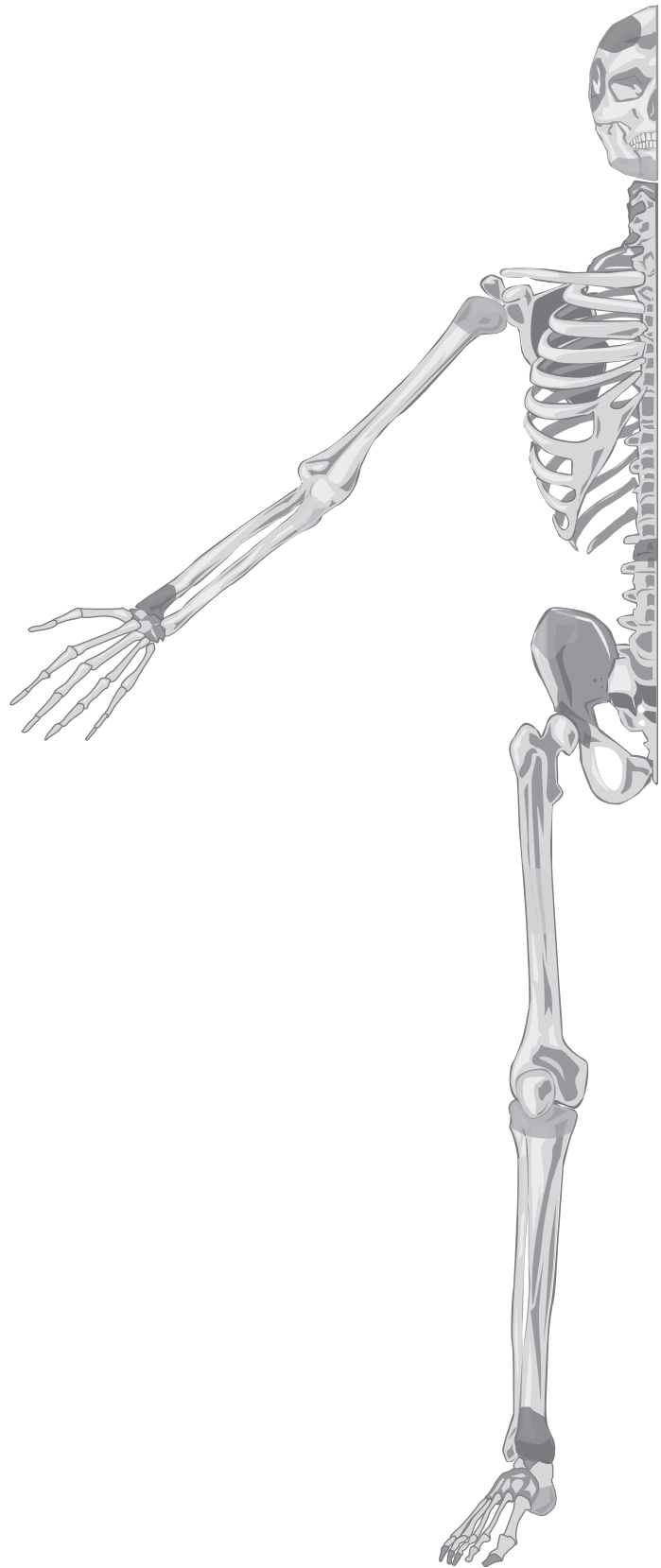
- Titanium foam in segmental defects of rat femora, Netherlands society for Biomaterials and Tissue Engineering 20th annual meeting, Lunteren, The Netherlands	2011
- Botssubstitutiematerialen: current state of the art, Zuid West Nederland overleg trauma (ZWOT), Rotterdam, The Netherlands	2012
- Guided bone regeneration in critical defects using porous titanium scaffolds loaded with gelatin nanosphere-based gels for controlled release of BMP-2 and FGF-2, European Orthopaedic Research Society 20th annual meeting, Amsterdam, The Netherlands	2012
- Guided bone regeneration in critical defects using porous titanium scaffolds in combination with nanostructured colloidal gelatin gels for controlled release of BMP-2 and FGF-2, Orthopaedic Research Society annual meeting, San Antonio, United States	2013
- Hypertrophic chondrocyte differentiated MSC pellets as artificial fracture callus to enhance bone healing of critical bone defects, BMM/ TeRM annual meeting, Ermelo, The Netherlands	2013
- Hypertrophic chondrogenic differentiated MSC pellets stimulate bone regeneration in segmental bone defects, European Cells & Materials annual meeting, Davos, Switzerland	2013

Other

-

2. Teaching

	Year	Workload (ECTS)
Lecturing		
- Lecturing 3rd year medical students attending the minor "Orthopaedic Sports Traumatology"	2012-2013	2,0
Supervising practicals and excursions		
- Examination of Basic Life Support (EHBO) of 1st year medical students	2009-2010	1,0
- Practicals in bone pathology, 2nd year medical students	2012-2013	2,0
Supervising master theses		
- Development of in vitro screening methods for the evaluation of osteoinductive properties of porous metal implant surfaces, Yvonne de Jong, Biomedical Sciences, Leiden University Medical Center, Leiden, The Netherlands	2010	2,0
- Osteostatin-coated porous titanium scaffolds for bone regeneration in segmental bone defects in rats, Angela P. Bastidas Coral, Biomedical Sciences, Radboud University Nijmegen Medical Center, Nijmegen, The Netherlands	2012	2,0

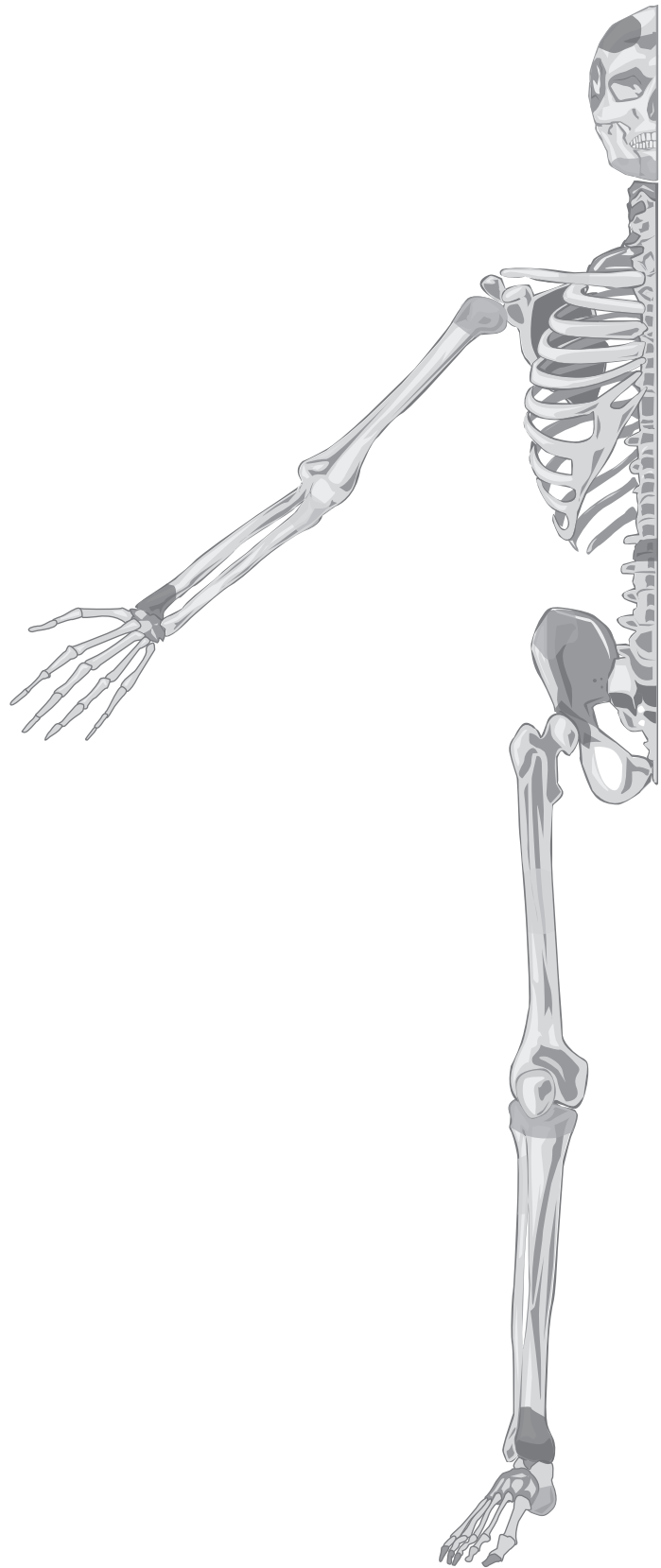


List of publications

List of publications

- 2007 ***Metabolic and genetic regulation of cardiac energy substrate preference***
Kodde IF, van der Stok J, Smolenski RT, de Jong JW.
Comp Biochem Physiol A Mol Integr Physiol. 2007 Jan;146(1):26-39.
- 2011 ***Bone substitutes in the Netherlands – a systematic literature review***
van der Stok J, Van Lieshout EMM, El-Massoudi Y, van Kralingen GH, Patka P.
Acta Biomater. 2011 Feb;7(2):739-50.
- 2012 ***The influence of genetic factors on the osteoinductive potential of calcium phosphate ceramics in mice***
Barradas AM, Yuan H, van der Stok J, Le Quang B, Fernandes H, Chatterjea A, Hogenes MC, Shultz K, Donahue LR, van Blitterswijk C, de Boer J.
Biomaterials. 2012 Aug;33(23):5696-705.
- 2013 ***Selective laser melting-produced porous titanium scaffolds regenerate bone in critical size cortical bone defects***
van der Stok J, Van der Jagt OP, Amir Yavari S, de Haas MFP, Waarsing JH, Jahr H, van Lieshout EMM, Patka P, Verhaar JAN, Zadpoor AA, Weinans H.
Journal Orthopaedic Research. 2013 May;13(5):792-9.
- 2013 ***Full-field strain measurement and fracture analysis of rat femora in compression test***
Amin Yavari S, van der Stok J, Weinans H, Zadpoor AA.
J Biomech. 2013 Apr 26;46(7):1282-92.
- 2013 ***Predicting the therapeutic efficacy of MSC in bone tissue engineering using the molecular marker CADM1***
Mentink A, Hulsman M, Groen N, Licht R, Dechering K, van der Stok J, Alves H, Dhert W, van Someren E, Reinders MJT, Van Blitterswijk CA, De Boer J.
Biomaterials. 2013 Jun;34(19):4592-601.
- 2013 ***Inflammatory response and bone healing capacity of two porous calcium phosphate ceramics in a critical-sized rat long size cortical bone defect***
van der Stok J, Chatterjea A, Danoux CB, Yuan H, Habibovic P, van Blitterswijk CA, Weinans H, de Boer J.
Journal of Biomedical Materials Research Part A. 2013 Jun 3.
- 2013 ***Enhanced Bone Regeneration of Cortical Segmental Bone Defects Using Porous Titanium Scaffolds Incorporated with Colloidal Gelatin Gels for Time- and Dose-Controlled Delivery of Dual Growth Factors.***
van der Stok J, Wang H, Amin Yavari S, Siebelt M, Sandker M, Waarsing JH, Jahr H, Zadpoor AA, Leeuwenburgh SCG, Weinans H.
Tissue Engineering Part A. 2013 Aug 17.
- 2013 ***Properties of commonly used calcium phosphate cements in trauma and orthopaedic surgery***
van der Stok J, Weinans H, Kops K, Siebelt M, Patka P, van Lieshout EMM.
Injury. 2013 Oct;44(10):1368-74.
- 2013 ***Subxiphoid pericardial window to exclude occult cardiac injury after penetrating thoracoabdominal trauma.***
Hommes M, Nicol AJ, van der Stok J, Kodde IF, Navsaria PH
British Journal of Surgery. 2013 Oct; 100(11):1454-8.

- 2013 ***Sustained release of BMP-2 in bioprinted alginate for osteogenicity in mice and rats.***
Poldervaart MT, Wang H, van der Stok J, Weinans H, Leeuwenburgh SCG, Öner FC, Dhert WJ, Alblas J.
PLoS One. 2013 Aug 19;8(8):e72610.
- 2013 ***Fatigue behavior of porous biomaterials manufactured using selective laser melting***
Amin Yavari S, Wauthle R, van der Stok J, Riemsdag AC, Janssen M, Mulier M, Kruth JP, Schrooten J, Weinans H, Zadpoor AA.
Materials Science Engineering Part C. 2013 Dec 1;33(8):4849-58.
- 2013 ***Chondrogenically differentiated mesenchymal stromal cell pellets stimulate endochondral bone regeneration in critical-sized bone defects.***
Van der Stok J, Koolen MKE, Jahr H, Kops N, Waarsing JH, Weinans H, Van der Jagt OP.
European Cells & Materials. 2014 Feb 19;27:137-48
- 2014 ***Bone regeneration performance of surface-treated porous titanium***
Amin Yavari S, van der Stok J, Chai YC, Wauthle R, Tahmasebi Birgani Z, Habibovic P, Mulier M, Schrooten J, Weinans H, Zadpoor AA.
Biomaterials, 2014 Aug;35(24):6172-81
- 2014 ***Effects of bio-functionalizing surface treatments on the mechanical behaviour of open porous titanium implants***
Amin Yavari S, Ahmadi SM, van der Stok J, Wauthle R, Riemsdag AC, Janssen M, Schrooten J, Weinans H, Zadpoor AA.
Journal of the Mechanical Behavior of Biomedical Materials, 2014 Apr 26;36C:109-119
- 2014 ***Mechanical analysis of a rodent segmental bone defect model: the effects of internal fixation and implant stiffness on load transfer***
Amin Yavari S, Van der Stok J, Ahmadi SM, Wauthle R, Schrooten J, Weinans H, Zadpoor AA.
Journal of Biomechanics. 2014 Aug 22;47(11):2700-8
- 2015 ***Growth factor-induced osteogenesis in a novel radiolucent bone chamber***
Poldervaart MT, van der Stok J, De Haas MFP, 't Hart MC, Cumbur Oner F, Dhert WJA, Weinans H, Alblas J.
European Cells and Materials. 2015 Jan 2;29:35-41
- 2015 ***Additively manufactured porous tantalum implants***
Wauthle R, van der Stok J, Amin Yavari S, van Humbeeck J, Kruth JP, Zadpoor AA, Weinans H, Mulier M, Schrooten J.
Acta Biomaterialia. 2015 Mar 14;217-25
- 2015 ***Osteostatin-coated porous titanium can improve early bone regeneration of cortical bone defects in rats***
van der Stok J, Lozano D, Chai YC, Amin Yavari S, Bastidas Coral AP, Verhaar JAN, Gómez-Barrena E, Schrooten J, Jahr H, Zadpoor A, Esbrit P, Weinans H.
Tissue Engineering. 2015 Jan 28 (Epub ahead of print)
- 2015 ***Full regeneration of segmental bone defects using porous titanium implants loaded with BMP-2 containing fibrin gels***
van der Stok J, Koolen MKE, de Maat, M, Amin Yavari S, Alblas J, Patka P, Verhaar JAN, van Lieshout EMM, Zadpoor AA, Weinans H, Jahr H.
European Cells and Materials. 2015 Mar 4;29:141-54



Dankwoord

Tot slot wil ik alle mensen bedanken die mij hebben geholpen bij de totstandkoming van dit proefschrift.

Prof.dr.ir. H. Weinans, beste Harrie, ik ben je enorm dankbaar voor jouw grote vertrouwen in mij. Jouw onuitputtelijke enthousiasme voor de wetenschap heb jij op een geweldige manier overgedragen. Dit heeft mij gedurende de afgelopen jaren gemotiveerd tot het doen van steeds meer onderzoek. Het was ook heel erg fijn om dagelijks met jou te mogen samenwerken, een fijnere supervisor had ik me niet kunnen wensen!

Prof.dr. J.A.N. Verhaar, beste professor, ook u ben ik zeer dankbaar voor het vertrouwen en de oprechte interesse en betrokkenheid in mijn werk. Uw ervaren en deskundige klinische blik heeft ertoe bijgedragen dat verkregen resultaten konden worden vertaald naar toekomstige toepassingen in de trauma en orthopaedische chirurgie. Ik kijk er naar uit om in de nabije toekomst nog veel meer van u te kunnen leren over het vak orthopaedie!

Prof.dr. P. Patka, beste professor, ik wil u bedanken voor het feit dat u mij de kans heeft geboden om als onderzoeker aan de slag te gaan. Uw jarenlange expertise op het gebied van botgenezing en botsubstitutiematerialen heeft enorm geholpen bij de totstandkoming van dit proefschrift.

Dr. E.M.M. van Lieshout, beste Esther, bedankt voor de begeleiding en voor de altijd razend-snelle feedback op mijn werk.

Dr. van der Jagt, beste Olav, zonder jou was dit proefschrift misschien wel nooit tot stand gekomen. Jouw bijdrage is onmisbaar omdat jij mij, toen we elkaar troffen in het Sint Franciscus ziekenhuis, in contact bracht met Harrie. Ik heb met veel plezier met jou samengewerkt en ik ben bovenal erg trots op de door ons bereikte resultaten. Ik hoop dat we in de nabije toekomst een vervolg kunnen geven aan dit boeiende werk.

Dr. Zadpoor, beste Amir, ik wil jou in het bijzonder bedanken voor alle begeleiding bij de totstandkoming van dit proefschrift. Je was altijd laagdrempelig beschikbaar voor feedback en je stond altijd open voor nieuwe ideeën. Je hebt enorm veel voor mij gedaan en het was fantastisch om met jou te werken aan het ontwikkelen van poreuze titanium implantaten. Een onderwerp waar ik graag met jou in de toekomst nog verder aan zou willen werken!

Beste Saber en Ruben, dankzij jullie enorme inzet en bovenal harde werk ontstond er een unieke samenwerking tussen de TU Delft, Layerwise en het Erasmus MC. Hierdoor ontstond een uiterst efficient team, maar bovenal droeg de samenwerking bij aan het plezier dat ik heb gehad tijdens het doen van al het onderzoek. Jongens, heel erg bedankt!

Beste Holger, beste Erwin, ik wil jullie hier ook in het bijzonder bedanken omdat jullie enthousiasme, kennis en ervaring onmisbaar is geweest bij de totstandkoming van dit proefschrift. Jullie input is duidelijk zichtbaar in meerdere hoofdstukken en daar ben ik jullie beiden zeer dankbaar voor!

Collega's, stuk voor stuk ook vrienden, ik wil jullie ook graag bedanken. Michiel, Rintje, Jasper, dat we ieder een andere voetbalclub aanmoedigen stond een zeer fijne tijd op het lab niet in de weg. In het bijzonder dank voor de vele (te) gezellige vrijdagavonden in Boudewijn! Marianne, super gezellige collega, ik vind het mooi dat het onderzoek naar nieuwe botssubstitutiematerialen momenteel voortzet in Utrecht, succes! Marjan, super leuk dat je me achterna bent gegaan naar het Maasstad ziekenhuis, altijd fijn om even met jou van gedachten te wisselen. Angela, je was een fantastische master student, dank voor al je inzet en werk met osteostatin. Sandra, bedankt voor al jou hulp bij de laatste loodjes! En dan volgt er een hele lijst met stuk voor stuk fijne collega's: Anna, Belle, Gerben, Gerjo, Guus, Job, Lizette, Maarten, Marloes, Max, Mieke, Mirthe, Nienke, Nicole, Roberto, Tijs, Tom, Yvonne, Vincent, Wendy en Wu.

Daarnaast heb ik het geluk gehad te mogen samenwerken met diverse zeer enthousiaste en kundige onderzoeksgroepen buiten het Erasmus MC. Huanan Wang en Sander Leeuwenburg van de Radboud Universiteit, Nijmegen. Daniel Lozano and Pedro Esbrit of the Instituto de Investigación Sanitaria-Fundación Jiménez Díaz, Madrid. Anindita Ganguly en Jan de Boer van de Technische Universiteit, Twente. Yoke Chin Chai en Jan Schrooten van de Katholieke Universiteit, Leuven. Stuk voor stuk hebben jullie een belangrijke bijdrage geleverd aan dit proefschrift.

Vrienden van de Kantelaar, jullie hebben helemaal niets bijgedragen aan dit proefschrift. Toch mogen jullie absoluut niet in dit dankwoord ontbreken, omdat jullie stuk voor stuk zulke unieke en waardevolle vrienden voor mij zijn. Dank voor de vele legendarische avonden waarop ik voor even kon ontsnappen aan de dagelijkse kommer en kwel van het onderzoek doen. Ik hoop dat er nog vele mooie avonden mogen volgen!

Klaas Hartholt, bedankt dat je mijn paranimf wilde zijn! Doordat ik jouw promotie als paranimf van dichtbij mocht meemaken, wist ik wat er op me af zou komen de laatste maanden. Samen was het altijd gezellig in de verder toch wat suffe gang van het Z-gebouw in het Erasmus MC.

Sjaak Kodde, ook jij bedankt dat je mijn paranimf wilde zijn! Samen delen we veel mooie herinneringen en omdat wij samen onze eerste publicatie schreven in 2006 in Londen,

moest jij hier natuurlijk ook bij zijn. Na Londen beleefde ik samen met jou het absolute hoogtepunt van mijn studietijd: een half jaar coassistent zijn op de beroemde Trauma Unit van het Groote Schuur ziekenhuis in Kaapstad. Gelukkig blijven we naast goede vrienden ook nog eens collega's in een schitterend vak!

Als laatste wil ik mijn familie bedanken. Pa en ma, jullie zijn een stelgeweldige ouders! Het is altijd fijn om thuis te komen in Maasdijk. Het feit dat jullie altijd bereid zijn om even een handje te helpen met de dagelijkse dingen, is een grote steun geweest. Hierdoor kon ik dit proefschrift met volle overgave schrijven. Het gemak waarmee jullie iets voor een ander doen is uniek, ik doe mijn best om hierin op jullie te mogen lijken. Ingrid en Lianne, jullie hebben beide dezelfde motivatie en inzet voor jullie eigen werk, en dat is super mooi om te zien! Ik wil jullie, en tegelijkertijd ook Arwin, bedanken voor jullie steun de afgelopen jaren.

And finally, Niamh, I want to thank you for walking into the lab on the 16th floor of the Erasmus Faculty Building that ordinary day in 2012! From that day onwards you've been a great support and motivation to get this PhD thesis done! I also want thank you and your family for welcoming me in Ireland and introducing me to all the traditional habits including the occasional relaxing drink of a big pint in the pub. Pòg mòr!

About the author



Johan van der Stok werd geboren op 24 februari 1985 in Delft. Hij groeide op in het Westlandse dorpje Maasdijk, waar hij naar de protestants-christelijke basisschool Het Kompas ging. Na de basisschool behaalde hij zijn vwo-diploma op de Interconfessionele Scholengemeenschap Westland in Naaldwijk. Tijdens zijn middelbareschooltijd ontstond zijn passie voor de medische wereld en in 2003 begon hij met de studie geneeskunde aan de Erasmus Universiteit Rotterdam. Een korte buitenlandse stage in het Harefield Heart Science Centre, onderdeel van het Imperial College Londen, was zijn eerste kennismaking met wetenschappelijk onderzoek. Tijdens zijn coschappen in het Sint Elisabeth ziekenhuis in Tilburg ontstond de voorkeur voor trauma en orthopaedische chirurgie. In het kader daarvan besloot hij zeven maanden coschappen te lopen op de trauma-afdeling van het Groote Schuur ziekenhuis in Kaapstad. Terug in Nederland voltooide hij in 2009 zijn artsexamen en besloot hij direct aansluitend te starten met een promotieonderzoek. Dat onderzoek, met dit proefschrift als resultaat, is een samenwerking geworden tussen de afdeling Orthopaedie en de afdeling Heelkunde en Traumatologie, van het Erasmus MC. In 2014 is hij gestart met zijn vooropleiding heelkunde in het Maasstad ziekenhuis en medio 2015 zal hij zijn vervolgopleiding tot orthopaedisch chirurg starten in het Reinier de Graaf Gasthuis en aansluitend het Erasmus MC.

